Generating and characterising chimeric antigen receptors to target the tumour vasculature

Lewis Blair Cawkwell

A thesis submitted to the University of Birmingham for the degree of
DOCTOR OF PHILOSOPHY

Institute of Immunology and Immunotherapy
College of Medical and Dental Sciences
The University of Birmingham
August 2017

Abstract

Tumour associated endothelial cells have been found to express markers not normally found within the mature, stable, adult vasculature network. These markers, termed tumour endothelial markers (TEMs) are potential targets for chimeric antigen receptor (CAR) T cell therapy. This project attempts to generate and characterise CARs against the novel TEMs: ROBO4, ELTD1, GRIND2 and MCAM.

In the first part of the project, ROBO4-specific CARs that signal through CD3ζ and CD28 signalling domains were characterised. ROBO4 CARs specifically retarget T cells to mouse and human ROBO4 in multiple in vitro assays of T cell function. ROBO4 CAR T cells also showed a slight but insignificant reduction in tumour growth compared to control CAR T cells. However, ROBO4 CAR T cells caused toxicity at high doses and whole body cryoimaging showed that ROBO4 CAR T cells accumulated in the lung and liver of healthy mice.

In the second part of the project, the ETH2-GOLD phage display library was used to recover novel antibodies with the aim of generating CARs. However, the generated ELTD1 CAR was non-functional in T cells and significant problems occurred while searching for antibodies to GRIN2D and MCAM.

Acknowledgements

Thank you to everyone who has helped me throughout this PhD project, in the lab and out the lab.

Contents

Figures

Tables

1. Introduction

1.1 Vasculogenesis

The cardiovascular system is the first organ to begin formation in the developing embryo. Vasculature can form through vasculogenesis and angiogenesis. Vasculogenesis is de novo vasculature formation through the differentiation of vascular precursor cells (angioblasts). Angiogenesis is the expansion or remodelling of pre-existing vasculature. This vascularisation in the developing embryo is essential in delivering oxygen to other developing organs. After birth the vascular system remains stable, however, post-natal vascularisation occurs in the ovaries, wound healing and some pathological conditions. The vascular system consists of thick arteries, which branch into arterioles which branch further into smaller capillaries. These vessels are made up of endothelial cells, which form the inner lining of the vessel. Around large vessels, smooth muscle cells surround the endothelium and pericytes surround the smaller capillaries.

The first site of embryonic vascularisation occurs on the yolk sac, around embryonic day (E) 7.5 in mice. Here, hemangioblast cells, derived from mesodermal cells, form aggregates which become blood islands. The hemangioblast is a common precursor for the angioblast and hematopoietic cells (Choi et al. 1998). The islands inner hemangioblast cells become hematopoietic cells, whereas outer cells differentiate into angioblasts which give rise to endothelial cells, forming blood vessel lining. These endothelial cells then form a primary plexus giving rise to the yolk sac vasculature. Similarly, in the embryo proper, angioblasts are found at E7.5 which give rise to a primary plexus and endocardial tube leading to the dorsal, aortae and cardinal veins (Conway et al. 2001).

Adult vasculargenesis was previously thought only to occur through angiogenesis, but evidence now exists for endothelial progenitor cells (EPCs) to persist in the adult and initiate vasculogenesis (Urbich & Dimmeler 2004). Asharara *et al* first described adult EPCs which could differentiate to endothelial cells *in vitro* and contribute to neovascularisation in animal models of Ischemia (Asahara et al. 1997). It was later shown that murine bone marrow derived cells could incorporate into tumour endothelium and stroma (Asahara et al. 1999). Several studies have now described non bone-marrow derived EPCs (Urbich & Dimmeler 2004). After initial embryonic vasculogenesis, angiogenesis is responsible for the majority of vascular development. Angiogenesis results in remodelling of the primary plexus forming a complex branching vessel network. Angiogenesis can occur in a sprouting or intususceptive manner. Sprouting involves endothelial cell detachment from the basement membrane and migration as a sprout towards an angiogenic stimuli and fusing to another blood vessel. Intersussceptive angiogenesis involves the splitting of a single vessel into two.

1.2 VEGF and vascularisation

The vascular endothelial growth factor (VEGF) family consist of VEGFA, VEGFB, VEGFC, VEGFD and placental growth factor (PGF) (Ferrara et al. 2003). VEGFA is considered the prototype member and is a key regulator of vascularisation.

VEGFA's importance is emphasised by mice embryo's lacking one VEGFA allele dying around E11 to E12 and exhibiting defective vascularisation (Carmeliet et al. 1996; Ferrara et al. 1996). It is capable of binding VEGF receptor (VEGFR) 1, VEGFR2, neuropilin (NPR) 1 and NPR2. VEGFR2 is essential in vasculogenesis, since VEGFR2 knock out mouse embryos do not develop blood islands due to a lack of endothelial cell differentiation, dying around E8.5 to E9.5 (Shalaby et al. 1995). VEGFR1 knock-out mice also die around E8.5 to E9.5, largely due to an overproliferation of angioblasts (Fong et al. 1999). It is possible that VEGFR1 therefore acts as a decoy receptor (Park et al. 1994; Ferrara et al. 2003). Studies have described VEGF to have a higher affinity for VEGFR1 than VEGFR2, but VEGFR1 has poor signal transduction capacity and due to alternative splicing can exist as a secreted soluble receptor, capable of sequestering surrounding VEGF, agreeing with its prediction as a decoy receptor (Takahashi et al. 1997; Park et al. 1994). NPR1 and NPR2 have been described as VEGFR2 coreceptors, enhancing VEGF signalling (Ferrara et al. 2003).

VEGFA exists in four different isoforms due to alternative splicing known as $VEGF_{121}$, $VEGF_{165}$, $VEGF_{189}$ and $VEGF_{206}$ (Houck et al. 1992; Park et al. 1993). Variants 189 and 206 retain a heparin binding domain and therefore are sequestered within the extracellular matrix (ECM) or cell surface through high affinity heparin interaction. Variant 121 lacks this domain and is therefore soluble. Variant 165 has intermediate heparin binding properties with some sequestered within the ECM. Interestingly mice expressing only the non-heparin binding soluble VEGFA exhibit reduced complexity in vessel branching early in development (Ruhrberg et al. 2002). It was also shown that heparin binding variants are capable of forming a VEGFA gradient as they are secreted and mostly retained in close proximity to the producing cells (Ruhrberg et al. 2002). VEGFR2, VEGF and its gradient play a key role in branching angiogenesis.

VEGFR2 expressed on endothelial cells can interact with free VEGF, initiating endothelial filipodia formation leading to an endothelial sprout, with a migrating tip cell and proliferative stalk cells. Blockage of VEGFR2 or sequestration of VEGF can inhibit this fillipodia initiation (Gerhardt et al. 2003). The gradient of VEGF can subsequently guide endothelial tip cell filipodia towards the site of VEGF production (Ruhrberg et al. 2002). Similarly, sequestration of VEGF during migration causes filipodia to lose the tip cells responsible for guidance (Gerhardt et al. 2003). VEGF signal transduction in endothelial cells can activate the notch ligand Delta-like ligand 4 (Dll4) (Lobov et al. 2007; Liu et al. 2003). Dll4 expression is restricted to the developing vascular endothelium (Shutter et al. 2000). Similar to VEGFA, the knock-out of a single copy of the Dll4 gene is embryonic lethal (Gale et al. 2004).

A VEGF mediated Dll4 upregulation in responding endothelial cells is important in differentiation into a leading tip cell and following stalk cells. Furthermore, Dll4 expression on the tip cell surface can interact with its notch receptors, notch 1 and notch 4, on adjacent endothelial cells. Notch signalling results in the generation of a Notch intracellular domain (NICD) which is a transcriptional regulator. This transcriptional regulation includes a downregulation of VEGFR2 and an upregulation of VEGFR1, resulting in cells becoming less responsive to VEGF. Therefore, the endothelial cell with the highest concentration of VEGF can initiate a greater Dll4 upregulation and impose greater notch signalling to surrounding cells. The high Dll4 expressing cell then adopts a tip cell phenotype whereas the adjacent cells become stalk cells. In this regard, Dll4/Notch signalling is an important negative feedback of VEGF, allowing a regulated differentiation of tip and stalk cells.

Extending filipodia are important in guiding tip cells up the VEGF gradient. Another feature of the tip cell is a proteolytic phenotype. This is important in degradation of the surrounding basement membrane and the ECM to allow endothelial cell release from the blood vessel and migration into avascular regions. The matrix metalloproteinases (MMPs) are heavily implicated in angiogenesis as are the A disintegrin and metalloproteinase domain (ADAMs) family and the A disintegrin and metalloproteinase with thrombospondin motifs (ADAMTS) family (van Hinsbergh & Koolwijk 2008). However, membrane type-1 (MT-1) MMP is described as the dominant proteinase during angiogenesis.

MT-1 MMP is a membrane bound proteinase. MT-1 MMP Knock-out mice exhibit serious problems with angiogenesis (Zhou et al. 2000). MT-1 MMP was found to be required for endothelial cell migration and vessel formation in 3-dimensional collagen gel matrices *in vitro* and *in vivo* (Koike et al. 2002; Chun et al. 2004). Furthermore, MT-1 MMP expression is mostly limited to the endothelial tip cells during angiogenesis (Yana et al. 2007). Mathematical modelling has suggested MT1 MMP, MMP2 and TIMP7 as required for ECM degradation and endothelial tip cell migration into avascular regions (Karagiannis & Popel 2006). After angiogenic vessel branching is complete, the resolution phase begins. This involves the shutdown of endothelial cell proliferation and recruitment of pericytes and vascular smooth muscle cells (VSMCs). Endothelial cells lose their proteolytic phenotype, the vessel lumen closes up, stabilises and a basel membrane is produced. As blood flows through the vessel, oxygenation of the surrounding tissues can occur. This can decrease local VEGF, ending vascularisation.

Intussusceptive angiogenesis also plays a role in vascularisation although much less is known about its molecular regulation (Burri et al. 2004). It is thought to be more important in plexus formation and vessel remodelling. Electron microscopy has identified important stages in intussusceptive angiogenesis (Burri et al. 2004). Firstly, endothelial cells on opposing sides of the vessel lumen protrude towards each other, making contact and creating a transluminal bridge. The endothelium becomes perforated forming a cylindrical pillar. The pillar increases in size as invasive fibroblasts and pericytes are recruited and eventually, two separate vessels are formed.

1.3 Tumour Vasculogenesis

After the completion of embryonic vascularisation, the adult vascular system is largely quiescent with the exception of the ovarian cycle, wound healing and certain diseases. It has been found that tumours can grow up to $1mm^3$ before neovascularisation is required to promote further growth by supplying oxygen and nutrients (Muthukkaruppan et al. 1982) (figure 1.1). Intriguingly, both vasculogenesis from an endothelial precursor cell and angiogenesis from existing vessels appear to have roles in tumour vascularisation (Asahara et al.

1999)(Folkman 1971). However, there are notable differences between normal and tumour vessels.

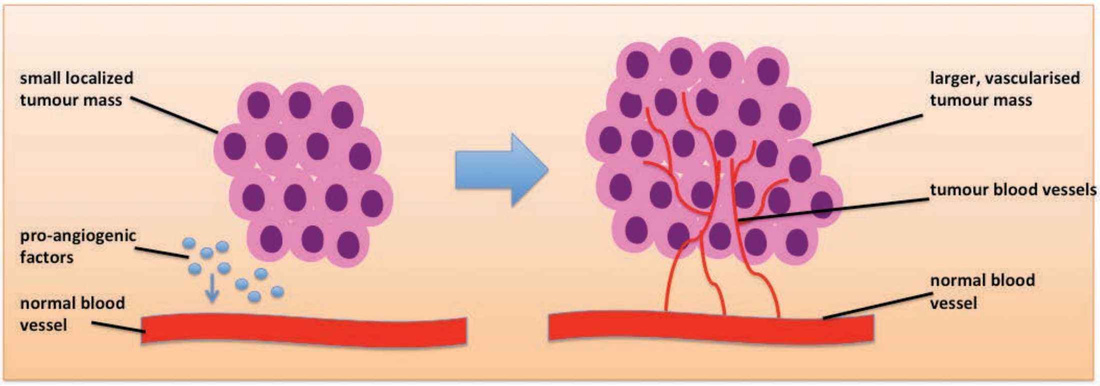

Figure 1.1: tumour angiogenesis. Small, localised tumours can grow and survive without a dedicated blood supply. However once the tumour reached around 1mm^3 it requires a blood supply for continues growth and survival. The tumour can initiate angiogenesis by releasing pro-angiogenic factors such as VEGF. These factors induce normal blood vessels in adjacent healthy tissues to begin angiogenesis. New blood vessels can then grow into the tumour and generate a tumour vasculature network, supporting continued tumour growth and survival.

Tumour vessels are tortuous in shape and disorganised in structure with irregular branching (Warren et al. 1978; Konerding et al. 1999; McDonald & Choyke 2003)). Vessels are also dilated and leaky and have chaotic blood flow (McDonald & Choyke 2003). Whereas normal endothelium is a single monolayer of cells, the tumour endothelium tends to be patchy, with endothelial cells of variable shape. Vessels may also be mosaic, where CD31, an endothelial marker, gives a spotted staining pattern. This feature can be due to a complete lack of endothelium with blood in contact with the tissues or where tumour cells are themselves incorporated into the vasculature, adopting an endothelial-like phenotype (Dudley 2012; Furuya et al. 2009). Similarly, vasculogenic mimicry can occur where a tumour blood vessel is lined solely with tumour cells with an endothelial-like cell phenotype (Furuya et al. 2009). Despite these differences, Folkman proposed that anti-angiogenesis therapy could be used to treat cancer (Folkman 1971).

The discovery and characterisation of the VEGF signalling pathway paved the way for anti-angiogenic therapy. Murine tumour models provided the proof of concept of targeting VEGF with a monoclonal anti-VEGF antibody (Kim et al. 1993). The same antibody became humanised (Presta et al. 1997) and showed success in clinical trials (Hurwitz et al. 2004). This antibody, named bevacizumab is now approved in the treatment of various cancers including colorectal cancer, although only works in combination with chemotherapy. Other approved molecules include sorafenib, sunitinib and vandetanib. These small molecule tyrosine kinase inhibitors can bind and inhibit the catalytic domain of tyrosine kinase of several molecules, including VEGFR2 (Bergers & Hanahan 2008).

However, in several cases, any beneficial effect of these anti-VEGF signalling molecules is only temporary (Bergers & Hanahan 2008). This is due to several reasons including angiogenic redundancy through vascularisation via other VEGF-independent pathways and protection of tumour vessels through recruitment of inflammatory cells, pericytes and tumour cell incorporation into vessels (Bergers & Hanahan 2008). Thus tumours can again vascularise and grow again. In almost all patients, tumours will gain resistance and become progressive.

There is also considerable concern around the toxicity of molecules targeting VEGF signalling. VEGF is required for the long term maintenance of endothelial cells (Carmeliet 2003) and is important in kidney function through glomerular vascularisation (Masuda et al. 2001). VEGF targeting has been associated with serious side effects such as gastric perforation, poor wound healing and thrombocytic events (Hurwitz et al. 2004). There is therefore a need to identify new targets on the tumour vasculature.

1.4 T cells

T cells are a group immune cells that form part of the adaptive immune system. They express a T cell receptor (TCR) responsible for recognising antigen expressed as peptide on MHCI and MHCII molecules. CD8 cytotoxic T cells recognise peptide-MHCI and are generally responsible for killing infected or malignant cells. CD4 helper T cells recognise peptide-MHCII and assist the immune response through activation of innate immune cells, B cells, CD8 T cells and non-immune cells (Zhu & Paul 2008). The classical subsets of CD4 T cells are the T helper (Th) 1 cells and Th2 cells. Th1 cells are typically involved in pro-inflammatory responses such as against intracellular pathogens and their signature cytokines are IFNγ and IL2. Th2 cells are typically involved in defence against extracellular parasites such as helminths. Their signature cytokines include IL4, IL5, IL10 and IL13. Further subsets now include Th17, T follicular helper cells, and regulatory T cells (Tregs). Th17 cells mediate responses against extracellular bacteria and fungi. T follicular helper cells assist B cell antibody responses. Tregs negatively regulate the immune response and help to maintain self-tolerance.

T cells arise from common lymphoid progenitors that migrate from the bone marrow, into the thymus and their development has previously been reviewed elsewhere (Germain 2002). Briefly, the first stage in T cell development is as a double negative (DN) thymocyte that lacks the expression of the CD8 and CD4 coreceptors. During DN development, the T cell receptor (TCR) is expressed. The TCR is a heterodimer that consists of either the αβ chain pair or the γδ chain pair. The loci of each chain contain multiple variable (V), multiple junctional (J) and constant gene segments. The β and δ chains additionally contain diversity (D) segments. Each loci must rearrange its DNA, bringing individual V(D)J segments and the constant region together to form a functional chain. The random recombination of these individual segments generates significant TCR diversity. Further diversity is generated from an often imprecise joining of segments.

TCRβ, TCRγ and TCRδ rearrangement begins at DN stage 2 (Krueger et al. 2017). Successful TCRγ and TCRδ rearrangement leads to a γδ TCR, driving a clonal proliferation and differentiation into a γδ T cell. A functionally rearranged TCRβ can pair with a pre-TCRα molecule to form the pre-TCR. Successful pre-TCR expression will induce allelic exclusion of TCRβ, clonal proliferation, transcriptional silencing of the TCRγ locus and differentiation into a double positive (DP) CD8 and CD4 expressing cell. DP cells then initiate TCRα rearrangement. Functional rearrangement allows the expression of the αβTCR.

From this large pool of αβTCR expressing DP cells, selection must occur to choose for useful cells. Firstly, cells undergo positive selection. Here, cells must be capable of recognising self-peptide expressed on MHCI or MHCII molecules to initiate TCR signalling. In the absence of TCR signalling, DP cells die by apoptosis. Around 90% of DP cells die at this stage. During positive selection, cells will also become single positive (SP) by expressing only one coreceptor.

After positive selection, SP cells undergo negative selection. Here, cells are again presented self-peptide on MHCI or MHCII. If the SP cells TCR induces too great a signal upon self-peptide/MHC interaction, they may be deleted or in some cases differentiate into regulatory T cells (Tregs). Cells that survive negative selection can leave the thymus as immature T cells and enter circulation in the periphery. In the periphery, T cells will migrate into secondary lymphoid organs where they move into the T cell zones. Here they will survey antigen presenting cells (APCs) for cognate peptide. Upon recognition of cognate peptide, the T cell may be activated.

The TCR contains 6 complementary determining regions (CDRs), three in each chain, which are important in peptide-MHC recognition. CDR1 and 2 are formed from germline DNA of the V segment whereas CDR3 is formed from somatically rearranged DNA of V(D)J recombination (Rangarajan & Mariuzza 2014). X ray crystallography has revealed the αβ TCR sits diagonally over the peptide within the MHC molecule (Rangarajan & Mariuzza 2014). The germline encoded CDR1 and 2 loops have been found to position over the MHC α helices, whereas the

CDR3 loop positions over the peptide, although variations of this exist (Rangarajan & Mariuzza 2014).

T cell activation and downstream signalling events have been reviewed elsewhere (Rossy et al. 2012). Briefly, upon TCR engagement with peptide-MHC, the CD8 or CD4 coreceptor is recruited which also interacts with the MHC molecule. The Src family kinases, which include Lck, are associated with the coreceptor. Once brought into the vicinity of the TCR complex, they can phosphorylate the immunoreceptor tyrosine-based activation motifs (ITAMs) on CD3 and ζ chains. Double phosphorylated ITAMs can recruit the Syk kinase family member, Zap-70, through its two Src homology 2 (SH2) domains. Once recruited into the complex, Lck can phosphorylate the activation tyrosines of Zap-70.

Adaptor proteins are crucial in linking the early signalling events with downstream molecules. Linker for activation of T cells (LAT) is a membrane bound adaptor recruited to the TCR complex. Multiple LAT tyrosines are phosphorylated by Zap-70. Further molecules essential in downstream signalling pathways such as P13K, PLCγ, Grb2 and SLP76 are then recruited through SH2 domains. The downstream effect of these molecules leads to T cell cytoskeletal rearrangements, activation of transcriptional factors, intracellular calcium signalling and cell survival. The TCR signalling cascade for CD4 T cells is summarised in figure 1.2.

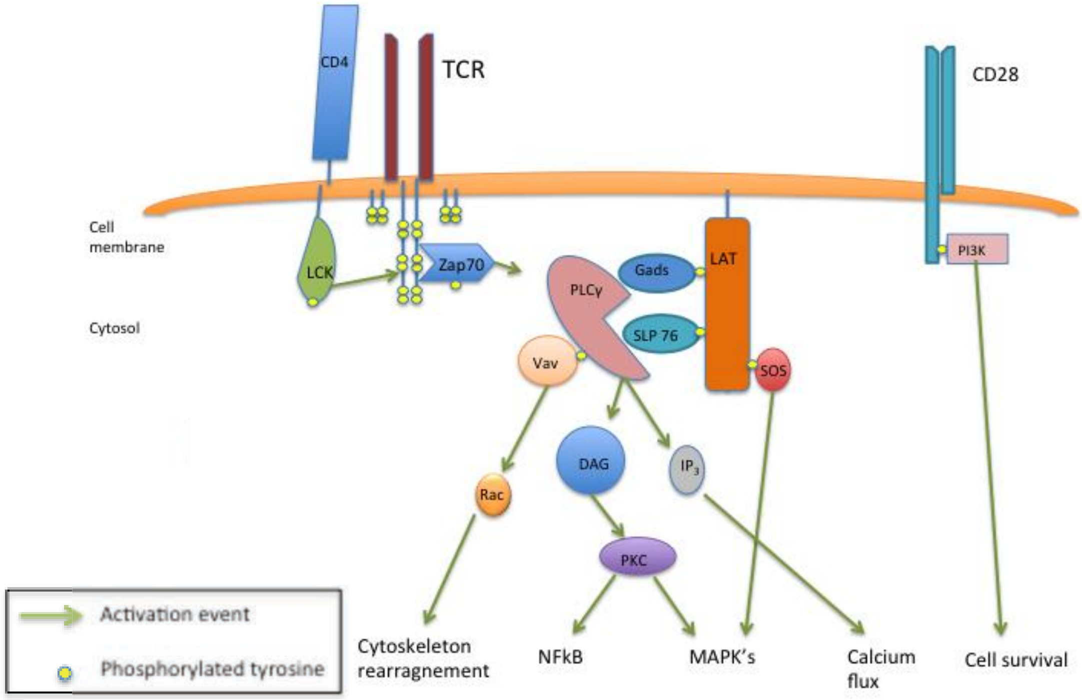

Figure 1.2: summary of CD4 T cell TCR signalling. After antigen stimulation of the TCR, the CD4 co- receptor comes into proximity, bringing with it Lck. Lck phosphorylates the ITAMs of the CD3 chains and zeta chains associated with the TCR. Zap70 is recruited to the ITAMs and phosphorylated and activated by Lck. Zap70 can then phosphorylate LAT and the several molecules that it recruits, forming a signalling complex. PLCγ can cleave membrane bound phosphoinositol biphsophate (not shown), generating IP3 and DAG. IP3 acts as a secondary messenger facilitating calcium flux. DAG can activate isoforms of PKC without calcium, and isoforms with calcium. The MAPK's ERK, JNK and P38 are important in many cell signalling cascades and processes. TCR, T cell receptor; PLCγ, phospholipase C gamma; DAG, diacylglycerol; LAT, linker for activation of T cells; SOS, son of sevenless; P13K, phosphoinositide 3 kinase; IP3, inositol triphosphate; PKC, phosphokinase C; ZAP-70, zeta chain associated protein kinase 70; NFκB, nuclear factor Kb.

1.5 T cell therapy

Haematopoietic stem cell transplant (HSCT) has long been used to combat haematopoietic-cell cancers, where the host blood cells are depleted by radiation or chemotherapy, then replaced with donor cells. Non-malignant donor cells can then reconstitute the blood of the host. However, relapse is common. Relapse has been found to be increased in patients receiving syngeneic donor cells; those under immunosuppression after transplant; and those receiving T cell depleted donations (Deol & Lum 2010). It was first demonstrated that following leukemia relapse after HSCT, lymphocytes from the same donor could be giving to trigger graft versus leukaemia (GvL) resulting in remission (Kolb et al. 1990). The principle is based on allogeneic donor T cells recognising host malignant blood cells as foreign and thereby destroying them. This therapy, known as donor lymphocyte infusion (DLI) has been effective in chronic myeloid leukaemia but less so in acute myeloid or lymphoid leukaemia (Deol & Lum 2010). A high incidence of graft versus host disease (GVHD) and aplasia is also reported In DLI (Deol & Lum 2010).

Patients are typically immunocompromised after HSCT before the immune system is fully reconstituted. This timeslot is associated with viral infections including Cytomegalovirus (CMV) and Epstein Barr virus (EBV), largely due to the disruption in the CD8 T cell control of infected cells. This may be due to reactivation of the virus in remaining host cells, or donor cells. Adoptive cell transfer can be performed where T cells are expanded *ex vivo* before transferring into the host. This was demonstrated with CMV specific CD8 T cell clones which were expanded and transferred after HSCT from the same allogeneic donor and were capable of providing CMV immunity (Walter et al. 1995). Similarly, patients who developed CMV infection and failed to respond to antivirals developed CMV immunity after transfer of expanded anti-CMV CD8 T cell clones (Einsele et al. 2002).

Infection with, or reactivation of EBV after HSCT can lead to post transplant lymphoproliferative disease (PTLD). Infected B cells can be transformed by EBV and grow uncontrolled due to an immunocompromised immune system. EBV lymphoma is associated with expression of highly immunogenic viral antigens. Therefore, it was shown that donor derived EBV specific CD8 T cells can be adoptively transferred to patients and successfully provide prophylaxis to EBV infection (Rooney et al. 1995; Rooney et al. 1998). On top of this, EBV specific T cell infusion can decrease EBV levels to normal control levels and resolve EBV immunoblastic lymphoma (Rooney et al. 1995; Rooney et al. 1998). EBV specific clones persist in the host and are now reported to have 100% efficacy in prophylaxis and 80% efficacy in treatment of EBV complications (Heslop 2009).

1.6 Tumour infiltrating lymphocyte therapy

The presence of tumour infiltrating lymphocytes (TILs) insinuates the existence of a host anti-tumour response. In parallel with this the presence of TILs can correlate with a better prognosis (Zhang et al. 2003; Galon et al. 2006). The collection of these cells from the host tumour, followed by *in vitro* expansion and activation with IL2 then infusion back into hosts along with IL2 is known as TIL therapy. TIL therapy, being an autologous transfer therefore bypasses any GVHD problems and makes use of the polyclonal reactivity.

The concept of TIL therapy was first shown in mice as therapy against lung and liver cancers (Rosenberg et al. 1986). It was then demonstrated how human TILs from melanoma could be isolated, expanded in IL2 then exhibit *in vitro* specificity for autologous melanoma antigen (Muul et al. 1987). The first clinical trial using TIL therapy successfully demonstrated tumour regression in 34% of 84 patients with metastatic melanoma (Rosenberg et al. 1988). However, despite an initial objective response, cells failed to persist and many patients quickly relapsed as cells had short persistence *in vivo.*

Studies from animal models subsequently showed the need for depletion of the host immune system before adoptive cell transfer. Host lymphodepletion helped to eliminate regulatory T cells (Tregs) and reduce competition with endogenous lymphocytes for homeostatic cytokines such as IL7 and IL15 (Antony et al. 2005; Gattinoni, Finkelstein, et al. 2005). Later clinical trials have incorporated chemotherapy to induce lymphodepletion prior to TIL infusion and demonstrated an objective response in 51% of metastatic melanoma patients (Dudley et al. 2002; Dudley & Rosenberg 2003). Other centres have also reported response rates of around 50% in metastatic melanoma patients, many with prolonged engraftment and durable responses (Besser et al. 2009).

Furthermore, the addition of total body irradiation with chemotherapy before TIL therapy led to an increased objective response rate of up to 72% (Rosenberg et al. 2011). Complete tumour regression was also reported in 22% of this cohort, with 95% still completely regressed 3 years later (Rosenberg et al. 2011). Of note, the inclusion of total irradiation was also associated with increased toxicities including renal problems and pulmonary hypertension. Overall, TIL therapy has been successful for metastatic melanoma. However, it's estimated that as little as 45% of patients with metastatic melanoma can receive TIL therapy due to some patients with insufficient sized lesions as well as poor growth of cells *ex vivo* (Rosenberg et al. 2011). Traditionally, TIL therapy has been most successful in melanoma. This may be due to the large number of melanoma tumour antigens recognised by T cells and the fact that unlike many other solid tumours, melanoma tumour tissue is relatively easy to access (Boon et al. 2006). Similarly, melanoma tumours exhibit the greatest level of somatic mutations (Lawrence et al. 2013). Therefore this cancer can express multiple neo-antigens that can be targeted by the host immune response. However, in recent years, TIL therapy is now emerging as a promising therapy for non-melanoma cancers such as breast cancer and pancreatic cancer (Ravelli et al. 2017; Hall et al. 2016).

1.7 Genetic engineering

As identified from TIL therapy, some naturally occurring T cells carry specificity to tumour associated antigens. With the exception of viral associated tumours however, tumour associated antigens are derived from self. Immune tolerance has acted to shape the T cell repertoire against self-reactivity. During T cell development, antigen-expressing cells in the thymus can present peripheral tissue antigen to thymocytes. Here, central tolerance can take place so that reactive T cells may be deleted, become FOXP3 expressing regulatory T cells or possibly become unresponsive. Furthermore, cells that escape central tolerance and show self-reactivity can be subjected to peripheral tolerance, where regulatory T cells and so called tolerogenic or immature dendritic cells can prevent activation of self-reactive T cells.

Therefore, tumour specific T cells are relatively rare, and those with high affinity to tumour-associated antigens are even rarer. However, with genetic engineering, genes encoding a TCR specific to a tumour-associated antigen can be transduced into peripheral blood T cells to confer upon these engineered cells the same tumour specificity. Several papers have demonstrated the ability to identify tumour specific TCR's and transduce them into human T cells (Hughes et al. 2005; Morgan et al. 2003; Zhao et al. 2005; Cohen et al. 2006; Cohen et al. 2005; Cohen et al. 2007; Kuball et al. 2005; Engels et al. 2005; Roszkowski et al. 2005; Clay et al. 1999). There are a variety of ways to find tumour specific TCR's.

Often TILs from one patient may be recovered and tumour specific clones identified before isolating the TCR. This has been performed from melanoma TIL's against the differentiation antigens MART1 (Morgan et al. 2006; Hughes et al. 2005), gp100 (Morgan et al. 2003), the cancer-testis antigen NY-ESO-1 (Zhao et al. 2005) and tyrosinase (Roszkowski et al. 2005). T cells engineered to express these cloned TCR genes were then shown to have *in vitro* specificity to the appropriate tumour antigen. TILs have also provided a TCR with tumour specificity to renal cell carcinoma, although the antigen was never identified (Engels et al. 2005). However TILs are not always accessible, especially in non-melanoma cancers. Furthermore, although TCRs reactive to these self-derived tumour antigens can sometimes be found, they are often of low affinity. It has been shown how TCR's to cancer associated self-antigens have a much lower binding affinity compared to TCR's to foreign viral antigens (Aleksic et al. 2012). This likely reflects the action of central and peripheral tolerance on the TCR repertoire.

Another method for generating tumour specific TCR's involves transgenic mice. Mice expressing the human HLA system can allow the generation of murine TCR's with specificity to peptides on human MHC molecules. Since the mouse

TCR repertoire will have been shaped against mouse proteins, they are unlikely to be tolerised to human-derived antigen. The effects of central tolerance are therefore bypassed, and high avidity anti-human tumour TCR's can be identified. HLA transgenic mice have been used to generate human-specific TCR's to the adenocarcinoma associated differentiation antigen carcinoembryonic antigen (CEA), common in colorectal cancer (Parkhurst et al. 2009); the melanoma antigens gp100 (Johnson et al. 2006) and MAGE-3 (Chinemassey 2011); and the tumour associated antigens overexpressed in a variety of cancers, p53 (Kuball et al. 2005; Cohen et al. 2005) and MDM2 (Stanislawski et al. 2001).

The first clinical trial of TCR gene transfer using genetically engineered autologous T cells was published by Morgan and colleagues in 2006 (Morgan et al. 2006). They utilised a TIL from a patient that showed a near complete response following TIL therapy for melanoma (Dudley et al. 2002). The anti-MART1 TCR was then isolated and transduced into metastatic melanoma patients. Of a 15 patient cohort, only 2 (13%) responded to treatment, although they showed a sustained complete regression of tumour over 2 years (Morgan et al. 2006).

It was hypothesised that this low response rate of 13% was due to the low affinity TCR used. The same authors described the isolation of another MART1 specific TCR of higher affinity from a melanoma TIL infusion that also facilitated tumour regression (Johnson et al. 2006). This TCR was later incorporated into another clinical trial for metastatic melanoma (Johnson et al. 2009). In this second trial, of the 20 patients, 30% exhibited an objective response. However, most also experienced destruction of normal melanocytes by the engineered T cells, with 14 exhibiting skin rash with T cell infiltrate and 11 exhibiting ear or eye toxicity. The same trial also incorporated a high affinity murine TCR against gp100, developed in a HLA transgenic mouse. Of the 16 patients receiving engineered T cells specific to gp100, a 19% response rate was found. Similarly, several patients exhibited off target toxicities against normal melanocytes.

Notably, these trials, even with high avidity TCR's gave low response rates compared to the 50-70% rates seen in TIL therapy. Likewise, TIL therapy is rarely associated with toxicity to normal melanocytes (Rosenberg et al. 2011). These trials suggest monoclonal T cell infusion may not be sufficient for *in vivo* anti-tumour efficacy. They also suggest that melanoma differentiation antigens may not necessarily be the only antigen targets of therapeutic TILs. Recent studies have developed tumour exomic sequencing in order to identify mutated antigens responsible for TIL anti-tumour responses (Robbins et al. 2013; van Rooij et al. 2013) and successfully isolated mutation-reactive T cells from patients (Cohen et al. 2015). These studies are laying the foundations for future personalised T cell therapies.

Carcinoembryonic antigen (CEA) is another differentiation antigen highly expressed in many colorectal cancers and certain other epithelial cancers. HLA transgenic mice were used to generate CEA specific TCRs which were then modified with amino acid substitutions within in the complimentary determining regions to increase the affinity of the receptors (Parkhurst et al. 2009). These receptors were successfully transduced into human CD4 and CD8 T cells. One TCR was selected and used to transduce T cells from three patients with metastatic colorectal cancer (Parkhurst et al. 2011). Only one patient responded according to RECIST criteria with a partial response at 4 months, but became progressive at 6 months. All three patients exhibited a transient severe autoimmune colitis, due to toxicity from the engineered T cells recognising normal levels of CEA in the colonic mucosa. The trial also used 100 fold fewer cells than typically used in TIL therapy, highlighting the potency of these engineered cells. Together, these clinical trials in melanoma and colon cancer indicate that targeting these antigens is not safe with high affinity receptors.

Alternative antigen targets include the cancer testis antigens. This group of antigens, of which more than 40 have been described, are usually only expressed in germ cells and trophoblasts but can also be expressed in several different cancers (Simpson et al. 2005). Crucially, MHCI molecules are not expressed in the testes and therefore specific CD8 T cells cannot cause damage here. NY-ESO-1 is an example of a cancer testis antigen, expressed in spermatogonia and primary spermatocytes and with low level transcripts detected in placenta, pancreas and normal breast tissue (although protein was not detected in the breast) (Nicholaou et al. 2006). NY-ESO-1 expression has been described in 10-45% of melanomas through immunohistochemistry and reverse-transcriptase (RT) PCR. It has also been described in 80% of synovial sarcomas (Jungbluth et al. 2001).

A TCR specific to NY-ESO-1, originally isolated from a patient with melanoma (Jäger et al. 1998) was edited with amino acid substitutions to the CDR regions to create a higher affinity receptor (Robbins et al. 2008). A high affinity receptor was used to transduce T cells from patients with metastatic melanoma (n=11) and patients with synovial sarcoma (n=6) with tumours expressing high levels of NY-ESO-1 (Robbins et al. 2011). An objective response was described in 45% (n=5) of melanoma patients, with 2 exhibiting complete regression beyond 20 and 22 months and one patient with a partial response persisting beyond 9 months. 67% (n=4) of the synovial sarcoma patients responded, with one partial response persisting until 18 months. Importantly, no toxicities were reported in this trial, likely due to lack of NY-ESO-1 protein expression in normal tissue. This was the first trial to target the NY-ESO-1 using transduced T cells and the first report of tumour regression in non-melanoma tumours using TCR engineered T cells.

However, other trials targeting cancer-testis antigen have been less successful and have highlighted toxicity problems. The cancer-testis antigen MAGE-A3 is commonly expressed in melanomas, non-small-cell lung carcinoma, bladder cancers, squamous oesophageal cancers and hepatocellular carcinoma (Fratta et al. 2011). HLA A2 transgenic mice were used to generate a TCR specific to a human MAGE-A3 peptide (Chinnasamy et al. 2011). The TCR was subsequently edited in the CDR3 region through amino acid substitutions to further improve avidity and function. In the clinical trial that followed, 7 patients with metastatic melanoma, one with synovial sarcoma and one with esophageal cancer had their T cells transduced with the MAGE-A3 specific TCR (Morgan et al. 2013). In total, five patients, (all melanoma) exhibited a clinical response. One patient had a complete response ongoing at 15 months and one a partial response ongoing at

12 months. Despite this, three patients displayed severe neurologic toxicity, including the ongoing partial responder. Two of the patients (not the ongoing responder) later died from the neurological complications.

MAGE-A3 was found not to be expressed in the brain. However, it was known that the TCR recognised a similar peptide from MAGE-A12 with a higher affinity. Despite no previous reports of MAG3-A12 expression in the brain, the authors detected MAGE-A12 at the RNA level in the brains of the two deceased patients and several non-diseased control brains. The authors also suggested the neurologic toxicity was associated with a higher cell dose.

Another study used a MAGE-A3 specific TCR isolated from a patient with melanoma which had several substitutions introduced into the CDR2 region of the alpha chain, creating a higher affinity receptor (Linette et al. 2013). Two patients, one with melanoma and one with myeloma expressing MAGE-A3 had their T cells transduced with this high affinity TCR. After T cell infusion, both patients developed fever, hypoxia and subsequently died after progressive cardiogenic shock (Linette et al. 2013). Autopsy revealed myocardiocyte necrosis and a T cell infiltration of the myocardium. Despite this toxicity in the heart, MAGE-A3 expression was not detected here and pre-clinical experiments detected no cross-reactivity. However, further analysis identified a peptide from the unrelated protein titan, which is also recognised by the high affinity MAGE-A3 TCR (although not by the non-mutated TCR). Critically, titin is highly expressed in normal heart tissue (Cameron et al. 2013). Although not recognised in a static culture of cardiomyocytes (because such cells lack titin expression), beating cardiomyocytes were recognised and killed by the high affinity TCR expressing T cells. Therefore the affinity enhancement of this TCR has introduced cross-reactivity to a new epitope from another protein. This trial has highlighted the dangers of site-directed mutagenesis in causing off-target toxicity and how cross-reactive responses to self-antigen may only be recognised under certain in vitro culture conditions.

1.8 Chimeric Antigen Receptors

An alternative method of engineering T cells to direct specificity to particular antigens is with chimeric antigen receptors (CARs). CARs are recombinant receptors typically carrying the variable domain of an antibody fused to one or more intracellular T cell signalling domains. CARs therefore combine the antigen specificity of an antibody with the potent cytotoxic and immune regulatory activity of a self-replicating T cell. CARs recognise whole native antigen and are not MHC restricted. Therefore they can be used to treat patients regardless of HLA type. It also means that common tumour immune evasion strategies of downregulating HLA expression or peptide processing are not problematic for CAR based therapies. CARs can theoretically be directed to any surface marker. Although this means one shortcoming of CARs is the inability to target intracellular antigens, a recent report has successfully generated a CAR which can target intracellular protein epitopes expressed on MHC molecules, although this now makes the CAR MHC restricted (Tassev et al. 2012).

1.9 The beginning of CAR technology

Early studies would fuse the variable domains of the light chain (V_L) and the heavy chain (V_H) to the TCR alpha or beta chain constant domains as two separate molecules (Gross et al. 1989). These two constructs could successfully be introduced into a T cell hybridoma cell line to form a functional CAR capable of recognising antigen directed by the V_L and V_H domains and initiating target cell cytolysis and IL2 production. CARs went through further advancements by Eshhar and collegues (Eshhar et al. 1993). First, the V_L and V_H domains were fused together with a flexible peptide linker to form what is known as a short chain variable fragment (scFv). The variable domain may then be fused to a single intracellular domain, instead of two separate chains.

Normal T cell signalling involves the CD3 complex which includes chains containing ITAM signalling motifs which are subsequently phosphorylated and transduce intracellular signalling (Rossy et al. 2012). For this reason, the second advancement in CAR technology was to fuse the scFv directly to a CD3ζ chain or the FcRγ chain (which follows a similar signalling pathway to TCR signalling) (Eshhar et al. 1993). CARs with CD3ζ or FcRγ could both form functional receptors in hybridomas although a later study suggests *in vivo* function and anti-tumour efficacy was superior in CD3ζ CARs in a murine colon cancer model (Haynes et al. 2001). Most CARs have since utilised the CD3ζ rather than FcRγ signalling domain. The scFv domain is linked to the transmembrane domain through a flexible hinge. The Hinge is typically derived from immunoglobulin or immunoglobulin-like domains (Cartellieri et al. 2010) and the relative length of the hinge can affect function of the receptor (Patel et al. 1999).

In contrast to early studies in T cell hybridoma cell lines, resting T cells from transgenic mice responded poorly upon CAR stimulation with transient or no proliferation and little cytokine production (Brocker 1995; Brocker 2000). However, if previously activated, T cells could respond after CAR stimulation. Furthermore, CD3ζ CAR transduced primary human T cells showed poor cytokine production and proliferation in response to repeated antigen exposure (Gong et al. 1999). From this, it was predicted that signalling only through the CD3ζ ITAM was insufficient to activate T cells which is consistent with the longstanding two-signal hypothesis that T cells require two signals to be functionally activated, one from TCR signalling and one from costimulation (Bretscher & Cohn 1970). On top of this it has been observed that stimulation of the TCR alone can result in anergy, where cells remain in an unresponsive state (Gimmi et al. 1993; Harding et al. 1992). This anergic state can be overcome with costimulation, for example through CD28 signalling (Gimmi et al. 1993; Harding et al. 1992).

1.10 Introducing costimulation with CAR technology

CD28 signalling is the best-described costimulation pathway. It is expressed on all murine T cells, and around 95% and 50% of human CD4 and CD8 cells respectively (Lenschow et al. 1996). It's activating receptors, B7-1 and B7-2 are expressed on activated APCs where engagement along with TCR stimulation can promote T cell proliferation, differentiation, survival and IL2 production (Lenschow et al. 1996). It was first hypothesised in 1970 that T cells require two signals for complete activation, one from the TCR signalling pathway and another signalling pathway from the antigen presenting cell, thereby helping discriminate self/non-self peptide presentation (Bretscher & Cohn 1970). The discovery of the CD28 signalling pathway helped enforce this two-signal hypothesis.

In order to satisfy the requirement for two signals, investigators began to incorporate CD28 signalling into CAR constructs. This was first done by introducing the CD28 signalling domain, which does not signal through ITAMs, as a separate antigen specific construct (Krause et al. 1998; Alvarez-Vallina & Hawkins 1996). This CD28 construct was referred to as a chimeric costimulatory receptor (CCR) and could induce IL2 production and prevent activation induced cell death (AICD) in primary human T cells. Finney and colleagues were the first to introduce the CD28 signalling domain with the CD3ζ signalling domain into a single CAR construct (Finney et al. 1998). This duel-signalling CAR was introduced into a T cell hybridoma cell line and gave 20-fold greater IL2 production than a CAR expressing only the CD3ζ domain. Interestingly, constructs with the CD28 domain membrane proximal and the CD3ζ domain membrane distal showed superior cell expression compared to constructs with the reversed combination. However, this positional preference for the CD28 domain was only seen in T cell hybridomas and not in primary T cells (Maher et al. 2002). The addition of a single costimulation domain to the construct became known as second generation CARs as opposed to the CD3ζ/FcRγ only constructs known as first generation CARs.

The superiority of second generation CARs was subsequently demonstrated in primary T cells. Several *in vitro* studies have demonstrated that second generation CARs with a CD28 signalling induce greater proliferation, IL2 production, IFNγ production and GMCSF production compared to first generation CARs (Maher et al. 2002; Hombach et al. 2001; N M Haynes et al. 2002). Finney and colleagues later showed that the additional costimulation domain of CD28 allowed an antigen specific upregulation of the anti-apoptotic gene Bcl2, not found with CD3ζ only CARs (Finney et al. 2003). Notably, compared to first generation CARs, the CD28 domain could allow activation of even naïve primary T cells in the absence of exogenous costimulation from antigen-specific target cells (Friedmann-Morvinski et al. 2005). Further studies in animal models have again confirmed the greater efficacy of second generation CARs which were also shown to induce proliferation, cytokine production and tumour eradication *in vivo* in mouse models more efficiently than first generation CARs (Nicole M Haynes et al. 2002; N M Haynes et al. 2002).

The requirement for costimulatory domains within the CAR is also emphasised by the fact that few tumours actually express costimulatory ligands. It was described how a first generation CAR to CD19 failed to control a B cell tumour cell line unless it expressed B7 in a severe-combined immunodeficiency (SCID) mouse model (Brentjens et al. 2003). A recent trial in humans described how a second generation CAR to CD19 enhanced *in vivo* expansion when compared directly to a first generation CAR (Savoldo et al. 2011). Although costimulation through CD28 is the best-studied pathway, several other costimulatory pathways exist.

OX40 and 41BB, both members of the TNF receptor superfamily, are two such pathways investigators have utilised in CARs (Imai et al. 2004; Carpenito et al. 2009; Pulè et al. 2005). Both OX40 and 41BB are not normally expressed on resting T cells but are expressed within 24 hours of stimulation, peaking a few days later before downregulating (Croft 2003). CD28 signalling is not a prerequisite but does enhance OX40 or 41BB expression. The OX40 and 41BB ligands, OX40L and 41BBL respectively, are expressed on APCs hours to days after activation. The functions of OX40 and 41BB have been studied primarily in CD4 and CD8 T cells respectively. These studies have found both are important in the later stages of activation after initial activation through the TCR and CD28 where they allow continued survival and sustained proliferation (Croft 2003). For this reason, OX40 and 41BB can be described as late costimulation compared to the early costimulation of CD28.

The 41BB signalling domain has been incorporated into a CD19 CAR instead of CD28 (Imai et al. 2004). *In vitro* culture experiments found 41BB-ζ CARs allowed greater target cell lysis, proliferation and IL2 production compared to the ζ only CAR. However this study did not compare CARs with 41BB to CARs with CD28 domains. A later study did compare CD28 and 41BB CARs and found that in an *in vivo* murine leukemic xenograft model, 41BB containing CARs had significantly enhanced anti-tumour efficacy and persistence than CD28 or first generation CARs (Milone et al. 2009). This was despite 41BB CARs reduced induction of IL2 and TNFα compared to CD28 CARs *in vitro.* The authors also suggest that 41BB CARs exhibited some form of antigen independent survival and/or proliferation.

In contrast, second generation CD19 CARs with a CD28 domain had superior in vitro proliferation and cytokine production compared with the same CAR with the 41BB domain (Brentjens et al. 2007). Another study compared second generation CARs with either CD28, OX40, 41BB or ICOS domains (Finney et al. 2003). All enhanced IL2 production, with CD28 giving the highest production. CD28 and ICOS could also induce greater TNFα, IFNϒ and GM-CSF. *In vitro* target cell cytolysis could be enhanced by CD28, ICOS or OX40 but not by 41BB, with the greatest effect seen with ICOS.

Furthermore, a study of CARs to CEA found that the inclusion of 41BB or OX40 signalling domains with CD3ζ did not improve CAR driven proliferation of T cells (Hombach & Abken 2007). They also found that only inclusion of the CD28 domain could induce high IL2 production. CD28 gave the best cytolysis although OX40 but not 41BB could also enhance cytolysis. Likewise, an in depth comparison of second generation CARs with either CD28; DAP10; 41BB or OX40 found that CD28 signalling CARs resulted in the greatest proliferation and IL2 and IFNγ production (Brentjens et al. 2007). In line with the theory of OX40 and 41BB acting as late costimulators both, particularly OX40, could enhance survival of effector memory T cells. The authors therefore combined both CD28 and OX40 with CD3ζ to form what is known as a third generation CAR. This CAR had enhanced IL2 and target cell cytolysis *in vitro* as well as a greater anti-tumour activity in an *in vivo* SCID mouse model compared to the CD28 second generation CAR.

Another study found that second generation CARs with CD28 could not initiate a full T cell activation but the inclusion of the OX40 domain to from a third generation CAR allowed full activation with sustained proliferation, more IL2 and a greater target cell cytolysis *in vitro* (Pulè et al. 2005). Several other studies have further analysed other third generation CARs including 41BB with CD28 (Zhong et al. 2010; Milone et al. 2009) and Lck with CD28 (Geiger et al. 2001). *In vitro* assays from these studies certainly suggest third generation CARs are the future. However, more *in vivo* (including clinical) studies are still required to determine their superiority.

Together, these studies show that the inclusion of a costimulation domain within the CAR can improve function, yet there are conflicting reports of which domains are optimal. This likely reflects the different antigens targeted and different construction and design of each CAR. A more extensive analysis directly comparing the effects of different costimulatory domains in a range of CAR specificities is required to determine the advantages or disadvantages of each costimulation molecule.

1.11 Clinical development of CARs - CD19 as a target

CD19 is a marker expressed on the surface of normal mature B cells, B cell precursors and notably it is also expressed on malignant B cells (Uckun et al. 1988). Recently, it has become a favoured target in B cell cancer therapy. Monoclonal antibodies targeting CD19 are already available as treatments for B cell malignancies. Several groups have been developing CD19 specific CARs. Pre-clinical studies in murine lymphoma models have shown how CD19 CARs can effectively cure disease with long term removal of B cells, normal and malignant (Kochenderfer et al. 2010). CAR treatment was also more effective than monoclonal antibody treatment in this model. Notably, successful CAR treatment was dependent on prior conditioning (irradiation) of the host.

Early trials focused on Non-Hodgkin's lymphoma (NHL) such as chronic lymphocytic leukaemia (CLL) (Till et al. 2008; Jensen et al. 2010; Savoldo et al. 2011). These trials used first generation CARs to CD19 without pre-conditioning patients with lymphodepleting chemotherapy. There was no clinical response in these trials. Savoldo and colleagues infused both first and second generation CARs (Savoldo et al. 2011). The second generation CARs, containing CD28 costimulation showed an improved in vivo proliferation and persistence compared to the first generation CARs. Brentjens and colleagues at Memorial Sloan Kettering Cancer Centre (MSKCC) performed a small trial with 19-28z CARs (second generation CAR to CD19, signalling through CD28 and CD3ζ) that included patients receiving prior conditioning chemotherapy and patients receiving no conditioning (Brentjens et al. 2011). Clinical efficacy was poor, with two CLL patients who did receive lymphodepletion exhibiting stable disease and one with reduced lymphadenopathy. However this was an improvement compared to patients who did not receive lymphodepletion, whose disease rapidly progressed. Of note, the prior lymphodepletion did increase persistence of CAR expressing T cells. Also, patients were previously refractory to chemotherapy, suggesting conditioning had little direct effect on tumour cells and that the improved effect was due to CAR expressing T cells (Davila et al. 2012).

Following this, a study based at the National Cancer Institute (NCI) (Kochenderfer et al. 2012) described the clinical trial of a second generation CAR to CD19, signalling through CD28 and CD3ζ to treat 8 patients with advanced B cell lymphoma or CLL. Patients first underwent lymphodepletion followed by T cell infusion with high dose IL2. Five patients showed a partial response and one patient had a complete response ongoing 15 months. University of Pennsylvania (UPENN) used a second generation CAR to CD19 containing 41BB rather than the CD28 costimulation domain to treat advanced CLL (Kalos et al. 2011). This CAR, which previously showed greater efficacy than CD28 signalling CARs in a murine leukemic xenograft model (Milone et al. 2009), was used following lymphodepletion and resulted in a complete ongoing response in 2 of 3 patients. The third patient exhibited a partial response. Of note from this study was the massive *in vivo* expansion of CAR expressing T cells and the fact that IL2 was not administered. It has been argued that conditioning with chemotherapy may have also had anti-tumour effects in these three patients since recruited patients had not been shown to be previously refractory to chemotherapy (Davila et al. 2012).

Several groups are now consistently reporting robust clinical responses with prior conditioning. UPENN reported an overall response of 57% (n=8/14) including a complete response (CR) rate of 29% (4/14) with the 19-BBz CAR (Porter et al. 2015). CR patients were still disease free at time of report. The proliferation and persistence of CAR T cells in patients was also found to correlate with clinical response. NCI have reported complete response rates of 75% (3/4) CLL patients and 44% (4/9 with two patients not evaluated) of diffuse large B cell lymphoma (DLBCL) patients with a 19-28z CAR (Kochenderfer et al. 2015). All the CLL CR patients and 3/4 of the DLBCL CR patients were ongoing at the time of report. The Fred Hutchinson Cancer Research Centre (FHCRC) also used a 19-BBz CAR (Turtle et al. 2015). They noted improved results by using a combined chemotherapy regime of Fludarabine and cyclophosphamide compared to cyclophosphamide alone. Using the combined chemotherapy, they reported CR rates of 38% (3/8) in DLBCL patients, 67% (2/3) in follicular lymphoma patients and 50% (3/6) in CLL patients.

Even more impressive results have been seen with CD19 CARs to B cell acute lymphoblastic leukaemia (B-ALL). UPENN have used the 19-BBz CAR to treat relapsed/refractory ALL. After an initial report of two paediatric patients (Grupp et al. 2013), they have expanded the cohort to 25 paediatric and 5 adult patients (Maude et al. 2014). An impressive 90% (27/30) patients showed a complete response and 73% (22/30 with 2 patients not tested) were free of minimal residual disease. After a follow up of 2-24 months, 19 patients were in sustained remission. Similar to results in CLL, the persistence of the CAR correlated with clinical outcome. Intriguingly, CAR T cells persisted as long as 2 years in this cohort (3 years in CLL). 6 patients who relapsed exhibited a loss of CAR T cell persistence, and one exhibited a CD19 negative tumour.

MSKCC expanded an initial cohort of 5 adults (Brentjens et al. 2013) to 16 adults with ALL (Davila et al. 2014). All were treated with a 19-28z CAR and exhibited a CR rate 88% (14/16) and 75% (13/16) were free of minimal residual disease. Sustained CR was only reported in the patients that went on to receive allogeneic stem cell transfer. In contrast to other studies, CAR T cells failed to persist for long periods. The median persistence was only 30 days, however most patients were in CR within this time. The NCI also treated patients with a 19-28z CAR and reported a CR of 70% (14/20) and 60% (12/20) of patients with no minimal residual disease (Lee et al. 2015). 10 of the 12 patients went onto receive allogeneic stem cell transfer. Again, this study reported a poor persistence of CAR T cells. CAR T cells were not detected beyond 2 months, but again, patients showed a rapid clearance of tumour cells.

The FHCRC recently reported a CR rate of 93% (27/29) with an 86% (25/29) free of minimal residual disease using a 19-BBz CAR (Turtle et al. 2016). This trial also noted the development of T cell immunity to the murine scFv within the CAR in five patients. This anti-murine scFv immunity appeared to result in the loss of CAR T cells and a relapse with $CD19^+$ disease. Further infusion of CAR T cells resulted in no CAR T cell expansion or persistence or any anti-tumour effect in these patients. The authors show that the use of fludarabine as well as cyclophosphamide increases CAR T cell persistence, possibly by preventing a anti-murine host T cell response. Despite the impressive response rates, two patients died of CAR T cell related toxicities of severe cytokine release syndrome (CRS) and neurological complications, highlighting the potential dangers of this therapy, as discussed in the next section.

1.12 Toxicities associated with CD19 CARs

CRS is one of the most common toxicities associated with CD19 CAR therapy. In the most recent trial, 25/30 ALL patients developed CRS (Turtle et al. 2016). CRS can occur when a high number of intravenous infused T cells are activated in one site, resulting in a massive inflammatory response. This large-scale inflammatory response in the patient can lead to a drop in blood pressure and low oxygen delivery to organs. Symptoms may only be mild fever or ultimately, patients may succumb to multi-organ failure and require intensive care. Intriguingly, most groups have reported that severe CRS correlates with a high tumour burden as well as high T cell dose (Lee et al. 2015; Davila et al. 2014; Maude et al. 2015; Turtle et al. 2016) CRS can be self-limiting but cases of severe CRS have been successfully treated with the biologics etanercept and tocilizumab, which bind to TNFα and IL6 respectively or the use of steroids (Maude et al. 2015; Lee et al. 2015; Porter et al. 2015; Turtle et al. 2016; Davila et al. 2014). Steroids however, have been associated with poor CAR T cell proliferation and early relapse (Davila et al. 2014). Tocilizumab in contrast, has the ability to reverse CRS with little impact on CAR T cell efficacy (Barrett et al. 2016). Tocilizumab has now become the standard treatment of CRS and was FDA approved this year. Interestingly, in vivo mouse models of solid tumours found only intravenous CAR T cell delivery was associated with CRS, whereas regional intraperatoneal delivery in the tumour area was not associated with CRS. (van der Stegen et al. 2013). However, intraperatoneal delivery may have little application against blood cancers.

Another common condition is neurotoxicity, which usually occurs during or after the resolution of CRS. Symptoms range from confusion, delirium to seizures requiring intensive care. Again, this condition is usually transient and reversible, however one patient died due to irreversible neurotoxicity in a recent trial at FHCRC (Turtle et al. 2016) and several patients have died during the recent trials of JCAR015 at UPENN. JCAR015 has since been discontinued. The exact cause of neurotoxicity is not known, however, CAR T cells have been detected in the CSF of patients (Maude et al. 2015). Despite this, not all of the patients with CAR T cells in the CSF developed neurotoxicity. Tocilizumab also had no effect on neurotoxicity symptoms in this study.

The targeting of CD19 will indiscriminately result in the killing of normal, non-malignant mature and pre-cursor B cells, resulting in B cell aplasia and hypogammaglobulinemia. All groups have reported this during trials. In fact, B cell aplasia acts as a marker of CAR T cell function and persistence. The loss of CAR T cells correlates well with the return of host B cells. B cell aplasia may last for years in patients with persistent CAR T cells. Patients can be treated with regular infusions of gamma globulin as a replacement therapy, although it's not known what the long-term consequences will be for chronic B cell aplasia.

1.13 Targeting solid tumours

Despite this great success targeting CD19 in haematological malignancies, there has been relatively little success targeting solid tumours. One of the first ever-completed CAR therapy trials used first generation FcRγ signalling CARs specific to α-Folate Receptor in ovarian cancer (Kershaw et al. 2006). 14 patients were treated along with IL2 cytokine support however all showed progressive disease. Furthermore, T cells showed poor tumour homing and poor persistence. With the exception of one patient, T cells were only detectable for up to 3 weeks. A first generation CD3ζ CAR to L1-CAM was used in a trial with metastatic neuroblastoma patients (Park et al. 2007). From the 6 treated patients, 5 had progressive disease while one showed a partial response that later relapsed. Again, CAR T cell persistence was poor in this study.

Another trial found no clinical response using first generation CARs to CAIX in renal cell carcinoma (Lamers et al. 2013). This study used a first generation FCγR based CAR to treat 12 patients. The original cohort of 3 patients in this trial experienced significant on target/off tumour toxicity causing cholangitis and bile duct epithelial cell damage (Lamers et al. 2006). An anti-CAR immune response also occurred resulting in poor T cell persistence. Interestingly, by pre-treating patients with a CAIX-specific antibody, on target/off tumour toxicity was prevented and CAR T cell persistence was improved (Lamers et al. 2013). The antibody dose at the time of infusion was less than the in vitro dose required to saturate CAIX epitopes on renal cell carcinoma cell lines and prevent their lysis by CAR T cells. Despite this, no anti-tumour response was seen.

In general, authors related poor efficacy against solid tumours with a lack of *in vivo* persistence due to poor signalling of first generation CARs as well as host antibody responses to murine derived scFv sequences of CARs. Some first generation CARs have resulted in clinical efficacy, for example CARs specific to

GD2 that were used to treat 19 neuroblastoma patients (Louis et al. 2011)(Pule et al. 2008). Intriguingly, the authors used the strategy of engineering host T cells specific for EBV as well as non-EBV T cells. The theory was that natural EBV-specific T cells could receive activation signals through EBV infected B cells in patients, thereby improving persistence of such cells also expressing a CAR. Initially, EBV specific T cells expressing the CAR were of greater proportion *in vivo* although by 6 weeks both EBV and non-EBV T cells were at similar levels in each patient. Three of eleven patients with active disease at time of infusion achieved complete regression of tumour and this correlated with persistence of either EBV or non-EBV specific CAR expressing T cells.

A recent study used a first generation CD3ζ CAR specific to IL13Rα2 (Brown et al. 2015). This study tested the feasibility of intracranial delivery of CD8 CAR T cells to treat 3 glioblastoma patients. Intracranial delivery was tolerated well, with only mild CNS inflammation. However, all patients showed progressive disease despite CAR T cell persistence for up to 6 months. Trials have explored the use of second generation CARs against solid tumours. An RNA based BBz CAR specific to mesothelin was used to treat four patients (three with mesothelioma and one with pancreatic adenocarcinoma) (Maus et al. 2013). Since RNA CAR expression is transient, one mesothelioma patient was given further infusions, however this resulted in severe anaphylaxis due to an acquired immune response to the CAR T cells. Nevertheless, the patient quickly recovered and showed a transient partial tumour response. The authors suggested completing CAR T cell infusions within 21 days before class switching to IgE occurs to prevent such severe anaphylaxis. Since targeting mesothelin was otherwise well tolerated in this study, a further trial using lentiviral CAR transduced T cells to target mesothelin was recently completed although no result have been posted (https://clinicaltrials.gov NCT02159716).

A CD28z CAR specific to CEA has been used to treat patients with adenocarcinoma with liver metastasis (Katz et al. 2015). This trial tested the feasibility of using hepatic artery injection to allow a more direct CAR T cell delivery. Although hepatic artery injection was safe and well tolerated, five patients showed progressive disease, one patient had stable disease and CAR T cells only persisted for around 2 weeks.

HER2 has been targeted in one patient with colon cancer using a high dose of T cells expressing a third generation BB28z CAR (Morgan et al. 2010). However, this patient quickly succumbed to a fatal respiratory distress apparently due to on target/off tumour toxicity in the lung. More recently, a CD28z CAR specific to HER2 has been used to treat sarcoma patients (Ahmed et al. 2015). This study used a dose escalation protocol to treat 19 patients and found of the 17 evaluable patients, 4 exhibited stable disease for up to 14 months. CAR persistence varied, with less than half of evaluable patients having detectable CAR T cells, although in one patient they were detectable for up to 18 months. This dose escalation approach demonstrates that by controlling the T cells dose, overexpression markers may be targeted safely.

1.14 Overcoming the tumour microenvironment

Tumours can effectively induce the surrounding environment to support tumour growth and suppress anti-tumour immune responses. Multiple different suppressive immune cells are present within the tumour. This includes M2 macrophages, myeloid derived suppressor cells (MDSCs) and regulatory T cells. The suppressive microenvironment consists of proteases to aid in tumour cell invasion and metastasis; pro-angiogenic molecules to induce tumour vascularisation; and immunosuppressive cytokines to inhibit anti-tumour immune responses.

TGFβ is an immunosuppressive cytokine commonly found within the tumour microenvironment. Often it is produced by tumour cells but additionally can be produced by local suppressive and regulatory cells. It has been shown *in vitro* that TGFβ can repress the proliferation of T cells expressing a first generation CAR to CEA after antigen specific stimulation, whereas IFNγ and cytolytic activity were unaffected (Koehler et al. 2007). This repression could be overcome with CD28 costimulation, suggesting that CD28 second generation CARs could have better efficacy against solid tumours. Indeed, the CD28-ζ CAR induced better tumour regression compared to the first generation CAR in immune compromised mice with TGFβ secreting tumours.

However, the same authors later found the high IL2 secreted by CEA specific CD28-ζ CAR-expressing T cells supported regulatory T cell expansion and showed less anti-tumour activity than the first generation CAR (Kofler et al.

2011). By editing the CD28 domain to prevent Lck binding, IL2 signalling was prevented but higher proliferation and IFNγ production *in vitro* remained. This modified CAR showed improved anti-tumour activity in the presence of Tregs. Another strategy to counteract the tumour environment has been to introduce a non-functional TGFβ receptor (Foster et al. 2008). EBV specific T cells transduced with such receptor had improved *in vivo* anti-tumour activity against TGFβ secreting EBV positive lymphoma cell lines. As well as using antibodies to direct CAR specificity, endogenous receptors may be used to target specific cell surface antigens. NKG2D is a receptor that can recognise multiple stress related ligands that are often expressed in tumours. By fusing NKG2D to CD3ζ and transducing T cells, a vastly improved anti-tumour response to an ovarian cancer model was seen (Barber et al. 2009). T cells were also capable of directly killing Tregs.

IL12 is a proinflammatory and anti-angiogenic cytokine capable of activating both innate and adaptive immunity. In anti-tumour immunity it can support activation of NK, CD4 and CD8 T cells, driving a pro-inflammatory Th1 response. Murine Pmel-1 CD8 T cells specific for gp100 have been engineered to constitutively secrete IL12 (Kerkar et al. 2010). Even small numbers of these cells could induce B16 tumour regression despite low *in vivo* persistence. Another study created a CAR inducible form of IL12, therefore, upon CEA engagement within the tumour, a local production of IL12 ensued (Chmielewski et al. 2011). As well as eradication of CEA^+ tumours in SCID mice, CEA^- tumour cells within a tumour chimera could be eradicated due to an IL12 mediated recruitment and activation of macrophages.

1.15 Checkpoint inhibitors

The T cell coinhibitory receptors cytotoxic T-lymphocyte–associated antigen 4 (CTLA4) and programmed death 1 (PD1) are an essential part of peripheral tolerance. Both have recently become targets in cancer therapy using so called checkpoint inhibitors: antibodies that block their function/signalling. CTLA4 expression is induced upon TCR stimulation and enhanced by CD28 or IL2 signalling. The stronger the TCR signal, the greater the expression of CTLA4 (Egen & Allison 2002). Once CTLA4 is upregulated it can then interact with receptors CD80 or CD86 on APCs. Since it has a greater affinity for these receptors than the costimulatory molecule CD28, it can effectively outcompete CD28 and prevent costimulatory signals. Thus, depending on the relative surface expression levels of CTLA4, T cell activation can be suppressed and anergy can be induced. As well as competitive binding of CD80/CD86, it's possible that CTLA4 may mediate intracellular inhibitory signalling (Walker & Sansom 2015). Interestingly, its been found that activated T cells can endocytose CD80/CD86 molecules from APCs and degrade them in lysosomes (Qureshi et al. 2011). This depletion of APC CD80/CD86 results in poor ability of the APCs to activate further T cells. Correlating with a control on T cell activation, CTLA4 deficient mice succumb to a severe lymphoproliferative disease (Waterhouse et al. 1995).

CTLA4 is also constitutively expressed on Tregs where it seems to be important for suppressive Treg function. CTLA4 on Tregs can accumulate CD80/CD86 on APCs, thus limiting their availability to conventional T cells and inhibit APC costimulation (Wing et al. 2008). In addition, in a CTLA4-dependent way, Tregs can induce APC indoleamine-pyrrole 2,3-dioxygenase (IDO) expression causing a local depletion of Tryptophan, a limiting factor in conventional T cell activation (Fallarino et al. 2003). Giving the apparent importance of CTLA4 in Treg function, it's not surprising that CTLA4-blocking antibody can supress Treg function in vivo (Read et al. 2006). Furthermore, anti-CTLA4 antibody has been found to selectively deplete tumour-infiltrating Tregs in an Fc dependent manner (Simpson et al. 2013). Ipilimumab is a human monoclonal antibody specific to CTLA4 and is now FDA approved for use in advanced melanoma. A phase III trial found that ipilimumab increased metastatic melanoma patient survival by more than 3 months (Hodi et al. 2010).

PD1 is upregulated after T cell activation. Its receptors, PD ligand 1 (PDL1) and PD ligand 2 (PDL2) are expressed on a variety of cell types, including tumour cells (Intlekofer & Thompson 2013). In contrast to CLTA4 which functions primarily in the T cell activation stage, PD1 acts on the effector stage. PD1 signalling inhibits T cell function and reduces T cell survival. Furthermore, PDL1 expression in APCs has been found to be essential in Treg differentiation and function (Francisco et al. 2009). Correlating with inhibiting effector T cells, PD1 deficient mice suffer a delayed onset, organ-specific autoimmunity that varies depending on the genetic strain (Intlekofer & Thompson 2013). PD1 was also found to be overexpressed in exhausted hypofunctioning T cells during chronic viral infection (Barber et al. 2006). On top of this TILs commonly express high levels of PD1 and other exhaustion markers (Sfanos et al. 2009; Ahmadzadeh et al. 2009) and TIL inflammatory cytokine production can actually induce tumour cell PDL1 expression (McGray et al. 2014; Cherkassky et al. 2016). Along with the fact that many different tumour types express PDL1 (Zou & Chen 2008) and some myeloid cells of the tumour microenvironment also express PDL1 (Kuang et al. 2009; Curiel et al. 2003), PD1 signalling is a promising target for cancer immunotherapy.

Clinical trials using either monoclonal blocking antibodies to PD1 or to PDL1 have shown improved clinical response and survival in patients with melanoma, non small cell lung cancer and renal cell carcinoma (Topalian et al. 2012; Brahmer et al. 2012) (McDermott et al. 2015; Garon et al. 2015). Pembrolizumab and nivolumab are both PD1 blocking antibodies that are FDA approved for metastatic melanoma and refractory non-small cell lung cancer. Interestingly, Pembrolizumab outperformed Ipilimumab in a trial with advanced melanoma patients, with higher response rates and survival rates (Farolfi et al. 2012). The combination of blocking both CTLA4 as well as PD1 has resulted in enhanced anti-tumour responses in murine models compared to only blocking one (Curran et al. 2010). Likewise, a trial using the combination of ipilimumab and nivolumab resulted in an increased response rate and survival compared to ipilimumab alone with metastatic melanoma patients (Weber et al. 2015) and this combination is now approved for forms of metastatic melanoma. Of note, the combination of the two antibodies also increased the incidence of immune-related toxicity.

In a murine model, the addition of a PD1 blocking antibody in combination with HER2 CD8 CAR T cells improved the anti-tumour efficacy and T cell function (Liza B. John et al. 2013). Interestingly, the authors also observed a decrease in the numbers of MDSCs in the tumour microenvironment with the blocking PD1 antibody. Another study in murine models also demonstrated how the inclusion of a PD1 blocking antibody could help restore function and anti-tumour activity in CAR T cells (Cherkassky et al. 2016). The authors also tried an alternative approach of cotransducing CAR T cells with a non-signalling PD1 molecule that had some success in protection from PD1 mediated inhibition in vivo. Therefore, there is scope for combining CAR therapy with the checkpoint inhibitors. In fact, a clinical trial is now ongoing for B cell malignancies combining ipilimumab with CD19 CARs (https://clinicaltrials.gov NCT00586391).

1.16 Migration of CAR T cells into tumour tissue

A problem more associated with solid tumours than haematological tumours is the ability of specific T cells to migrate from the blood into the tumour tissue, and to do so in high enough numbers not to succumb to the suppressive microenvironment. Recruitment into peripheral tissues requires multiple interactions involving selectins, chemokines and integrins. Chemokines are small molecules, which are responsible for attracting cells via chemokine receptors. Over 50 chemokines and 20 G-protein coupled receptors exist. They have roles in cell migration, polarisation, adhesion as well as gene expression. Several chemokines can be produced from the tumour site that can attract tumour reactive T cells. However, should reactive T cells lack the responding chemokine receptor, they may never reach the tumour site. Tumour biopsies following the trial with GD2 specific CARs found a poor infiltration of transduced T cells despite presence in the peripheral blood (Pule et al. 2008).

T cells transduced with the chemokine receptor CXCR2 showed *in vitro* chemotaxis to CXCL1, a chemokine associated with melanoma tumours (Kershaw et al. 2002). Another study showed how T cells could co express GD2 CAR and a CCR2b chemokine receptor (Craddock et al. 2010) which greatly improved *in vitro* migration to neuroblastoma tumour and improved *in vivo* migration and tumour eradication in a neuroblastoma xenograft mouse model. Therefore, it is possible to enhance migration of tumour reactive T cells, provided the required homing phenotype can be defined.

Additionally, the tumour vasculature has been described as a poor recruiter of T cells, essentially acting as a barrier. Tumour vasculature fails to upregulate adhesion markers in response to inflammatory cytokines and T cell show poor ability to roll and arrest (Fisher et al. 2011). Intra-vital microscopy has suggested that T cells are actually recruited into blood vessels in the peritumour area rather than the central tumour vasculature (Boissonnas et al. 2007). Interestingly, some studies have found that anti-angiogenic therapy normalizes the vasculature leading to increased recruitment of T cells, improving adoptive cell therapy in murine models (Shrimali et al. 2010). Fas ligand (FasL) is expressed within the tumour endothelium of many human and mouse tumours (Motz et al. 2014) which can kill effector T cells but not Tregs, correlating with a low number of effector T cells and high number of Tregs found in tumours with FasL+ vascular endothelium. The inhibition of FasL greatly increased the recruitment of effector T cells.

1.17 Toxicity and safety

So far, TAA's targeted by CARs have been self-antigens, therefore, the potential for toxicity to normal cells and tissues must be considered. The successful use of CD19 as a target for B cell malignancy comes with the depletion of normal B cells since they also express CD19. However, this loss is considered acceptable since it can be managed using intravenous or subcutaneous immunoglobulin therapy to make up for the loss in B cell immunity. Most of the antigens targeted on solid tumours are normal proteins overexpressed on tumour cells, but often still expressed at lower levels on normal cells. This may result in on-target/off-tumour toxicity where CAR T cells target normal tissue.

The trial targeting CAIX resulted in on-target toxicity through CAIX expression on normal biliary epithelial cells (Lamers et al. 2011). The case report of a third generation CAR to HER2 in a colon cancer also described on-target toxicity resulting in a massive and fatal pulmonary infiltrate of T cells and cytokine storm most likely due to low level antigen expression on lung epithelium (Morgan et al. 2010). This was despite no toxicity and good efficacy seen in a pre-clinical murine xenograft model (Zhao et al. 2009). Furthermore, the CAR was constructed from the humanised monoclonal antibody Herceptin, which is an established breast cancer treatment and no or little toxicity was found in an ERBB2 epitope vaccine trial (Morse et al. 2007) or ERBB2 specific CD8 T cell clone therapy in breast cancer (Bernhard et al. 2008). This highlights the danger of targeting overexpressed normal self-antigens.

However, a recent study has targeted a novel tumour specific antigen (Morgan et al. 2012). EGFRvIII is a novel protein arising from gene-rearrangement commonly found in glioblastomas. The authors constructed a 3rd generation CAR that specifically recognised EGFRvIII but not normal EGFR or any of the normal cells investigated. Not only did this construct show *in vitro* efficacy, the same authors developed a murine version of this CAR which could cure glioblastomas in an immune competent glioma model (Sampson et al. 2014). A clinical trial is now recruiting patients for treatment with the EGFRvIII CAR (http://clinicaltrials.gov, NCT01454596).

Suicide or safety switches can be engineered into infused T cells as a way to trigger T cell death should high toxicity occur. Herpes simplex virus thymidine kinase (HSV-TK) is a particular suicide gene that has been used clinically in cancer therapy before and is regarded as effective and safe (Bonini 1997). HSV-TK phosphorylates ganciclovir, which can subsequently incorporate into DNA, inhibiting DNA synthesis. However, due to its viral origin, it is immunogenic (Berger et al. 2006) and could result in elimination of transferred T cells. Also, being cell cycle dependent means it may take time for it to effectively kill enough transferred T cells to repress any toxicity.

Inducible caspase 9 is an alternative suicide switch mechanism. When caspase 9 dimerises it induces an apoptotic-signalling pathway. A fusion construct has been developed so that when engineered into T cells, it forms a dimer upon binding extracellularly to a synthetic drug, resulting in dimerization and activation of the its intracellular caspase 9 domains, leading to induction of apoptosis (Di Stasi et al. 2011). It was tested in patients receiving high dose allodepleted donor T cells after allogeneic stem cell transplantation. Donor T cells expressed the inducible caspase 9 construct, and upon signs of GVHD, drug administration resulted in eradication of 90% of engineered T cells in half an hour, effectively stopping GVHD. The NCI group has now developed a 3rd generation CAR to GD2, which incorporates the inducible caspase 9 construct. A trial is now underway using this CAR. Another group has also recently developed a CD20 CAR expressing the inducible caspase 9 construct which resulted in efficient removal of engineered T cells *in vitro* and in a murine model upon drug administration (Budde et al. 2013).

The majority of genetic engineering studies have used γ retroviral or lentiviral vectors to transduce T cells. There has been concern surrounding the possibility of insertional mutagenesis and oncogene activation. Mature T cells are considered highly resistant to insertional mutagenesis, however it has occurred *in vitro* (Newrzela et al. 2011). Despite this, the transformed clones were not capable of causing tumours when transplanted into mice. Furthermore, over 200 patients have now been treated with genetically engineered T cells, with no case of transformation occurring (Maher 2012). Even though the chance of transformation is extremely low, it may be difficult to grant approval for clinical protocols involving multiple rounds of engineering, for example, separate transduction of a CAR and a chemokine receptor, as this doubles the risk of insertional mutagenesis.

In contrast to viral vectors, transposons can integrate into more specific sites in the genome and can be used to express transgenes including CARs in primary human T cells (Huang et al. 2008; Manuri et al. 2010). An alternative to DNA insertion is to perform CAR mRNA electroporation that can be expressed without the need for genetic insertion (Barrett et al. 2013) (Maus et al. 2013). Although this will result in only temporary expression, this could be useful in initial trials with concern for toxicity.

1.18 Targeting the tumour vasculature using T cells

The ability to specifically target the tumour endothelium was first demonstrated in 1993 when an immunotoxin was targeted to the endothelium within a neuroblastoma tumour in mice (Burrows & Thorpe 1993). The toxin disrupted tumour endothelium and caused substantial tumour regression whereas an immunotoxin targeting the actual tumour had little effect. In contrast to tumours, the endothelium is considered genetically stable, hence tumour evasive mutation strategies involving target antigen downregulation is less likely to affect the vasculature. However, abnormal chromosome numbers have been described in tumour endothelial cells in mice and humans (Hida et al. 2008; Akino et al. 2009). Nonetheless, cancer cells such as colorectal cancer have been documented to have up to 11,000 genomic alterations, highlighting their genomic instability (Stoler et al. 1999).

The discovery of the VEGF signalling pathway led to hope of anti-angiogenic therapy. However, only temporary responses are seen and toxicity is common using biologics inhibiting this pathway. As previously mentioned, the tumour vasculature is abnormal in structure. It is now appreciated that endothelial cells of the tumour vasculature also differ in gene expression compared to endothelial cells from normal vasculature.

A landmark paper analysed freshly isolated endothelial cells from patient matched human normal and malignant colorectal tissue (St Croix et al. 2000). Serial analysis of gene expression (SAGE) was performed allowing quantification of all mRNA transcripts within the tumour and normal endothelial tissues. 79 differentially expressed transcripts between normal and tumour endothelial cells were identified, 46 of which were specifically upregulated ten-fold or more in tumour endothelial cells including 9 novel genes. The 9 novel genes were also validated at the mRNA level using reverse transcriptase PCR. Such overexpressed markers are termed tumour endothelial markers (TEMs). Most of the novel genes discovered in this study were also overexpressed in the endothelial cells of several other cancers.

Similar studies have identified TEMs associated with glioma (Madden et al. 2004), breast cancer (Parker et al. 2004) and ovarian cancer (Buckanovich et al. 2007; Lu et al. 2007). Several of these were validated at the protein level in some studies. Despite some shared TEMs between different cancers (Aird 2009; St Croix et al. 2000), other TEMs are restricted such as HEYL, only found in invasive breast cancer (Aird 2009; Parker et al. 2004). An ideal TEM should have high expression in tumours with no expression in normal cells or during normal angiogenesis. Most of these global gene expression studies only compared TEM expression to normal tissue adjacent to the tumour tissue. The expression of the identified TEMs were not investigated in normal tissue throughout the body therefore all the markers require further validation.

For example, many of the novel TEM genes identified from the landmark report from St Coix have since been found to be expressed in normal tissue or are not surface markers making them unsuitable targets. Only one marker from this report, TEM8, is currently still being considered (Chaudhary et al. 2012). Along with this marker, several others are still being investigated. ROBO4 was first identified as a putative TEM in 2000 (Huminiecki & Bicknell 2000) and it has come up again in further expression screens (Herbert et al. 2008; Masiero et al. 2013). Another marker, CLEC14A has recently been discovered as a promising TEM, showing a broad expression pattern on various different tumour endothelium (Mura et al. 2012). ELTD1 has recently gained interest as a TEM in various cancers (Towner et al. 2013; Dieterich et al. 2012; Masiero et al. 2013). All of these markers also play a role in angiogenesis and could be targets of anti angiogenic therapy.

However, given the success of T cell therapies described above, T cell therapy targeting TEMs is a promising treatment strategy. Very few published reports have involved targeting the tumour vasculature using T cells. A T cell mediated destruction of tumour-associated vasculature has the potential of starving tumours and inducing tumour necrosis. One notable series of reports targeting the tumour vasculature is described below.

The most advanced study to target the tumour vasculature has come from the Rosenberg group against VEGFR2 (Chinnasamy et al. 2010; Chinnasamy et al. 2012; Chinnasamy et al. 2013). VEGFR2 is highly expressed on tumour endothelium and is considered a tumour endothelial marker (TEM). The major advantage of targeting tumour endothelial markers is that multiple different tumour types can express the same marker. Using a third generation CAR to VEGFR2, tumour regression was successful in 5 different syngeneic mouse models including melanoma and colon cancer models (Chinnasamy et al. 2010). Both lymphodepletion and IL2 were required for regression. Despite tumour reduction and the increased tumour free survival compared to control groups, the majority of mice succumbed to the tumour.

Leading on from previous reports into IL12, the authors included an inducible IL12 producing construct with the CAR (Chinnasamy et al. 2012). The inclusion of IL12 production by CAR expressing T cells resulted in an increased tumour free survival with many mice essentially cured. Similarly, by co-administrating T cells expressing a TCR to melanoma antigens present in the malignant cells along with VEGFR2 specific CAR expressing cells, an increased tumour response was seen compared to administration of only one cell type alone (Chinnasamy et al. 2013). These results led to a recently completed clinical trial treating 23 patients with metastatic melanoma and renal cancer (http://clinicaltrials.gov NCT01218867). Despite pre-clinical success, clinical response was poor, with 1 stable disease and 1 partial response. Nevertheless, the safety and efficacy of using CARs to target other TEMs is an area that has largely been unexplored.

1.19 Project aims

This project explores the use of CARs to target the TEM ROBO4. It is hypothesised that ROBO4 can be safely targeted using CAR T cells to efficiently prevent tumour growth through disruption of the tumour vasculature. To test this, ROBO4 specific CARs were generated and tested for function in vitro before in vivo experiments were performed to analyse safety and toxicity as well as anti-tumour activity.

Another section of the project involved using antibody phage display in an attempt to discover monoclonal antibodies specific to several other TEMs in order to develop further CARs. It is hypothesised that CARs can be generated from novel antibodies specific to TEMs.

2. Materials and Methods

2.1 ROBO4 CAR development

2.1.1 Cell media

T cell medium (TCM)

- 500ml RPMI 1640 (sigma)
- 10% Fetal Bovine Serum (Gibco)
- 2mM L-Glutamine (Gibco)
- 100mg/ml streptomycin (Gibco)
- 100 IU/ml penicllin (Gibco)
- 1% Human serum (TCS Biosciences)

LCL

- 500ml RPMI 1640 (sigma)
- 10% Fetal Bovine Serum (Gibco)
- 2mM L-Glutamine (Gibco)
- 100mg/ml streptomycin (Gibco)
- 100 IU/ml penicillin (Gibco)

ELISA media

- 500ml RPMI 1640 (Sigma)
- 10% Fetal Bovine Serum (Gibco)
- 2mM L-Glutamine (Gibco)
- 100mg/ml streptomycin (Gibco)
- 100 IU/ml penicillin (Gibco)

- 50 IU/ml IL2 (Sigma)

Phoenix cell medium

- 500ml DMEM (Sigma)
- 10% Fetal Bovine Serum (Gibco)
- 2mM L-Glutamine (Gibco)
- 100mg/ml streptomycin (not included during transfection) (Gibco)
- 100 IU/ml penicillin (not included during transfection) (Gibco)

CHO cell medium

- 500ml DMEM (Sigma)
- 10% Fetal Bovine Serum (Gibco)
- 100mg/ml streptomycin (Gibco)
- 100 IU/ml penicillin (Gibco)

HUVEC cell medium

- 500ml Human Large Vessel Endothelial Cell Basal Medium (Cellworks)
- 10ml Growth supplement (Cellworks)
- 100mg/ml streptomycin (Gibco)
- 100 IU/ml penicillin (Gibco)

All cell cultures at 37°C were performed in a 5% CO_2 in a humidified incubator.

ROBO4 CAR construct generation

Two ROBO4 CARs, named R1 and R2, were generated. Two scFv sequences (named R1 and R2) from two mouse-derived monoclonal antibodies specific to human/mouse ROBO4 proteins were provided by Roche (confidentially agreement prevents the sequences being published). The scFv sequences were inserted into pUC57 plasmid vectors with a 5' Not1 and a 3' Cla1 restriction site (GenScript). An MP71 vector containing a second generation Clec14A-specific CAR was used as a template vector for the ROBO4 CARs. The MP71 vector contains a Not1 and a Cla1 restriction site at the 5' and 3' end of the Clec14A respectively. A Not1/Cla1 double digest of the MP71 vector allowed removal of the Clec14A-specific scFv and an open vector. A Not1/Cla1 double digest of the pUC57 vector generated the ROBO4 scFv products. The ROBO4 scFv DNA was then ligated into the MP71 vector. The CAR construct is as follows: long terminal repeat (LTR) of the myeloproliferative sarcoma virus (MPSV); truncated CD34 (tCD34); a 2A peptide (obtained from picornaviruses, 22 amino acids); R1 or R2 scFv; the transmembrane and cytoplasmic domain of human CD28; and an intracellular human CD3z chain (see figure 3.2a in chapter 3). With the 2A peptide, several proteins within a single vector are expressed at a 1:1 ratio through a ribosomal skipping mechanism (Szymczak et al. 2004). Therefore, the truncated CD34 acts as a reporter gene to quantify CAR expression.

Mice:

C57BL/6 mice (CD45.2 allele) were obtained from Charles River Laboratories (London, UK) and BoyJ mice (C57BL/6 congenic mice with the CD45.1 allele) were obtained from a colony maintained at the Biomedical Services Unit of the University of Birmingham. All mice were housed at the Birmingham Biomedical Services Unit (Birmingham, UK). All animal experimentation was carried out in accordance with Home Office License number PPL 40 3686 held by Steve Lee. All mice were female and aged between 8 and 12 weeks at the experimental start point.

2.1.2 Trypsinisation

Media was removed and cells were rinsed in sterile PBS (School of Cancer Sciences, University of Birmingham). PBS was removed and cells were incubated with 2ml of 1x Trypsin/EDTA (Gibco) for a T50 culture plate. Plate was incubated for 5 minutes at 37°C before washing in 10ml of culture media, by centrifugation at 500g for 5 minutes.

2.1.3 HUVEC cell culture

Culture plates were incubated in 5ml of 0.1% porcine gelatine (Sigma) in PBS for a T50 culture flask for 20 minutes at 37°C. Plates were then rinsed in PBS before seeding with $4x10^6$ cells in 10ml of HUVEC media. Plates were incubated at 37°C and when they became confluent they were trypsonised and split. Cells were grown for a maximum of 5 passages.

2.1.4 Human Cell isolation and activation

Adult peripheral blood mononuclear cells (PBMCs) were isolated from apheresis cones, supplied by the blood donor centre, using lymphoprep (StemCell). Cells were resuspended to $1x10^6$ cells/ml in T cell media (TCM). For activation, Anti-CD3 antibody (OKT3) (eBiosciences, UK) and anti-CD28 (Invitrogen) were added at 30ng/ml with 300U/ml of IL2 (Sigma). For transduction, cells were incubated for 48 hours at 37°C.

2.1.5 Mouse cell isolation and activation

Spleens from BoyJ mice were removed and mashed through a 70µM strainer then washed in RPMI by centrifugation at 1800rpm. Red blood cells were lysed using lysing buffer (BD) at 1x concentration diluted in sterile water. Cells were then washed in LCL. Cells were resuspended to $3x10^6$ cells/ml in LCL and activated with Concanavalin A (Sigma) at 2ug/ml and mouse IL7 (eBiosciences) at 1ng/ml. Cells were then added into a 6 well TC plates and incubated for 48 hours at 37°C.

2.1.6 Human T cell Transduction

A T50 culture flask (Corning) of phoenix amphotropic packaging cells (Orbigen) in phoenix cell medium were transfected with the pCL Ampho retroviral packaging vector (9µg), with the specified CAR construct vector (9µg) and PEI (72µg) then incubated for 48 hours at 37°C. Supernatant containing retrovirus was recovered and plated into retronectin (Takara, Shiga, Japan) coated wells of a non-tissue culture 6 well plate (2ml/well). Plates were centrifuged at 2000g for 2 hours at 32°C. Supernatant was removed and preactivated cells were seeded into wells at $2x10^6$ cells/well containing IL2 at 100IU/ML. Plates were then centrifuged at 400g for 5 minutes before incubating at 37°C. 24 hours later cells were transferred into tissue culture treated 6 well plates at to $1x10^6$ cells/ml in TCM with 100IU/ml IL2. Plates were cultured at 37°C/5% CO_2 in a humidified incubator with TCM and IL2 replaced every 3 to 4 days.

2.1.7 Mouse T cell transduction

A T50 culture flask of phoenix ecotropic packaging cells (Orbigen) in phoenix cell medium were transfected with the pCL Eco retroviral packaging vector (9µg), with the specified CAR construct vector (9µg) and Fugene 6 (Promega) (120µl) prepared in OptiMEM (Gibco) then added to the phoenix cells in phoenix cell medium and incubated for 48 hours at 37°C. Supernatant containing retrovirus was recovered and plated into retronectin coated wells of a non-tissue culture 6 well plate (2ml/well). Plates were centrifuged at 2000g for 2 hours at 32°C. Supernatant was removed and preactivated cells were seeded into wells at $2x10^6$ cells/well containing IL2 at 100IU/ML. Plates were then centrifuged at 400g for 5 minutes before incubating at 37°C. 24 hours later cells were either prepared for infusion or transferred into tissue culture treated 96 well plates TCM with 100IU/ml IL2. Plates were cultured at 37°C with TCM and IL2 for up to 3 days before an IFNγ ELISA is performed.

2.1.8 Flow cytometry to check transduction efficiency

For all antibody incubations in flow cytometry experiments, cells were resuspended in 40μl of media and the antibodies were added at the stated dilutions.

Flow cytometry was performed to confirm transduction of T-cells by staining with CD34. Four days (for human T cells) or one day (for mouse T cells) after transduction, $1\text{-}2x10^5$ transduced T cells were washed in PBS and stained with LIVE/DEAD (Invitrogen) at 1/30 from a 1:100 stock for 20 minutes at room temperature. LIVE/DEAD is a viability dye that distinguishes live cells from dead cells based on cell membrane integrity and access to available amines. Cells were then washed in MACs buffer (PBS with 0.5% BSA and 2.5mM Ethylenediaminetetraacetic acid (EDTA) (School of Cancer Sciences, University of Birmingham)) and stained with antibodies to CD34, CD8 and CD4 for 30 minutes at 4°C in the dark (tables 2.1 and 2.2). Alternatively, where stated, cells were stained only for CD34. Cells were then analysed on the LSRII flow cytometer (BD).

Table 2.1 Antibodies for human T cells.

Antibodies for human T cells	Manufacturer	Concentration
Human CD4-FITC	BD	1/8
Human CD8-PE	Abcam	1/40
Human CD34-APC	Biolegend	1/20

Table 2.2 Antibodies for mouse T cells.

Antibodies for mouse T cells	Manufacturer	Concentration
Mouse CD4-PE	Abcam	1/20
Mouse CD8-FITC	Abcam	1/20
Human CD34-APC	Biolegend	1/20

2.1.9 Human T cell IFNγ ELISA

Coating buffer

- 3.7 g NaHCO3
- 0.64 g Na2CO3
- 1 L of distilled water

Blocking buffer

- 2% BSA in PBS

Protein:
Recombinant extracellular human or mouse ROBO4-His protein (Sino biological) was diluted in PBS and added to a 96 well non-TC plate. Protein was added to triplicate wells at the indicated concentration(s) and plate was incubated for 4 hours at 37°C. Wells were then washed in sterile PBS. T cells were resuspended in ELISA media and added to aspirated wells at $2x10^5$ cells/well or media was added alone. Plates were incubated overnight.

Cells:
The following target cells were used: Chinese hamster ovary (CHO) wild type (WT) cells (Bicknell Lab, University of Birmingham); Human ROBO4 overexpressing cell line CHO magic roundabout full length (MRFL) (Bicknell Lab, University of Birmingham); human umbilical cord endothelial cells (HUVEC) (Gibco). Target cells were seeded into 96 well TC plates at $5x10^4$ cells/ml in 200ul of target cell media. Plates were incubated for at least 3 hours then media was aspirated. T cells were resuspended into ELISA media and added to target cells or empty wells at 100ul/well. T cells were added at a top concentration of $2x10^5$ cells/well and at dilutions (unless otherwise stated) of $1x10^5$, $5x10^3$ and $2.5x10^3$ cells/well. Plate was incubated overnight. A 96 well maxisorp ELISA plate (nunc) was coated in 0.75ug/ml anti-human IFNγ (Invitrogen) in coating buffer then stored overnight at 4°C.

ELISA development:
Coating was removed from the ELISA plate and plate was blocked for 2 hours in blocking buffer at room temperature (RT) before washing in Tween20 (Sigma) 0.05% in PBS. The 96 well culture plate was centrifuged at 600g for 5 minutes then 50ul of supernatant from each well was added to the blocked ELISA wells. A standard dilution of recombinant human IFNγ (Sigma) in ELISA media from 20,000pg/ml to 312.5pg/ml was performed and added to triplicate wells of the same ELISA plate for each dilution. ELISA media alone was also added for the standard.

ELISA plates were incubated for 3 hours at RT then washed as before. Biotinylated anti-IFNγ (Invitrogen) at 1/1333 dilution in blocking buffer was added to each well and the plate was incubated for 1 hour at RT. After washing as before, Extra-avidin (Sigma) diluted 1/1000 in blocking buffer was added to the ELISA plate 100ul/per well and incubated for 30 minutes at RT. After washing 8 times in Tween20 0.05% in PBS, 50ul/well of TMB substrate was added to each well and left to develop at RT for up to 20 minutes. The reaction was stopped by adding 30ul/well of 1M H_2SO_4. ELISA plate was read on a plate reader at 450nm and 605nm. The absorbance values at 605nm was removed from the absorbance values at 450nm. IFNγ concentration was determined by extrapolating form the standard curve values.

2.1.10 Mouse T cell IFNγ ELISA to whole cells

The target cells CHO MRFL and CHO WT were seeded into 96 well TC plates at $5x10^4$ cells/ml in 200ul of target cell media. Plates were incubated for 3 hours then media was aspirated. T cells were resuspended into ELISA media and added to target cells or empty wells at 100ul/well. T cells were added at a top concentration of $2x10^5$ cells/well and at dilutions of $1x10^5$, $5x10^4$ and $2.5x10^4$ cells/well. A 96 well maxisorp ELISA plate (nunc) was coated in 0.75ug/ml anti-mouse IFNγ (Sigma) in coating buffer then stored overnight at RT.

ELISA development:

ELISA plate was aspirated then blocked in 300ul of blocking buffer per well at RT for 1 hour before washing in Tween20 0.05% in PBS. The 96 well culture plate was centrifuged at 800g for 5 minutes then 50ul of supernatant from each well was added to the blocked ELISA wells. A standard dilution of recombinant mouse IFNγ (Sigma) in ELISA media from 24,000pg/ml to 625pg/ml was performed and added to triplicate wells of the same ELISA plate for each dilution. ELISA media alone was also added for the standard. ELISA plates were incubated overnight at RT before washing as before.

Biotinylated anti mouse IFNγ (Invitrogen) at 1/1333 dilution in blocking buffer was added to each well and the plate was incubated for 1 hour at RT. After washing as before, Extra-avidin (Sigma) diluted 1/1000 in blocking buffer was added to the ELISA plate 100ul/per well and incubated for 30 minutes at RT. After washing 8 times in Tween20 0.05% in PBS, 50ul/well of TMB substrate was added to each well and left to develop at RT for up to 20 minutes. The reaction was stopped by adding 30ul/well of 1M H_2SO_4. ELISA plate was read on a plate reader at 450nm and 605nm. The absorbance values at 605nm was removed from the absorbance values at 450nm. IFNγ concentration was determined by extrapolating form the standard curve values.

2.1.11 Intracellular cytokine staining

Target cells were seeded at 0.5×10^6 cells/well into wells of a 48 well TC plate. Plates were incubated for 5 hours (in their respective cell media). Mock, R1 and R2 transduced CAR T cells were washed and resuspended into LCL at 0.5×10^6 cells/ml. Target cell media was gently aspirated from the 48 well plate. T cells or media alone were then added to the target cells (or into T cell only wells) at 2.5×10^6 cells/well (1ml total media). The positive control wells that contain T cells only were incubated with 200ng/ml of staphylococcal enterotoxin B (SEB). Fluorescence minus one (FMO) controls also received the same concentration of SEB. Golgiplug (BD) was added to all wells, including an unstained control T cell well at 1ul/well. The plate was incubated overnight. The following day, T cells/media alone were removed from each well and added into FACs tubes before washing in MACs buffer. Cells were surface stained with antibodies (table 2.3) for CD34, CD4 and CD8 then incubated at 4°C for 30 minutes. Cells were washed in MACs buffer again before vortexing, adding 250ul of Cytofix solution (BD) per tube then vortexing again and incubated at 4°C for 20 minutes. Cells were washed in 1X Cytoperm solution (BD). Cells were stained with the antibodies for IL2, TNFα; IFNγ. Then incubated at 4°C for 30 minutes in the dark. Cells were washed in 1X Cytoperm solution, resuspended in MACs buffer and analysed on the LSRII. FMO controls were prepared for IL2, TNFα, IFNγ and CD34.

Table 2.3 Antibodies used for Intracellular cytokine staining.

Antibody	Manufacturer	Concentration
CD4-ECD	Beckman Coulter	1/40
CD8-AmCyan	BD	1/80
CD34-PE Cy5	BD	1/40
IL2-PE	BD	1/13
TNFα-PE Cy7	eBiosciences	1/80
IFNγ-FITC	Biolegend	1/8

2.1.12 CFSE proliferation assay

$2x10^5$ of target cells were added to wells of a 96 well TC plate in TCM and the plate was incubated at 37°C for 4 hours. For CFSE labelling, CFSE (Invitrogen C1157) was added to PBS at a concentration of 1:10,000 and mixed then incubated in a water bath at 37°C while protecting from light. R1, R2 or mock-Transduced T cells, with R1 and R2 equalised for transduction efficiency, were resuspended in warmed PBS/CFSE mix at $1x10^6$ cells/ml concentration and incubated at 37°C for 15 minutes. Cells were then washed and resuspended in

TCM at a concentration of $1x10^6$ cells/ml and incubated at 37°C for 30 minutes. Cells were washed then resuspended at $2.5x10^6$ cells/ml in TCM with 100U/ml IL2. T cells were added to appropriate wells of the 96 well TC plate. One well also contained unlabelled mock T cells at the same concentration. Plate was incubated for 4 days. Cells were then removed from the wells for staining. Cells were washed in PBS, then stained with LIVE/DEAD (Invitrogen) for 20 minutes at RT before washing in MACs buffer. Cells were then stained with antibodies for CD34, CD4 and CD8 in MACs buffer for 30 minutes at 4°C (table 2.4). Cells were washed in MACs then resuspended in MACs before analysis on the LSRII. An unlabelled and unstained mock T cell well was mixed a CFSE labelled, unstained mock T cell well to make a CFSE control well and measured on the FITC channel of the LSRII.

Table 2.4 Antibodies used for CFSE analysis.

Antibody	Manufacturer	Concentration
Human CD4-ECD	Beckman Coulter	1/40
Human CD8-PE	BD	1/40
Human CD34-APC	BD	1/20
LIVE/DEAD	Invitrogen	1/30 from 1/100 stock

2.1.13 Restimulation assay

R1, R2 or No scFv transduced human T cells were equalised for transduction efficiency. Cells were counted then resuspended in TCM with 50 IU/ml IL2 and seeded into wells of a non-TC plate precoated in human ROBO4-His protein at a concentration of 1μg/ml in PBS or into wells precoated in PBS alone. The cells were incubated for 48 hours at 37°C then transferred into new wells of a TC plate and incubated for another 5 days at 37°C before they were counted again and re-plated again into ROBO4-His protein or PBS coated wells. Again, cells were transferred to TC wells after 48 hours and incubated for 5 days then counted. This process was repeated one last time. During incubation with the TC wells, TCM was replaced every 2-3 days by removing the top half of media without disturbing the cells with the addition of fresh TCM and IL2 at 50 IU/ml.

2.1.14 Chromium release assay

10ul (50uCi) of ^{51}Cr was added to $1x10^6$ target cells. Cells were gently mixed then incubated for 2 hours at 37°C while resuspending every 20-30 minutes. T cells were resuspended in LCL media and added at 100ul/well in triplicate wells of a 96well V bottom plate at a top concentration of $5x10^4$ cells/well and at dilutions of $2.5x10^4$ and $1.25x10^4$ cells/well. ^{51}Cr labelled target cells were washed in LCL twice at 800g for 3 minutes. Target cells were then resuspended to $2.5x10^4$ cells/ml in LCL media and added to appropriate wells at $2.5x10^3$ cells/well. Target cells alone were incubated in sodium dodecyl sulphate (SDS) to induce lysis of all cells and provide a reading for maximum lysis. Target cells incubated in media alone provide a reading for minimum lysis. Plates were centrifuged at 400g for 3 minutes then incubated at 37°C for 5 hours. 100ul supernatant per well was harvested then analysed for ^{51}Cr levels. The percentage of specific lysis was worked out from the maximum target cell lysis control minus the minimum lysis control. The minimum lysis controls provide the level of lysis at 0% while the maximum lysis controls provide the level of lysis at 100%. The average for each triplicate sample and its specific lysis percentage can then be worked out.

2.1.15 Mouse T cell infusion

C57BL/6 mice were irradiated with 4Gy of total body irradiation in the afternoon. The following morning, T cells that were transduced the previous day were prepared for infusion. T cells first underwent a Histopaque 1083 (Sigma) filtration. This involved layering activated/transduced T cells over 15ml of Histopaque 1083 in a 50ml tube. The Tube was centrifuged at 400g, for 30 minutes, at room temperature. After centrifugation, cells at the interphase of the Histopaque were removed and made up to 40ml in RPMI. Cells were then centrifuged at 400g for 10 minutes at room temperature. The supernatant was removed and cells resuspended in LCL before centrifugation at 250g for 10 minutes at room temperature. Supernatant was removed, cells were resuspended in Hanks buffered salt solution (Sigma) and counted before injection into the tail vain of irradiated mice.

2.1.16 Tail Bleed Analysis

35ul of tail blood was collected from each mouse into a preweighed eppendorf along with 20ul of Heparin (50units/ml). Eppendorfs were weighed after collection to provide an exact value for amount of blood removed. 100ul of PBS with 10units/ml of Heparin was added to each tube and centrifuged at 600g for 3 minutes. Plasma was removed from sample (and stored at -80°C if mentioned) and remaining blood was lysed of red blood cells using lysing buffer (BD) at 1x concentration diluted in sterile water. Cells were then washed in PBS and stained using the LIVE/DEAD marker as before. Cells were then washed in MACs buffer and stained for CD34, CD4, CD8 and CD45.1 for 30 minutes at 4°C (table 2.5). Cells were washed in MACs buffer then flow count beads (BD) were added at a concentration of 1000 beads/µl. Cells were then analysed on the LSRII.

Table 2.5 Antibodies for tail bleed analysis.

Antibody	Manufacturer	Concentration
Mouse CD4-PE	Abcam	1/20
Mouse CD8-FITC	BD	1/20
Human CD34-APC	Biolegend	1/20
Mouse CD45.1 PE Cy7	BD	1/40
LIVE/DEAD	Invitrogen	1/30 from 1/100 stock

2.1.17 Lewis Lung Carcinoma tumour study

Lewis Lung Carcinoma (LLC) cells were resuspended at a 5×10^6 cells/ml in HBSS then mixed with an equal volume of phenol red-free matrigel (Corning). The side of each mouse was shaved and 200ul of LLC in matrigel was injected sub-cutaneously into each mouse so they received 0.5×10^6 cells each. One mouse received no tumour. Three days after LLC injection, mice were irradiated with 4G then injected with either No scFv or R1 transduced BoyJ cells as before, but in a blinded manner. The mouse that did not receive any tumour was injected with mock-transduced BoyJ cells and acted as a mock control to assist with CD34 gating for tail bleed analysis.

Callipers were used to measure the volume of each tumour by using the formula: (longitudinal (mm) x width^2 (mm))/2). Tail bleeds were performed when indicated as before, but data was not analysed until the end of the experiment to reduce any bias towards tumour measurements based on presence/absence of CAR T cells. At the end of the experiment, the tumours were removed and frozen in OCT medium (Fisher). 8μm sections of tumour were cut by a technician from the Lee Lab and stained as described below.

2.1.18 Immunofluorescence staining

All incubations were at RT unless otherwise stated.

Sections were fixed in Acetone at -20°C for 10 minutes before washing in PBS three times for 5 minutes each. Sections were blocked with goat serum (Sigma) for 30 minutes. Sections were stained with the appropriate primary antibodies (table 2.6) for 1-2 hours in the dark before washing again in PSB as before. Sections were then stained with the appropriate secondary antibodies (table 2.7) for 1 hour. Sections were washed again as before then rinsed in tap water. A drop of DAPI Prolong Gold Antifade (Life Technologies) was added onto coverslips and placed on top of the sections. Sections were analysed on a confocal microscope. The DAPI channel was malfunctioning during analysis so was excluded from analysis.

For cleaved caspase 3 analysis, the intensity of cleaved caspase 3 staining on endothelial cells was quantified using ImageJ. A threshold was generated for the 488 channel (cleaved caspase 3) using the MaxEntropy algorithm. The mean pixel intensity of the 568 channel (MECA32) within this threshold was then measured. Automated thresholding was used to remove any chance of bias in the analysis.

Table 2.6 Primary antibodies for Immunofluorescence staining

Primary antibodies	Manufacturer	Concentration
MECA32 (CD31)	BD	1/50
Human CD34	Abcam	1/50
Cleaved caspase 3	Cell signalling	1/400
ROBO4	Generon	1/25 to 1/200
ROBO4 R1 scFv fused to rabbit IgG Fc	Roche	10ug/ml to 1000ug/ml

Table 2.7 Secondary antibodies for Immunofluorescence staining

Secondary antibodies	Manufacturer	Concentration
Goat anti rat-Alexa 568	Life Technologies	1/200
Rat anti-rabbit-Alexa 488	Life Technologies	1/50

2.1.19 Luminex

The mouse magnetic luminex assay (R&D Systems) was used to detect a total of 26 cytokines on the BioRad Bio-Plex 200 machine. Frozen serum from the tail bleed analysis during the tumour experiment was prepared and analysed according to manufactures instructions. Tested cytokines: TNFα; IL5; GMCSF; IL12 p70; IL1β; IL2; EGF; IL10; IL17A; CXCL10; GCSF; IL1α; CXCL12; FGF-basic; IL7; CCL2; VEGF; IL4; IL6; IFNγ; CCL5; CCL3; CCL4; Granzyme B; CCL11.

2.1.20 QDOT 625 experiments

10nM of QDOT 625 labelling solution (Thermo) was prepared according to manufacturers instructions. Mouse cells were resuspended to $1x10^7$ cells/ml and QDOTS were added according to manufactures instructions. Cells were incubated at 37°C for 60 minutes with mixing every 15 minutes. Cells were then washed twice in TCM or LCL. For analysis on the LSRII, the QDOT 605 filter was used for QDOT 625 detection.

For the initial experiment to test QDOT detection in mouse spleens, C57BL/6 mouse splenocytes were activated as described for the BoyJ splenocytes previously. Two days after activation, cells were labelled with QDOT or left unlabelled then cells were prepared for tail vain infusion into irradiated C57BL/6 mice in HBSS as before. Four days later, the mice were euthanised and the spleens were frozen in OCT then sent for analysis at Maynooth University.

For whole mouse cryoimaging, C57BL/6 splenocytes underwent a CD3 cell sort using the Pan T cell MACs beads (Miltenyi) according to the manufacturers instructions. Sorted CD3 cells were activated just as splenocytes have been previously activated and transduced as described previously with the No scFv CAR or the R1 CAR. On the day of infusion, both CAR T cells were initially stained with CD34-APC as previously described for flow cytometry experiments then labelled with QDOT. Cells were then prepared for a cell sort using a FACs single cell sorter. Sorted cells were washed and resuspended in HBSS. Cells were then infused into irradiated mice as before. Mice were euthanized using CO_2 three days later and mice were frozen whole in OCT using liquid nitrogen then were sent to BioInvision, USA, for analysis.

2.2 Phage display

2.2.1 Protein

- Bovine serum albumin (BSA) (Sigma)
- Human and murine extracellular ELTD1 protein - Protein cloned into HEK 293 cells and purified using a His tag by the protein expression facility, University of Birmingham
- Human GRIN2D-GST (Henry Ferguson, Bicknell lab, University of Birmingham)
- Human GRIN2D-Fc (Henry Ferguson, Bicknell lab, University of Birmingham)
- Human MCAM-Fc (Acro Biosystems, USA)
- Murine MCAM-His (Sino Biological, China)

- Murine GRIN2D-Fc made in house (DNA construct provided by Henry Ferguson, Bicknell lab, University of Birmingham)
- Purified human IgG-Fc (Bethyl Laboratories)

2.2.2 Media

2xTY media (1 litre)

- 16g Bacto-Tryptone (BD)
- 10g Bacto-Yeast extract (BD)
- 5g NaCl (Sigma)
- 1L water
- with AMP (if specified) – 100µg Ampicillin (Roche)
- with Kan (if specified) – 25µg Kanamycin (Sigma)
- with GLU (if specified) – 1% Glucose (Sigma)

2xTY agar

- as media, with 15g bacteriological agar (Sigma) per 1L

2.2.3 Primers

Oligonucleotide	Sequence (5' to 3')
fdseq1	GAATTTTCTGTATGAGG
DP47CDR2back	TACTACGCAGACTCCGTGAAG
M2tinsertfor	TGCTGCTGACCCAGAGGACC
MP71 reverse primer	CAGAACAAATATGGGTATAA
ELTD1-3' Not1	AAAGCGGCCGCGCCTAGGACGGTCAGCTTGG

2.2.4 Phage Selection

2.2.4.1 Immunotubes

A maxisorp immunotube (Nunc) was coated overnight in 4 ml of the specified protein in PBS at the specified concentration at room temperature (RT) overnight. The tube was then rinsed three times in PBS then blocked with 4ml of 2% milk (Sigma) PBS for 2 hours at RT. For the first round of selection, one 1ml vial of library phage with a titre of 10^{12} titre units (TU) per ml was diluted in milk PBS to make a final 4ml solution at 2% milk concentration. This phage solution was added to the blocked immunotube. The tube was sealed and repeatedly inverted gently for 30 minutes at RT then left to stand upright for 1.5 hours at RT. The supernatant was then discarded and the tube was washed 10 times in 0.1% Tween20 in PBS then 10 times in PBS. Remaining bound phage were then eluted from the immunotube by the addition of 1ml of 100nM triethylamine (Sigma), then sealing the tube followed by repeated inversion for 8 minutes at RT. The solution was then poured into a microcentrifuge tube and neutralised with 0.5ml of 1M Tris/Cl (Sigma) at pH 7.4.

For additional rounds of selection, 1ml of PEG purified phage were added to the immunotube. The same selection process was repeated as above unless otherwise stated.

2.2.4.2 Biotinylation and selection

Protein was first biotinylated using the EZ-link NHS-SS-Biotin kit (Thermo) according to manufactures instructions at a ratio of 50:1 biotin to protein. Excess free biotin was removed by buffer exchange using PD-10 desalting columns (GE healthcare) according to manufactures instructions. For round one of selection, one 1 ml vial of library phage with a titre of 10^{12} TU was diluted to 5ml PBS with 2% milk protein, 0.1% Tween 20 and 50µM of biotinylated protein in a 15ml tube. The tube was gently rotated at RT for one hour. 100µl of M280-streptavidin dynabeads (Thermo) were blocked by incubating with 600µl of 5% milk in PBS for 15 minutes at RT. A magnet was used to separate the dynabeads from the blocking medium. Dynabeads where then resuspended in 200µl of PBS. 150µl of the blocked beads were then added into the phage-protein mix and rotation was continued for another 15 minutes at RT. A magnet was again used to accumulate the beads and remove the supernatant. The beads were then washed five times in 1ml of PBS with 0.1% Tween 20 then five times in 1ml of PBS using the magnet each time to accumulate the beads and remove the supernatant. Phage/protein was then eluted from the dynabeads by adding 300µl of 50Mm dithiothreitol (Sigma) in PBS and incubated for 5 minutes at RT before beads were accumulated with a magnet and the 300µl phage containing supernatant was removed.

2.2.5 Phage rescue

The whole 1.5ml of phage mix recovered from the immunotube or 150µl of the phage mix recovered from the biotinylation method was added to 10ml of exponentially grown TG1 and incubate at 37°C for 30 minutes. Following this, 10µl of neat TG1, 10µl of a 1:100 dilution of TG1 and 10µl of a 1:10,000 dilution are plated onto TY-AMP-GLU plates to allow an estimation of phage titre. The remaining TG1 culture was centrifuged at 3,300g for 10 minutes, resuspended in

0.5ml of 2xTY and all of it is spread on a large TY-AMP-GLU plate. All plates were incubated overnight at 30°C.

The following day, the titre is estimated from the dilution plates. The lawn of TG1 grown on the large plate was scraped off into a glycerol stock of 2xTY-15% glycerol (Glycerol from School of Cancer Sciences, University of Birmingham). The stock was used to inoculate 50ml of 2xTY-AMP-GLU media to an OD^{600nm} of 0.05 to 0.1. This culture was then grown in a shaker at 37°C until exponential growth was reached (OD 0.4-0.5). At this point, 10ml of culture is removed and infected with 100µl of VCS-M13 helper phage (Agilent Technologies, UK) at a concentration of 10^{12} TU/ml. The infected culture was incubated at 37°C for 30 minutes before centrifugation at 3,300g for 10 minutes. Supernatant was removed and the TG1 pellet was resuspended in 100ml of 2xTY-AMP-KAN media and grown at 30°C while shaking at 200RPM overnight. The following day, the culture was centrifuged at 10,800g for 10 minutes. The supernatant was removed and phage was isolated as described below.

2.2.6 Phage PEG purification

300ml of supernatant was incubated with 75ml of PEG/NaCl (20% polyethylene glycol 6000 (Sigma), 2.5M NaCl (Sigma)) then incubated on ice for 1.5 hours. The supernatant was then centrifuged at 10,800g for 30 minutes at 4°C. The pellet was resuspended in 40ml of water and 10ml of PEG/NaCL then incubated on ice for 30 minutes. After another round of centrifugation as before, the pellet was resuspended in 2ml of PBS. The phage PBS mix was split into 2x 1ml fractions in microcentrifuge tubes and centrifuged at 3,300g for 10 minutes to remove any debris. The 1ml phage PBS mix supernatant was removed and stored in 15% glycerol at -70°C or was stored at 4°C in PBS alone if it was to be used within a few days.

2.2.7 Polyclonal phage ELISA

All incubations at room temperature and one hour unless otherwise stated. All washes in PBS+0.1% Tween 20; all rinses in PBS. A 96 well Maxisorp plate (Nunc) was coated in 100μl/well of protein diluted in PBS and incubated overnight. Wells were blocked in 200μl of 2% milk-PBS for 2 hours. After rinsing, 10μl of precipitated phage and 90μl of PBS added per well, except no phage control wells, which received 100μl of 2% milk-PBS, before incubating, washing and rinsing. 100μl/well of Mouse Anti-M13 HRP (GE-healthcare, UK) at 1:1000 in 2% milk-PBS added before incubating, washing and rinsing. 100μl/well of goat anti-mouse HRP (Sigma) added at 1:1000 in 2% milk-PBS before incubating washing and rinsing. 100μl/well of blue POD substrate (Roche, UK) added to develop ELISA, then 30μl of 1M phosphoric acid added 10-20 minutes after to stop ELISA. Plates were measured at 450nm.

2.2.8 Polyclonal phage ELISA against biotinylated protein

A StreptaWell high bind 96 well plate (Roche, UK) was coated with protein diluted in PBS 0.1% BSA, at 100nM per well (100μl/well). The plate was then incubated at RT for 30 minutes before washing three times with 200ul/well of PBS-0.1% BSA. The plate was then blocked with 2% BSA-PBS, 200ul/well, for 1.5 hours at RT before washing as before. Precipitated phage from rounds of selection were added to appropriate wells with 10ul of phage and 90ul PBS 0.1% BSA per well. No phage control wells were coated with 10ul PBS and 90ul of PBS

0.1% BSA per well. Plate was incubated for 1 hour at RT before washing 3x in PBS 0.1% tween then 3x in PBS 0.1% BSA, leaving each wash on for 3-5 minutes each time. The primary antibody, mouse anti-M13 HRP, diluted 1:1000 in PBS 0.1% BSA was added at 100ul/well. The plate was incubated at RT for one hour before washing as before. The secondary, goat anti-mouse HRP diluted at 1:10,000 in PBS 0.1% BSA was added at 100ul/well. Leave for 30 minutes at room temperature. The plate was incubated at RT for 30 minutes before washing as before. 100ul/well of blue POD substrate was then added for up to 15 minutes before stopping reaction by adding 30µl of 1M acid. The plate was then read on a plate reader at 450nm and 655nm

2.2.9 Monoclonal phage ELISA

Single colonies of TG1 bacteria from selection titre plates from phage display selection were picked into 96-well plates with 150µl 2xTY-Amp-Glu and growing for 3 hours at 37°C shaking at 150RPM. Each well was infected with 1×10^9 TU of helper M13 phage for 40 minutes at 37°C. Plates were centrifuged at 1800g for 10 minutes at 4°C and media removed from each colony before resuspension in 200µl of 2xTY-Amp-Kan then growing overnight at 30°C at 150RPM. For ELISA, the same procedure as polyclonal was performed with the exception of wells receiving 70µl of supernatant from plates with 30µl of 2% milk-PBS.

2.2.10 PCR

Reaction mix was prepared as below in table 2.8.

Table 2.0.8 PCR reaction mix

Component	Volume per reaction (ul)
Q5 high fidelity DNA polymerase (NEB)	0.25
Q5 buffer	5.0

dNTPs (10mM) (NEB)	0.5
Forward primer (10uM)	1.25
Reverse primer (10uM)	1.25
GC enhancer (NEB)	5
PCR grade water (Sigma)	13.25

1ng of DNA made up to 25ul of PCR grade water (no DNA added to negative control). DNA/water mixture was then added to the reaction mixture. The DNA reaction mix then underwent PCR for 35 cycles according to the reaction kinetics below (table 2.9).

Table 2.9 PCR reaction kinetic cycle

	Initial denaturing	Cycle step 1: denaturing	Cycle step 2: annealing	Cycle step 3: extension	Final extension	Hold
Temperature (ºC)	98	98	72	72	72	4
Time (seconds)	30	10	20	20	120	∞

2.2.11 Agarose gel electrophoresis

A 1.5% agarose gel (0.75h high purity agarose into 50ml of 1x TAE (Geneflow with 1:10 000 SYBR safe DNA gel stain (Invitrogen)) was set up. Samples were loaded with 6x buffer (Promega). A 1kb ladder and a hyperladder iv (Bioline) were also loaded. The gel was run for 1 hour at 100V. An ultraviolet (UV) image was acquired of the gel using the BIO Imaging System machine. The desired band was excised using a scalpel.

2.2.12 Gel extraction of DNA

The scFv or plasmid DNA was extracted from the excised agarose band using the QIAgen gel extraction kit (QIAgen) according to manufactures instructions.

2.2.13 DNA digestion

Cla1 and Not1 (both Roche) DNA digestion was performed according to manufacturers instructions in buffer H (Roche). The DNA of a Clec14A specific CAR in the MP71 second-generation CAR vector incorporating a CD28 costimulatory domain also underwent Cla1 and Not1 digestion to remove the Clec14A scFv.

2.2.14 DNA ligation

DNA ligation was then used to ligate the ELTD1 scFv into the MP71 vector. For ligation, vector and scFv inert DNA ligated using T4 DNA ligase (NEB) according to manufactures instructions. Ligated DNA product was transformed into an eppendorf of supercompetent DH5α bacterial cells prepared in house. Cells were thawed on ice and 2ul of ligation DNA was added. Cells were incubated on ice for 30 minutes then placed in a water batch at 42ºC for 90 seconds before placing on ice again. 200ul of warm SOC medium was then added before incubating tubes for 1 hour at 37ºC, shaking at 200 RPM. Bacteria were then plated out onto LB-Amp agar plates and incubated at 37ºC overnight.

Colonies were picked the following morning and plasmid DNA was recovered using the QIAgen plasmid miniprep kit (QIAgen) according to manufacturers instructions. After confirmation of DNA sequence (see below), the QIAgen plasmid endotoxin free maxiprep kit (QIAgen) was performed according to manufactures instructions making a stock of ELTD1 CAR DNA.

SOC medium

- SOB (BD) media, supplemented with 2% filter sterilised 20% glucose (Sigma)

LB broth (1 litre)

- 10g (Bacto-Tryptone (BD)
- 5g Bacto-Yeast extract (BD)
- 10g NaCl (Sigma)
- 1 litre water
- with AMP (if specified) – 100µg Ampicillin (Roche)

LB agar

- as broth, with 15g bacteriological agar (Sigma) per 1L

2.2.15 DNA sequencing

1µl of Miniprep DNA (300ng), 3.2µl of primer (diluted to 1mM) and 5.8µl of PCR grade water (Sigma) were sent to the Functional Genomics and Proteomics Facility, School of Biosciences, University of Birmingham for sequencing. Here the DNA mix was mixed with 10ul of BigDye Reaction Mixture (Life technologies). Data was analysed using Snapgene software (GSL Biotech LLC).

2.2.16 Mouse GRIN2D production

$6x10^6$ cells were plated onto a 15cm culture plate (Corning) in 20ml of phoenix media. The following day, HEK 293T cells (Bicknell lab) were transfected with the mGRIN2D-Fc construct. Each 15cm plate of HEK 293T cells was transfected using 2ml of OptiMEM, 18ug of DNA and 72ul of PEI (from 1mg/ml stock) in 20ml of Phoenix cell medium and incubated at 37˚C for 48 hours.

The medium was replaced with 20ml of fresh phoenix media (without penicillin and streptomycin) and plate was incubated for 48 hours at 37˚C. From this timepoint, media was removed and replaced every 48 hours. The removed media was stored at 4˚C with EDTA and a few phenylmethylsulfonyl fluoride (PMSF) crystals (Sigma). After two weeks of supernatant collection, the supernatant was filtered using a 0.22um filter and mGRIN2D protein was purified using a protein A column.

2.2.17 Protein A purification

All protein-A steps performed at 4˚C.

A HiTrap protein-A column (GE healthcare) was flushed with 20% ethanol, washed with filtered distilled water then equilibrated with 20mM Na_2PO_4 pH7. Supernatant containing protein was then run through the column at 1ml/minute before washing with 20mM Na_2PO_4 pH7. Protein was eluted from the column using 100mM NaCitrate pH3 into 25 eppendorf tubes, with 500ul volume eluted into each tube. Each tube was then neutralised with 110ul of 1M TRIS-HCl pH 9.5. Each tube was analysed for the presence of protein using the protein A280 programme on a NanoDrop spectrophotometer ND1000.

2.2.18 Coomasie gel staining

20ul of each fraction along with 5ul of 5x loading buffer were added to wells of a NOVEX Tris-Glycine gel (Invitrogen). The gel was loaded into an electrophoretic tank with NOVEX Tricene SDS running buffer (Invitrogen). The gel was run at

180V for 1 hour. The gel was removed then coomasie stained in 0.5% coomassie Blue G-250 (Thermo) (prepared in 50% methanol/10% acetic acid) then destained in 40% methanol/10% acetic acid.

2.2.19 Western blot

Samples were loaded into a NOVEX Tris-Glycine gel (Invitrogen) with 5x loading buffer (Invitrogen) and appropriate ladder. The gel was loaded into an electrophoretic tank with NOVEX Tricene SDS running buffer (Invitrogen). Electrophoresis was performed for 1 hour at 180V. The gel was transferred to a PVDF membrane (Invitrogen) in NOVEX Tris-Glycine transfer buffer (Invitrogen) for 1 hour at 30V. After transfer, the PVDF membrane was blocked in 5% milk PBS 0.1% tween on a rocker at room temperature (RT) for 30 minutes. The membrane was washed in PBS-0.1% Tween for 5 minutes on a rocker at RT 3 times. After washing, the membrane was stained using the appropriate antibody (anti-Fc HRP at 1:1000 (Abcam); streptavidin HRP at 1:2500 (GE healthcare) diluted in PBS-0.1% tween on a rocker for 30 minutes at RT. The membrane was washed 3 times as before. Membrane was incubated in ECL reagent (GE Healthcare) for 1 minute before exposing the membrane to photographic film.

3. Results – in vitro function of ROBO4 CARs

3.1 An introduction to ROBO4

The roundabout family of proteins were first discovered in drosophila and have been implicated in neuronal axon guidance and development (Seeger et al. 1993; Kidd et al. 1998). The transmembrane ROBO proteins interact with large secreted proteins called SLIT proteins. During development of the nervous system, SLIT interaction with ROBO in axons induces repulsive signals to prevent excessive axon growth (Brose et al. 1999). Both SLIT and ROBO protein families are evolutionary conserved and are also found in vertebrates, including mammals (Brose et al. 1999). SLIT-ROBO signalling is now known to be involved in several different processes, including myogenesis (Kramer et al. 2001), leukocyte migration (Wu et al. 2001) and more recently, tumourigenesis (Legg et al. 2008).

There are 4 members of ROBO found in mammals. ROBO1, ROBO2 and ROBO3 are highly expressed in the developing nervous system (Park et al. 2003). The most recently discovered member, ROBO4, is unique in that it is not found within the nervous system but in the vasculature (Huminiecki et al. 2002). ROBO4 was first identified as an endothelial specific gene, expressed in areas of active angiogenesis. Later studies have also identified ROBO4 expression in haematopoietic stem cells (Forsberg et al. 2005; Smith-Berdan et al. 2011). Although haematopoietic stem cells expression is concerning for a anti-cancer target, it would be hoped that overall ROBO4 expression is lower in these rare cells than in tumour endothelium. Furthermore, ROBO4 may not be expressed on all haematopoietic stem cells, as ROBO4 knock-out mice have a normal blood cell differentiation and composition (Zhao et al. 2016). ROBO4 is also the smallest of the ROBO proteins. It contains 2 extracellular Ig domains and 2 extracellular fibronectin domains (figure 3.1). The Ig domains of human ROBO4 (hROBO4) are most similar to the first two Ig domains of human ROBO1 (Legg et al. 2008). ROBO4 also contains two conserved cytoplasmic motifs, CC1 and CC3, also found in ROBO1. However, the other two conserved cytoplasmic motifs of ROBO1, named CC0 and CC2, are no longer present in hROBO4 (Legg et al. 2008).

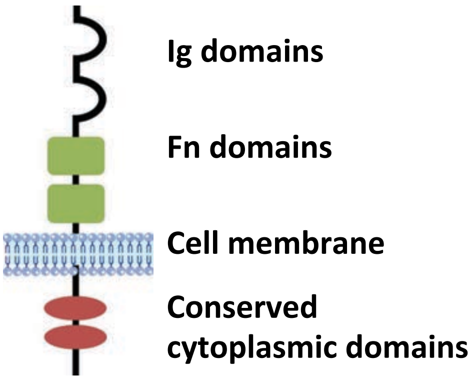

Figure 3.1: Human ROBO4. The image summarises the structure of ROBO4 with its two extracellular immunoglobulin (Ig) domains and two extracellular Fibronectin (Fn) domains. After spanning the cell membrane an intracellular domain contains two conserved cytoplasmic domains.

3.2 Function of ROBO4

The function of Robo4 in the endothelium has been investigated greatly since its discovery. Yet contrasting findings mean its function has become hotly debated. A role in angiogenesis seems clear. In zebrafish, ROBO4 was found to be expressed in tip and stalk cells of sprouting vessels (Bedell et al. 2005). Morpholino knockdown as well as overexpression of ROBO4 in zebrafish embryos both resulted in similar defects in intersomitic vessel sprouting including vessel positioning and sprout timing. Interestingly, the knockdown phenotype was rescued using hROBO4, suggesting a conserved evolutionary role in vascularisation. It should be noted that zebrafish ROBO4 contains three Ig domains and is also expressed within the nervous system, making this result less translatable.

ROBO1 expression has been reported in endothelium, and ROBO1-SLIT2 signalling promotes angiogenesis (Wang et al. 2003). Studies have also indicated that ROBO4 is pro-angiogenic. Sheldon et al. demonstrated in vitro that knockdown of ROBO1 or ROBO4 in HUVEC inhibited cell migration and tube formation in matrigel (Sheldon et al. 2008). Meanwhile, overexpression of ROBO4 increased filipodia formation in HUVEC, but not in the absence of ROBO1. ROBO1 and ROBO4 were also found to form a heterodimer together. Consistent with a role in cell movement, ROBO4 was found to interact with Wiskott-Aldrich Syndrome protein (WASP), an actin-regulating protein. The authors propose a model whereby a ROBO1/ROBO4 complex interacts with SLIT2 to promote actin directed cell movement. Here, ROBO1 is responsible for SLIT2 binding, and ROBO4 is responsible for signal transduction.

Kaur et al. found similar results with ROBO4 overexpression in cell lines (Kaur et al. 2006). ROBO4 overexpression increased active levels of the Rho family GTPases Cdc42 and Rac and enhanced cell adhesion and migration. Knockdown of ROBO4 in zebrafish resulted in lower active levels of the Rho GTPases Cdc42 and Rac in embryo lysates. Both the extracellular and cytoplasmic domains of ROBO4 were required for Cdc42 activation in endothelial cells. The Rho family

GTPases regulate various actin-dependent dynamics including cell migration (Hall 2012). Together, these results suggest ROBO4 acts as a chemosensory molecule to promote angiogenesis, helping to guide sprouting vessels.

In a later study the same authors found ROBO4 knockdown in endothelial cells had increased levels of active Cdc42 and Rac compared to control cells (Kaur et al. 2008). Serum-starved ROBO4 knockdown cells failed to migrate to serum, yet ROBO1 knockdown cells were unaffected. However, ROBO4 knockdown cells show a greatly increased migration towards SLIT2. SLIT2 was shown to bind to endothelial cells and this interaction was less efficient when ROBO4 was knocked down. Interestingly, SLIT2 had no effect on Rho GTPase activity in endothelial cells, suggesting that Rho GTPase activity is not involved in SLIT2-mediated inhibition of cell migration. The authors also found that ROBO1 and ROBO4 could interact together, according to immunoprecipitation with transfected cell lines. Together, the authors propose various models where serum and SLIT2 impose different signalling pathways through ROBO4 and ROBO1.

In contrast to Sheldon et al. 2008 and Kaur et al. 2006, multiple studies have suggested ROBO4 to inhibit angiogenesis. Park et al. overexpressed ROBO4 or SLIT2 in HEK293 cells (Park et al. 2003). ROBO4-expressing HEK293 cell migration towards SLIT2-rich media was greatly inhibited compared to control HEK293. Pre-incubating the SLIT2-rich media with soluble ROBO1 to deplete SLIT2 abolished this inhibition. After incubating cell lysates, ROBO4 and SLIT2 co-immunoprecipitated together, suggesting a direct SLIT2-ROBO4 interaction.

Furthermore, ROBO4 also co-immunoprecipitated with MENA, a known cytoplasmic signalling molecule in SLIT-ROBO signalling.

HUVEC overexpressed with ROBO4 were inhibited from migrating towards VEGF or FGF compared to control HUVEC (Seth et al. 2005). HUVEC migration towards VEGF was inhibited when the media was conditioned with SLIT2. The addition of soluble extracellular ROBO4 abolished the inhibitory effect of SLIT2 addition. The phosphorylation of focal adhesion kinase (FAK) is an important step in FGF mediated cell migration (Schlaepfer et al. 2000). ROBO4 overexpressing HUVEC had a decrease in FAK phosphorylation. SLIT2 treatment also resulted in a reduced FAK phosphorylation in control HUVEC, an effect that was reversed with the addition of soluble ROBO4. Similarly, it's been shown that knockdown of ROBO4 in HUVEC facilitates a SLIT2-ROBO1 mediated migration (Enomoto et al. 2016).

Jones et al. used ROBO4 knockout mice for two models of pathologic eye disorders (Jones et al. 2008). Corneal injection of SLIT2 inhibited the VEGF-mediated angiogenic response and leakage of vessels in control mice. This inhibition was not present in ROBO4 knockout mice, suggesting SLIT2 works in a ROBO4-dependent manner. In sites of retinal angiogenesis, ROBO4 was found more within the stalk cells rather than tip cells, which contrasts with the consensus of ROBO4 acting as a chemosensory and guidance molecule for sprouting vessels. Other studies have also reported that SLIT2 signals through ROBO4 in the endothelium to inhibit VEGF-mediated angiogenesis in vivo

(London et al. 2010; Marlow et al. 2010) and in vitro (Yu et al. 2014). Thus ROBO4 appears to function in stabilising the vasculature in these models.

It has been demonstrated that SLIT2-ROBO4 signalling in endothelial cells recruits the GTPase activating protein GIT1 (Jones et al. 2009). This induces GTP hydrolysis in the GTPase ARF6. This inactivates ARF6, which in turn reduces the activation of Rac, thereby maintaining the integrity of endothelium (Jones et al. 2009). Mouse models of breast cancer have shown increased tumour growth and metastasis in ROBO4 knockout mice (Zhao et al. 2016). Knockout of ROBO4 resulted in increased angiogenesis, vessel leakage and decreased endothelial tight junction protein ZO-1. By treating mice with a small drug to inhibit ARF6 activation, tumour growth was reduced and ZO-1 was increased in endothelial cells. The authors proposed that the small drug enhances ROBO4's downstream signalling to inhibit angiogenesis within the tumour.

Despite these reports of SLIT2-ROBO4 interaction, there is considerable evidence against this interaction. Suchting et al. also found soluble ROBO4 to inhibit angiogenesis *in vivo* in the mouse sponge assay and rat aortic ring assay. It also inhibited HUVEC proliferation and migration (Suchting et al. 2004). However, Biacore and immunoprecipitation analysis failed to show SLIT1, 2 or 3 interacting with ROBO4, though all SLIT proteins interacted with ROBO1. This is in direct contrast to Park et al who found Slit2 and ROBO4 to co-immunoprecipitate. One reason for this difference may be that Suchting et al. used a harsher detergent in their assay, making a ROBO4-SLIT2 interaction unfavourable. Despite this, the Biacore analysis from Suchting et al. is a more sensitive assay, yet never recovered any ROBO4-SLIT interaction. It's also possible that any ROBO4-SLIT2 interaction requires a co-receptor, such as ROBO1 (Sheldon et al. 2008). The co-receptor would also have to be present to allow detection of any ROBO4-SLIT2 interaction

A study using conditional genetic knockouts of ROBO and SLIT gene found that, in the post-natal retina of mice, SLIT2 promotes angiogenesis through ROBO1 and ROBO2 and loss of ROBO4 had no effect in this model (Rama et al. 2015). ROBO1 and ROBO4 share 42% sequence identity in the N-terminal Ig domains. Yet, ROBO4 is missing the sequences responsible for strengthening the SLIT2 interaction in ROBO1 (Fukuhara et al. 2008). It's also been suggested that ROBO4 can only bind weakly to SLIT2 (Hohenester et al. 2006). Furthermore, in zebrafish embryos, SLIT2 and ROBO4 expression did not overlap at any time (Bedell et al. 2005).

Koch et al found that ROBO4 interacted with another transmembrane receptor, UNC5B. UNC5B is expressed within endothelium and has previously been shown to inhibit angiogenesis (Lu et al. 2004). It was shown that ROBO4 acts as a ligand for UNC5B and that ROBO4-UNC5B signalling inhibits downstream VEGF signalling and maintains vessel integrity (Koch et al. 2011). ROBO4 was also shown not to interact with SLIT2, whereas ROBO1 did interact with SLIT2.

SLIT3 has also been found to interact with ROBO4 (Zhang et al. 2009), despite reports of ROBO4 failing to bind SLIT3 on the Biacore (Suchting et al. 2004). SLIT3 is expressed in endothelial cells and was found to interact with both

ROBO1 and ROBO4. SLIT3 was capable of inducing endothelial cell migration and this was inhibited by an anti-ROBO4 antibody, but not by an anti-ROBO1 antibody (Zhang et al. 2009). SLIT3 secreted by mouse mesenchymal stem cells was also capable of inducing and directing endothelial cell migration in a ROBO4-dependent manner in a transplant model (Paul et al. 2013).

Taken together, many of these studies contradict each other and it's difficult to conclude the function of ROBO4 in endothelial cells. However, some functions may be context dependent. Zhaung et al. propose a context dependent model of ROBO4 function in endothelial cells (Zhuang et al. 2011). During angiogenic sprouting, the expression of ROBO4 in the tip cell functions in a proangiogenic manner where it acts as a chemosensory molecule to guide sprouting vessels. Whereas low levels of ROBO4 in resting endothelium acts to maintain vessel integrity by inhibiting angiogenic signals. Here ROBO4 may interact with UNC5B on adjacent endothelial cells.

Similarly, the function of SLIT2 on ROBO1/ROBO4 signalling may also depend on context. SLIT-ROBO GTPase activating protein (srGAP) has been shown to interact with the CC3 domain of ROBO1 and it functions to increase the hydrolytic activity of Cdc42 (Yadav & Narayan 2014). This increases the conversion of GTP into GDP, leading to inactive Cdc42. Inactive Cdc42 leads to reduced actin polymerisation and reduced cell movement. Similarly, GTPase activating protein VILSE can interact with ROBO4 and leads to inactive Cdc42 (Kaur et al. 2008). Yadav and Narayan propose that, in the context of ROBO1/ROBO4 heterodimers, srGAP is prevented from binding ROBO1, and

VILSE is prevented from binding ROBO4, thus keeping Cdc42 in its active, GTP-bound state and allowing actin polymerisation and cell movement. In this context, SLIT2 signalling promotes cell movement in a ROBO4-dependent manner.

3.3 ROBO4 in tumour endothelium

ROBO4 has been found to be upregulated within the endothelium of multiple different tumours (Huminiecki et al. 2002; Seth et al. 2005; Mura et al. 2012; Zhao et al. 2016; Gröne et al. 2006). Huminieki et al. identified ROBO4 expression in the endothelium of colorectal liver metastasis, ganglioglioma, bladder and breast cancer sections according to immnohistochemistry (Huminiecki et al. 2002). Various normal adult tissue sections, including the liver, brain, colon and prostate, were all absent of ROBO4 expression. Seth et al. used immunohistochemistry to identify high ROBO4 expression in the vessels of tumour tissues including metastatic melanoma, lung, kidney and liver cancers (Seth et al. 2005). Its relative expression in normal tissues was far lower. Another study using qPCR found endothelial ROBO4 to be overexpressed in 72% (36/50) of patients with colorectal cancer compared with normal tissue (Gröne et al. 2006). 44% of these patients (22/50) had a 2-fold and 16% (8/50) had a 4-fold overexpression in the tumour tissue. Mura et al. compared tissue sections from normal and cancerous tissues (Mura et al. 2012). Immunostaining consistently identified ROBO4 expression in the vessels from over 80% of pancreatic and bladder cancer sections and over 60% of stomach, prostate, lung and kidney cancer sections (the number of patients/sections was not provided). ROBO4 was absent in normal tissues in this study.

None of these studies provided any quantifiable level of ROBO4 expression, only identifying that the relative expression is increased in cancerous tissues compared to normal tissues.

Given the low level or absence of ROBO4 expression found in normal adult tissues, ROBO4 could be described as a tumour endothelial marker. Little is known about the function of ROBO4 within tumour endothelial cells, but studies have indicated ROBO4 may function to inhibit tumour angiogenesis. A recent study found that endothelial ROBO4 expression inhibits breast cancer growth and metastasis in a mouse model (Zhao et al. 2016). Hypoxia-induced epigenetic changes in expression within human germ cell tumours results in an increase in angiogenesis (Ueda et al. 2014). One of these changes included a downregulation of ROBO4, indicating to the authors a potential role in suppression of angiogenesis. In vitro, glioma-conditioned media was capable of inducing endothelial cell proliferation, migration and tube formation (Cai, Xue, Li, et al. 2015). This effect was significantly reduced when ROBO4 was overexpressed in the endothelial cells. Here ROBO4 suppressed the VEGR2-mediated PI3K and FAK pathways. Additionally, incubating endothelial cells in glioma-conditioned media caused a reduction in ROBO4 expression.

Despite this, a higher expression of ROBO4 within human glioma tumours correlated with poorer prognosis (Cai, Xue, Liu, et al. 2015). ROBO4 mRNA levels also correlated with an increased microvessel density, a reflection of angiogenesis. In contrast, increased endothelial ROBO4 expression within early stage non-small cell lung cancer correlated with an increased survival (Pircher et al. 2013). Also, lower ROBO4 expression within tumours has been found at the time of cancer progression compared with stable disease after patients underwent anti-angiogenic therapy (Pircher et al. 2016).

The expression of ROBO4 can be regulated by shear stress (Mura et al. 2012). When HUVEC are cultured in vitro under static conditions, ROBO4 is highly expressed. When HUVEC are cultured under flow conditions at a pressure of 2Pa, comparable to that in large vessels, almost 100% of the ROBO4 expression was inhibited. Tumour blood vessels are typically poorly formed and leaky. Therefore blood flow in these vessels is also poor, occasionally even static or reversed (McDonald & Choyke 2003; Jain 1988). Shear stress has also been accounted to regulate 3% of genes in endothelial cells (Chu & Peters 2008). Although the function of ROBO4 within tumour endothelium may not be well known, its consistently high expression within multiple different tumours make it an attractive anti-angiogenic or anti-cancer target.

Internalising antibodies conjugated to toxins have been generated against VEGR2 and ROBO4 (Yoshikawa et al. 2013). The internalisation of these antibodies induced significant anti-tumour effects. This was the first report of a ROBO4-targeted anti-cancer therapy. Crucially, although VEGFR2 antibodies caused some toxicity, no toxicity was seen with ROBO4 antibodies. Another study vaccinated mice with ROBO4, which induced a strong ROBO4 antibody response (Zhuang et al. 2015). Vaccinated mice exhibited a reduced growth of Lewis lung carcinoma. This reduction was dependent on B cells and IgG1, but not

CD8 T cells. Again, there were no signs of toxicity due to ROBO4 vaccination. Furthermore, wound healing was not affected.

3.4 Tumour-related ROBO4 expression in non-vasculature tissue

ROBO4 expression has also been reported in HSCs where it functions to facilitate homing to the bone marrow through CXCR4 (Smith-Berdan et al. 2011). Interestingly, leukemic stem cells have also been reported to express ROBO4 (Forsberg et al. 2005) and an increased ROBO4 expression within the bone marrow correlated to poorer prognosis in AML patients (Chen et al. 2015). ROBO4 is also expressed within the endothelial cells of the bone marrow (Smith-Berdan et al. 2012) where it has a role in localising HSCs at this site. Together, ROBO4 within leukemic cells and within bone marrow endothelium may play a role in preventing leukemic stem cell mobilisation and protection from chemotherapy by keeping leukemic cells within the bone marrow niche.

3.5 Redirecting T cells to target ROBO4 using chimeric antigen receptors (in vitro studies)

ROBO4 is a potential TEM which has been found to be overexpressed within the endothelium of multiple different cancers (Huminiecki et al. 2002; Mura et al. 2012). However, nobody has attempted to target T cells to ROBO4. In this study, two CARs are created to redirect T cell specificity to ROBO4. Retroviral transduction is an efficient and well-established way to transfer transgenes into T cells. The vector MP71 has previously been shown to provide high transgene expression in both human and mouse T cells (Engels et al. 2003). The Lee lab has previously used this vector to generate first and second generation CAR constructs. Since second generation CARs have consistently outperformed first generation CARs, it was decided that only second generation ROBO4 CARs would be generated for this study.

Roche provided the sequences for two humanised monoclonal murine antibodies. Both antibodies are cross-reactive to human and mouse ROBO4 and both recognise separate epitopes (personal communication, Roche). The scFv DNA for each antibody was then synthesised by a commercial company (Integrated DNA Technologies, USA). The DNA sequences were then cloned into a previously generated second generation CAR within an MP71 retroviral vector, replacing the original scFv. The two generated CAR constructs (figure 3.2a) were named R1 and R2 for all future experiments. Both R1 and R2 CAR vectors contain a truncated, non-signalling human CD34 domain (Fehse et al. 2000). This serves as a tag to detect successful CAR vector expression, since CD34 is not normally found on T cells. The CD34 domain is linked to the CAR domain through the self-cleaving peptide 2A linker from the Foot and Mouth Disease Virus (Szymczak et al. 2004). The peptide 2A linker allows both CD34 and the CAR to be expressed at a 1:1 ratio through a ribosomal skipping mechanism. Detection of the CD34 domain on the T cell surface is therefore a marker of successful CAR vector transduction.

In order to transduce human T cells, PBMCs are first activated with anti-CD3 and anti-CD28. This activation of T cells can then allow transduction with the recombinant retrovirus, uptake of the MP71 vector and subsequent transgene expression of CAR DNA. Although not specifically sorted for T cells, the activation process and culture conditions mean the majority of cells present after a few days of culture are T cells. Human T cells were transduced with R1 and R2 vectors or mock transduced without any DNA. Three days later, cells were analysed for CD34 surface detection using flow cytometry (figure 3.2b). Both R1 and R2 CAR transduction resulted in a high frequency of CD34 positive cells compared to mock transduced T cells. Of the CAR transduced T cells, many show a high mean fluorescent intensity of CD34 expression, suggesting a high level of CAR expression. A high level of CAR expression may be important, since T cells expressing a low number of TCR molecules had poor function (Labrecque et al. 2001).

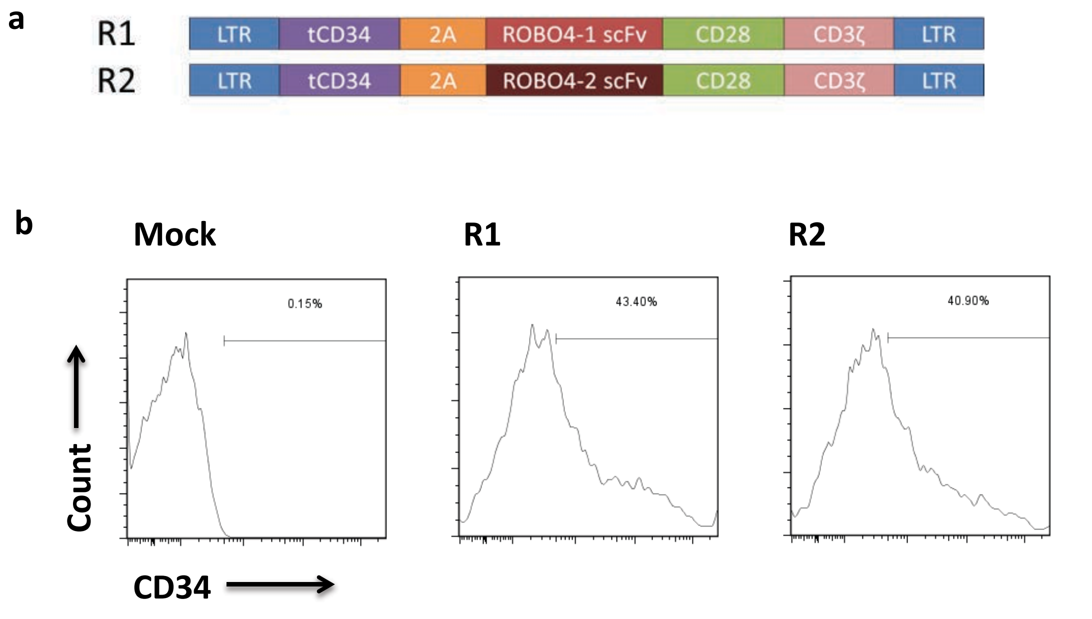

Figure 3.2: R1 and R2 CAR constructs. (a) the DNA constructs for both the R1 and R2 CARs are shown. Both contain and N and C terminus long terminal repeats (LTR). A truncated CD34 (tCD34) domain acts as an extracellular tag. tCD34 is linked to the CAR through the peptide 2A linker (2A). The CAR DNA contains the ROBO4 specific scFv domain. This is followed by the CD28 transmembrane and intracellular signalling domain (CD28), then the CD3ζ signalling domain (CD3ζ). (b) Human PBMCs have been activated with anti-CD3 and anti-CD28. Two days later they have been transduced with the R1 or R2 CAR DNA or mock-transduced with no DNA as a control. The flow cytometry plots show PBMCs that have been gated for a viability marker then gated with a lymphocytes gate. These cells have been analysed for CD34 expression as a marker for CAR surface expression. The CD34 gate was set using the mock-transduced cells. Result is representative of eight independent experiments.

3.6 Testing ROBO4 specific CAR T cell function

3.6.1 IFNγ production

The ability of R1 and R2 expressing human T cells to specifically respond to ROBO4 was tested in a variety of in vitro functional assays. IFNγ is a pro-inflammatory cytokine that is produced by Th1 cells, cytotoxic T cells and natural killer cells (Ikeda et al. 2002). IFNγ production has essential roles in immune protection to intracellular infections as well as tumour control (Ikeda et al. 2002). An in vitro production of IFNγ in response to ROBO4 would therefore be indicative of a potential anti-tumour function in vivo.

R1 and R2 transduced T cells were prepared for the assay by ensuring they had the same transduction level by diluting one or the other with mock-transduced T cells. R1, R2 or mock T cells were incubated with an increasing concentration of human or mouse recombinant extracellular ROBO4 protein prebound to maxisorp plates. After overnight culture, the supernatant was tested for the presence of IFNγ. IFNγ was below 200pg/ml for T cells cultured alone (data in appendix) and for recombinant protein cultured alone (data not shown) and can be considered background levels. As seen in figure 3.3a and 3.3b, both R1 and R2 T cells produced IFNγ in response to human or mouse ROBO4 protein whereas mock T cells produced only background levels. There was an increased detection of IFNγ as ROBO4 protein concentration was increased until detection plateaued at or just above 1ug/ml of protein. Greater levels of IFNγ were detected from R2 T cells compared to R1 T cells in response to both human and mouse protein. T cells expressing the R1 CAR showed similar levels of response to ROBO4 derived from both human and mouse, whereas T cells expressing R2 showed a stronger response to the human protein at all concentrations from as little as 0.03ug/ml. However, the half maximal IFNγ concentration was achieved at the same protein concentration of around 0.3ug/ml for human.

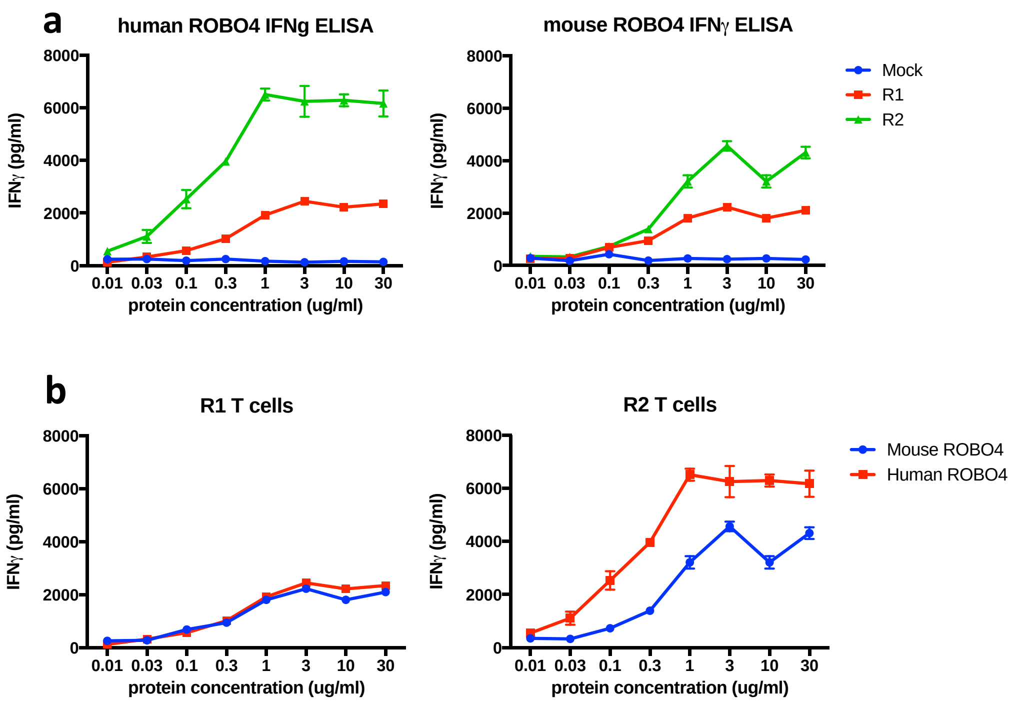

Figure 3.3: IFNγ response to recombinant human and mouse ROBO4 protein. R1 and R2 CAR Transduced R1 and R2 T cells were matched for transduction percentage by dilution with mock-transduced T cells. R1, R2 and mock-transduced T cells were incubated with an increasing concentration of recombinant human or mouse extracellular ROBO4 protein. After an overnight incubation the supernatant was analysed for IFNγ production. (a) shows the comparison of mock, R1 and R2 transduced T cells to either human or mouse protein. (b) shows the same data but with a direct comparison of mouse and human protein incubated with R1 or R2 T cells. Data is the mean of triplicate wells with error bars showing the standard deviation (SD). Result is representative of three individual experiments.

These data not only demonstrate that both CARs are functional when expressed in human T cells, but also that they respond to both mouse and human forms of the ROBO4 protein. However, in these assays the recombinant protein has been adsorbed onto plastic wells. The adsorption of protein onto plastic may cause the protein to denature and lose its native confirmation. Since the CAR T cells will need to recognise native ROBO4 expressed on tumour endothelial cells in vivo, the ability of T cells to produce IFNγ in response to cell lines expressing the target protein was investigated. CHO cells have previously been stably transfected with human ROBO4 protein and were provided by the Bicknell lab. HUVEC are human endothelial cells derived from umbilical cord. It's previously been shown that when HUVEC are growing under static conditions in vitro, they naturally express ROBO4 (Mura et al. 2012).

R1 and R2 transduced T cells were equalised for transduction levels by dilution with one or the other with mock-transduced T cells. R1, R2 and mock-transduced T cells were incubated with wild type CHO (CHO WT), human ROBO4 expressing CHO cells (CHO MRFL) or HUVEC target cells. After overnight incubation, the supernatant was tested for the presence of IFNγ. IFNγ was for all T cells cultured alone at the highest dose and for target cells cultured alone were less than 500pg/ml and were considered background level (T cell data in appendix). Mock T cells at all T cell doses produced background levels of IFNγ to all three target cells (figure 3.4). R1 and R2 T cells at all doses also produced background levels of IFNγ in response to CHO WT cells (figure 3.4).

Both R1 and R2 CAR T cells responded well to ROBO4 expressing cells lines. Although only low levels of IFNγ are detected from R1 T cells at the lowest dose in response to CHO MRFL and HUVEC cells, all three increasing doses resulted in high levels of IFNγ to a maximum of 7000pg/ml. Low to background levels of

IFNγ were also detected at the lowest dose of R2 T cells to CHO MRFL and HUVEC. Moderate levels of IFNγ were then detected at the three higher doses to a maximum of 3400pg/ml.

The high R1 T cell IFNγ levels were roughly double that of levels detected with R2 T cells to both CHO MRFL and HUVEC at the three highest T cell input number. This was surprising since R2 T cells gave a stronger IFNγ response to recombinant ROBO4 protein. This may be due recombinant ROBO4 undertaken an unnatural confirmation when adsorbed onto plastic compared to when it is expressed on the cell surface. As both R1 and R2 CARs are derived form antibodies recognising different epitopes, its possible these epitopes may be presented differently between an adsorbed and cell surface expression confirmation. Recombinant extracellular protein may also lack normal glycosylation found in the full length, cell surface expressed ROBO4. Ultimately, these data demonstrate that both R1 and R2 T cells can detect ROBO4 on the cell surface of target cells.

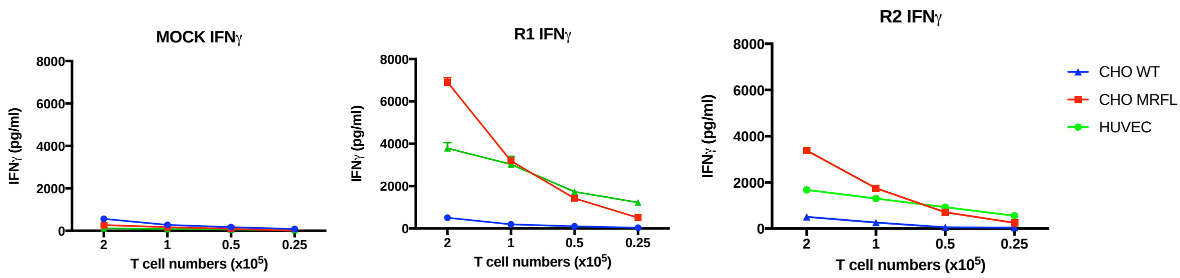

Figure 3.4: IFNγ ELISA to T cells incubated with target cells. R1 and R2 CAR Transduced T cells were matched for transduction percentage by dilution with mock-transduced T cells. R1, R2 and mock-transduced T cells were incubated at decreasing concentrations with the cell lines CHO WT, CHO MRFL or HUVECs overnight. The supernatant was then analysed for the presence of IFNγ. Data is the mean of triplicate wells with error bars shown the (SD). Result is representative of four individual experiments

3.6.2 Testing for multiple cytokine production

Rather than rely on IFNγ production alone, further experiments explored additional functional responses of these engineered T cells to assess their potential anti-tumour efficacy (Seder et al. 2008). The ability of T cells to produce multiple cytokines has been associated with a more effective immune response to infectious disease and vaccines (Darrah et al. 2007; Caccamo et al. 2010; Betts et al. 2006; Precopio et al. 2007; Lindenstrøm et al. 2009; Duvall et al. 2008). Data has also suggested that CD4 T cells that only produce IFNγ are much less likely to form memory cells than IL2 or IL2 and IFNγ producing cells in vivo (Younes et al. 2003; Reece et al. 2004; Hayashi et al. 2002). For this reason, intracellular cytokine staining (ICCS) was performed for the Th1 polarised cytokines IFNγ, TNFα and IL2. R1 and R2 transduced T cells were equalised for transduction levels by dilution of one or the other with mock-transduced T cells. R1, R2 and mock-transduced T cell were incubated overnight with CHO WT or CHO MRFL cells. T cells were then removed and analysed for cytokine production by ICCS. The gating strategy for ICCS analysis along with representative FACs plots are shown in figures 3.5 and 3.6 for R1 CAR T cells incubated with CHO MRFL and CHO WT respectively.

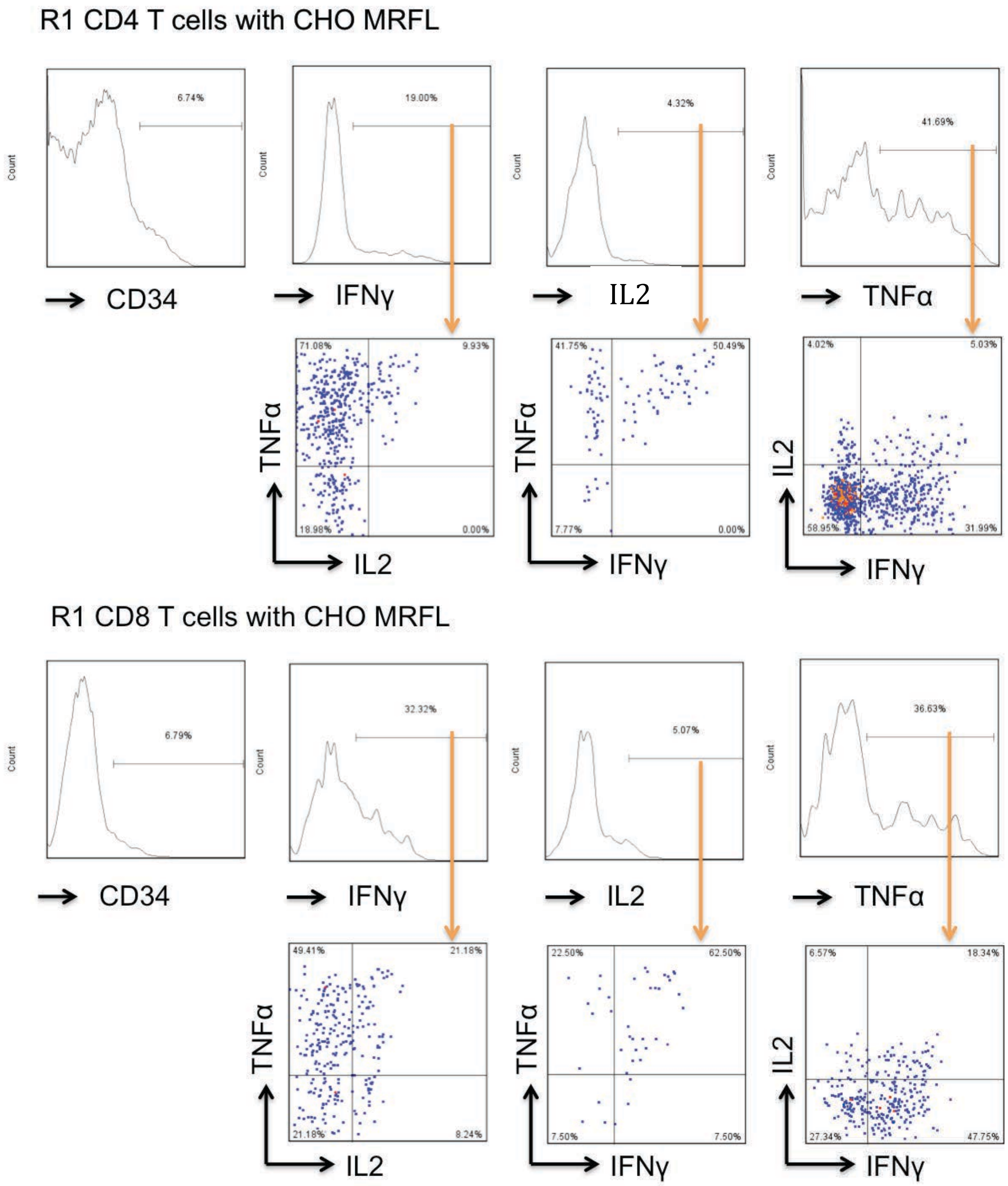

Figure 3.5: gating strategy for ICCS with representative plots for R1 CAR T cells with CHO MRFL. Cells have been gated for lymphocytes; single cells then live cells using a viability marker (not showing). CD34-expressing T cells (CAR transduced) have been gated. Within the CAR T cells gate, IFNγ, TNFα or IL2 positive cells have been gated for. From the cytokine positive gates, the proportion of these cells that also produce another cytokine gated for. All gates have ben set using fluorescence minus one controls to set gates for each fluorescent marker. Results are representative of three individual experiments.

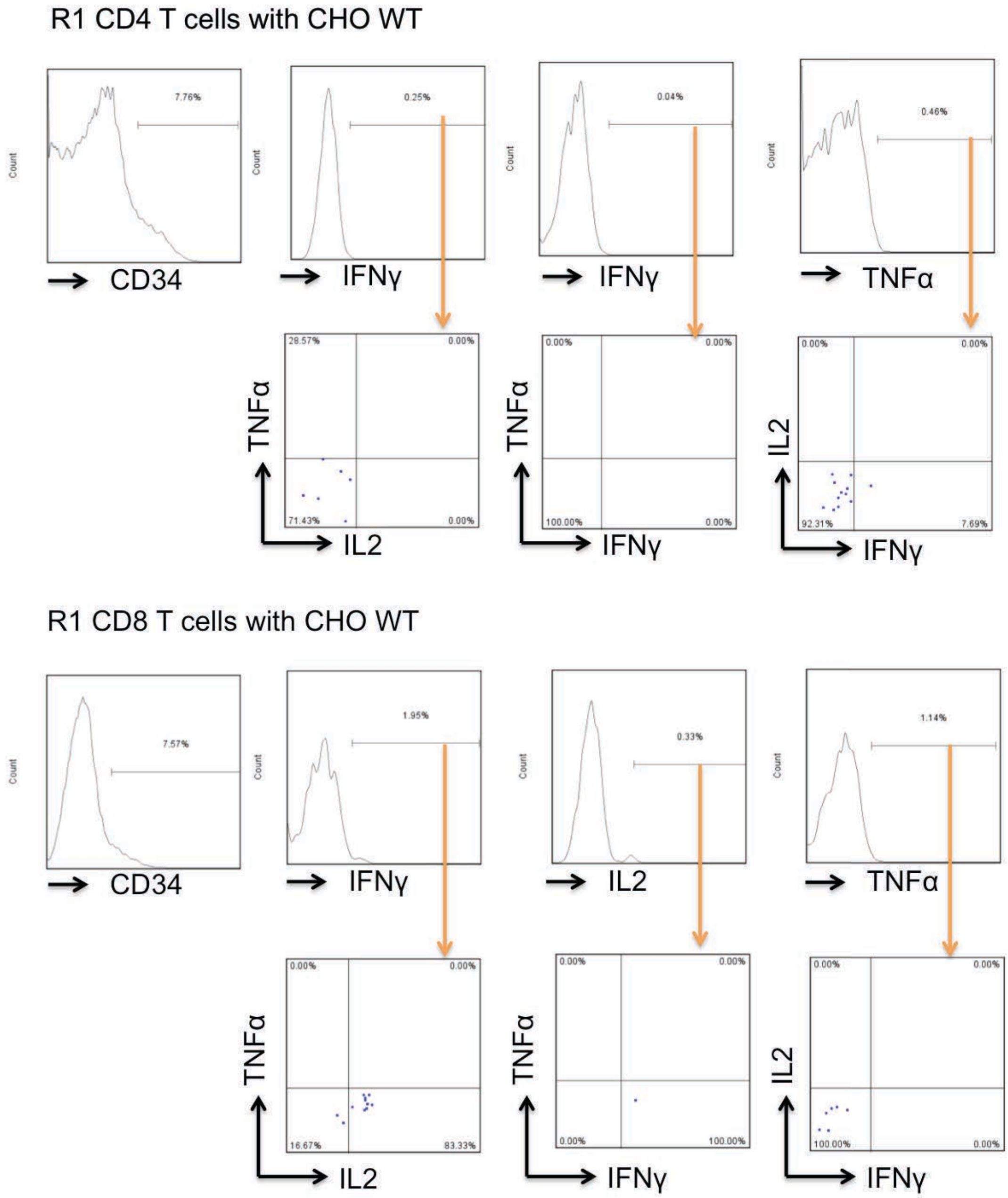

Figure 3.6: gating strategy for ICCS with representative plots for R1 CAR T cells with CHO WT. Cells have been gated for lymphocytes, single cells then live cells using a viability marker (not showing). CD34-expressing T cells (CAR transduced) have been gated. Within the CAR T cells gate, IFNγ, TNFα or IL2 positive cells have been gated for. From the cytokine positive gates, the proportion of these cells that also produce another cytokine gated for. All gates have ben set using fluorescence minus one controls to set gates for each fluorescent marker. Results are representative of three individual experiments.

Single cytokine production

A monofunctional T cell, one that produces only a single type of cytokine is this assay, can be deciphered using the gating strategy described in figures 3.5 and 3.6. Less than 0.5% of mock T cells were positive for any tested cytokine to CHO WT or CHO MRFL (figure 3.7a-b), however mock T cells did respond with cytokine production to the positive control SEB (data not shown). R1 and R2 CAR T cells showed a minimal cytokine response to CHO WT (figure 3.7c-f). However, a large proportion of R1 and R2 CAR T cells produced a single cytokine in response to CHO MRFL (figures 3.7c-f). Of these monofunctional T cells, most produced TNFα. Only a small proportion produced only IL2.

Double cytokine production

Although the majority of CAR T cells showed a monofunctional cytokine response to CHO MRFL, many are also double positive. Looking at double positive cytokine production, a higher frequency of CAR T cells produce IFNγ and TNFα together compared to any other double cytokine combination (figure 3.8a-b). IFNγ and TNFα double positives made up around 14% of R1 CAR CD4 and 16% R1 CAR CD8 T cells in response to CHO MRFL. The proportion of IFNγ and TNFα double positives was smaller in R2 CAR T cells, with around 8% of CD4 CAR and 7% of CD8 CAR cells in response to CHO MRFL. Only a small proportion of CAR T cells are double positive for IFNγ and IL2 or TNFα and IL2 in response to CHO MRFL.

Triple cytokine production

The ability of T cells to produce IFNγ, IL2 and TNFα simultaneously has been associated with improved effector function in vivo (Darrah et al. 2007). A small but detectable proportion of R1 and R2 CAR T cells produce all three cytokines simultaneously in response to CHO MRFL (figure 3.8c-d). Around 2% of R1 CAR CD4 T cells and around 7% of R1 CAR CD8 T cells are triple positive. Again, this proportion is much less in R2 CAR T cells with less than 1% of CD4 and around 1% of CD8 CAR T cells positive for all three cytokines. Despite the low frequency of triple cytokine producing cells, the fact that at least some engineered cells possess this phenotype suggests they may mediate enhanced anti-tumour effects in vivo.

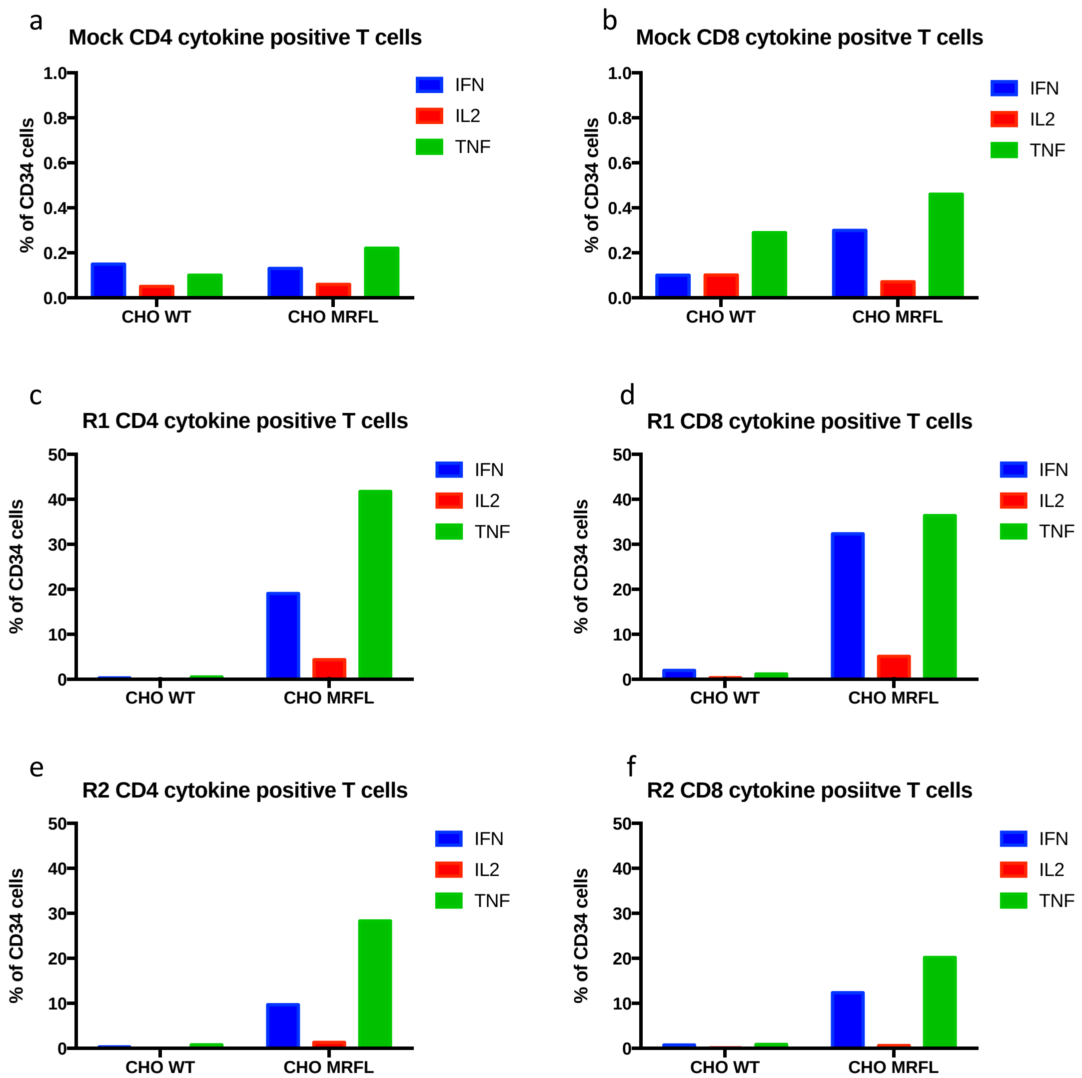

Figure 3.7: production of single cytokines by CD4 and CD8 CAR T cells. R1 and R2 CAR Transduced T cells were matched for transduction percentage by dilution with mock-transduced T cells. Mock, R1 or R2 transduced T cells were incubated with the cell lines CHO WT or CHO MRFL overnight. T cells were stained for surface markers then permeabilised before intracellular cytokine staining was performed for IFNγ, TNFα and IL2. Data shows the percentage of CD34 (transduced) CD4 or CD8 T cells that are expressing only a single cytokine in response to CHO WT or CHO MRFL. Data is from a single well from a single assay. Results are representative of three individual experiments.

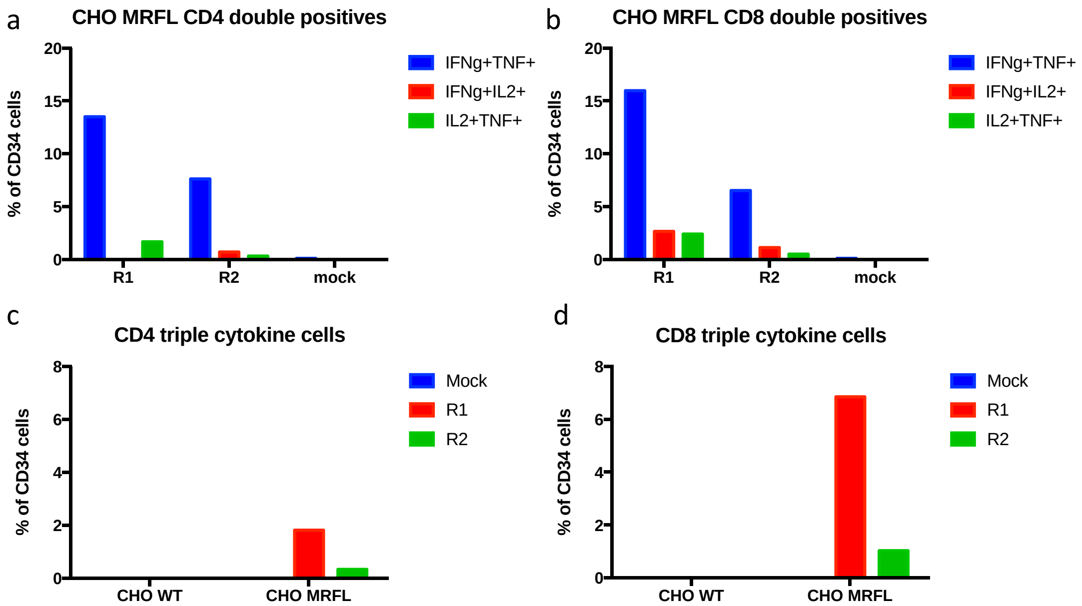

Figure 3.8: multicytokine production by CAR T cells. R1 and R2 CAR Transduced T cells were matched for transduction percentage by dilution with mock-transduced T cell. Mock, R1 or R2 transduced T cells were incubated with the cell lines CHO WT or CHO MRFL overnight. T cells were stained for surface markers then permeabilised before intracellular cytokine staining was performed for IFNγ, TNFα and IL2. Data shows the percentage of CD34 (transduced) CD4 or CD8 T cells that are expressing only two cytokines (a-b) or produced all three cytokines (c-d) in response to CHO WT or CHO MRFL. Data is from a single well from a single assay. Results are representative of three individual experiments.

3.6.3 Cytotoxic function

Another potential indicator of anti-tumour efficacy is the ability of the T cell to kill target cells. The target cells CHO WT, CHO MRFL and HUVEC, were labelled with a radioactive isotope of chromium (Cr51). R1, R2 or mock-transduced T cells (With R1 and R2 CAR T cells transduction levels matched) were incubated with these target cells at T cell to target cell ratios of 5:1, 10:1 and 20:1. The release of chromium from labelled target cells is indicative of target cell lysis. Therefore after incubation for 8 hours, levels of radioactivity present in the culture supernatants were quantified. Background levels of lysis to CHO WT target cells were seen with all T cells tested (figure 3.9). However, R1 and R2 CAR T cells showed increased levels of lysis of CHO MRFL, reaching greater than 60% of target cells at the highest T cell to target cell ratio (figure 3.9). R1 and R2 CAR T cells also showed a small to moderate level of HUVEC lysis at the two highest T cell to target cell ratios. Target cell lysis by mock T cells remained at background levels at all effector:target ratios with CHO MRFL and HUVEC target cells.

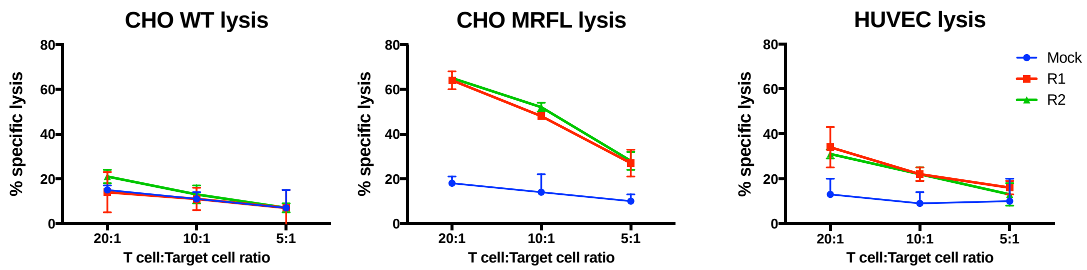

Figure 3.9: Chromium release assay. The target cells CHO WT, CHO MRFL or HUVEC were pre-labelled with ^{51}Cr. Labelled Target cells were then incubated with either Mock, R1 or R2 transduced T cells at different ratios for 8 hours. The % specific lysis was measured for all T cells and the target cells. Data shows the mean value from triplicate wells with the SD. Results are representative of four independent experiments.

3.6.4 T cell proliferation

The ability of T cells to proliferate in response to specific antigen stimulation is another property that is likely to be important for effective anti-tumour responses. If cells fail to proliferate in response to tumour antigen they may never reach the required numbers to be effective. R1, R2 or mock-transduced T cells (with R1 and R2 CAR T cells transduction levels matched) were pre-labelled with CFSE. Labelled T cells were then incubated for 4 days with the target cells CHO WT or CHO MRFL or in T cell media alone. A reduction in CFSE staining is indicative of cell division. Mock-transduced T cells showed no difference in CFSE levels in response to either target cell or media alone (figure 3.10a-b). However, R1 and to a lesser extent R2 T cells exhibited a clear and specific reduction in CFSE staining in response to CHO MRFL but not CHO WT. To explore T cell proliferation over a longer period and following repeated encounters with antigen, the No scFv CAR vector was included in a repeated stimulation experiment. The No scFv CAR vector is derived from the same CAR constructs as R1 and R2, but it lacks the scFv domain. Therefore, the No scFv CAR cannot bind the target antigen, but it still contains the CD34 tag (and CD28/CD3zeta signalling domains). This means that No scFv CAR T cells can be identified and tracked just like the R1 and R2 CAR T cells.

R1, R2 or No scFv transduced T cells (transduction levels matched to 33% (data not shown)) were incubated with plate bound human ROBO4 recombinant protein from day 0 to day 2. T cells were then removed from the stimulation plate and resuspended onto a new plate without antigen. On day 7, T cells were counted then resuspended again with plate bound human ROBO4 for two days. T cells were again removed from the stimulation plate and resuspended onto a new plate without antigen. T cells were counted again on day 14 and restimulated with ROBO4 protein for 2 days. T cells were counted for a final time on day 21. Throughout the experiment, 50U/ml of IL2 was used in the culture media.

After one round of ROBO4 stimulation, both R1 and R2 T cells have increased two-fold (figure 3.10c). After two rounds of ROBO4 stimulation, R1 T cells have increased almost 5 fold and R2 T cells have increased over 3 fold. However after three rounds of stimulation, R1 and R2 T cells have begun to contract in number. In contrast, No scFv T cells fail to proliferate in response to ROBO4 stimulation and slowly decrease in number throughout the experiment. The proliferation of R1 and R2 T cells is in response to the ROBO4 protein since in the absence of this protein, they fail to expand, in the same way as T cells expressing the no scFv CAR control (figure 3.10d).

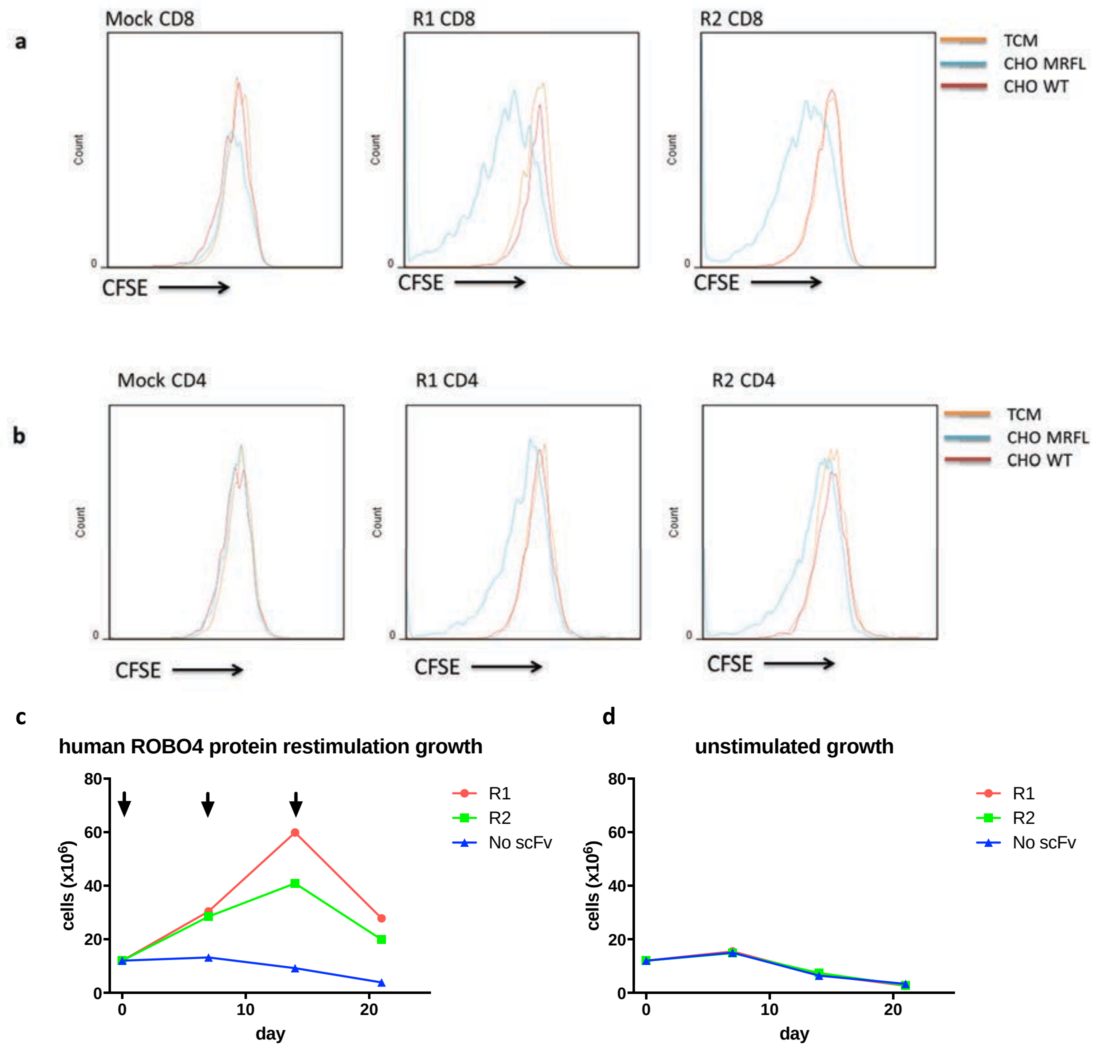

Figure 3.10: proliferation of CAR T cells in response to antigen. (a-b) R1 and R2 CAR Transduced R1 and R2 T cells were matched for transduction percentage by dilution with mock-transduced T cell. Mock, R1 or R2 transduced T cells were labelled with CFSE then incubated with the cell lines CHO WT or CHO MRFL or in T cell media alone for four days. The levels of CFSE were measured again for CD8 (a) and CD4 (b) T cells. Cells have been gated using a lymphocyte gate then a single cells gate. Cells were then gated for live cells using a viability dye. Transduced R1 and R2 CAR T cells were gated using mock T cells to set the CD34 gate. (c) R1, R2 and No scFv CAR Transduced R1 and R2 T cells were matched for transduction percentage by dilution with mock-transduced T cells. Matched numbers of R1, R2 and No scFv CAR T cells were counted then incubated for two days in a well coated in human extracellular recombinant ROBO4 protein on day 0. After two days of stimulation cells were washed and resuspended in a well without the protein. The two days of ROBO4 protein incubation were repeated in days 7 and 14. Cells were again counted on days 7,14 and 21. (d) The same process as in figure c, but without ROBO4 protein stimulation. All results are plotted from individual wells. Results are representative of one individual experiment.

3.7 Chapter 3 discussion

In the previous section, two ROBO4 specific CARs have been developed and tested in vitro for functionality. The CAR T cells responded well to ROBO4 in vitro, demonstrating the ability produce multiple effector cytokines kill target cells and proliferate. The significance of these findings is now discussed below.

3.7.1 IFNγ and T cell function

IFNγ is a pro-inflammatory cytokine produced by effector CD8, T helper 1 CD4, natural killer and natural killer T cells (Ikeda et al. 2002). The receptor for IFNγ is found on all nucleated cells including T cells and is composed of a heterodimer of IFNγR1 and IFNγR2 proteins. Consequently, IFNγ has a wide range of effects. It is involved in macrophage activation, activation of the immunoproteosome and enhancement of MHC-peptide presentation, cell division and induction of inflammatory T cell responses (Ikeda et al. 2002).

IFNγ has long been described as essential in a host's anti-tumour response (Ikeda et al. 2002). Its roles include assisting in tumour surveillance, negative effects on tumour growth and survival, inhibiting tumour angiogenesis and promoting innate and adaptive anti-tumour immune responses (Ikeda et al. 2002). Despite this, mixed results have been seen using IFNγ clinically in cancer treatment (Miller et al. 2009). In terms of T cell function, IFNγ appears to have roles in the expansion of effector T cells and subsequent contraction and apoptosis of effector T cells during infection (Whitmire et al. 2005; Green et al. 2013; Haring et al. 2006; Badovinac et al. 2000; Dalton et al. 2000).

ROBO4 specific CAR T cells were observed to specifically respond to ROBO4 protein with a substantial production of IFNγ compared to mock transduced T cells. A CAR T cell ACT murine model for solid tumours found IFNγ was important in destruction of the tumour stroma (Textor et al. 2014). IFNγ was also essential in tumour eradication in mice receiving CAR T cells (Darcy et al. 2000). The large production of IFNγ by the ROBO4 CAR T cells should therefore be a beneficial marker in this study.

3.7.2 TNFα and T cell function

TNFα exists as both a membrane bound and soluble form (Chen & Oppenheim 2011). Both forms can bind to the receptors TNFR1 and TNFR2, although the soluble form induces limited signaling through TNFR2. TNFR1 is expressed constitutively on most nucleated cells. TNFR2 is restricted to immune cells where its expression is regulated. Both receptors can also be released as soluble receptors. Macrophages are key producers of TNFα but T cells, B cells, mast cells and endothelial cells also produce significant amounts. TNFα is a proinflammatory cytokine with roles in health and disease. It is heavily involved in septic shock, cancer cachexia and various autoimmune diseases. Some of its main immune functions include macrophage activation, inflammatory cell recruitment and granuloma formation. It is also heavily implicated in protection from intracellular bacteria and parasites. Although originally named after its in vitro tumour lysing ability, its in vivo anti-tumour capacity is linked to its immune activation rather than direct tumour lysis (Hock et al. 1993).

TNFα signalling on T cells has been found to act as costimulation in T cell activation and assists in proliferation, recruitment and protection from chronic infections (Chen & Oppenheim 2011) (Chatzidakis et al. 2007) (Calzascia et al. 2007) (Allie et al. 2013; Saunders et al. 2004). Conversely, TNFα signalling can promote Treg expansion and function (Kleijwegt et al. 2010)(Grinberg-Bleyer et al. 2010). Overall, the high proportion of ROBO4 CAR T cells producing TNFα will likely be beneficial for an in vivo anti-tumour response

3.7.3 IL2 and T cell function

IL2 was originally discovered for its ability to expand T cells (Morgan et al. 1976). It is produced largely by activated CD4 T cells but also by activated CD8 T cells, NK cells and NKT cells (Boyman & Sprent 2012). There are two IL2 receptors. The high affinity trimeric receptor consists of CD25, CD122 and the common γ chain whereas the low affinity dimeric receptor consists of only CD122 and the common γ chain. The dimeric receptor is not normally expressed in naïve CD4 T cells but is expressed to a low level on naïve CD8 and memory CD4 T cells. It also highly expressed on CD8 memory T cells and NK cells. The trimeric receptor is highly expressed on T cells after TCR or IL2 stimulation. The production of IL2 by T cells depends on signalling through calcium and protein kinase C and is controlled by multiple transcription factors (Boyman & Sprent 2012). It has a wide range of effects on T cells ranging from proliferation, differentiation, memory formation and induction of apoptosis (Kundig et al. 1993; Williams et al. 2006; Bachmann et al. 2007)(Feau et al. 2011)(Williams et al. 2006) (Liao et al. 2011) (Boyman & Sprent 2012) (Ballesteros-Tato et al. 2012; Johnston et al. 2012; Oestreich et al. 2012).

High dose IL2 immunotherapy has been FDA approved for metastatic renal cell carcinoma since 1992 and metastatic melanoma since 1998 (Rosenberg et al. 2008). A complete response can be seen in 5-10% of patients. However, high dose IL2 can cause toxicity such as severe capillary leak syndrome, although it has only been fatal in less than 1% of patients. On the other hand, IL2 directly affects Treg cells. Mice deficient in IL2 signalling succumb to systemic autoimmune disease due to a lack of Treg development and Treg survival (Sakaguchi et al. 2008). IL2 enhances CD25 in Tregs, positively augmenting IL2 signalling and increasing FOXP3 expression. This helps to support Treg suppressive function (Fontenot et al. 2005; Barron et al. 2010). Concerns over Treg expansion have been raised with the superior IL2 production often seen with 28ζ CARs. A 28.ζ CAR was actually less efficient than a ζ only CAR against a Treg infiltrated solid tumour mouse model (Kofler et al. 2011). However, by mutating the CD28 signalling domain to prevent IL2 production yet maintain superior IFNγ production, proliferation and cytolysis, anti-tumour efficacy was improved compared to the ζ only CAR.

Given the role of IL2 in T cell expansion, differentiation and memory cell formation, it could be vital for adoptive cell transfer. Most clinical protocols for adoptive cell transfer include a high-dose IL2 immunotherapy. The addition of exogenous IL2 has been found to improve CD8 T cell persistence in vivo after ACT (Yee et al. 2002). In contrast, mouse ACT model found that with administration of both CD4 and CD8 CAR T cells, exogenous addition of IL2 had no effect on T cell persistence (Mitsuyasu et al. 2000). Although only a small proportion of ROBO4 CAR T cells could produce IL2, there is potential for CAR produced IL2 to augment the non-IL2 producing CAR T cell population. The low frequency of IL2 producing cells may actually be beneficial in Treg-infiltrated tumours.

3.7.4 Multifunctional T cells

Both R1 and R2 T cells were capable of producing IFNγ, TNFα and IL2 alone and in combinations of two or all three cytokines. The ability of T cells to produce more than one cytokine has increasingly been implicated with improved in vivo immune responses. In mice infected with Leishmania major, the presence of CD4 T cells capable of simultaneously producing IFNγ, TNFα and IL2 (multifunctional) correlated with survival (Darrah et al. 2007). CD4 T cells producing only one cytokine had no correlation with survival. Multifunctional CD4 T cells also produced a higher amount of cytokine, on a per cell basis, than T cells positive for only one or two of the same cytokines. A human study investigating CD4 T cell responses to various viruses found multifunctional T cells also had a higher cytokine production on a per cell basis, greater levels of CD40L expression and greater degranulation ability than monofunctional T cells (Kannanganat et al. 2007). A human vaccine study found that the majority of vaccines induced long-term memory T cells simultaneously producing IFNγ, TNFα and IL2 cytokines (Lindenstrøm et al. 2009). A further study in this PhD project could involve investigating the phenotype of single, double and triple cytokine producers and whether triple cytokine producing T cells appear to be more memory-like. For example, the markers CCR7 and CD45RO are commonly used together to differentiate between naïve, effector, effector memory and central memory T cells (Mahnke et al. 2013). Furthermore, one study has described a long-lived memory-like T cells subset called stem cell-like memory cells. These cells display self-renewal capacity and multifunctionality with a unique naïve-like phenotype ($CD45^{+}$ $CD45RO^{-}$, $CCR7^{+}$, $CD45RA^{+}$, $CD62L^{+}$, $CD27^{+}$, $CD28^{+}$ and IL-$7R\alpha^{+}$). T cells with this phenotype also outperformed T cells with the traditional memory phenotypes, with greater in vivo proliferation and anti-tumour ability (Gattinoni et al. 2011). The presence of such a phenotype may therefore be desirable within CAR populations.

Another study analysed the in vitro ability to produce the three cytokines and found that most (>90%) human T cells are initially monofunctional (Han et al. 2012). After monitoring real-time secretion of cytokines by individual cells, it was found that multifunctionality was only a transient state as cells begin to sequentially express different cytokines rather than simultaneously (Han et al. 2012). In this regard, it is unknown whether the small population of multifunctional ROBO4 specific CAR T cells in this study are truly capable of simultaneously producing all three cytokines long-term or whether it is only a transitional phenotype. A further experiment in this project cold involve ex vivo functionality. CAR T cells could be used in a tumour model as before, then removed and re-tested for multifunctional cytokine production. This could give insight into long-term functionality and multifunctionality.

Note that although such multifunctional T cells may be very important in mediating anti-tumour effects, when preparing human PBMCs the frequency of the CD4 and CD8 T cells can vary in individuals and in some cases the frequency of CD4 T cells may be very low. Pre-clinical murine studies have reported superior anti-tumour responses with equal number of CD4 and CD8 tumour specific T cells (Moeller et al. 2005). A recent CD19 clinical trial performed separate activation and transduction of CD4 and CD8 T cells before pooling together at a 1:1 ratio to overcome differential subset ratios (Turtle et al. 2016).

3.7.5 T cell differentiation status and cancer therapy

Traditionally, the ability of T cells to produce IFNγ and kill tumour cells during in vitro culture has been the deciding factor for selection of clones for adoptive cell transfer in patients with solid tumours (Yee et al. 2002; Dudley & Rosenberg 2003). However, an increased in vitro IFNγ and cytolytic ability does not always correlate with improved anti-tumour function in vivo (Yee et al. 2002; Dudley et al. 2001).

In fact, it has been found that T cells producing less IFNγ and reduced target cell cytolysis in vitro have exhibited superior anti-tumour responses in mouse models of adoptive cell transfer (Gattinoni, Finkelstein, et al. 2005; Hinrichs et al. 2009; Klebanoff et al. 2005). Several animal models have now indicated that less differentiated T cells function better in vivo ((Klebanoff et al. 2005; Gattinoni, Klebanoff, et al. 2005; Hinrichs et al. 2009; Berger et al. 2008). Effector T cells derived from less differentiated T cell populations such as naïve or central memory express lower levels of the exhaustion and senescence marker KLRG1, and apoptotic marker Fas ligand. They also showed an increased proliferative capacity and increased persistence in vivo.

Studies using human T cells have shown that effector cells derived from naïve populations produce the least differentiated effector phenotype with the lowest KLRG1 and CD57 but the highest CD27 and longest telomeres (Hinrichs et al. 2011). Additionally, engineered effector T cells derived from naïve cells expressed higher levels of transgenic TCR molecules and exhibited extensive proliferation compared to effector cells derived from more differentiated populations. These studies would argue against the use of bulk PBMCs, which comprise a mix of differentiated populations, for CAR transduction and adoptive cell transfer.

In this regard, T cells from human umbilical cord blood cells (CBs), in contrast to adult peripheral blood (PB), are mostly naïve and may be a good source for ACT. This lab has previously described the genetic engineering of CB T cells which retained a less differentiated phenotype compared to PB T cells (Frumento et al. 2013). Alternatively, future studies may wish to employ the use of IL7 and IL15 in transductions, which have can increase the frequency of naïve like T cells with improved in vivo function (Cieri et al. 2013). These results would indicate that it might be worth investigating the use of specific populations of CAR T cells and their overall anti-tumour efficacy.

3.7.6 Proliferation and persistence

Both R1 and R2 T cells were capable of expansion when cultured with target cells or recombinant ROBO4 protein. After a single recombinant ROBO4-mediated stimulation, R1 and R2 CAR T cells expanded 2-fold and after two stimulations, R1 CAR T cells have expanded almost 5-fold (figure 3.10c). Given that 33% of the starting T cell culture actually expressed the CAR (data not shown), and given that the unstimulated T cells showed negligible expansion (figure 3.10d), the actual expansion of CAR T cells may be greater than 5 fold. Of course, the CAR negative T cells may also undergo bystander expansion from IL2 produced by CAR expressing T cells. Future experiments could use flow cytometry to analyse the percentage of CAR T cells after stimulation.

The CFSE dilution only indicates a limited proliferation compared to the impressive expansion seen in the restimulation assay, although, the CFSE assay measured cells after only 4 days whereas the restimulation assay counted cells after 7 days. The high proliferation in the restimulation assay may indicate a superior proliferative response to recombinant protein rather than ROBO4 expressed on CHO cells. Cell surface ROBO4 may be more difficult to access due to the different glycosylation, steric hindrance from accessory cell surface proteins or alternatively, the epitope may be a out of reach for some CAR molecules. A spacer domain in the CAR may assist in this context (Qin et al. 2017). Recombinant fixed protein may be at a higher concentration than when found on a cell, and/or be easier to access. Alternatively, it may be because the T cells used in the CFSE assays were approaching exhaustion as they had already undergone a large proliferative expansion during the 12 day culture with IL2 before starting the assay. The cells used in the restimulation assay were cultured only a matter of days after transduction before starting the assay. Despite the T cells only being recently activated, the large expansion was specific to ROBO4 recognition, as the No scFv T cells as well as CAR T cells cultured in absence of ROBO4 failed to expand.

A recent study identified that human CAR T cells that were cultured at the minimal time required for lentiviral transduction (3 days after T cell activation) showed superior in vivo anti-tumour activity in a xenogeneic model compared to T cells cultured for longer (5 days or 9 days after activation) (Ghassemi et al. 2016). The in vivo mouse experiments in this PhD project also used a minimal culture time of 3 days after activation for mouse T cells. These data support the use of a human T cell adoptive cell transfer clinical protocol with a shorter in vitro culture period although the limiting factor in human T cell adoptive cell transfer is often T cell numbers.

The repeated antigen stimulation assay suggests both R1 and R2 CAR T cells lose their ability to proliferate after three antigen specific stimulations (figure 3.10c). In fact, T cells reduced dramatically number, suggesting the possible onset of AICD. Alternatively, T cells may simply have died off after excessive in vitro culture or due to a poor persistence. Non-stimulated CAR T cells also show a large reduction in number by day 21 (figure 3.10d). Flow cytometry could be used to detect the expression of exhaustion and apoptopic markers such as inhibitory receptors, Fas and FasL after each round of ROBO4 stimulation. It is possible that incorporation of “late” costimulatory molecules such as OX40 or 41BB in addition to (or instead of) CD28 in the CAR molecule could improve proliferation and reduce AICD in this setting. Studies have found that 41BB second generation CARs persist longer than CD28 second generation CARs in vitro after CAR stimulation (Zhao et al. 2015; Kawalekar et al. 2016). On top of this, one study showed that second generation CARs containing 41BB reduced T cell exhaustion after persistent antigen stimulation compared to CD28 containing CARs (Long et al. 2015).

In fact, CD28 or 41BB mediated CAR costimulation can result in remarkably different outcomes (Kawalekar et al. 2016). CD28 costimulation results in an increased glucose uptake and aerobic glycolysis with cells resembling an effector phenotype. 41BB costimulation results in an increased oxidative metabolism and anaerobic fatty acid oxidation, with cells resembling a central memory phenotype. An in vivo mouse tumour model found that CAR T cells with CD28 costimulation resulted in more rapid tumour destruction than 41BB CARs (Zhao et al. 2015). However, 41BB CARs persisted longer in vivo and eventually cleared the tumour. By combining CD28 and 41BB into a third generation CAR, T cells were capable of rapidly clearing tumours along with an extensive persistence. The optimal CAR design is unknown however and will depend entirely on the type of cancer and the antigen and epitope that is targeted.

3.7.8 Cytolysis of target cells

Cytotoxic CD8 T cells form an immunological synapse (IS) with target cells in order to induce apoptosis, killing the target cell. Formation of the IS is induced upon TCR stimulation. Once formed, the IS can direct perforin and granzymes towards the target cell across the synaptic junction. Perforin forms pores in the membrane of the target cell (Keefe et al. 2005). The pores induce endocytosis of both perforin and granzymes into vesicles called gigantisomes. After around 15 minutes, the gigantisomes break up and granzymes are released into the target cell cytosol where they can induce apoptosis (Thiery et al. 2011).

Mouse models have demonstrated that perforin, as well as IFNγ are essential in anti-tumour efficacy of CAR T cells (N M Haynes et al. 2002; Darcy et al. 2000). In this project, both R1 and R2 CAR T cells were capable of specifically lysing ROBO4 expressing CHO cells and HUVEC cells. Both R1 and R2 CAR T cells showed an equivalent killing ability at each T cell dose tested. Both CAR T cells showed a much greater ability to lyse CHO MRFL target cells than the HUVEC cells. In fact, at the lowest tested T cell:target cell ratio of 5:1, HUVEC lysis was near to the background levels seen with mock T cells (figure 3.9). This may be reflective of a possible higher expression level of ROBO4 seen on the CHO MRFL cells than HUVEC cells although this has not been investigated. Overall, both R1 and R2 CARs are clearly capable of a ROBO4-mediated target cell killing in vitro, whether it is by IFNγ or perforin. Interestingly, although R1 CAR T cells produce more IFNγ than R2 CAR T cells in response to CHO MRFL (figure 3.2) at the highest T cell dose, R1 CAR T cells did not induce greater CHO MRFL lysis than R2 CAR T cells (figure 3.9).

4. Testing CAR T cells in vivo

Now that the function of the ROBO4 CARs have been established in human T cells mouse models were investigated to explore their function in vivo, since both the R1 and R2 CAR T cells were capable of recognising mouse ROBO4 protein.

4.1 Transduction and function of ROBO4 specific mouse CAR T cells

If mouse T cells transduced with ROBO4 CARs can also recognise ROBO4 protein, then immune competent models can be used to develop test the CARs in vivo. Before any in vivo experiments are performed in mice, the function of R1, R2, No scFv and mock-transduced mouse T cells were tested in vitro. An IFNγ ELISA was performed using the target cell lines CHO WT and CHO MRFL. T cells were incubated overnight with target cells at four different T cell doses.

T cells incubated alone, especially R1 T cells, resulted in an IFNγ production of up to 3000pg/ml (data not shown). This likely reflects the fact that the mouse T cells were activated only 6 days ago. Compared to human T cells, mouse T cells culture poorly, thus must be used in functional assays within a few days after transduction and high background levels of IFNγ are expected. There was a notable amount of IFNγ after incubation with CHO WT for R1 and mock T cells (figure 4.1). Despite these background levels, ROBO4-specific responses are clearly detectable. R1 CAR T cells produced a strong IFNγ response to CHO MRFL (figure 4.1). At the highest T cell dose, the response was off the scale, greater than the most concentrated standard of 25,000pg/ml. R2 CAR T cells responded moderately to CHO MRFL. Mock and No scFv T cells were equally unresponsive. The particularly high IFNγ responses seen in this assay may reflect the fact that there was a high transduction percentage of around 76% for CD8 T cells and 95% for CD4 T cells (data in appendix), rather than the levels seen for human T cell assays, typically 20-40%.

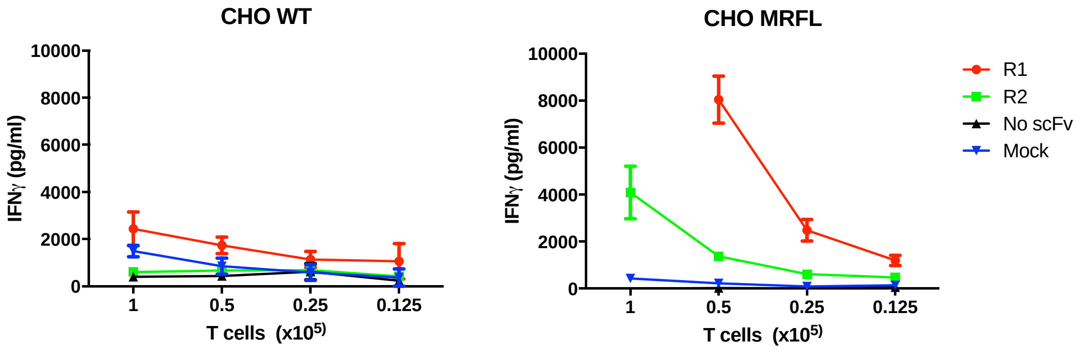

Figure 4.1: CAR Transduced mouse T cells are functional. Mouse T cells transduced with R1, R2 or No scFv CAR DNA or mock-transduced T cells were incubated overnight with either the CHO WT or CHO MRFL target cells. The supernatants were then tested for the presence of IFNγ. Each T cell concentration was tested in triplicate and results shown are mean values. Error bars represent the SD. Experiment was representative of two independent experiments

Together the results show that mouse R1 and R2 CAR T cells do respond to ROBO4 in terms of IFNγ production. R1 has a greater response than R2 CAR T cells. No scFv CAR T cells showed a negligible IFNγ response and should therefore be a suitable control for in vivo experiments.

4.2 Toxicity test using low dose of CAR T cells

For the first in vivo experiment, a low dose of transduced R1, R2 or No scFv CAR T cells were prepared for injection into healthy C57 BL/6 mice (figure 4.2a). Splenocytes from congenic CD45.1 BoyJ mice were activated with concanavilin A and IL7. The congenic marker CD45.1 from BoyJ mice allows cells to be identified and tracked in CD45.2 C57 BL/6 mice. Two days later, the activated cells were transduced with the R1, R2 or No scfv CAR construct. The following day, the T cell transduction efficiency was measured by flow cytometry staining for the CD34 tag (figure 4.2b). On this occasion, the transduction efficiency of CD4 and CD8 T cells was low for all CAR constructs. The MFI of the transduced T cells was also very low, suggesting that they were expressing relatively few CARs on their surface. On the same day, CAR expressing T cells were injected into the tail vein of healthy C57BL/6 mice (irradiated with 4Gy the previous day) in numbers that meant each would receive 1 million CAR expressing T cells. Two mice did not receive any T cells and acted as a control group.

Over the course of the experiment, experienced members of staff in the animal unit checked mice regularly but there were no signs of ill health, and all mice continued to gain weight normally (figure 4.2c), suggesting no significant toxicity. Tail bleeds were performed on days 3, 7 and 12 after T cell injection to analyse the presence of CAR engineered T cells. Representative FACs plots show a single mouse for R1, R2 and No scFv on day 3 (figure 4.3a) Despite the low numbers of engineered CAR cells injected into the mice, No scFv CAR T cells were clearly detectable at each timepoint (figure 4.3b-d). No scFv CAR CD4 and CD8 T cells were highest at day 3 before dropping slightly by day 10 to 2000 cells/ml of blood. Both R1 and R2 CAR T cells were barely detectable at any timepoint and the few cells that could be detected were CD4+.

The percentage of No scFv CAR T cells within infused T cells drops slightly compared to the pre-injection transduction levels, but remains steady in mice throughout the experiment. (figure 4.3e-g). The percentage of R1 and R2 CAR T cells within infused cells drops to 1-3% and remains low throughout the experiment. This is despite R1 CD4 T cells starting with a relatively greater transduction efficiency of 16.5%. The data suggests that there was a selective loss of ROBO4 specific CAR CD4 and CD8 T cells from the peripheral blood of mice, whereas the No scFv control CAR T cells persisted. However, mice exhibited no sign of toxicity.

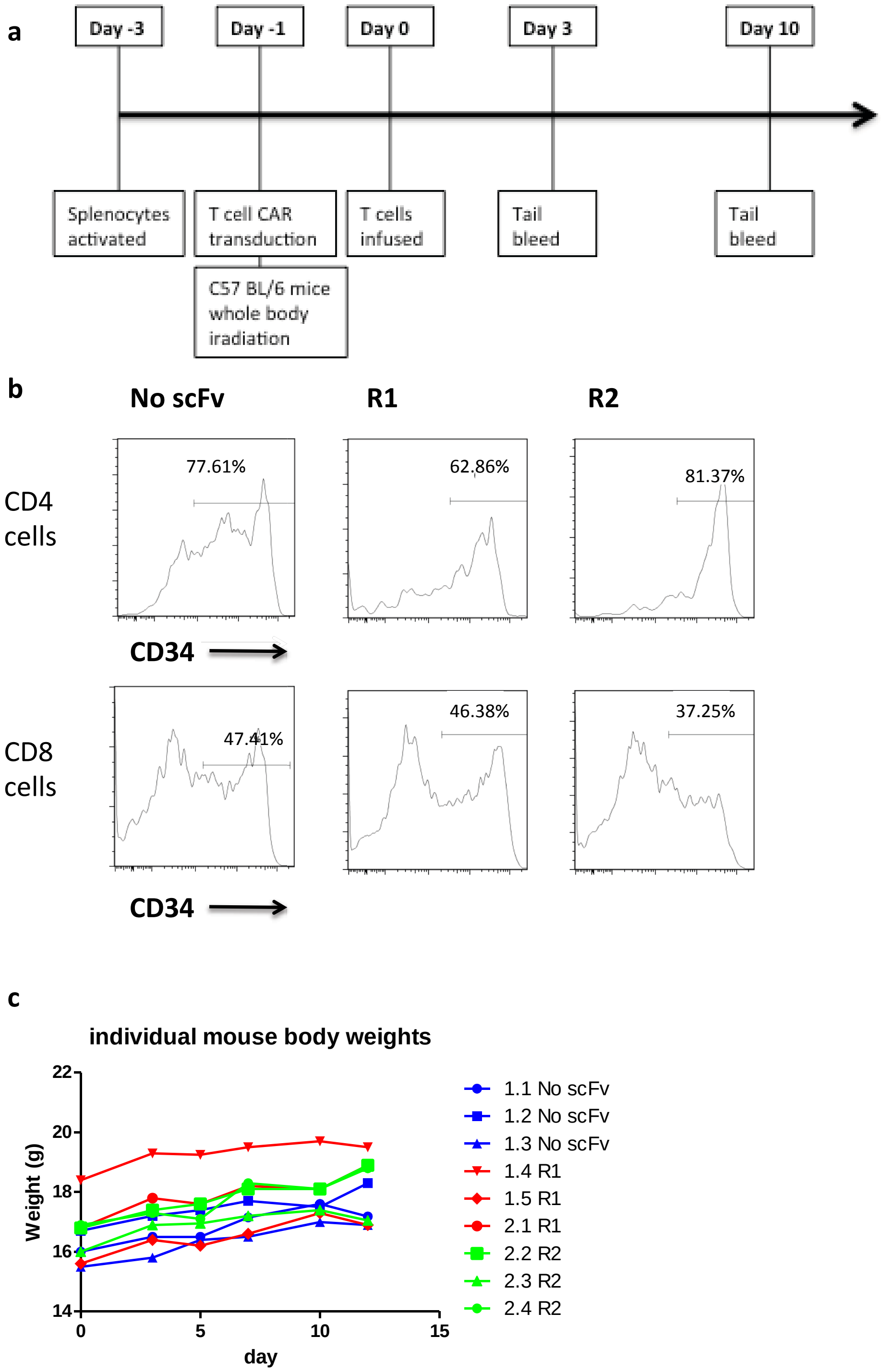

Figure 4.2: toxicity experiment 1. In (a) the experimental set up is summarised. On day -3 splenocytes are harvested from BoyJ mice then activated using Concanavilin A and IL7. On day -1, BoyJ T cells were transduced with R1, R2 or No scFv CAR DNA. C57/BL6 mice were also irradiated with 4Gy of irradiation. On day 0, transduced T cells are injected in the tail vein of C57/BL6 mice. On day 3, 7 and 12, tail bleeds are performed to analyse engraftment of transduced T cells. In (b), the CD4 and CD8 T cell transduction levels were analysed on day 0 before infusion by flow cytometry staining for CD34. Cells were gated on a lymphocyte gate, then single cells gate. These cells were then gated for live cells using a viability dye. Live cells were then gated for CD4 or CD8 cells before a CD34 gate was set using an FMO control. In (c) the body weights of all mice were analysed every 2 to 3 days from day 0.

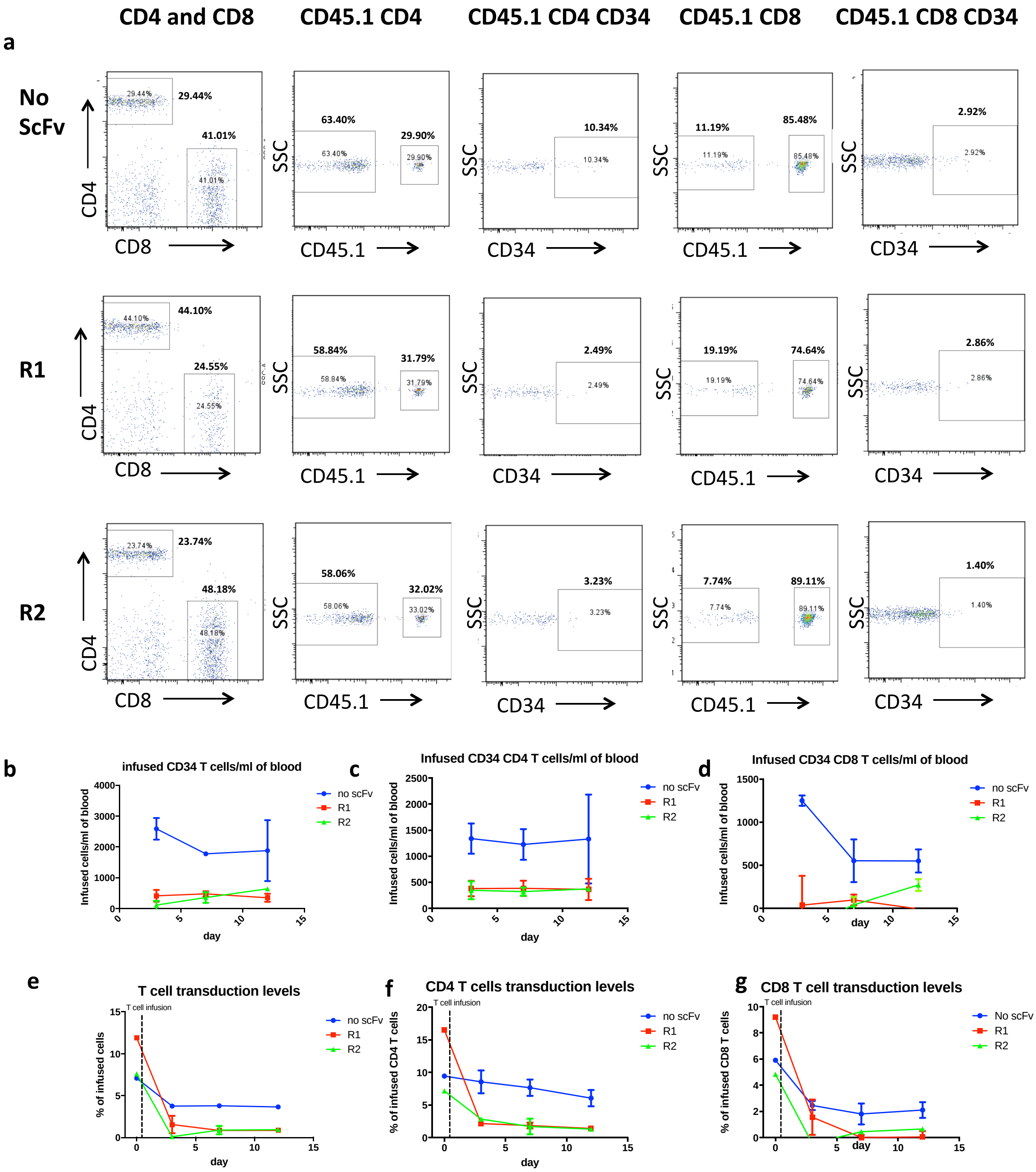

Figure 4.3: CAR T cell engraftment in toxicity experiment 1. No scFv, R1 or R2 CAR T cells were injected into C57 BL/6 mice. Staining for CD45 can identify infused T cells. The infused CAR T cells were analysed by flow cytometry of tail veins on days 3, 7 and 12 after injection. Staining CD45+ cells for CD34 can identify transduced infused T cells. (a) Shows representative FACs plots of T cells three days after tail vein injection for one mouse receiving No scFv, R1 or R2 T cells. Side scatter = SSC. The infusion of CAR T cells per ml of blood of mice over day's 3-12 post injection is summarised for all CAR T cells (b), CD4 CAR T cells (c) and CD8 CAR T cells (d). The percentage of CAR T cells within the T cell culture at day 0 before injection and the percentage of CAR T cells within all infused cells (e), infused CD4 T cells (f) and infused CD8 T cells (g) is summarised. Results plot line mean for each group of mice and the error bars show the S.D. n = 2 mice per group.

4.3 Toxicity test with an increased dose of CAR T cells

The relative loss of ROBO4 specific T cells from the circulation compared to the No scFv CAR T cells suggests that there may be targeting of healthy tissues recognising low-level ROBO4 or cross reacting with another protein in tissues. Indeed, a clinical trial found that CAR T cells quickly disappeared from the periphery is cases of on-target/off-tumour toxicity in the liver (Lamers et al. 2006). Although no overt signs of toxicity were observed in the mice, this may reflect the relatively low numbers of transduced cells injected into each animal. Therefore the experiment was repeated with an increased dose of T cells. Mouse T cells were activated and transduced with the R1, R2 or No scFv CAR construct as before (figure 4.4a). The transduction efficacy of all CARs was greater than the previous experiment (figure 4.4b). CD4 T cell transduction was 77.6%, 62.9% and 81.4% for No scFv, R1 and R2 respectively. CD8 T cell transduction was 47.4%, 46.5% and 37.3% for No scFv, R1 and R2 respectively. A range of CD34 expression levels in engineered T cells was apparent for each CAR construct. Three healthy C57 BL/6 mice (all irradiated the previous day with 4Gy of irradiation) each received five million R1, R2 or No scFv CAR expressing T cells. All mice gained weight over the course of the experiment suggesting no significant toxicity (figure 4.4c). Tail bleeds were taken on days 3 and 10 after injection. As expected, the increased dose of T cells injected meant that a larger number of No scFv CAR T cells were detected in the blood compared to the previous experiment (figure 4.5a-d). 3 days after T cell injection the number of No scFv CAR T cells per/ml of blood ranged from 10,000 to 38,000. 10 days after T cell injection, the No scFv CAR T cells were around 10,000 cells per/ml of blood in all three mice. In this experiment, most of the No scFv CAR T cells in the blood were CD8 T cells. Again, both R1 and R2 CAR T cells were barely detectable at both timepoints.

The percentage of infused T cells that express the No scFv CAR drops from the pre-injection level but still persists at a relatively high level of 35-40% (Figure 4.5e). However, the high pre-injection level of CD4 T cell transduction drops to a much lower level of around 25% (Figure 4.5f), whereas CD8 T cell transduction remains relatively high. This reflects the fact that most No scFv T cells present in the blood are CD8 rather than CD4 (figure 4.5c-d). For both R1 and R2, transduction levels drop dramatically from the pre-injection levels (figure 4.5e-g). Although CD4 T cell transduction percentage appears to still be reasonable for both R1 and R2 at day 3 (figure 4.5f), this value may be unreliable since so few infused CD4 T cells were detectable in the mice at this stage (figure 4.5a, c).

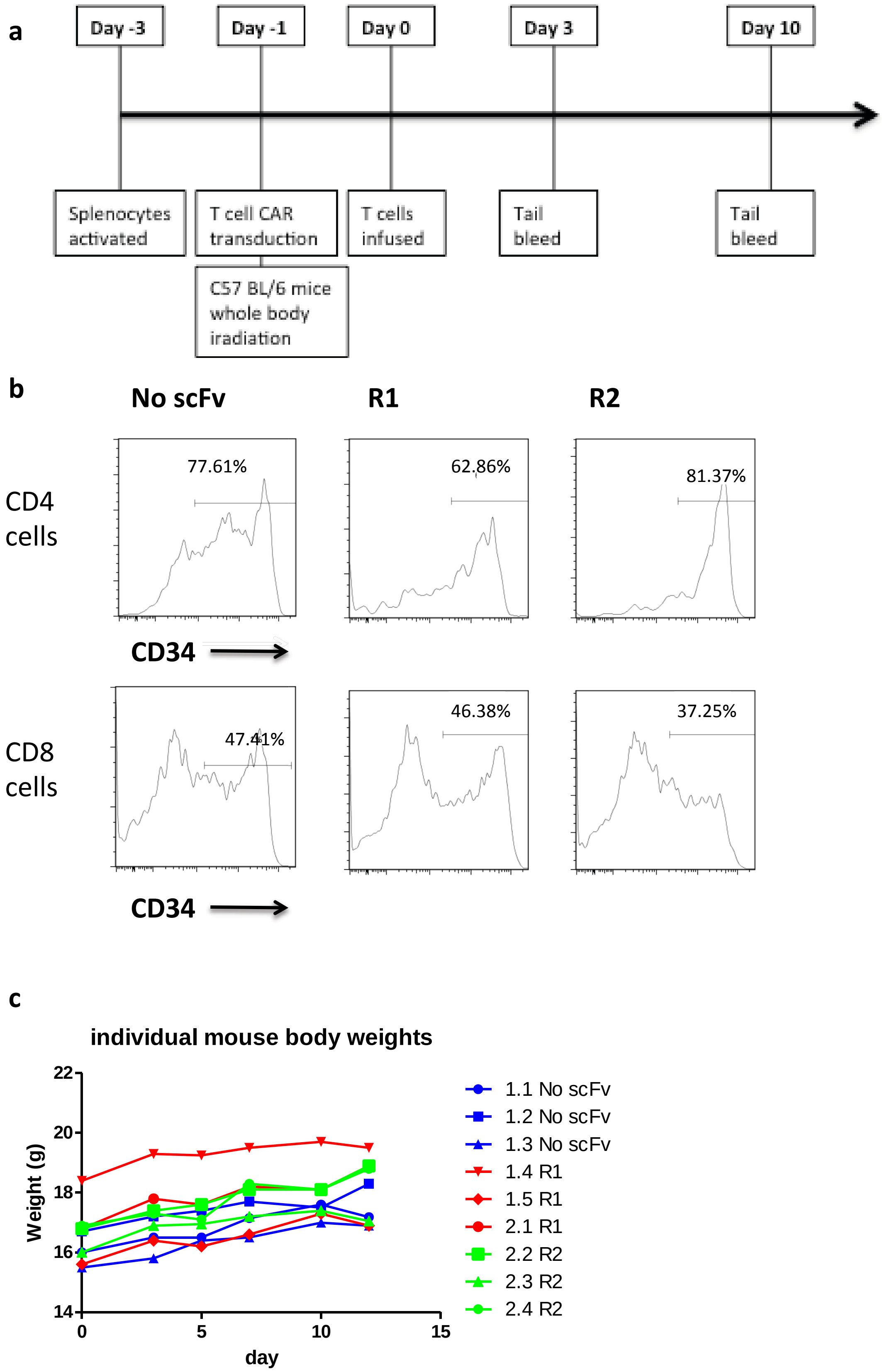

Figure 4.4: toxicity experiment 2. (a) shows the experimental overview. On day -3 splenocytes are harvested from BoyJ mice then activated using concanavalin A and IL7. On day -1, BoyJ T cells are transduced with R1,

R2 or No scFv CAR DNA. C57/BL6 mice are also irradiated with 4Gy of irradiation. On day 0, transduced T cells are injected in the tail vein of C57/BL6 mice. On day 3 and 10, tail bleeds are performed to analyse engraftment of transduced T cells. In (b), the CD4 and CD8 T cell transduction levels were analysed on day 0 before infusion by flow cytometry staining for CD34. Cells were gated on a lymphocyte gate, then single cells gate. These cells were then gated for live cells using a viability dye. Live cells were then gated for CD4 or CD8 cells before a CD34 gate was set using an FMO control. In (c) the body weights of all mice were analysed every 2 to 3 days from day 0. n = 3 mice per group.

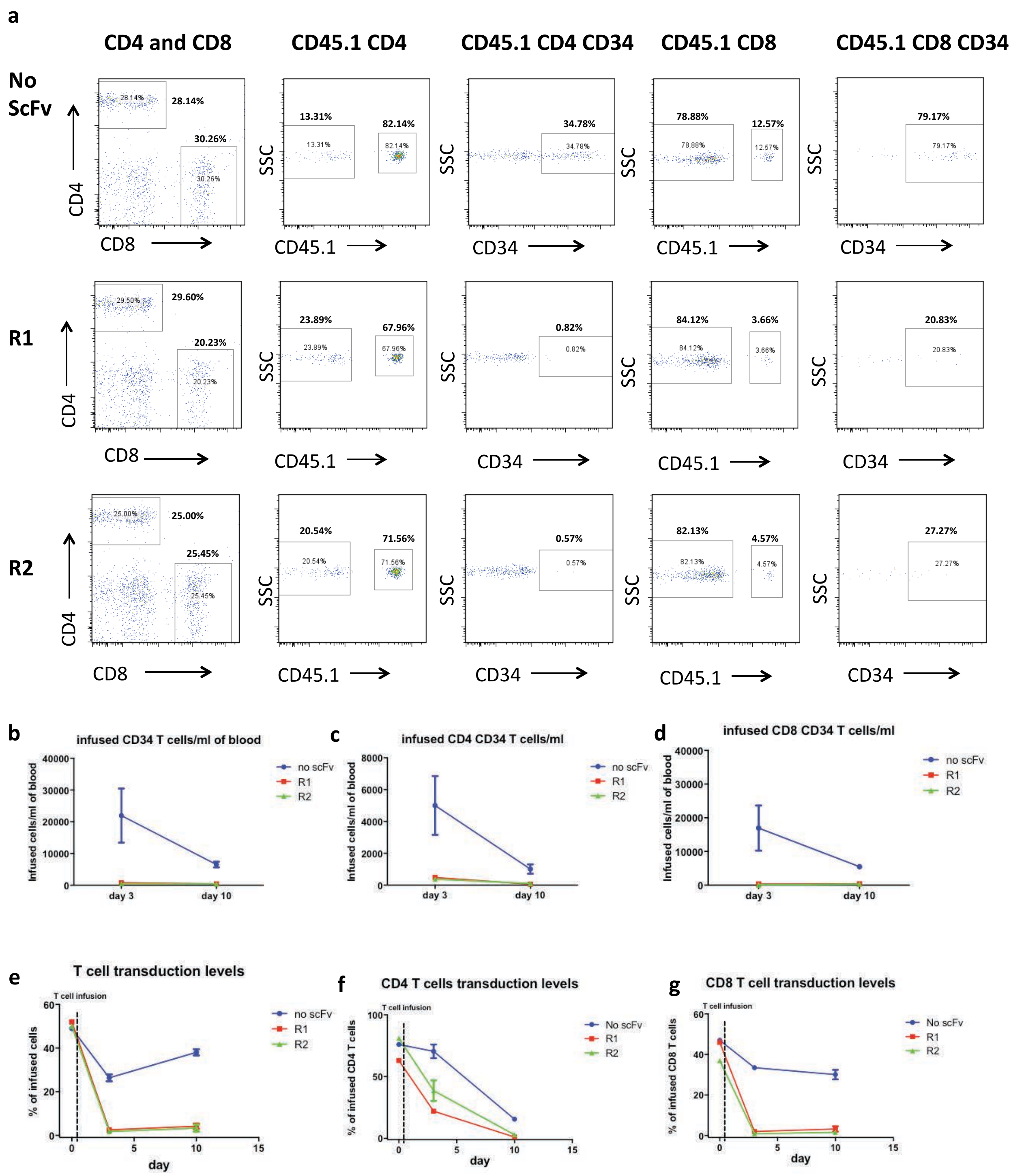

Figure 4.5: CAR T cell engraftment in toxicity experiment 2. No scFv, R1 or R2 CAR T cells were injected into C57 BL/6 mice. Staining for CD45 can identify infused T cells. The infused CAR T cells were analysed by flow cytometry of tail veins on days 3 and 10 after injection. Staining CD45+ cells for CD34 can identify transduced infused T cells. (a) Shows representative FACs plots of T cells three days after tail vein injection for one mouse receiving No scFv, R1 or R2 T cells. Side scatter = SSC. The infusion of CAR T cells per ml of blood of mice over day's 3-10 post injection is summarised for all CAR T cells (b), CD4 CAR T cells (c) and CD8 CAR T cells (d). The percentage of CAR T cells within the T cell culture at day 0 before injection and the percentage of CAR T cells within all infused cells (e), infused CD4 T cells (f) and infused CD8 T cells (g) are summarised. Results plot the mean of each CAR group and the error bars show the SD. n = 3 mice per group.

4.4 Toxicity test using a further increased dose of T cells

Due to the lack of toxicity in the previous experiments, the T cell dose was increased again to further test toxicity. Mouse T cells were activated and transduced with the R1, R2 or No scFv CAR construct as before. A very high transduction efficiency was achieved for CD4 T cells at 96.8% 94.5% and 95.6% for No scFv, R1 and R2 respectively (figure 4.6a). A high transduction efficiency was also achieved for CD8 T cells at 76.8%, 76.9% and 75% for No scFv, R1 and R2 respectively. Three mice each received 17.5 million R1, R2 or No scFv CAR expressing T cells. However, 24 hours after injection, all three mice receiving R2 CARs, and two of the three mice that received R1 CARs showed signs of toxicity and were euthanized. Toxicity included a hunched posture, lack of activity, pinched faces and closed eyes. Unfortunately, organs were not recovered in time from the euthanized mice. There was also a slight drop in weight in these mice the day after T cell injection (figure 4.6b). The weights from mice in the previous toxicity experiments were not noted 24 hours after injection so may also have dropped before increasing by the time they were measured.

Despite this, the single remaining R1 mouse appeared healthy, as did all three No scFv mice. The weight of all remaining mice was stable until the end of the experiment, 5 days after T cell injection (figure 4.6b). 3 days after T cell injection, tail bleeds were performed on all remaining mice. Again, high numbers of No scFv CAR T cells were detected in the blood, averaging around 40,000 cells/ml of blood (figure 4.7a-d). The majority of these cells were CD8 T cells. Consistent with the previous experiments, CAR T cells have been selectively depleted from the circulation in the remaining R1 mouse. Only 3400 transduced cells/ml of blood were detected in the R1 mouse. It was surprising that this mouse also didn't show any signs of toxicity. It is possible that a lower than expected number of T cells were actually injected into the vein with the remainder injected into the surrounding tissue instead. However, the number of non-transduced CD45.2 T cells was similar between the R1 mouse and all No scFv-treated mice (figure 4.7e). Since only transduced cells are disappearing from the blood, a similar number of non-transduced cells suggest that the R1 mouse did receive a similar T cell dose.

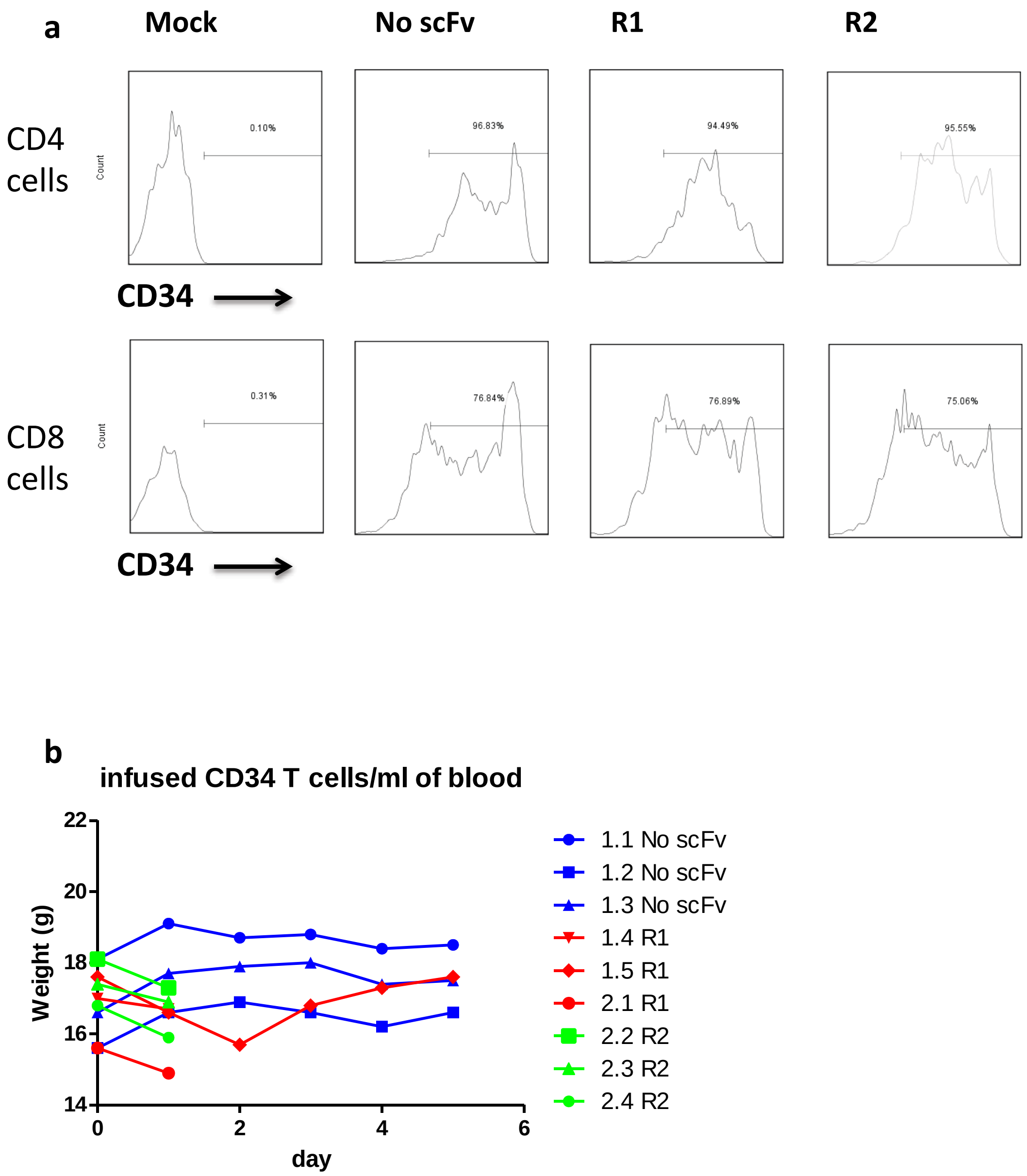

Figure 4.6 toxicity experiment 3. On day -3 splenocytes are harvested from BoyJ mice then activated using Concanavilin A and IL7. On day -1, BoyJ T cells are transduced with R1, R2 or No scFv CAR DNA. C57/BL6 mice are also irradiated with 4Gy of irradiation. On day 0, transduced T cells are injected in the tail vein of C57/BL6 mice. In (a), the CD4 and CD8 T cell transduction levels were analysed on day 0 before infusion by flow cytometry staining for CD34. Cells were gated on a lymphocyte gate, then single cells gate. These cells were then gated for live cells using a viability dye. Live cells were then gated for CD4 or CD8 cells before a CD34 gate was set using mock T cells. In (b) the body weights of all mice were analysed every day from day 0.

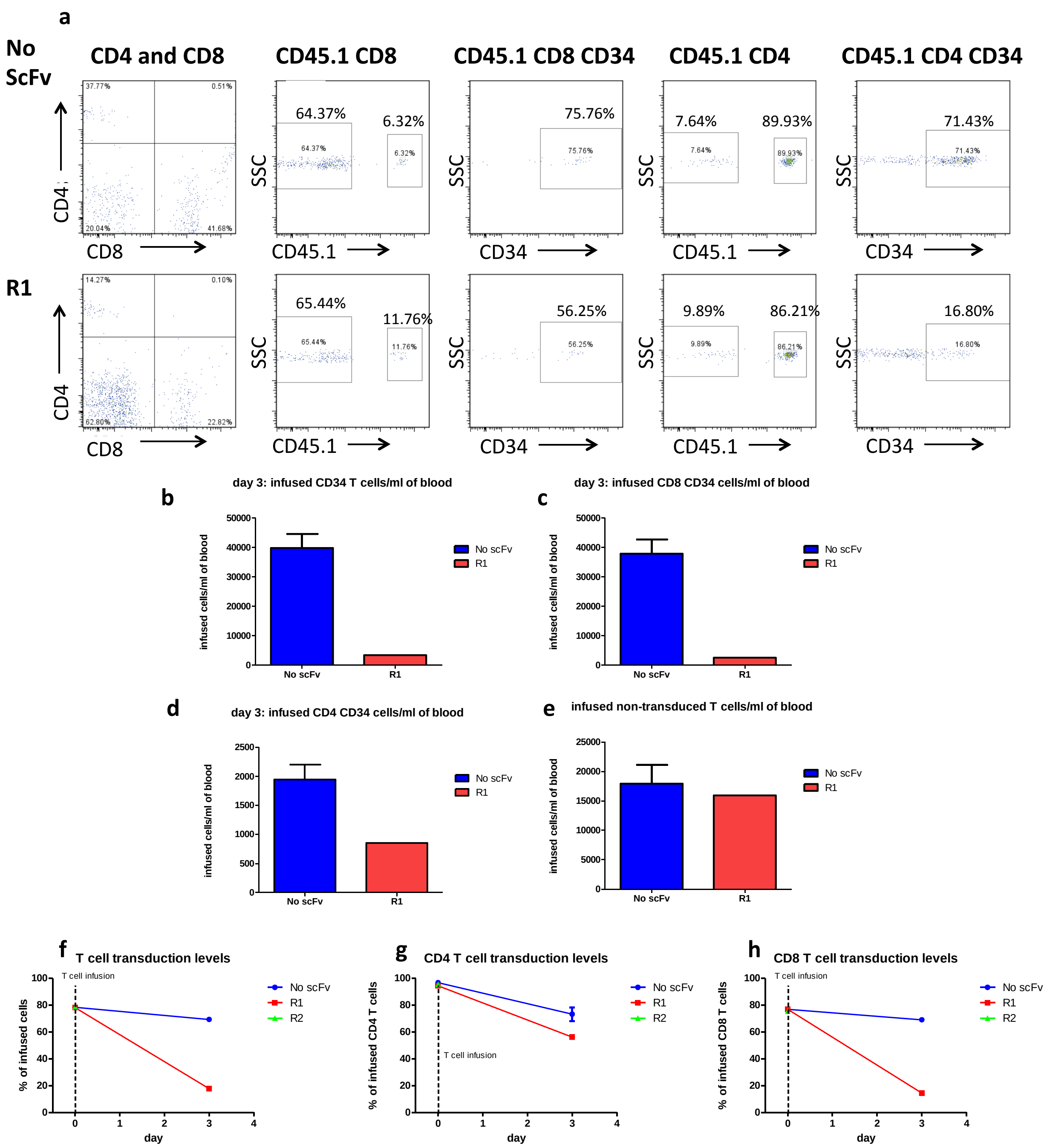

Figure 4.7: CAR T cell engraftment in toxicity experiment 3. No scFv, R1 or R2 CAR T cells were injected into C57 BL/6 mice. Staining for CD45 can identify infused T cells. All R2 mice and 2 of the 3 R1 mice were euthanized the following day due to toxicity. For the remaining mice, the infused CAR T cells were analysed by flow cytometry of tail veins on day 3. Staining CD45.1 cells for CD34 can identify transduced infused T cells. (a) Shows representative FACs plots of T cells three days after tail vein injection for one representative mouse receiving No scFv cells and the one remaining R1 mouse. Side scatter = SSC. For the three No scFv mice and the remaining R1 mouse, the infusion of all CAR T cells (b), CD8 CAR T cells (c), CD4 CAR T cells (d) and non-transduced T cells (e) per ml of blood is summarised. Results plot the mean for No scFv and the individual R1 mouse. Error bars show the SEM. The percentage of CAR T cells within the T cell culture at day 0 before injection and the percentage of CAR T cells at day 3 within all infused cells (f), infused CD4 T cells (g) and infused CD8 T cells (h) is summarised. Data shows the mean of each CAR group and the error bars show the SD. Note the R2 group could not be evaluated on day 3 as all mice were euthanized on day 1.

4.5 Testing the anti-tumour ability of ROBO4 specific CAR T cells

The toxicity studies reported above indicated that T cells expressing either R1 or R2 CARs may be responding to normal tissue and, if given at high dose, such cells are toxic. Nevertheless, since lower doses of these T cells appeared to be well tolerated it was explored whether a lower dose could be safely used to mediate an anti-tumour effect, especially if high ROBO4 expression within the tumour tissue leads to preferential targeting by ROBO4-specific T cells. Lewis Lung Carcinoma (LLC) is a mouse-derived tumour that has previously been shown to express high levels of ROBO4 within the tumour endothelium (Zhuang et al. 2015). Previous experiments from the lab have shown that the injection of LLC cells mixed with matrigel results in a more evenly formed tumour with lower risk of ulceration. Eleven C57 BL/6 mice were subcutaneously injected with 0.5×10^6 LLC cells mixed with matrigel (figure 4.8a). The transduction levels for No scFv were 69.58% of CD4 and 54.25% for CD8 T cells (figure 4.8b). The transduction levels for R1 were 56.06% of CD4 and 36.73% of CD8 T cells (figure 4.8b). Three days after LLC injection, a total of 7×10^6 No scFv or R1 CAR expressing T cells from BoyJ mice were injected into five and six mice respectively, in a blinded manner. The day before infusion, mice went under 4Gy of total body irradiation. Although higher levels of irradiation can temporarily inhibit LLC tumour growth (Cheng et al. 2013), levels of 4Gy are regularly used in the Lee lab, with little effect on LLC growth (unpublished data, Lee Lab). An additional mouse that did not receive tumour cells did receive 7×10^6 mock-transduced T cells. The mock mouse assisted with tail bleeds and the setting of the CD34 threshold during flow cytometry analysis.

The body weights of mice were measured three times a week throughout the experiment. All mice gradually gained weight throughout the experiment (figure 4.8c). Tail bleeds were taken at three, seven and fifteen days after T cell injection. As seen in the previous toxicity experiments, the transduced No scFv T cells persist in the blood throughout the experiment. Interestingly, the No scFv CD4 T cells increased 2 fold in number within the blood of mice by fifteen days after injection (figure 4.8d) whereas the No scFv CD8 T cells drop from around 40,000 to 10,000 cells/ml of blood where they then persist. This was the first experiment that CD4 CAR T cells outnumbered the CD8 CAR T cells. Similar to previous experiments, only low numbers of the R1 T cells are detectable three days post T cell injection (figure 4.8d-f). By seven days post injection R1 CD4 and CD8 T cells were almost undetectable.

Looking at the percentage of T cell transduction within infused T cells, a similar pattern is seen. The No scFv transduction percentage drops from the pre-injection level but remains fairly high at around 40% for both CD4 and CD8 T cells. The R1 transduction percentage rapidly drops for both CD4 and CD8 T cells by three days after injection and remains low to undetectable after this (figures 4.8g-i). The size of the tumours in mice was measured three times a week. Tumours were detectable seven days after LLC cell injection (figure 4.9a). Initially there was no notable difference in tumour size between the R1 and No scFv treated groups. However, from fifteen days after LLC cell injection (twelve days after T cell injection) the mean tumour volume of the R1 treated group is reduced compared to the No scFv control treated group (figure 4.9a). This difference is even greater at twenty-two days after LLC cell injection (nineteen days after T cell injection). Despite this, the difference in tumour volume between the two test groups was not significant at any timepoint. However, these results may have been skewed by a single mouse that was treated with No scFv expressing T cells that had a particularly slow growing tumour (figure 4.9b).

Although there was no significant difference in the size of tumours between the groups, the slight reduction in the R1 group may be indicative of a R1 CAR T cell mediated immune response. Since ROBO4 is known to be highly expressed within the blood vessels of LLC tumours, the colocalisation of CD31, an endothelial marker, and cleaved caspase 3, an apoptotic marker, was investigated. An increased colocalisation of cleaved caspase 3 within the endothelium would indicate killing of blood vessels. However, there was no difference between the R1 and No scFv treated tumours (figure 4.9c). The majority of cleaved-caspase 3 staining actually appeared at non-endothelial sites (figure 4.10). To investigate the possibility of cytokine storm, the serum from the first tail bleed at 4 days after T cell injection was tested using luminex. Luminex was performed for a range of 32 cytokines, but only 7 were detectable in at least one mouse. CXCL12 and CCL11 were the two highest concentrated cytokines for both mice receiving R1 or No scFv CAR T cells (figure 4.9d). Overall, the levels of cytokine production were similar between the R1 and No scFv groups. Therefore, there is no indication of any ROBO4-mediated cytokine storm.

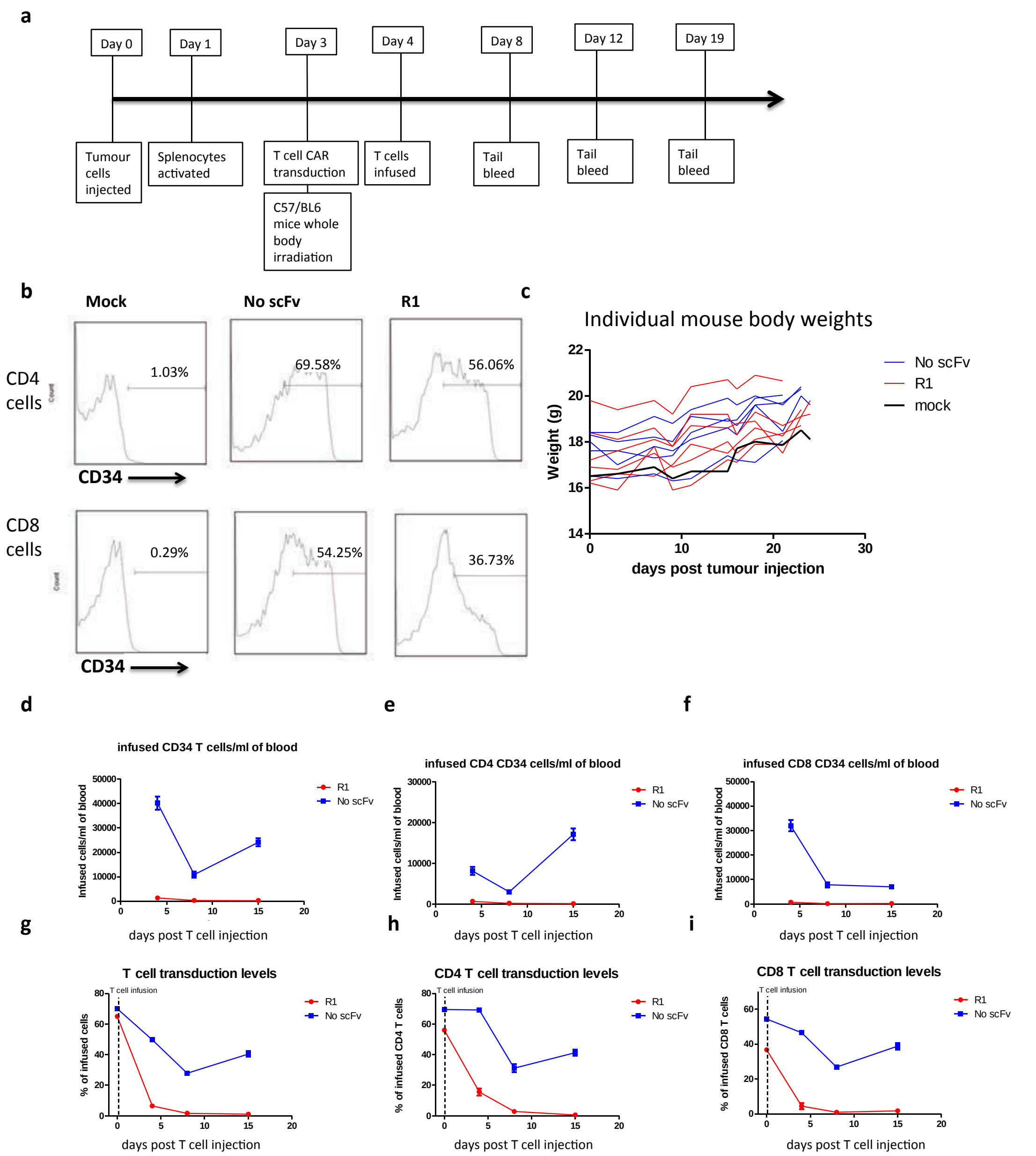

Figure 4.8: CAR T cells for a tumour challenge experiment. (a) shows the experimental overview. On day 0, Lewis Lung Carcinoma (LLC) cells were injected s.c. into C57BL/6 mice. On day 1, splenocytes from BoyJ mice were harvested and activated using Concanavalin A and IL7. On day 3, BoyJ T cells are transduced with either No scFv or R1 CAR DNA. The tumour bearing C57BL/6 mice were also irradiated with 4Gy of irradiation. On day 4, irradiated tumour bearing mice were injected with either 7×10^6 No scFv or R1 CAR transduced T cells into the tail vain. Tail bleeds were performed on days 8, 12 and 19 (days 4, 8 and 15 post T cell injection).), in (b), the CD4 and CD8 T cell transduction levels were analysed on day 4 before infusion by flow cytometry staining for CD34. The CD34 gate was set using mock-transduced T cells. In (c) the body weights of all mice were analysed every 2 to 3 days from day 0. A mock mouse receiving mock-transduced T cells was also included in this analysis. The infusion of CAR T cells per ml of blood of mice over day's 4-15 post T cell injection is summarised for all CAR T cells (d), CD4 CAR T cells (e) and CD8 CAR T cells (f). The percentage of CAR T cells within the T cell culture at day 0 before injection and the percentage of CAR T cells within all infused T cells (g), infused CD4 T cells (h) and infused CD8 T cells (i) are summarised. Results plot the mean of each group; the error bars represent the SEM. n = 5-6 mice per group except for mock (n=1).

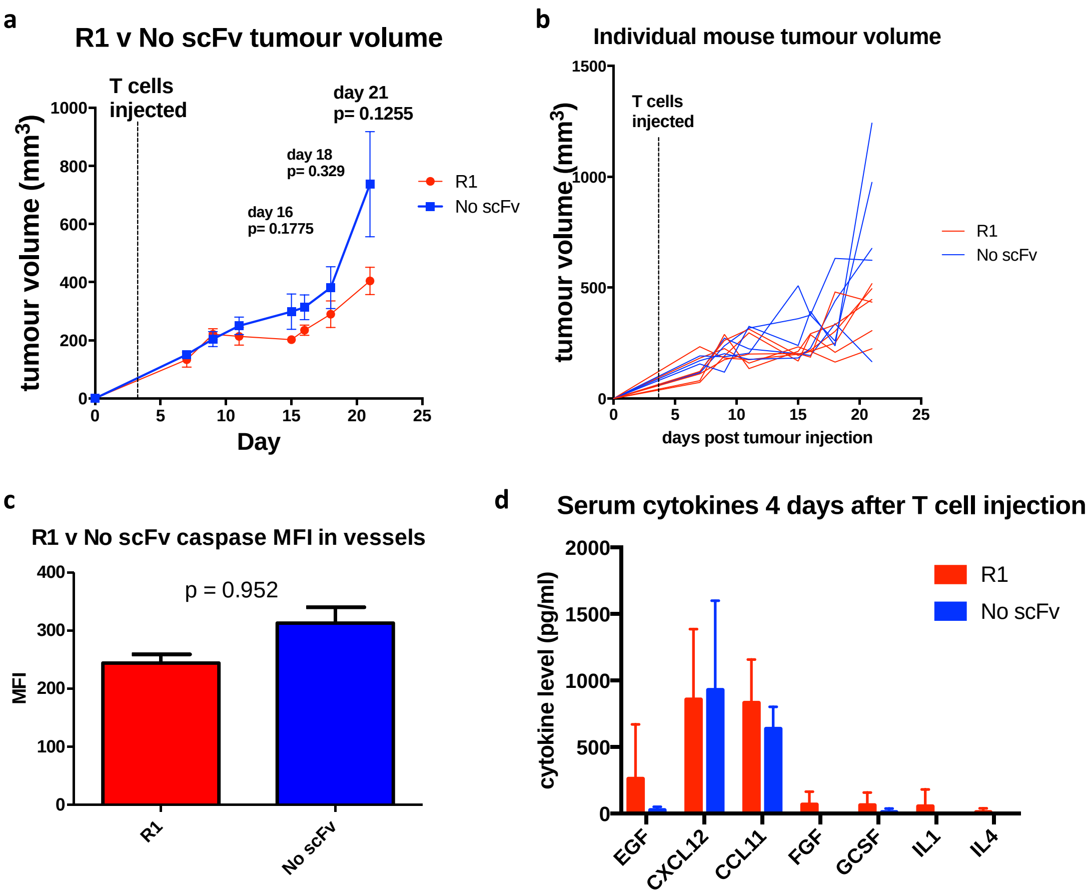

Figure 4.9: anti-tumour response of CAR T cells. Lewis Lung Carcinoma cells were injected s.c. into mice on day 0. 7x10^6 No scFv or R1 transduced T cells were injected into the tail vein on day 4. Tumour size was measured using callipers two to three times per week until day 22. The growth of tumours is summarised for both the R1 and No scFv group (a). Plots represent the mean tumour volume for each group, the error bars represent the SEM. The Mann-Whitney test was performed for each timepoint and the p value is showing for days 16, 18 and 21. In (b), the individual tumour volume of each mouse is plotted. The tumours were removed and frozen on day 22 before being sectioned and immunofluoresence was performed to stain for the colocalisation of tumour endothelium and cleaved-caspase 3. The mean fluorescence intensity of cleaved-caspase 3 within vessels is then summarised (c). n= 6 in the R1 group and n=5 in the No scFv group. The Mann-Whitney test was performed and the p value is shown. (d) 1 week after T cell injection, tail bleeds were performed and serum was removed. Serum was tested for a range of cytokines using luminex but only those that were detectable in at least one mouse are shown. n = 5-6 mice per group.

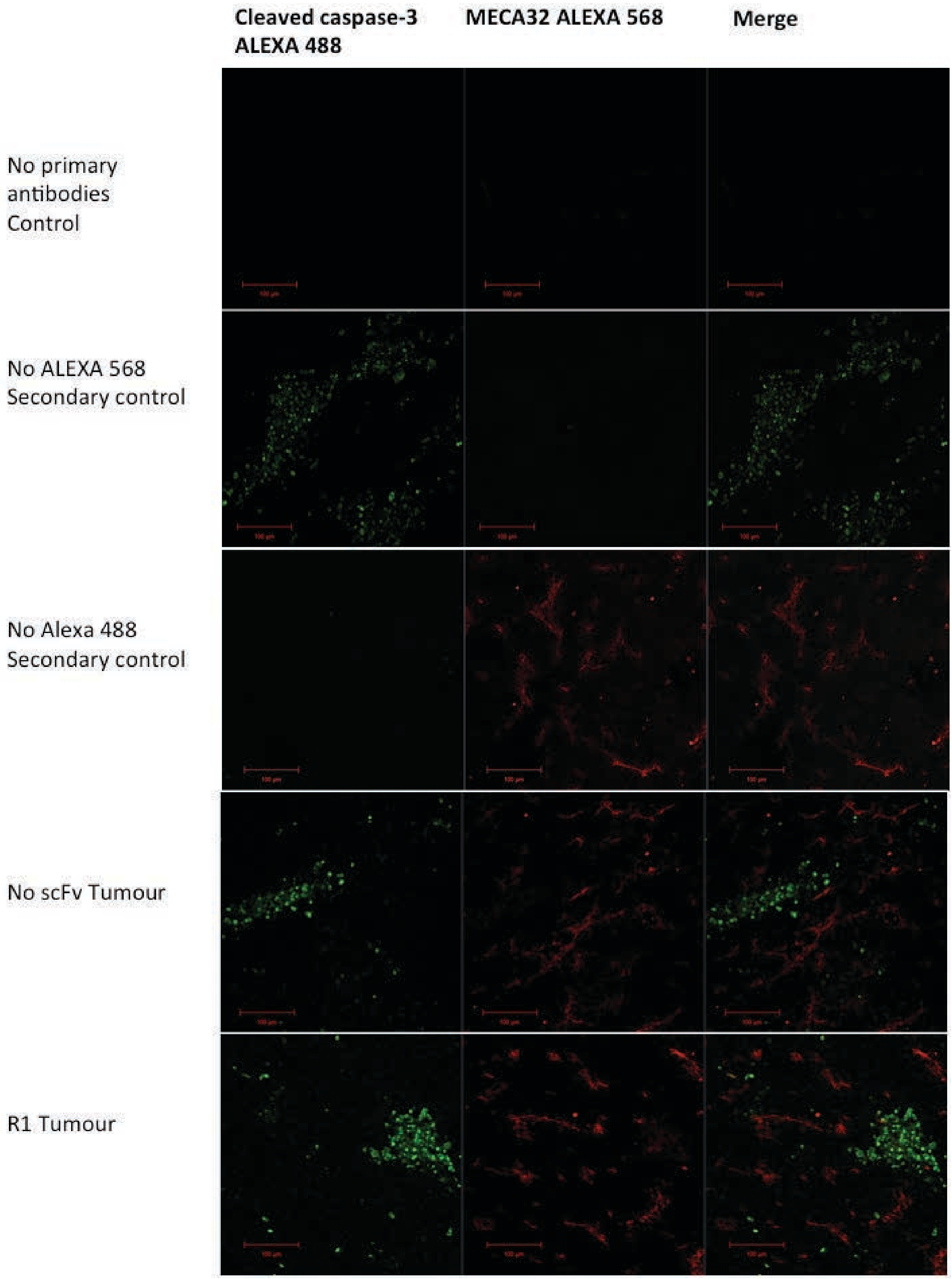

Figure 4.10: immunofluorescence staining of LLC tumour sections. LLC Tumour sections have been taken from mice that had received either No scFv or R1 CAR T cells. Cleaved caspase-3 with the secondary Alexa 488 in green is shown in the left hand side column. The Vasculature marker MECA32 with the secondary Alexa 568 is shown in red in the middle column. The merge of Cleaved caspase-3 Alexa 488 and MECA32 Alexa 568 images is shown on the right hand side column. The top row shows a section that received no primary antibodies. The second row and third row show sections that received no secondary Alexa568 or Alexa 488 conjugated antibody respectively. The fourth and fifth rows show representative tumour sections from mice that received either No scFv or R1 CAR T cells respectively.

4.6 Staining tissue for ROBO4 and CAR T cells

Given the rapid disappearance of ROBO4 specific cells from the blood and the toxicity seen in mice receiving higher doses of ROBO4 specific T cells, it was hypothesised that ROBO4 CAR T cells were reacting to self-tissue. The T cells may be recognising ROBO4 or cross-reacting to another antigen. In order to investigate the possibility of the CAR T cells recognising ROBO4 in normal tissues, immunofluorescence-based antibody staining of tissues was attempted to detect ROBO4 expression. However, ROBO4 staining is notoriously difficult (Roy Bicknell, personal communication). The scFv of the R1 CAR was used to test the detection of ROBO4 in mouse placenta. The scFv has been fused to a Rabbit IgG Fc domain and was provided by Roche. Placenta is an active site of angiogenesis where ROBO4 has previously been detected in the endothelial cells (Huminiecki et al. 2002). Despite this, the scFv only came up with background staining (figure 4.11). The experiment was repeated at different concentrations and with a commercially available ROBO4-specific antibody, but ROBO4 could not be detected even in this positive control tissue (data not shown). Even the use of a previously published protocol failed to work (Zhuang et al. 2015), although the antibody reagent used in this previous study was no longer available.

The CAR T cells contain a CD34 tag, which can be detected by flow cytometry using specific antibodies. Therefore in an attempt to identify the distribution of the infused T cells in tissues, the use of immunofluorescence staining to detect the CD34 tag on T cells within a mouse spleen section was explored. As a positive control, spleen sections were used from mice that received a high dose of CAR T cells specific to another TEM (CLEC14A) where the T cells were known to persist even in peripheral blood. Unfortunately, the human CD34 antibody also detects murine CD34, which is found on endothelial cells (Lin et al. 1995) (figure 4.12). Anti-CD34 clearly detects CD34 on endothelial cells but there was no obvious detection of CAR T cells (figure 4.12) so an alternative approach was explored as described below.

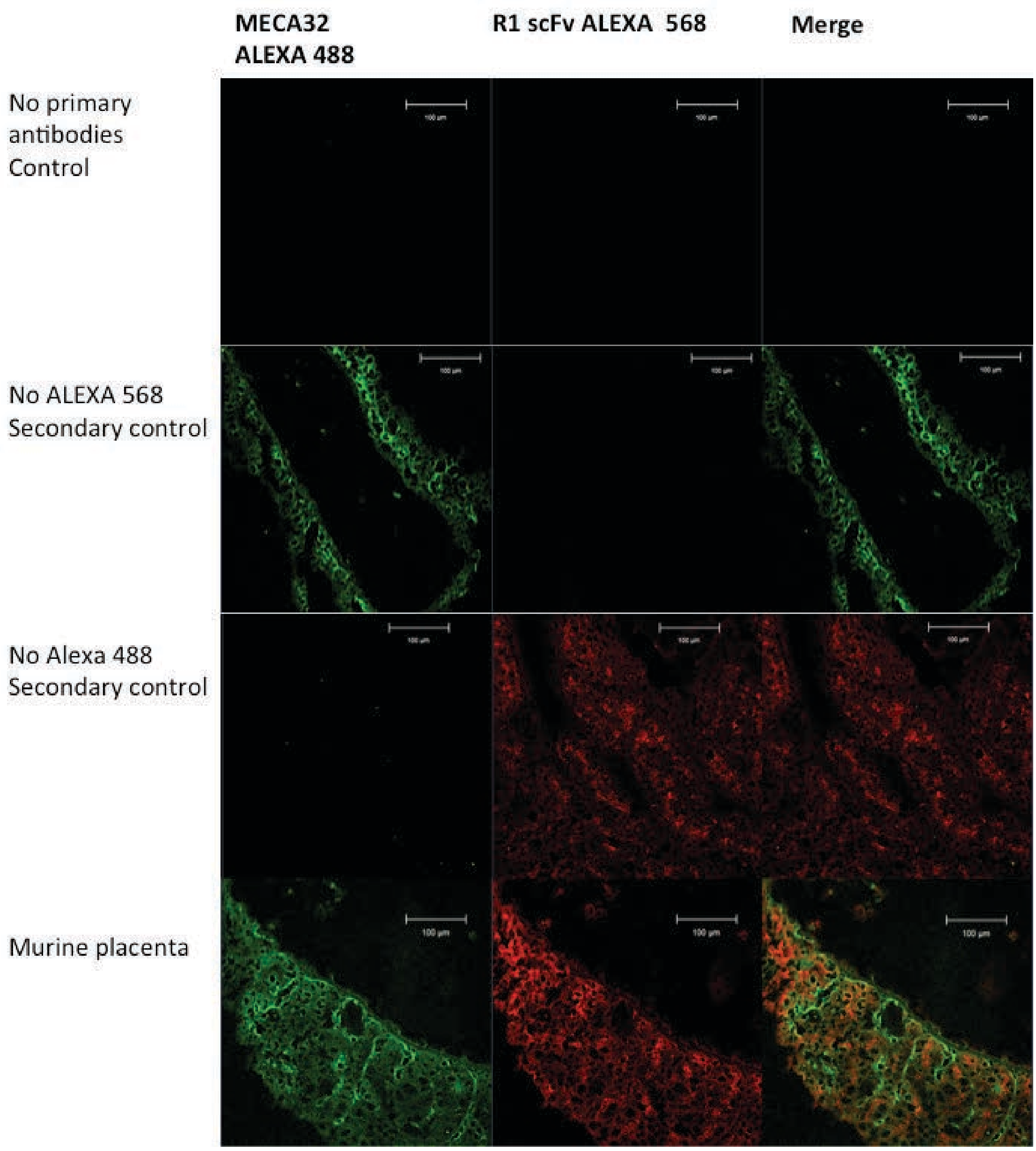

Figure 4.11: immunofluorescence staining of murine placenta for ROBO4. Murine placenta tissue was sectioned and stained for the ROBO4 in the vasculature. The left hand side column shows staining for the vasculature marker MECA32 with an Alexa 488 secondary, shown in green. The middle column shows staining for ROBO4 using the scFv derived from R1 which has been fused to Fc. ROBO4 detection with the Alexa 568 secondary is shown in red. The right hand side column shows the merge of the MECA32 Alexa 488 image and the R1 scFv Alexa 568 image. The top row shows a section that received no primary antibodies. The second and third rows show sections that received no secondary Alexa568 or Alexa 488 conjugated antibody respectively. The bottom row shows a section that received both primary and secondary antibodies.

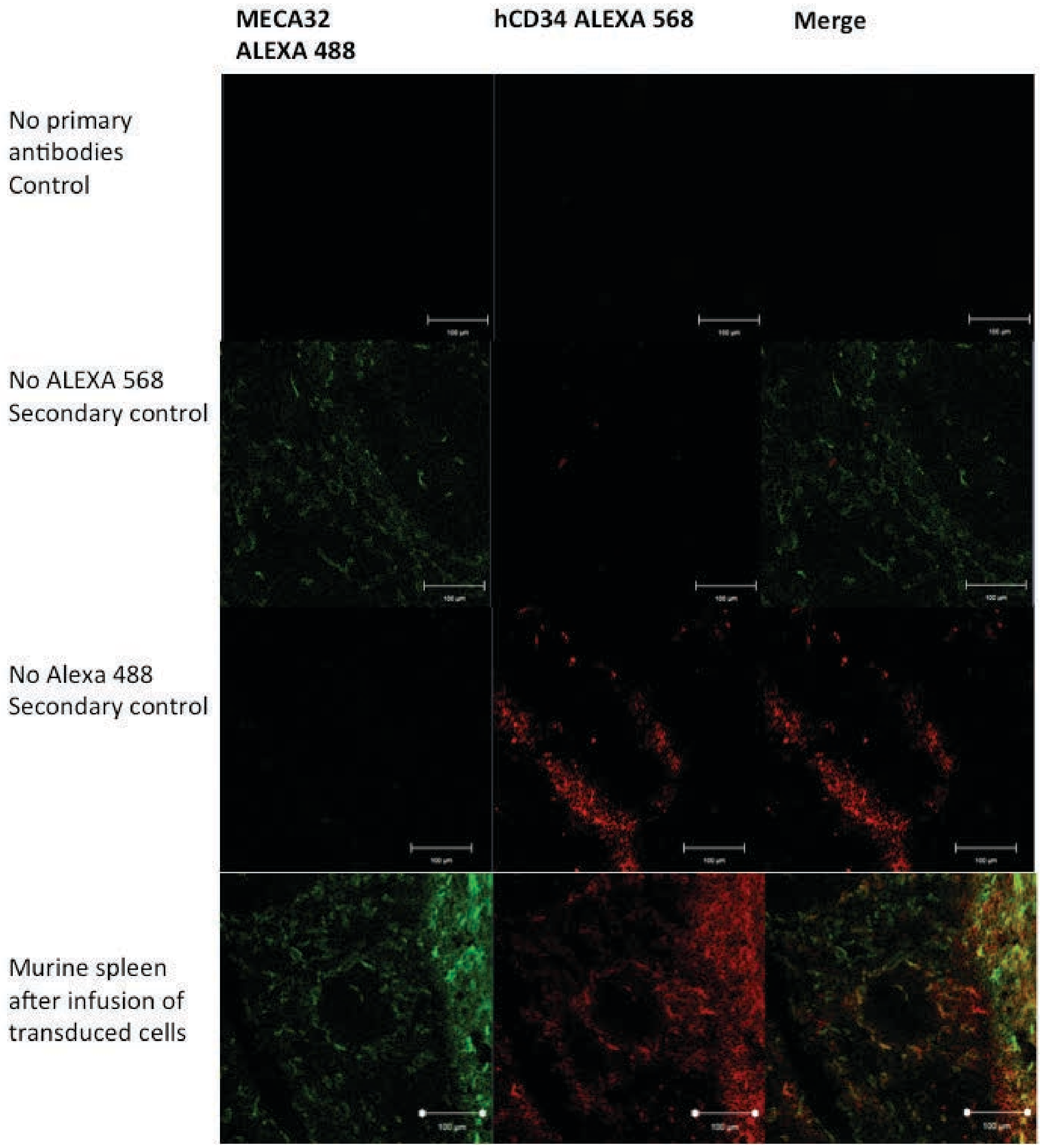

Figure 4.12: immunofluorescence staining of murine spleens for CAR T cells. C57BL/6 received 15 million BoyJ CAR T cells via the tail vain. Mice were sacrificed 5 days later. Spleen sections were analysed using MECA32 with the secondary Alexa 488, shown in green, as seen in the left hand side column. The middle column shows staining for human CD34 with the secondary Alexa 568, shown in red. The right hand side column shows the merge of the MECA32 Alexa 588 and human CD34 Alexa 568 images. The top row shows a section that received no primary antibodies. The second and third rows show sections that received no secondary Alexa568 or Alexa 488 conjugated antibody respectively. The bottom row shows sections that received primary and secondary antibodies.

4.7 Using cryo-imaging to detect CAR T cell location

Given the technical difficulties of CD34 staining in tissue, an alternative approach that permits whole body scanning (rather than having to focus on given tissues) was investigated. This involves fluorescently labelling the CAR T cells and detecting them using cryo-imaging (Wilson et al. 2008) (Roy et al. 2009; Steyer et al. 2009). Cryo-imaging uses a bright-field/fluorescence microscope with automated imaging of whole mouse body sections. Whole frozen mice are sectioned using an automated system. The sections are then imaged on the microscope, providing highly detailed, micron-resolution images. Even fluorescently labelled single cells can be detected (Steyer et al. 2009). Sequential images can be stacked to form a 3D image of a whole mouse, with brightfield anatomy and fluorescent detection of labelled cells. The relative location and distribution of fluorescently labelled cells can then be identified. T cells have previously been detected using this system (Steyer et al. 2009), so cryo-imaging to detect the distribution of the ROBO4-specific CAR T cells was used.

4.7.1 Labelling T cells and detection in the spleen

Since this was the first time this approach had been used in our Institute, initial studies explored labelling of T cells with quantum dots (QDOTs). QDOT nanocrystals can be loaded into cells where they can be traced for several populations and do not leak into neighbouring cells. Activated murine PBMCs were labelled with QDOT625 or left unlabelled. Flow cytometry confirmed successful QDOT625 labelling (figure 4.13). The ability to detect labelled mouse cells in the spleen was then tested. 6 million of the labelled activated or 6 million of the unlabelled activated PBMCs were injected into the tail vein of C57BL/6 mice. 3 days later, the spleens were harvested and frozen before being sent for cryo-imaging.

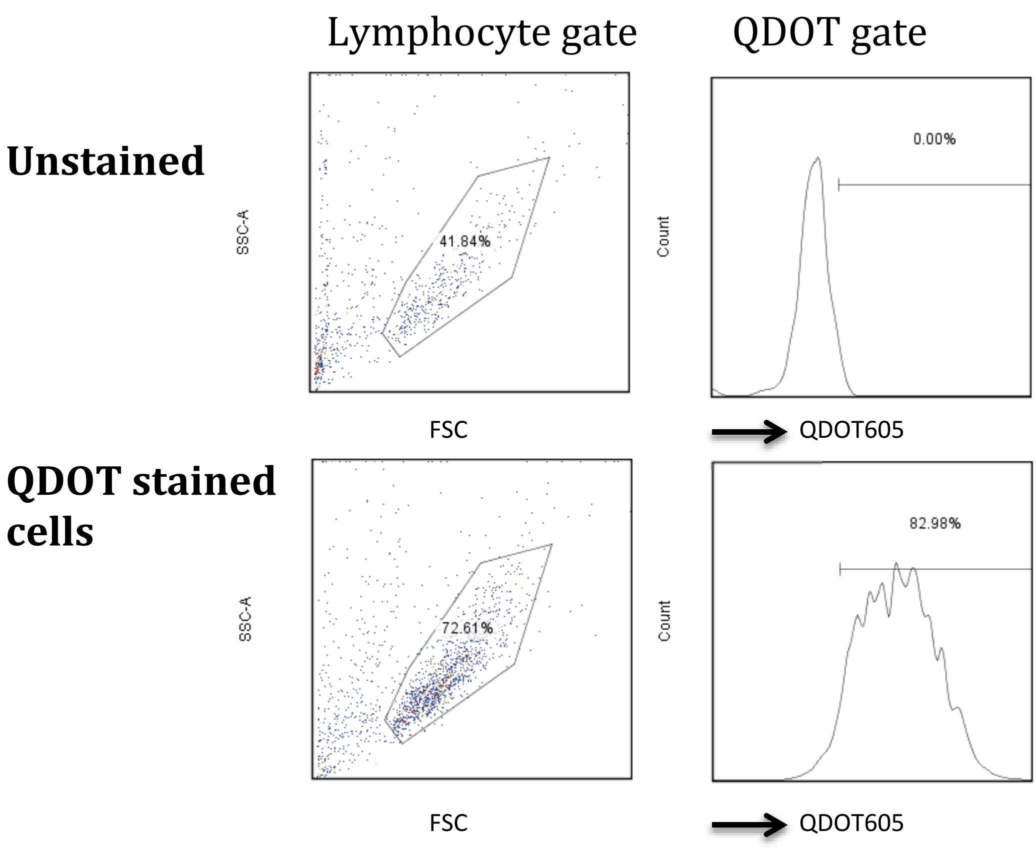

Figure 4.13: QDOT staining of activated murine PBMCs. Murine splenocytes were activated and cultured for three days, then labelled using QDOT625 nanocrystals. PBMCs were then analysed for QDOT625 staining. QDOT stained cells and unstained cells were gated for lymphocytes. A QDOT gate was then set using the unstained lymphocytes. QDOT625 could be detected in the QDOT605 channel on the LSRII.

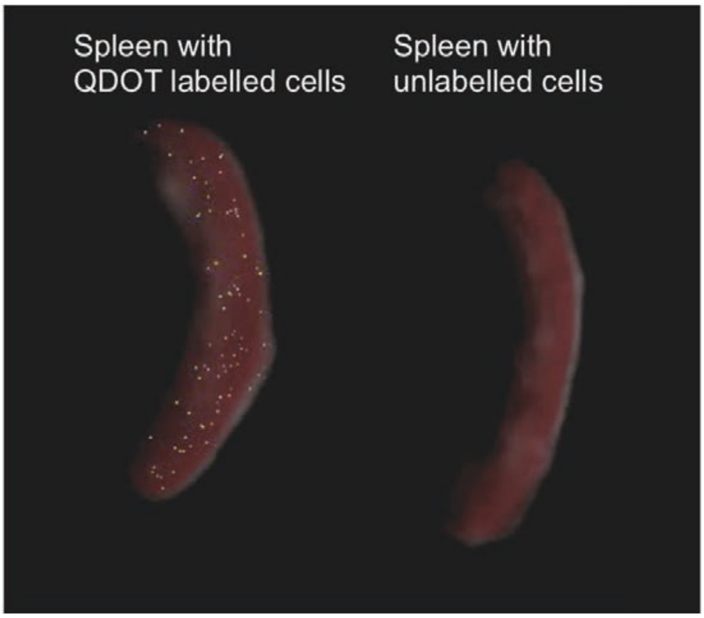

Figure 4.14: image of spleens from mice receiving either QDOT625 or unlabelled activated splenocytes. C57BL/6 mice were infused with QDOT labelled or unlabelled activated C57BL/5 splenocytes then euthanized three days later. The spleens were removed and frozen then cryoimaging was performed. The above image shows a snapshot of a 3D image of a merge of light microscopy and fluorescent microscopy of 62 individual 40μM sections throughout the spleens. QDOT detection is shown as yellow dots.

Table 4.1: QDOT cell detection. Table shows the numbers of QDOT625 labelled cells detected in the spleens of mice three days after receiving either QDOT labelled or unlabelled activated splenocytes. Cryoimaging was used to detect cells.

Mouse	cell count
QDOT spleen	610
Unlabelled spleen	0

The spleens were sectioned into 60μM thick sections. This allowed 62 sections of each spleen. QDOT labelled cells were clearly detected in the spleen receiving QDOT labelled activated cells whereas there was no detection in the negative control spleen receiving unlabelled activated cells (figure 4.14 and table 4.1).

4.7.2 Fluorescently labelled CAR T cells in whole mice with cryo-viz detection

For the cleanest data, QDOT labelled T cells should be sorted so that only QDOT positive, CAR expressing T cells are injected. Otherwise non CAR-transduced

QDOT-labelled cells, which may not disappear from the blood, could skew the results. Similarly, non-T cells could confuse the results. Therefore before transduction, splenocytes were negatively sorted using MACs beads to remove non-T cells. The remaining T cells were then activated as usual with concanavilin A and IL7. T cells were then transduced with either the R1 or No scFv CAR construct. Due to high costs associated with the cryoviz system, R2 was not included in this experiment.

The following day, transduced T cells were labelled with QDOT 625 then underwent FACs sorting for double positive CD34 QDOT T cells. Unfortunately, due to the unexpectedly low numbers of double positive R1 and No scFv T cells recovered after sorting, only one mouse could be treated with each T cell line. 3.36×10^6 R1 or No scFv T cells were infused into mice. Three days later, mice were euthanised, frozen and delivered to BioInvision. Representative cryoviz images are shown in figure 4.15 QDOT T cells were clearly detectable in the organs of both mice, especially the lung and the liver (figure 4.15 and 4.16). There was little detection of T cells in other sites (figures 4.15 and 4.16). Overall, a far greater number of R1 cells were detected in the tissues compared to No scFv cells (table 4.2). Note that any T cells that may still be in circulation will not be detected as the QDOT signal is quenched in blood.

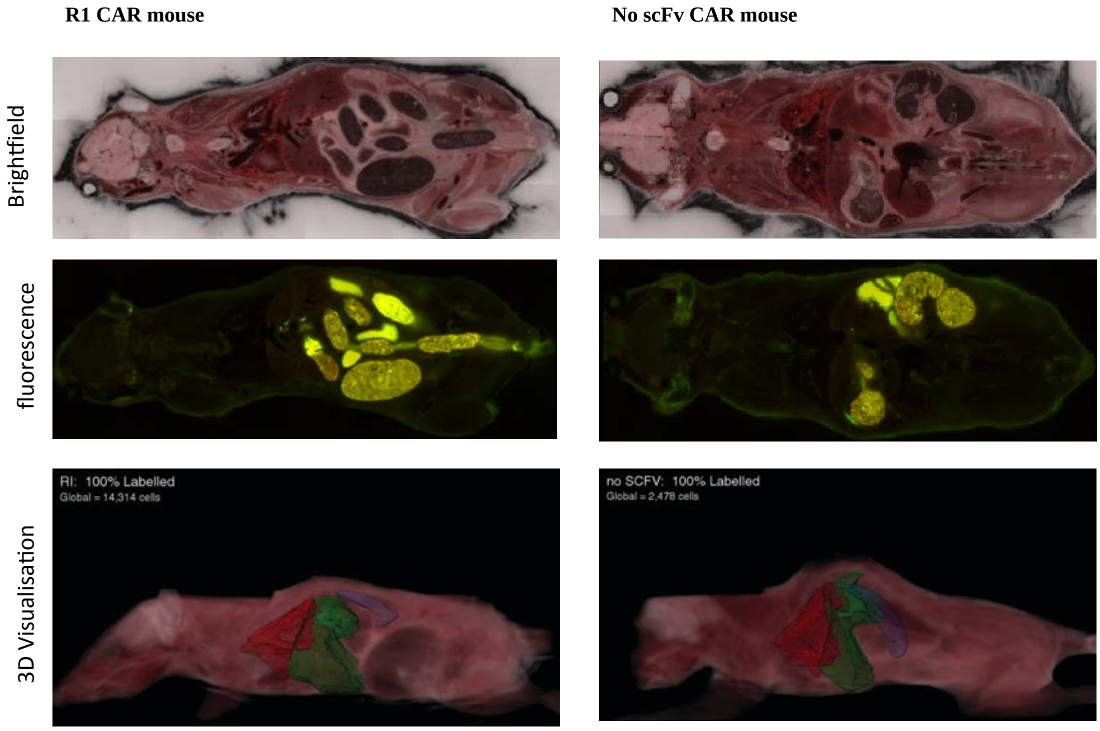

Figure 4.15: representative images from whole mouse cryoimaging. One C57BL/6 mouse was infused with mouse T cells that had been transduced with the R1 (left) or No scFv (right) CAR and have been labelled with QDOT625. T cells were sorted for double positive T cells that were CAR transduced and highly expressed QDOT625 using a FACs sorter. Cells were injected through i.v injection in the tail vain. Three days later mice were euthanized and frozen whole before cryoviz whole body imaging was performed. The top sections show representative brightfield image sections. The middle sections show representative fluorescent image sections. The bottom section shows representative sections from 3D visualisation. In the 3D images, the lungs (red), liver (green) and spleen (blue) are shown.

R1 QDOT labeled T cells (yellow clusters/dots) within Lung (red organ), liver (green organ) and spleen (blue organ)

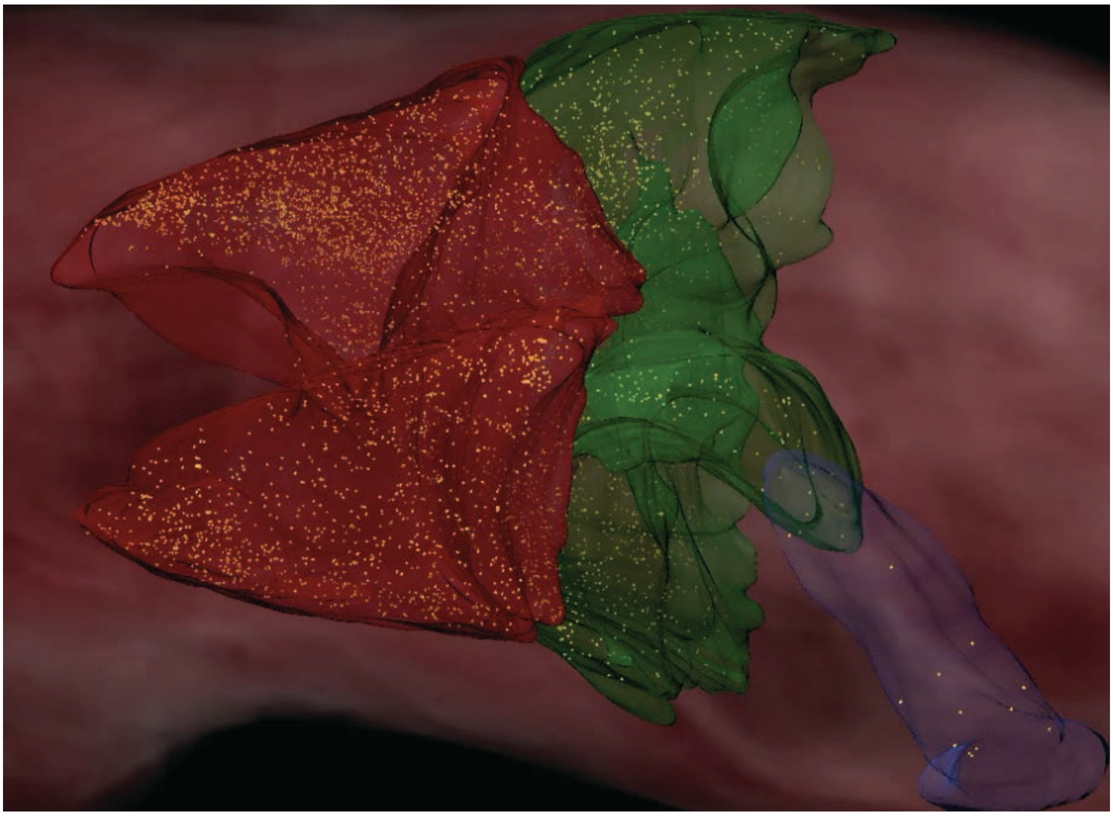

No scFv QDOT labeled T cells (yellow clusters/dots) within Lung (red organ), liver (green organ) and spleen (blue organ)

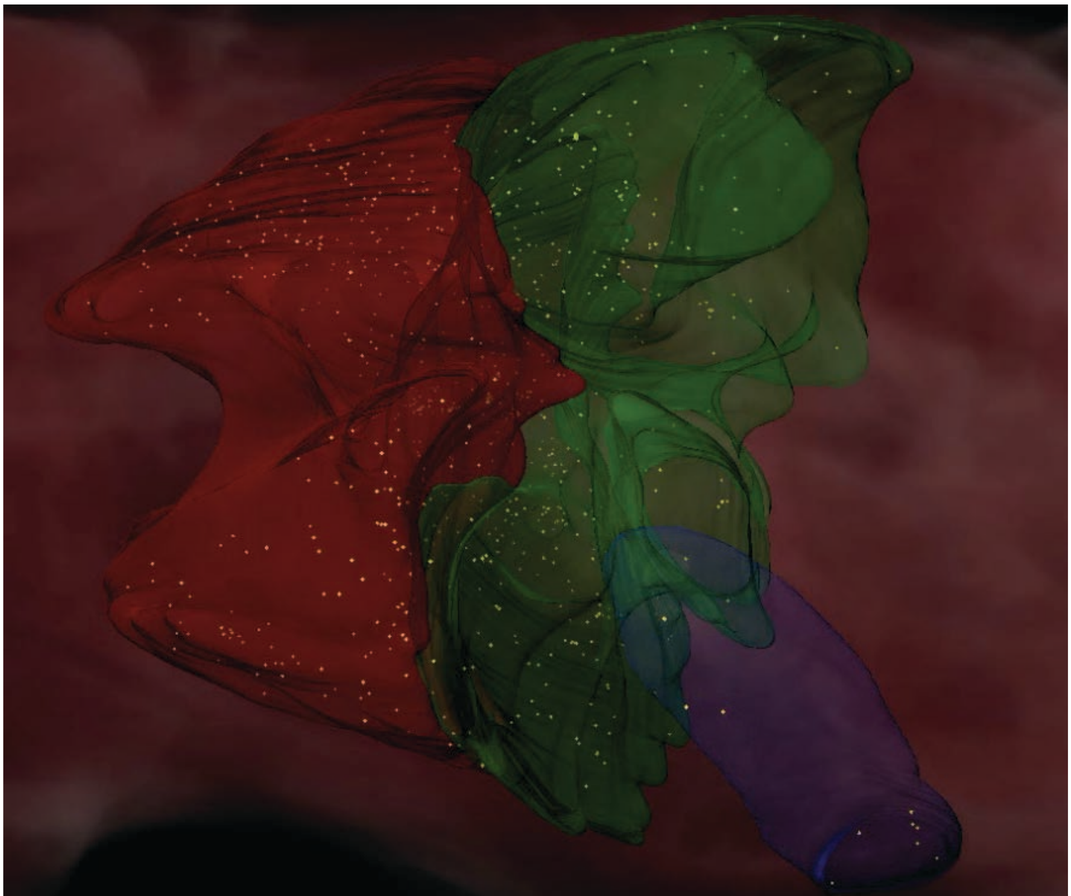

Figure 4.16: detection of QDOT labelled CAR T cells in the lung, liver and spleens of mice. C57BL/6 mice were infused with mouse T cells that had been transduced with the R1 or No scFv CAR and have been labelled with QDOT625. T cells were sorted for double positive T cells that were CAR transduced and highly expressed QDOT625 using a FACs sorter. Three days later mice were euthanized and frozen whole before cryoviz whole body imaging was performed. Images are a snapshot of a 3D image generated from fluorescent microscopy and brightfield microscopy from 1000's of 40µM sections of whole mouse. QDOT labelled cells are detected as yellow dots/clusters.

Table 4.2: overall detection of QDOT labelled CAR T cells in mice. One mouse received either 3.36 million C57BL/6 T cells that were FACs sorted for high QDOT625 expression and expressed either the R1 or No scFv CAR. Each mouse was then euthanized three days later and analysed for the presence of QDOT cells using cryoviz. Global refers to the total number of cells detected within the tissues of mice.

Mouse	Global	Lungs	Liver	Spleen
R1	14,314	7,406	6,445	41
No scFv	2,478	809	1,457	22

4.8 Chapter 4 discussion

In this chapter, ROBO4-specific CAR mouse T cells were tested for toxicity by dose escalation in healthy, immune-competent mice. ROBO4 CAR T cells were selectively depleted from circulation at a range of doses and caused severe toxicity at high doses. Whole body cryoimaging suggested that ROBO4 CAR T cells are accumulating in the lungs and liver. In addition, ROBO4 CAR T cells resulted in a slight but insignificant reduction in LLC growth. In the following discussion, the possibility of reducing ROBO4 CAR toxicity and increasing anti-tumour efficacy are examined.

4.8.1 The nature of ROBO4 CAR mediated toxicity

ROBO4 CAR T cells were selectively removed from the blood circulation. At higher doses, they caused severe toxicity within 24 hours. ROBO4 CAR cells were found to accumulate in the lung and liver especially. It is unknown whether ROBO4 CAR T cells are interacting with ROBO4 in these tissues or a cross-reactive antigen. The use of ROBO4 knockout mice could help identify this. If ROBO4 CAR T cells remain in the periphery and toxicity is absent in ROBO4 knockout mice and then this would suggest that the toxicity seen in this project is down to recognition of ROBO4 in normal tissues. Previous studies have identified ROBO4 expression within endothelial cells of the lung, liver, heart and kidney of adult mice (Park et al. 2003). The relative expression levels in this study were not explored, however ROBO4 expression was found to be higher in the heart and kidney than the lung and liver. Yet CAR T cells were not identified in the heart or kidney from whole body cryo-imaging in this project. ROBO4 has been identified in the liver of healthy C57 BL6 mice (Zhao et al. 2014), although the precise location and relative expression levels were not identified. Given that ROBO4 expression is controlled by shear stress (Mura et al. 2012), and given that liver sinusoids are often under lower shear stress than other normal blood vessels (MacPhee et al. 1995), it is possible that ROBO4 is expressed within liver endothelium. Although immunofluorescence failed to detect ROBO4 in normal liver endothelium compared to cancerous liver endothelium (Mura et al. 2012), this is something that should be investigated further. Due to the problems finding suitable commercial antibodies to ROBO4, a phage display library could potentially be used to recover murine ROBO4 specific scFv for use in IHC/IF. This has previously been done before for the large isoform of the glycoprotein tenascin-C, whose expression is largely restricted to the tumour stroma (Brack et al. 2006). Alternatively, gene microarrays could be performed to investigate ROBO4 expression within lung and liver cell lysates as well as the lysate of endothelial cells isolated from these tissues. Ideally, the tissues from mice experiencing ROBO4-mediated toxicity could be analysed by histology for damage and inflammatory infiltrate, particularly in the lung and liver. Unfortunately the organs of mice experiencing severe toxicity were not recovered in time in this project. There was no noticeable damage or infiltrate in the organs of mice that were recovered from the toxicity experiments in this project (data not shown). It is likely that by the time the experiments have ended and organs have been recovered, any inflammatory infiltrate and tissue damage will have been resolved.

4.8.2 Controlling CAR T cell activation/toxicity

The significant toxicity seen in the mice receiving high doses of ROBO4 specific T cells is another example of the potential dangers of targeting overexpressed antigens. It may be that the CAR derived antibodies obtained from Roche are of too high an affinity to safely target an overexpression antigen. The CAR studies in this project found that in general, the R2 CAR resulted in the reduced responses seen in some in vitro functional studies compared with R1. However, even R2 CAR T cells caused significant toxicity. Perhaps lower affinity antibodies are required, although this may reduce anti-tumour efficacy. CARs with reduced scFv affinity have been showing to spare low antigen-expressing cells but still detect high antigen expressed on tumour cells (Liu et al. 2015). Blocking antibodies to

CAIX has previously been used in human trials to prevent CAIX-specific CAR mediated off-tumour toxicity (Lamers et al. 2013). However this method could easily inhibit anti-tumour activity and it might be difficult to control the effective dose. In order for a ROBO4 specific CAR to be developed further, substantial CAR modifications may have to take place to improve safety.

Combinatorial CAR

One method is to split CAR costimulation signalling onto a separate CAR. By choosing a low affinity scFv for the first CAR with only a CD3ζ signalling domain, stimulation through this CAR alone is insufficient for T cell activation. With the inclusion of a second CAR that contains costimulation domains and is specific to a separate antigen, full T cell activation can occur once both antigens are detected. Using this method, Kloss and colleagues targeted the prostate tumour antigens PSCA and PMSA in xenogeneic tumours in mice (Kloss et al. 2013). The combinatorial CAR T cells could only destroy tumours expressing both antigens and not tumours expressing single antigens, even when these different tumours were in the same mouse (on different flanks). This combinatorial method could be utilised for ROBO4 CAR T cells. The ROBO4 CAR could signal only through CD3ζ and costimulation could be provided through a second CAR to another TEM. CD31 for example could be used to largely restrict activation to within the vasculature. However an additional TEM may be better suited if ROBO4 is also expressed within normal blood vessels (Park et al. 2003).

By requiring two TAAs for T cell activation, the risk of on-target toxicity to normal tissues is greatly reduced. However, it requires an overlapping expression pattern of two TAAs. Tumours may also escape recognition by losing expression of just one of these antigens. Another possible problem could be the induction of anergy after signalling only through the low affinity CAR upon encountering normal tissue. Signalling through one CAR may also result in activation in certain circumstances, such as a very high antigen expression in some tissues.

Inhibitory CAR

A different strategy is to use an inhibitory CAR (iCAR). Federov and colleagues designed a CAR that sends inhibitory signals using the PD1 or CTLA4 intracellular domains (Fedorov et al. 2013). iCARs were capable of greatly reducing T cell cytokine production, proliferation and killing ability. The PD1 based iCAR showed superior inhibition to the CTLA4 iCAR. The iCAR has the potential to prevent CAR T cell mediated damage of normal tissue. In a proof of principal in vivo study, T cells with an iCAR specific to PSMA and a conventional CAR specific to CD19 were unable to clear a PSMA^{+} CD19^{+} tumour. Tumour growth was similar to mice receiving control T cells. The major roadblock to using an activation CAR with an iCAR is choosing the correct iCAR antigen and balancing the signal threshold for activation. If the normal iCAR antigen has a broad distribution pattern T cells may receive significant iCAR stimulation before they reach the tumour site at which point they become unresponsive even in the presence of the activating CAR tumour antigen.

Notch CAR

Over the last year there has been an increasing interest in developing CARs with greater control of T cell activation. Roybal and colleagues have developed a dual receptor circuit CAR termed a synNotch Car (Roybal et al. 2016). Upon CAR recognition of its antigen, instead of sending activation signals it cleaves its intracellular transcriptional activator domain. This domain can then induce the expression of a second CAR. This second CAR is specific to a tumour-associated TAA and has typical activation signals. Therefore the T cell is only activated after encountering both the synNotch ligand and the TAA.

In vivo xenogeneic models using the synNotch CAR system showed that only tumours expressing both relevant antigens resulted in T cell activation and clearance of tumours (Roybal et al. 2016). Tumours expressing only the second antigen on the opposite flank of mice showed no evidence of bystander killing, demonstrating that the specific activation of T cells only occurred in the desired target microenvironment. This report showed an interesting proof of concept but would require further development since it utilised murine and yeast derived components that may cause the T cells to be immunogenic in human hosts. Furthermore, after in vitro synNotch CAR stimulation, it took 6 hours for half maximal second CAR expression and 12 hours for half maximal T cell activation, Since these T cells may not receive their initial synNotch CAR signals until they reach the tumour microenvironment, they would continue to be exposed to the tumour microenvironment for 12 hours before they may be sufficiently activated to mount an anti-tumour response. The external tumour microenvironment may actually prevent the T cells from becoming sufficiently activated in this time. There is also the danger of the second CAR remaining expressed after leaving the tumour and the CAR T cell is free to cause off-tumour toxicity until CAR expression is lost.

Switch CAR

A different approach is the switch CAR (sCAR). The sCAR is specific to a switch molecule that is typically linked to an antibody specific to a TAA. Therefore, T cells are only activated once a CAR-switch-TAA interaction has formed. This approach has used divalent avidin CARs specific to biotin or CARs specific to FITC (Tamada et al. 2012; Urbanska et al. 2012). Such CARs can then be redirected to TAA through biotin or FITC labelled antibodies. CAR T cells showed in vivo anti-tumour ability in the presence of the relevant labelled antibodies in both xenogeneic (Tamada et al. 2012; Urbanska et al. 2012) and syngeneic models (Tamada et al. 2012). However the syngeneic mouse study used tumours expressing human antigen as the antibody target. The possibility of on-target toxicity of normal tissue was therefore not investigated.

Two recent studies have used a peptide neo-epitope (PNE) derived from a yeast transcription factor linked to a CD19 specific fragment antigen-binding (FAB) domain (Rodgers et al. 2016) and FITC linked to a CD19 or CD22 FAB (Ma et al. 2016). The activation and function of both anti-PNE and anti-FITC sCAR T cells was dependent on the presence of the relevant switch molecule linked to antibodies specific to target cells. Furthermore, in vivo proliferation, cytokine production and tumour control could be controlled through different doses of the switch molecule. The common CAR related toxicity of CRS correlates with the expansion of CAR T cells and a high tumour burden. In one fatal study, a massive CAR T cells expansion correlated with severe TLS and CRS (Brentjens et al. 2010). Lower doses of switch molecule resulted in reduced T cell expansion, reduced cytokine levels and slower tumour clearance (Rodgers et al. 2016; Ma et al. 2016). However switch doses could be increased after the initial tumour response to accelerate tumour clearance in the absence of CAR related toxicities. B cell aplasia is another consequence of CD19 CAR T cell treatment. Ma et al showed that mouse T cells expressing the sCAR could be turned off after anti-CD19 switch molecule removal, therefore allowing the repopulation of CD19 cells in the periphery (Ma et al. 2016). In this way, once tumour clearance has been achieved, CAR T cells can effectively be switched off, allowing normal B cell repopulation despite the continued presence of CAR T cells. A further advantage of the sCAR is that one sCAR can potentially target multiple different antigens by the use of different switch molecules. Ma et al. showed that the same anti-FITC sCAR could be redirected with antibodies to CD20 (Ma et al. 2016).

A similar study developed a sCAR to target the breast cancer antigen Her2 (Cao et al. 2016). This study again demonstrated that sCAR T cells were only activated in the presence of the switch molecule and the specific target cells. sCAR T cells exhibited a similar in vitro target cell lysis ability and in vivo xenograft tumour control to conventional CAR T cells. Furthermore, despite the short half-life of the FAB based switch molecule, conjugating a dye to the FAB showed that it could be retained within the tumour for up to three days after I.V. injection. A key finding in all of these sCAR studies was that the design of the CAR length and/or position of PNE or FITC on the FAB significantly affected T cell activation and function (Rodgers et al. 2016; Ma et al. 2016; Cao et al. 2016). Different construct designs will have a great impact on the immunological synapse and subsequent CAR signalling capacity.

The use of sCARs to target overexpression antigens in solid tumours to reduce normal tissue destruction is also being investigated (Rodgers et al. 2016). In this situation, switch molecule FABs may preferentially accumulate within the tumour due to the high antigen expression rather than low expression within normal tissue. Therefore antigen expression levels in the tumour could be amplified. The use of monoclonal antibodies to overexpression markers has previously shown no toxicity but CARs using the same antibody have resulted in toxicity. Perhaps if a switch FAB controls the activation of sCAR T cells in this situation, no toxicity would be seen and T cells will only be activated within high switch molecule concentrations within the tumour. However, the concept of transduced T cells ignoring low expression of antigen in normal tissue is a dangerous one, as noted in this project with the potential low expression of ROBO4 in normal tissues.

On-switch CAR

Another method to avoid toxicity is the On-switch CAR (Wu et al. 2015). This CAR is formed from two separate components. The first component is the tumour recognition component and second is the on-switch component. For T cell activation, an exogenous small molecule must be supplied in order to induce heterodimerization of the tumour recognition component and the on-switch component. In a proof of principle study, rapalog was used as the small molecule responsible for heterodimerization of a CD19 specific on-switch CAR (Wu et al. 2015). In the absence of rapalog, On-switch CAR T cells fail to become activated and elicit effector responses in response to CD19 target cells. Furthermore, target cell killing is quickly stopped upon removal of rapalog, and quickly restarted upon addition of rapalog. In vivo killing of CD19 target cells also required the injection of rapalog. Despite these results the use of rapalog would be unsuitable for human use due to its extremely poor pharmokinetics. However, if a suitable small molecule with good pharmokinetics could be produced easily with little cost, it could be incorporated to form a ROBO4 on-switch CAR.

4.8.3 Improving CAR T cell function in the tumour microenvironment

ROBO4 CAR T cells resulted in a reduced tumour growth compared to control No scFv T cells, although the difference was not statistically significant. Given the toxicity caused by CAR T cells, the ability of CAR T cells to respond to ROBO4 in vivo may not be the core reason for poor anti-tumour efficacy. It is likely that ROBO4 CAR T cells are suppressed in the tumour microenvironment. Indeed, previous studies have shown CAR T cells isolated from established tumour exhibit hypofunction along with an upregulation of inhibitory markers including PD1 (Moon et al. 2014). It's also possible that given the numbers of ROBO4 CAR T cells accumulating in the lungs and liver, very few CAR T cells have the opportunity to migrate to the tumour tissue.

One challenge to overcome the tumour microenvironment is to firstly ensure a significant number of T cells home to the tumour. The report on 'on-switch' CARs is an example of 'smart' T cells whose function is controlled by an exogenously supplied small molecule. Another example of controlling T cells through small molecules is in the control of cell migration. Park and colleagues engineered G-protein coupled receptor (GPCR) into T cells (Park et al. 2014). The GPCR was capable of redirecting cell migration towards a small synthetic molecule. The authors demonstrated this in vivo where GPCR engineered T cells showed a preferential migration to an implanted bead releasing the small molecules rather than an implanted control bead. Perhaps the same small synthetic molecule could also activate an on-switch CAR, thus controlling CAR T cell migration to the tumour and activation within the tumour microenvironment.

Attempting to overcome the immunosuppressive tumour microenvironment, Liu and colleagues developed an activating PD1 CAR (Liu et al. 2016). This CAR was composed of the extracellular domain of PD1 with the intracellular signalling domain of CD28. T cells with a tumour specific second generation 41BB.ζ CAR and the PD1CD28 activation CAR exhibited an increased cytokine production and target cell killing in the presence of PDL1 expressing target cells than T cells with the tumour specific CAR alone. In vivo xenogeneic mouse models showed that the co-expression of PD1CD28 increased TIL numbers and TIL function as well as improving anti-tumour ability. Interestingly, the improved anti-tumour ability with the PD1CD28 CAR was superior to using a PD1 blocking antibody instead of the PD1CD28 CAR. PDL1 expression has recently been seen in tumour endothelium (Allen et al. 2017) and CD8 T cell activity is downregulated by PDL1 and PDL2 found on activated endothelium in vitro (Rodig et al. 2003).

It is possible that PDL1 is also expressed within the tumour endothelium of LLC. If this is the case then coexpression of a PD1CD28 CAR with the ROBO4 CAR could improve anti-tumour ability. FasL expression has been shown in human and mouse solid tumour vasculature and was responsible for selective effector CD8 T cell depletion but not of Tregs (Motz et al. 2014). Inhibition of FasL inhibited this CD8 T cell depletion. Future experiments could use IHC to investigate PDL1 and FasL expression within the endothelium of LLC.

The combination of anti-PD1 with CAR T cell therapy has shown efficacy in murine models (Liza B John et al. 2013; Cherkassky et al. 2016). Anti-PD1 may also benefit ROBO4 CAR therapy. A recent paper has demonstrated the ability to knockout the PD1 gene in primary human T cells using the CRISPR-Cas9 system (Su et al. 2016). T cells subsequently showed improved IFNγ production and target cell lysis in vitro. Additionally, a clinical trial using the CRISPR-Cas9 mediated PD1 knockout in cancer patients T cells for use in adoptive cell therapy have now started (https://clinicaltrials.gov NCT03081715). This non-viral method of PD1 knockout could potentially be combined with CAR transduction. Additionally it could replace the use of anti-PD1 checkpoint inhibitors as a safer alternative that specially affects only the infused CAR T cells rather than all host T cells.

The expression of cytokine constructs with CAR engineered T cells has also improved anti-tumour efficacy in murine models. The addition of an IL15 expressing T cell population enhanced the in vivo anti-tumour efficacy of VEGFR1 CAR T cells (Wang et al. 2013). The coexpression of an IL12 construct along with the VEGFR2 CAR has also been found to increase anti-tumour efficacy (Chinnasamy et al. 2012). The addition of a proinflammatory construct may benefit ROBO4 CAR T cells in the tumour microenvironment but of course the impact on toxicity in normal tissues may also be increased and would therefore need careful monitoring.

A hypoxic tumour microenvironment can negatively impact anti-tumour function of T cells. Tumour cells and macrophages of the tumour microenvironment are known to produce and release prostaglandin E2 (PGE2) that is known to suppress T cells. The tumour microenvironment also has highly hypoxic regions that can result in release of Adenosine, another inhibitor of T cells. Both PGE2 and Adenosine are capable of activating protein kinase A (PKA). PKA then localises to the T cell immune synapse by binding to the membrane-associated protein Ezrin. Here, PKA can inhibit TCR signalling. Newick and colleagues engineered CAR T cells to express a small peptide that inhibits PKA binding to Ezrin (Newick et al. 2016). These CAR T cells had increased cytokine production, proliferation and target cell lysis in the presence of PGE2 than conventional CAR T cells. They also had increased ant-tumour ability in mouse models.

5. Discovering Novel Antibodies to TEMs

5.1 Antibody Phage Display

The results presented in the previous two chapters, where CARs to ROBO4 were toxic at high cell doses, possibly due to ROBO4 expression on healthy tissues, highlight one of the greatest needs in the development of T cell based therapies for cancer. Namely, the need to identify antigens that can be safely and effectively targeted. Therefore we sought to develop CARs to other TEMs. However, this first required generating antibodies specific for these markers. Therefore, the use of a phage display library was explored.

Ideally, since the aim is to target the tumour vasculature, any CAR should be cross-reactive to human and mouse TEMs to allow pre-clinical development in mouse models. Due to immune tolerance, the murine hybridoma method of antibody production will rarely generate a cross-reactive human and mouse homolog specific antibody. In contrast, the use of in vitro phage display libraries can circumvents immune tolerance and can potentially generate species cross-reactive antibodies to conserved sites (Liang et al. 2006).

The ETH2 gold phage display library is an scFv based library (Silacci et al. 2005). All scFv from this library are originally derived from only 3 germline human variable (V) immunoglobulin genes. That is one heavy chain variable gene DP47 and two light chain variable genes: DPL16 and DPK22, from the lambda and kappa loci respectively. The ability of an antibody to recognise and bind to antigen is determined from three separate regions called the complimentary determining regions (CDR). The germline and non-germline amino acid variability found in these regions is what determines specificity. The CDR3 loop is considered the most important for antigen recognition. Therefore, DP47 has had a random 4-6 amino acid sequence introduced into the CDR3 site. Likewise, the CDR3 of both light genes have received 6 random amino acids with at least one proline for DPL16 and at least one proline and glycine for DPK22. scFv were then paired, with DP47 forming a lambda fraction with DPL16 or a kappa fraction with DPK22.

Therefore, despite starting with only 3 variable genes, the addition of random amino acids into each CDR3 has resulted in a huge repertoire of different lambda and kappa scFvs, with a diversity of $3x10^9$ different clones. Each of the scFv fragments has been inserted into a Phen1 phagemid vector. This vector (figure 5.1) contains an ampicillin resistance gene to allow selection. The scFv is linked to a PelB sequence that can allow secretion of the scFv, and a Myc tag that can allow scFv detection. Importantly, the scFv also links to the VCSM13 phage coat protein pIII gene. This can allow the production of a phage coat protein with the scFv expressed on the outside. Furthermore, the amber stop codon between the scFv and the pIII gene results in a stop in translation in suppressor strains of *E. coli.* In such strains, only the scFv protein is produced, along with its Myc tag and the PelB secretion leader sequence. This allows the production of scFv into the supernatant, which may then be purified.

Vectors have been introduced into the *Escherichia coli* strain TG1 by electroporation. The phage library is then supplied as a stock of scFv-phagemid containing TG1. The library was provided with four sub-library TG1 stocks. Each sub-library stock has been derived from separate rounds of CDR3 editing, with two stocks for kappa scFv and two for lambda scFv.

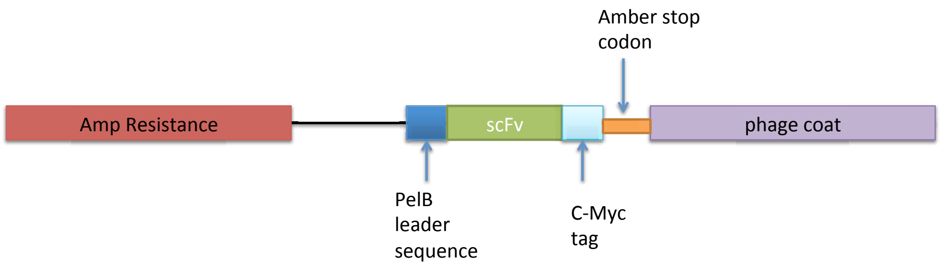

Figure 5.1: Figure 5.1: a section of the Phen1 phagemid vector. The vector contains an Ampicillin (Amp) resistance gene shown in red to allow positive selection. The scFv in green is linked to a C-Myc tag in light blue. Linked to this is the M13 phage coat gene in purple. Between the scFv-Myc and the phage coat is an amber stop codon in orange. In suppressor strains of *E.coli*, this is read as a stop codon and translation stops here. The scFv in this case can be secreted due to the PelB leader sequence in blue. In non-suppressor strains, the amber codon is not read as a stop codon and translation continues into the phage coat, linking the scFv protein to the phage coat protein.

Step one in setting up the library was to amplify each stock then aliquot. The Bicknell lab (University of Birmingham) previously completed this. The ETH2 Gold library of scFv expressing phage was then generated by growing each of the four TG1 sub-library stocks in media containing ampicillin, to select for TG1 that contain the phagemid vector, then superinfection of each sub-library culture with VCM13 helper phage. After infection, each culture was centrifuged then pooled together and resuspended in media with ampicillin and kanamycin. This allowed selection of TG1 that contain the phagemid vector and have been infected with the helper phage which carry a kanamycin resistance gene. Helper phage will replicate in TG1 and incorporate a new protein coat gene III from the phagemid vector. Thus creating new phage that now contain scFv fragments expressed on the protein coat. Newly assembled phage are released into the supernatant and can be purified through polyethylene glycol (PEG) precipitation and titred as described in the methods chapter. Precipitated phage were then aliquoted into 1ml vials of 10^{12} titre units (T.U)/ml.

The concept of phage selection involves the panning of library scFv-expressing phage against an antigen of interest, typically protein (figure 5.2). Phage with a specific scFv are captured on the antigen whereas non-specific scFv phage are washed away. The specific captured phage can then be released from antigen and amplified into larger numbers. Typically, panning requires further rounds of selection to enrich for antigen specific phage and depletion of non-specific phage.

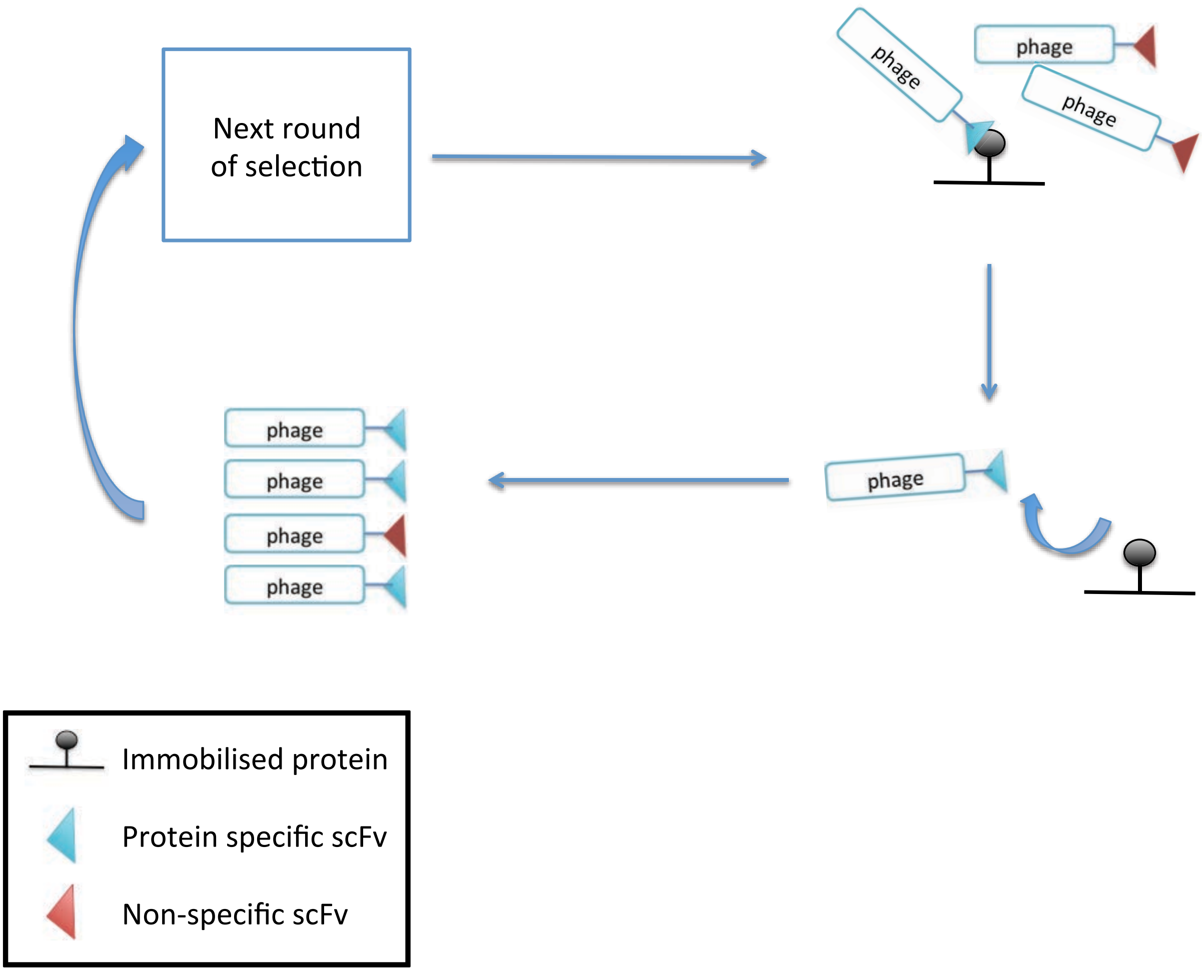

Figure 5.2: the concept of phage selection. A library of scFv expressing phage are incubated with an antigen of interest. Any phage with an scFv specific to this antigen can specifically bind to the antigen, such as the phage with a blue scFv in this figure. Non-specific scFv phage, such as the red scFv phage in this figure, fail to bind specifically and can be washed away. Specifically bound phage can then be eluted from the antigen before they are used to infect *E. coli*, allowing them to be amplified to greater numbers. Typically the specific phage is only enriched and non-specific phage will still be present. Therefore further rounds of selection are required to further enrich for specific phage.

5.2 Testing phage selection to BSA

Since this was the first time a phage display system had been used in our institute, selection began by attempting phage enrichment to bovine serum albumin (BSA) as a readily available protein target. An immunotube was coated overnight with 50ug/ml BSA in PBS. After blocking the tube with milk-PBS, 10^{12} T.U of library phage were added. The tube was left for 30 minutes on a shaker then left to stand upright for 1 hour. After selection, the supernatant was removed from the tube before washing the tube 10 times in PBS-tween then 10 times in PBS. Bound phage were then eluted from the tube using 100mM triethylamine. Eluted phage were then used to infect exponentially growing TG1 bacteria. After infection, dilutions of the infected TG1 were plated out on 2xTY Amp-Glucose plates to allow titre analysis. The titre can give an indication of selection efficiency. The remaining TG1 were plated onto a separate large 2xTY Amp-Glucose plate.

The following day, the phage titre was counted from the dilution plates (figure 5.3a). Amplification of the selected phage was performed by scraping the lawn of infected TG1 from the large plate. A small amount was then grown in a large culture followed by superinfection with helper VCSM13 phage. Infected TG1 were then grown overnight in 2xTY-Amp-Kan media. The next day the TG1 were centrifuged and the phage-containing supernatant was removed. Phage were subsequently removed from the supernatant by PEG precipitation and resuspended in 2x 1ml cultures.

1ml of precipitated phage was used for round 2 of selection to BSA. An immunotube was coated as before in BSA. Selected phage from round 1 were added to the tube for selection followed by washing, 20 times in PBS-tween and PBS before elution. Phage were amplified and precipitated as before. The titre of round 2 was noted to have decreased 10 fold from round 1, possibly indicating loss of phage through the extra washing or that fewer than 10^{12} T.U of phage were added in round 2 (figure 5.3a)

To determine if this process had successfully enriched for phage specific to BSA a polyclonal ELISA was performed. A Nunc maxisorp plate was coated with BSA at 50ug/ml in PBS, with other wells coated in PBS only. Phage from round 1 and 2 were diluted 1:5 in PBS and tested in triplicate wells to both BSA and PBS. Anti-M13-HRP was used to detect bound phage followed by goat-anti-mouse-HRP. Figure 5.3b shows that by round 2 of selection, phage have clearly been enriched for specificity to BSA.

a

	BSA selection Titre
Round 1	$1x10^6$
Round 2	$1.26\ x10^5$

b

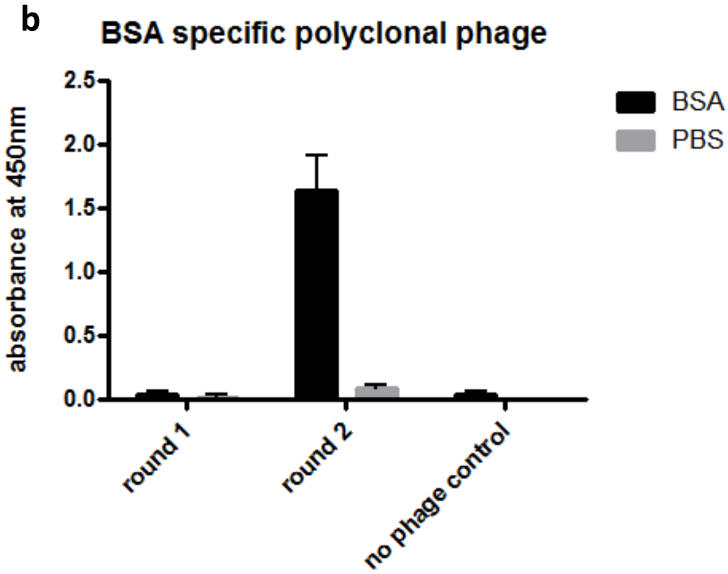

Figure 5.3: phage selection to BSA. Phage were subjected to two rounds of selection. The titre of phage rescue is shown in (a). (b) A polyclonal phage ELISA was performed to test the specificity of phage after round 1 and round 2 of selection to BSA. Results show the mean of triplicate wells, while error bars show the SD.

Having demonstrated the ability to enrich for phage with a given specificity, the phage library was then screened for scFvs specific for three defined tumour endothelial markers, ELTD1, GRIN2D and MCAM. The following pages will briefly introduce each of these markers and describe attempts to isolate scFvs specific to them.

5.3 Introduction to ELTD1

ELTD1 is a member of the G-protein coupled receptor (GPCR) superfamily. Within this superfamily, ELTD1 belongs to the adhesion group. It can then be further characterised into the sub-family, family 1/latrophilin-like. The human ELTD1 gene comprises 3527 nucleotides that are translated and spliced into a 690 amino acid protein (Favara et al. 2014). Similar to its group members, it contains a large extracellular domain (ECD), a seven transmembrane domain and an intracellular tail domain. Within the ECD is an epidermal growth factor (EGF) domain, a calcium binding EGF domain and a GPCR auto-proteolysis inducing (GAIN) domain. The GAIN domain contains a self-cleavage site. This site is cleaved during protein translation in the endoplasmic reticulum. However, the cleaved ECD rejoins non-covalently at the cleavage site before the protein is transported to the membrane. It's suggested this cleavage allows adhesion GPCR's to exchange their ECD with members and/or may be important for ligand binding and signalling. The ligand and signalling capabilities of ELTD1 are unknown. Its intracellular tail is the smallest of its sub-family members at 22 amino acids.

ELTD1 was first discovered in rat adult cardiomyocytes, bronchiolar cells, vascular smooth muscular cells and human adult heart (Nechiporuk et al. 2001). A comparison of human endothelial cell and non-endothelial cell complementary DNA (cDNA) libraries identified ELTD1 as a novel endothelial gene (Herbert et al. 2008). Similarly, ELTD1 was identified as a murine endothelial gene (Wallgard et al. 2008). Two papers identified an ELTD1 upregulation in the vessels of high grade glioma in humans and rat models (Dieterich et al. 2012; Towner et al.

2013). IHC found vascular staining of ELTD1 in grade IV glioma was significantly greater than in normal tissues (Dieterich et al. 2012). mRNA analysis also identified that ELTD1 expression was at least 2-fold greater in the vessels of grade IV glioma than in normal tissues (Dieterich et al. 2012). A landmark paper then identified ELTD1 as a TEM (Masiero et al. 2013). Masiero et al. compared the expression profiles from over 1000 primary human tumours of breast, head and neck and renal cell cancers. From this, ELTD1 was found to be one of the most overexpressed genes. Immunohistochemistry validated these data, finding higher ELTD1 expression in the vessels of 89% of renal (110/124 samples) and 82% of colorectal (98/119 samples) cancers compared with normal tissue samples. Although ELTD1 has been identified in normal cells and tissues, it is hoped that the elevated expression of ELTD1 in tumours can allow it to be safely targeted.

5.3.1 ELTD1 function

ELTD1 is believed to play a role in angiogenesis. Human endothelial cells increased ELTD1 expression in response to the angiogenic molecules VEGF-A and TGFβ2 (Dieterich et al. 2012). Silencing of notch1, resulting in an increase in delta-like ligand 4 (DLL4), caused an increase in ELTD1 in neovascular tip cells (158). Furthermore, Masiero et al. also found VEGF to increase and DLL4 to decrease ELTD1 expression in human umbilical vein endothelial cells (HUVECs). Silencing ELTD1 in HUVEC caused decreased angiogenic sprouting and tip cell formation. Together, since VEGF induces tip cell formation, whereas DLL4 represses this (Hellström et al. 2007), ELTD1 may play a role in tip cell differentiation and/or function. An *in vivo* role in vasculogenesis was also shown through ELTD1 knockdown in zebrafish embryos which resulted in severe vascular defects (Masiero et al. 2013).

Further to the report of expression in the heart, ELTD1 knock-out mice develop normally and appear healthy (Xiao et al. 2012). Yet, upon an increased blood pressure load, knock-out mice develop cardiac hypertrophy. End stage human heart failure patients also showed a decreased ELTD1 expression within the heart compared to normal heart controls. Other studies have identified ELTD1 polymorphisms Andes people living at high altitude; increased human and pig sub-cutaneous fat (Lee et al. 2011); dependence to cannabis (Agrawal et al. 2008); patient risks to GVHD following HSCT (Harkensee et al. 2013); and cattle tick burdon (Porto Neto et al. 2011). The increased tumour vessel expression of ELTD1 was noted to correlate with an increased prognosis in some cancers (Masiero et al. 2013). This lead to a hypothesis that ELTD1 may be important in vessel maturation with an increased ELTD1 expression leading to increased vascular density and maturity (Favara et al. 2014). This ultimately leads to a normalised vasculature that is less leaky with increased function and improved drug delivery. Other studies identified a greater expression of ELTD1 with higher grade gliomas and poorer prognosis (Dieterich et al. 2012; Towner et al. 2013).

5.3.2 Targeting ELTD1

Hypothesising a positive role in tumour angiogenesis, Masiero et al. silenced ELTD1 expression in two xenograft mouse tumour models. Both human derived ovarian and colorectal tumour growth were inhibited after injection of anti-murine *Eltd1* silencing RNA. The mice exhibited decreased size and number of tumour nodules, decreased areas of metastasis and an increased survival compared to control treated mice. Crucially, no signs of toxicity were noted and heart to body weight ratios were not affected. Of note, this lack of toxicity due to knocking down ELTD1 expression, does not mean that an agent which targets ELTD1 expressing cells for destruction (such as a CAR) will also be non-toxic since it has a different mechanism of action.

5.3.3 Selection of ELTD1 antibodies

The extracellular domain of human ELTD1 protein with a His tag was used to coat an immunotube at a concentration of 30ug/ml in PBS. 10^{12} TU of library phage were added to the immunotube. Selection was performed as before, with 10 washes in PBS-tween and PBS before elution. Amplification and PEG precipitation was performed as before. 1ml of precipitated phage was then used for a second round of selection with an immunotube coated in 30ug/ml of human ELTD1-His protein. The tube was washed 20 times before elution, followed by amplification and purification as before. After this second round, phage were tested in a polyclonal ELISA against human ELTD1-His protein at 20ug/ml in PBS and PBS alone. Phage were added to each well at a 1:10 dilution in PBS. From the figure 5.4, phage have been enriched for human ELTD1-His protein by round 2 of selection.

In order to explore both the anti-tumour efficacy and in particular, any possible toxicity, an antibody reagent that would cross react with both human and the murine homolog of the TEM was sought after. The extracellular domain of human and mouse ELTD1 share 65.3% amino acid sequence identity. Therefore there is a good chance of finding a cross-reactive scFv in the library. Selection was continued for another 3 rounds. For round 3 of selection, the murine extracellular domain of ELTD1 with a His tag was coated on an immunotube at 30ug/ml. 1ml of round 2 phage were added to the tube and selection continued as before, with 25 washes before elution. Round 4 used 20ug/ml of mouse ELTD1 with 30 washes. Round 5 used 20ug/ml of human ELTD1 with 40 washes. The titres of phage selection are summarised in figure 5.4a.

a

	ELTD1 selection Titre
Round 1	$4.3x10^{6}$
Round 2	$1.6x10^{5}$
Round 3	$1.26x10^{9}$
Round 4	$7.2x10^{8}$
Round 5	$7x10^{8}$

b

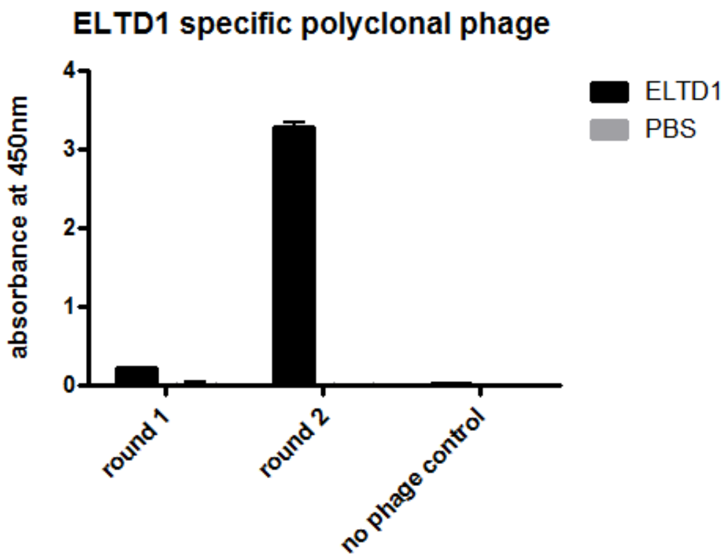

Figure 5.4: phage selection to ELTD1. Phage were selected against extracellular human ELTD1-His protein for 2 rounds initially. This was followed by 2 rounds to mouse ELTD1-His and a final fifth round to human ELTD1-His. The titre of phage rescue is shown in (a). (b) A polyclonal phage ELISA was performed to test the specificity of phage after round 1 and round 2 of selection to human ELTD1. Results show the mean of triplicate wells, while error bars show the SD. Result is representative of two experiments.

Due to a limited supply of murine ELTD1 protein, the polyclonal ELISA was not performed to confirm selection to human and mouse protein. Instead, a monoclonal phage ELISA was performed to first identify human ELTD1 positive scFv and selected clones would then be screened for reactivity to mouse ELTD1. The titre dilution plates from round 5 of selection were used to pick 93 individual colonies of phage-infected TG1. Each colony was grown in a single well of a 96 well plate. Superinfection with helper phage of each colony allowed the production and release of monoclonal selected phage from each colony. The supernatant of each colony was then used to test monoclonal phage against a single well coated in 5ug/ml of human ELTD1 and a single well coated in 2% BSA in PBS as a control. 13 clones were found to give a positive signal to human ELTD1 in the ELISA (figure 5.5a). A glycerol stock was prepared of these positive clones as well as a negative clone.

The 13 positive and 1 negative clone were grown again from glycerol stocks and superinfected before being tested in another monoclonal ELISA to human and mouse ELTD1 both at 4ug/ml as well as 2% BSA in PBS. All 13 clones were positive again and also cross-reacted to mouse ELTD1 (figure 5.5b). Clones 1 and 2 in particular gave the largest response to ELTD1 and were selected for further analysis. The glycerol stocks of TG1 clones 1 and 2 were both grown on separate 2xTY-Amp-Glu plates. 5 colonies were picked from each plate and the phagemid DNA from each was sequenced through the scFv insert using the fdseq1 Primer. All 5 subclones from clone 1 had identical sequences through the heavy gene and light gene CDR3 (figure 5.5c). Clone 1 was therefore considered a monoclonal scFv clone. Four of the five clone 2 subclones also had identical CDR3 sequences for both the heavy and light genes whereas one subclone had different CDR3 sequences (figure 5.5d). Interestingly, the four identical subclones from clone 2 were identical to the clone 1 sequence. Therefore clone 2 is not monoclonal but a polyclonal mix of clone 1 and another clone.

The scFv from clone 1 was selected to construct a CAR. Primers were designed to introduce a 5' Cla1 and a 3' Not1 site onto the scFv. The scFv was isolated through PCR (figure 5.6a). This allowed insertion of the scFv into the MP71 second generation CAR vector incorporating a CD28 costimulatory domain. After vector insertion, a double digest of the vector with Cla1 and Not1 restriction enzymes revealed 2 bands correlating to the scFv and cut vector (figure 5.6b). Forward and reverse DNA sequencing confirmed the scFv was inserted correctly into the MP71 vector. The ELTD1 CAR was then transduced into human PBMCs. Transduction efficiency was 20% (figure 5.7a). However, when T cells where functionally tested for IFNγ response by ELISA to recombinant ELTD1 protein (figure 5.7b) and ELTD1 overexpressing HEK293 cells (data not shown) no response was observed. The HEK293 cell line overexpressed human ELTD1 protein (a kind gift from Denim Li, Oxford University) (Masiero et al. 2013) was not available at the time of initial CAR development and so was not used to screen for phage that could detect native ELTD1 expression. All 13 clones that were positive to recombinant mouse and human protein were later screened for reactivity to this cell line in a whole cell ELISA and in flow cytometry, but no ELTD1 reaction was seen (data not shown).

a

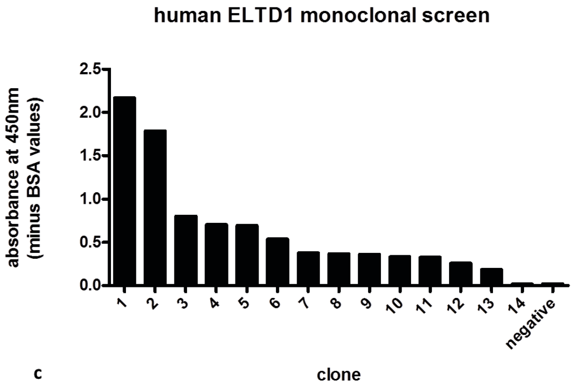

b

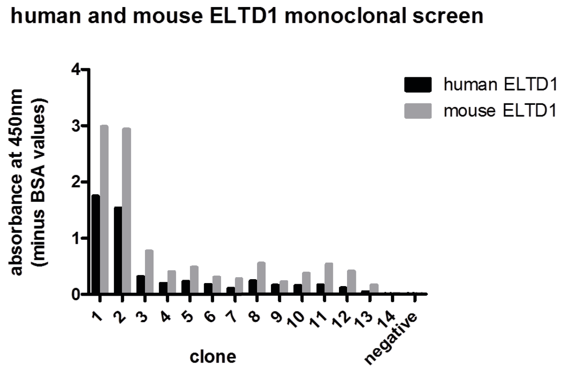

c

Clone	Heavy chain CDR3	Light chain CDR3
1a	gcgaaagctctgcgtgcgcggttttttgactac	aactcctctcatccccggcctcaggctgtggta
1b	gcgaaagctctgcgtgcgcggttttttgactac	aactcctctcatccccggcctcaggctgtggta
1c	gcgaaagctctgcgtgcgcggttttttgactac	aactcctctcatccccggcctcaggctgtggta
1d	gcgaaagctctgcgtgcgcggttttttgactac	aactcctctcatccccggcctcaggctgtggta
1e	gcgaaagctctgcgtgcgcggttttttgactac	aactcctctcatccccggcctcaggctgtggta

d

Clone	Heavy chain CDR3	Light chain CDR3
2a	gcgaaagctctgcgtgcgcggttttttgactac	aactcctctcatccccggcctcaggctgtggta
2b	gcgaaagctctgcgtgcgcggttttttgactac	aactcctctcatccccggcctcaggctgtggta
2c	gcgaaagctctgcgtgcgcggttttttgactac	aactcctctcatccccggcctcaggctgtggta
2d	gcgaaagctctgcgtgcgcggttttttgactac	aactcctctcatccccggcctcaggctgtggta
2e	gcgaaagggattagggcgtttgactac	aactcctctccctttttgtctcggggggtggta

Figure 5.5: monoclonal analysis of ELTD1 scFv. Ninety-three TG1 clones were analysed for phage-scFv specificity to human ELTD1. 13 clones were found to be positive to human ELTD1 as shown by the monoclonal phage ELISA in (a). Data shows the adsorption value from a single well for human ELTD1, minus the value seen to the BSA control well. Clone number 14 was a non-specific clone and the negative clone represents an ELISA using media only, i.e. no phage. Data shows the adsorption value from a single well for human or mouse ELTD1, minus the value seen to the BSA control well. All 14 clones were then tested again in an ELISA, to wells containing either human ELTD1, mouse ELTD1 or BSA (b). Data shows the values measured from a single well having subtracted adsorption levels to BSA. This ELISA is representative of two independent experiments and shows only the values measured from a single well. The scFv sequences from clones 1 (c) and 2 (d) were obtained from 5 individual subclones (labelled a-e) grown from each original clone. The sequences for the CDR3 of the heavy chain and light chain for each are shown.

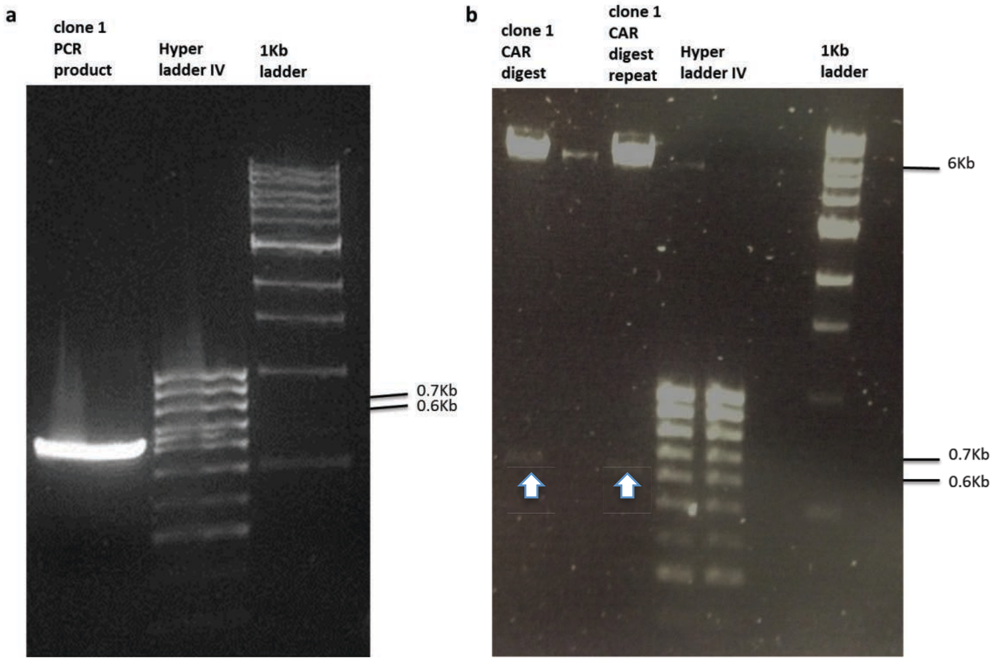

Figure 5.6: clone 1 scFv PCR product cloned into the CAR. The scFv from clone 1 was targeted using PCR to generate a product covering the whole of the scFv. The PCR product was run on a gel along with two ladders to confirm that its size matched the known size of the scFv (a). The scFv PCR product was then cloned into the MP71, second generation CAR vector, which has previously had its scFv removed by ClaI NotI digest and gel extraction. The clone 1-CAR product was then digested with Cla1 and Not1 restriction enzymes (b). This revealed 2 bands as indicated correlating to the scFv (as indicated by the white arrows) and cut vector.

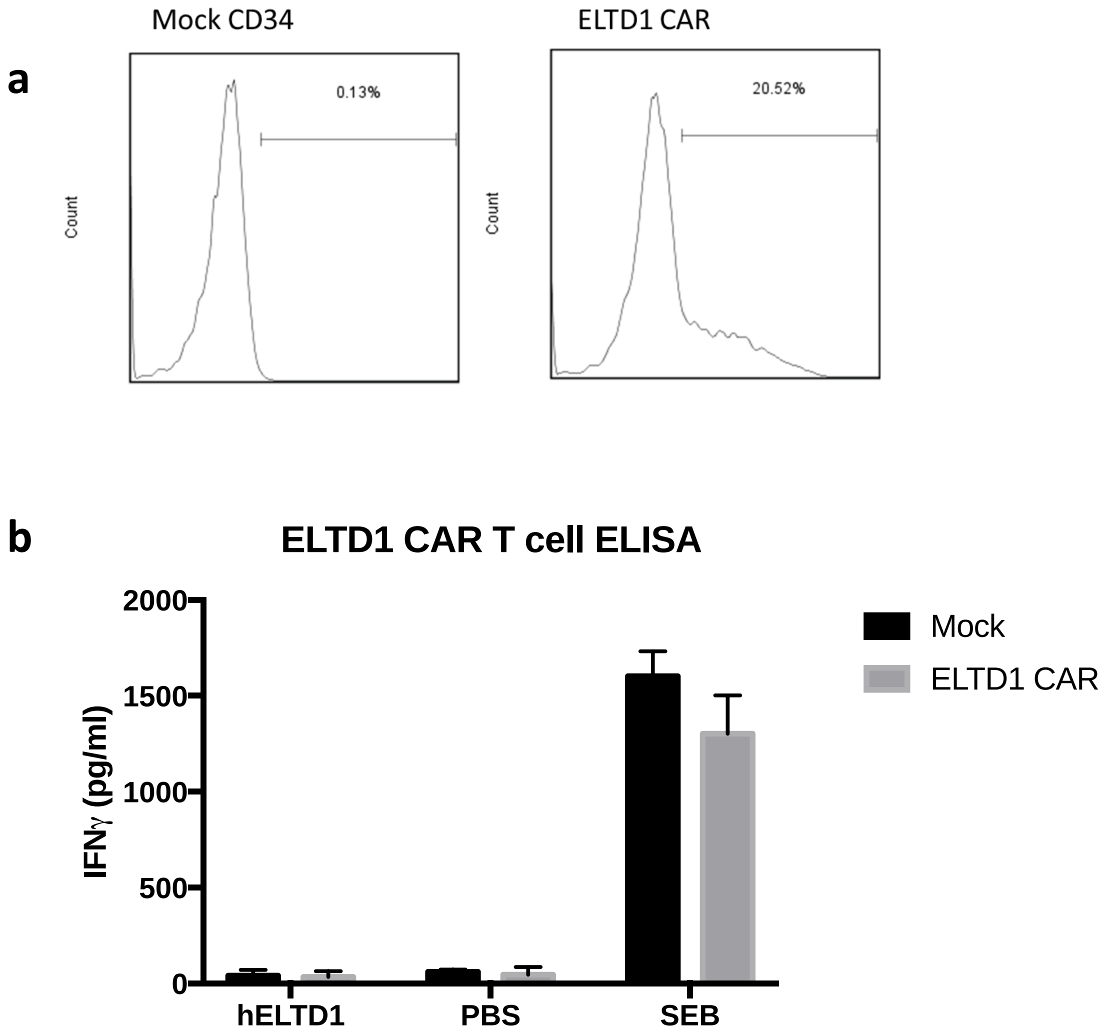

Figure 5.7: Human T cells transduced with the clone 1-CAR product (ELTD1 CAR). Human PBMCs were activated as before and mock-transduced or DNA-transduced as before with ELTD1 CAR DNA. (a) Cells were analysed by flow cytometry for CD34 expression. CD34 stained mock and CAR transduced T cells were gated for lymphocytes. The gate for CD34 was set on mock CAR T cells. (b) CAR T cells were tested in an IFNγ ELISA. Mock or ELTD1-CAR transduced T cells were incubated in wells precoated with recombinant human extracellular ELTD1-His protein at 1ug/ml in PBS or PBS alone. As a positive control, T cells were also incubated with 200ng/ml of SEB in ELISA media. Data shows the mean of triplicate wells and error bars show the SD.

Due to the apparent lack of ELTD1 specificity of the generated CARs, the inability for all clones to react to ELTD1 expressing cells, as well as a low supply of ELTD1 protein, other TEMs and phage selection methods where investigated.

5.4 An introduction to GRIN2D

Glutamate Receptor Ionotropic N-Methyl D-Aspartate 2D (GRIN2D) is a component of the NMDA receptor, a class of glutamate receptors. The release of glutamate from one neuron to another is essential in signal transmission and occurs at synaptic junctions. Presynaptic terminals release the neurotransmitter glutamine across the synaptic junction that can then interact with postsynaptic ionotropic glutamate receptors. The use of the agonist NMDA identified NMDA binding receptors (now known as NMDARs) and non-NMDA binding receptors (now known as AMPA and kainite receptors). NMDARs are unique in that they need two ligands for activation, glycine and glutamate (Johnson & Ascher 1987).

In a resting cell, magnesium ions block the NMDAR in a voltage dependent manner, preventing ions from entering the cell (Paoletti et al. 2013). This magnesium ion block can be disrupted by activation of non-NMDA receptors, the AMPA receptors. Upon glycine and glutamate binding, as well as membrane depolarisation to disrupt the magnesium block, a permeation of calcium and other cations into the cell occurs (MacDermott et al. 1986). NMDARs are involved in long-term potentiation within the CNS and are linked to learning and synaptic plasticity.

NMDARs are heterotetrameric molecules, composed of GRIN1, GRIN2 and GRIN3 subunits (Ishii et al. 1993). Usually, NMDARs are formed from two GRIN1 subunits and two GRIN2 subunits. There are four individual GRIN2 subunits, names A-D (Monyer et al. 1992). The differential pairing of GRIN1 and GRIN2 subunits forms receptors with distinct pharmacologic and kinetic properties (Monyer et al. 1994). GRIN1 subunits are responsible for binding glycine whereas GRIN2 are responsible for binding glutamate. The expression of the different GRIN2 subunits has distinct spatial-temporal patterns (Ritter et al. 2001; Meador-Woodruff et al. 2001; Scherzer et al. 1998; Akbarian et al. 1996). During embryonic development, only GRIN2B and GRIN2D are expressed in the brain. Early in the postnatal brain, a major shift in expression occurs, where GRIN2A expression increases to become the most expressed subunit whereas GRIN2D drops and is only found at low levels in the adult brain, typically within the diencephalon and mesencephalon. GRIN2B expression becomes mostly constrained within the forebrain of adults. GRIN2C occurs later cerebellum and olfactory bulb. The majority of research into GRIN2D has centred in its role in memory and learning in the developing brain. Furthermore abnormalities with NMDARs and subunit polymorphisms have been associated with neurological problems including schizophrenia (Meador-Woodruff et al. 2001; Moghaddam & Javitt 2012).

Microarray analysis from freshly isolated colorectal tumour endothelial cells and patient matched healthy colon identified GRIN2D as a putative TEM (Ferguson et al. 2016). Its endothelial specific expression was confirmed by IHC and PCR. Tissue arrays also found it to be most prevalent within tumours, especially colorectal. qPCR found GRIN2D to have around 30-fold greater relative expression in colorectal cancer endothelial cells than normal tissue endothelial cells. siRNA knockdown of GRIN2D identified a pro-angiogenic role in capillary tube formation as well as endothelial migration in vitro. A peptide unique to murine GRIN2D was then used to vaccinate mice. Vaccinated mice exhibited a decreased tumour growth as well as a reduction in tumour vessels per field after tumour section analysis. Toxicity was not reported in this study.

Despite its notable expression within colorectal tumour endothelium, there are still reports of its expression in normal tissue including the colon and within the brain and CNS (Zhou & Nicholas Verne 2008) (Del Valle-Pinero et al. 2007), although the expression is not quantified. Therefore it was again important to isolate scFvs that cross-reacted with both human and mouse GRIN2D to permit subsequent toxicity (and efficacy) testing in mouse models.

5.4.1 Phage selection using biotinylated antigen

A potential problem with the use of immunotubes for phage selection is that protein antigen is adsorbed onto the plastic. This will cause the protein to become denatured, thus changing confirmation and epitope availability. Phage selection is therefore performed with a denatured antigen. Any selected phage may not recognise the same native protein in its natural confirmation found on cell lines or in vivo. Similarly, phage screening to protein adsorbed on maxisorp ELISA plates will result in screening to denatured protein.

An alternative strategy is to use a biotinylated protein antigen for selection. Selection can be performed with protein antigen in solution before the antigen, along with any antigen specific phage attached, is recovered through addition of streptavidin-coated dynabeads that bind the biotin. An exterior magnet can then be used to secure the dynabead-bound antigen/phage complexes while supernatant is removed and washing is performed. Antigen-specific phage may then be eluted from antigen and recovered, then used to infect TG1 as before. Proteins containing primary lysines can be biotinylated using the EZ-link sulpho-NHS-SS-biotin (sulfosuccinimidyl-2-[biotinamido]ethyl-1,3-dithiopropionate). This biotin contains an extended spacer arm to decrease the likelihood of inducing steric hindrance of the protein once bound, potentially hiding available epitopes during selection. This biotin can furthermore be removed from the protein by incubation with a thiol. By separating the biotin from the protein antigen in this way before elution of phage, only those phage that bind the protein antigen, rather than the biotin, are recovered. Therefore, this alternative approach was adopted to screen the phage library for scFvs specific to other TEMs such as GRIN2D.

5.4.2 Selection of antibodies to GRIN2D

An extracellular 81 amino acid N terminus peptide segment from human GRIN2D and not found in other GRIN2 subunits, was linked to a GST tag (a kind gift from R. Bicknell, Birmingham, UK) (Ferguson et al. 2016). The extracellular fragment has been fused to a GST tag in the pGEX-2T vector for protein production in *E.coli.* 200ug of this protein was biotinylated according to manufacturer's instructions. Free unbound biotin was removed from the protein through buffer exchange. Biotinylated protein was then used at a concentration of $1x10^{-7}$ moles to screen the phage library. Protein was mixed with 10^{12} T.U of library phage on an orbital rotator for an hour in a 15ml tube. After this, dynabeads, preblocked in 2% milk-PBS, were added to the phage-protein mixture. Orbital rotation was continued for 15 minutes. The tube was placed in a holder with a magnet down one side. Dynabeads along with bound GRIN2D/phage complexes were drawn to the magnet. The supernatant was removed and the tube was washed 5 times with 0.1% tween-PBS then 5 times with PBS. Phage were eluted using DTT before phage containing supernatant was removed, while dynabeads were secured using the magnet. The Phage were then amplified and precipitated as before.

DTT cleaves biotin from the protein, thus releasing protein and any protein-bound phage along with it. However, phage are still capable of infecting TG1. 1ml of selected phage was used for round 2 of selection. Round 2 was completed with the same conditions as round 1. The titres from both rounds were noted and a polyclonal phage ELISA confirmed phage enrichment with specificity to biotinylated human GRIN2D-GST protein (figure 5.8a-b). Phage derived from 96 individual colonies of TG1 bacteria were then screened by ELISA, and 6 clones identified that specifically bound biotinylated human GRIN2D-GST protein (figure 5.8c). However, at this point the Bicknell lab realised that the GRIN2D-GST protein was in fact missing a 10kDa fragment (personal communication, Henry Ferguson), therefore the protein was switched to a human GRIN2D-Fc protein that was confirmed to express the full 88 amino acid extracellular domain (a kind gift from R. Bicknell).

a

	Titre
Round 1	$3x10^5$
Round 2	$1.6x10^3$

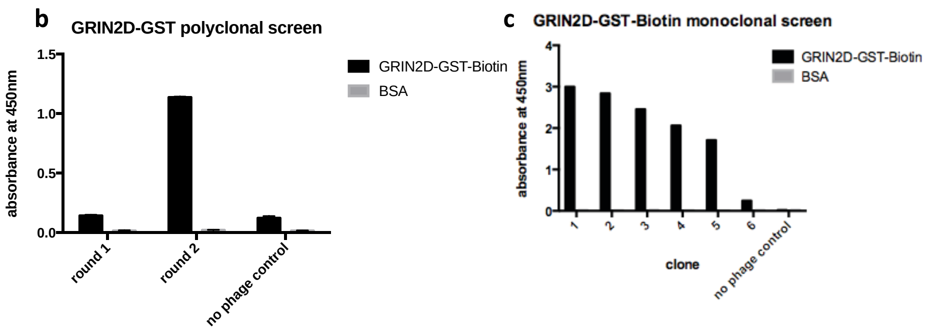

Figure 5.8: phage selection to GRIN2D. Two rounds of phage selection were performed to biotinylated human GRIN2D-GST protein. (a) The phage rescue titre was noted at round 1 and round 2. (b) A polyclonal ELISA was performed on polyclonal phage after rounds 1 and 2. Phage were tested for specificity to biotinylated human GRIN2D-GST and to BSA as a control. Data shows triplicate wells and error bars show the SD. (c) A monoclonal ELISA was performed using clones isolated after round 2 of selection. Of the 93 clones picked, 6 clones showed an absorbance to biotinylated human GRIN2D-GST but not to the BSA control. Data shows the absorbance values from individual wells.

The 81AA human GRIN2D fragment, has been linked to the 230AA Fc chain sequence of human IgG1 using the pIgG vector (pcDNA3.Fc) (Zhuang et al. 2015). Protein A purified human GRIN2D-Fc produced from vector transfected human epithelial kidney (HEK) cells was obtained from the Bicknell lab. A monoclonal phage screen showed the 6 selected clones were also reactive to human GRIN2D-Fc protein although clones 3 and 4 showed higher absorbance values than with the previous GRIN2D construct. For reasons described above, it was important to identify clones that would also cross-react with murine GRIN2D (mGRIN2D). Since the human 81AA sequence has a 78AA homolog in mGRIN2D (Ferguson et al. 2016), isolating cross-reactive scFv was thought to be possible. The Bicknell lab provided this 78AA murine sequence also in the pIgG vector.

HEK cells were transfected with this mGRIN2D pIgG vector and the mGRIN2D-Fc released into the supernatant was purified using a protein A column. 1.5 litres of collected supernatant was run overnight through the column. After washing, collected protein was eluted and released into twenty-five fractions of 500µl. Each fraction was then tested for the presence of protein using a NanoDrop machine. Samples from fractions 12-17 contained protein according to the NanoDrop (data not shown). These fractions were run on a gel and coomasie stained, confirming the presence of a protein around 35kDa, matching the predicted size of mGRIND2-Fc (figure 5.9a). The fractions were pooled together then buffer exchanged into PBS. Following this, a sample of the pooled fractions was tested on a western blot and stained for the Fc tag. This confirmed the presence of an Fc tagged protein around 35kDa (figure 5.9b). The 6 hGRIN2D-Fc-specific clones were then tested for specificity to mGRIN2D, however, there was no cross-reactivity to the mouse protein (figure 5.9c). Due to a lack of cross-reactivity, these clones could not be tested in mouse models to explore safety or anti-tumour efficacy. Therefore, the library was rescreened but this time selection was performed using both hGRIN2D-Fc and mGRIN2D-Fc proteins.

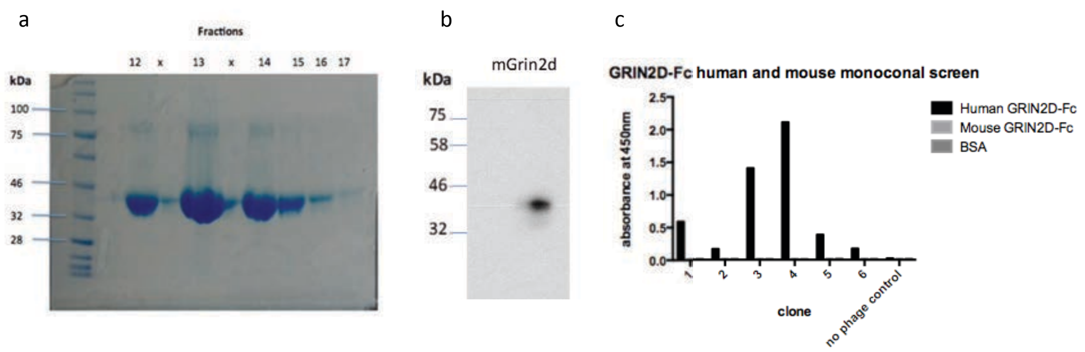

Figure 5.9: production of mGRIN2D-Fc and screening of monoclonal phage. Protein A purified mGRIN2D-Fc protein was eluted into 25 fractions. (a) Samples from fractions 12 to 17 were run on a gel and stained with coomasie blue to detect protein. "x" designates an empty lane. (b) Fractions 12 to 17 were then pooled together and a sample was run on a western blot and stained with an anti-Fc antibody. (c) The 6 monoclonal phage which were screened to and found to be specific to human GRIN2D-GST then underwent a monoclonal phage ELISA to hGRIN2D-Fc, mGRIN2D-Fc or BSA. Data shows the result form a single well. Predicted size of mGRIN2D-Fc = 35 kDa

hGRIN2D-Fc and mGRIN2D-Fc proteins were both biotinylated at a ratio of 50:1 biotin to protein (figure 5.10a-b). The titres of selection during GRIND2-Fc are summarised in figure 5.11a. Round 1 of selection was repeated as before using 1nM of human protein in 5ml of phage protein reaction mixture. The mixture was allowed to rotate for 1 hour before dynabead incubation. For round 2 of selection, 1nM of mGRIN2D-Fc was used for a smaller 1.5ml phage-protein reaction mixture. The reaction mixture was allowed to rotate for 40 minutes before the dynabeads were added and selection was continued as before. Selection rounds 3 and 4 using hGRIN2D-Fc and mGRIN2D-Fc respectively were performed using the same method as round 2.

Following 4 rounds of selection, phage from each round were tested for enrichment to both human and mouse GRIN2D-Fc. However, instead of using a standard maxisorp ELISA plate where protein is adsorbed onto the plastic, a streptavidin coated 96 well plate was used. These ELISA plates, named StreptaWell, are precoated in streptavidin. Biotinylated protein can therefore be coated to the wells and remain in a native confirmation rather than becoming adsorbed and losing its natural structure. As there was no remaining phage from the first round of selection, round 1 phage were not tested. However, phage from subsequent rounds of selection showed high absorbance values for both biotinylated human and biotinylated mouse GRIN2D-Fc as well as biotinylated Fc protein alone and biotinylated BSA (figure 5.11b). The high background to BSA may be due to lack of a blocking step and insufficient washing during the StreptaWell ELISA. This may also explain the high absorbance to Fc protein and both GRIN2D proteins, but the response to all three of these proteins is even higher than that seen to BSA suggesting enrichment for phage specific to Fc may have occurred. For this reason, a negative round of selection was performed against Fc protein using phage from round 4.

Negative selection at round 5 used 1nM of biotinylated Fc protein in a 1.5ml phage protein mixture. The mixture was rotated for 40 minutes. After incubating the mixture with dynabeads, a magnet was used to pull down the beads with Fc-protein along with any Fc specific phage. The supernatant was then removed from the tube, leaving Fc specific phage bound to the protein-beads secured with the magnet. The supernatant was added to a fresh tube and once again a magnet was used to pull down any remaining dynabeads. The supernatant, theoretically now depleted of Fc-specific phage but still containing GRIN2D specific phage, was then used to infect TG1.

Phage amplification and precipitation was continued as usual. Phage from rounds 2-5 were then tested in a StreptaWell ELISA. To reduce the high backgrounds seen in the previous StreptaWell ELISA, this time plates were blocked for 2 hours using 2% BSA in PBS and for washing steps (from phage addition onwards) PBS or PBS 0.1% tween was left in the wells for 3 minutes before removal. Phage from round two and above were then tested in a polyclonal phage ELISA (figure 5.11c), These modifications successfully reduced the background but there was no loss of response to Fc suggesting that attempts to remove Fc-specific phage had been unsuccessful.

Therefore a sixth round was performed with a negative selection against biotinylated Fc protein was using immunotubes that had been pre-coated with 50ug/ml of this protein (an approach previously used in this project to successfully remove other Fc-specific phage; data not shown). The tube was rotated and then left to stand as in previous immunotube selections. Then the supernatant, now hopefully depleted of Fc-specific phage, was removed from the immunotube and used to infect TG1 bacteria. Amplification and precipitation were performed as before. Phage from rounds 4 to 6 were then tested in a polyclonal StreptaWell ELISA (figure 5.11d). Although Fc specific phage have now been depleted as shown by the lack of response to Fc protein when using phage selected in round 6, the same phage also failed to bind either human or mouse GRIN2D-Fc. This suggests the majority of phage selected in the earlier rounds were Fc-specific.

As a final attempt, in case there were low numbers of GRIN2D specific phage present, two further rounds of selection were performed to human GRIN2D-Fc. Selection was performed with 1nM of biotinylated protein in a 1.5ml reaction mixture. Amplification and purification performed as before. However, no GRIN2D-Fc specific phage were recovered (figure 5.11e).

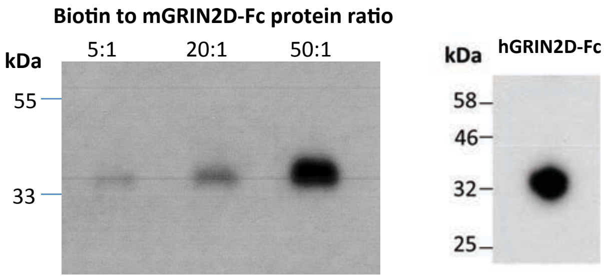

Figure 5.10: western blots showing the biotinylation of GRIN2D-Fc. (a) mGRIN2D has been biotinylated at ratio of 5:1, 20:1 and 50:1 biotin to protein. Samples were then tested for biotinylation on a western blot using streptavidin-HRP. (b) hGRIN2D has been biotinylated at a ratio of 50:1 biotin to protein. A sample was then tested for biotinylation on a western blot in the same manner.

	selection round	Titre
a	**Round 1: human GRIN2D-Fc**	1.6×10^5
	Round 2: mouse GRIN2D-Fc	3.4×10^7
	Round 3: human GRIN2D-Fc	2.5×10^8
	Round 4: mouse GRIN2D-Fc	4.5×10^8
	Round 5: negative	1.5×10^8
	Round 6: negative repeat	9.8×10^6
	Round 7: human GRIN2D-Fc	3.2×10^7
	Round 8: human GRIN2D-Fc	7.7×10^6

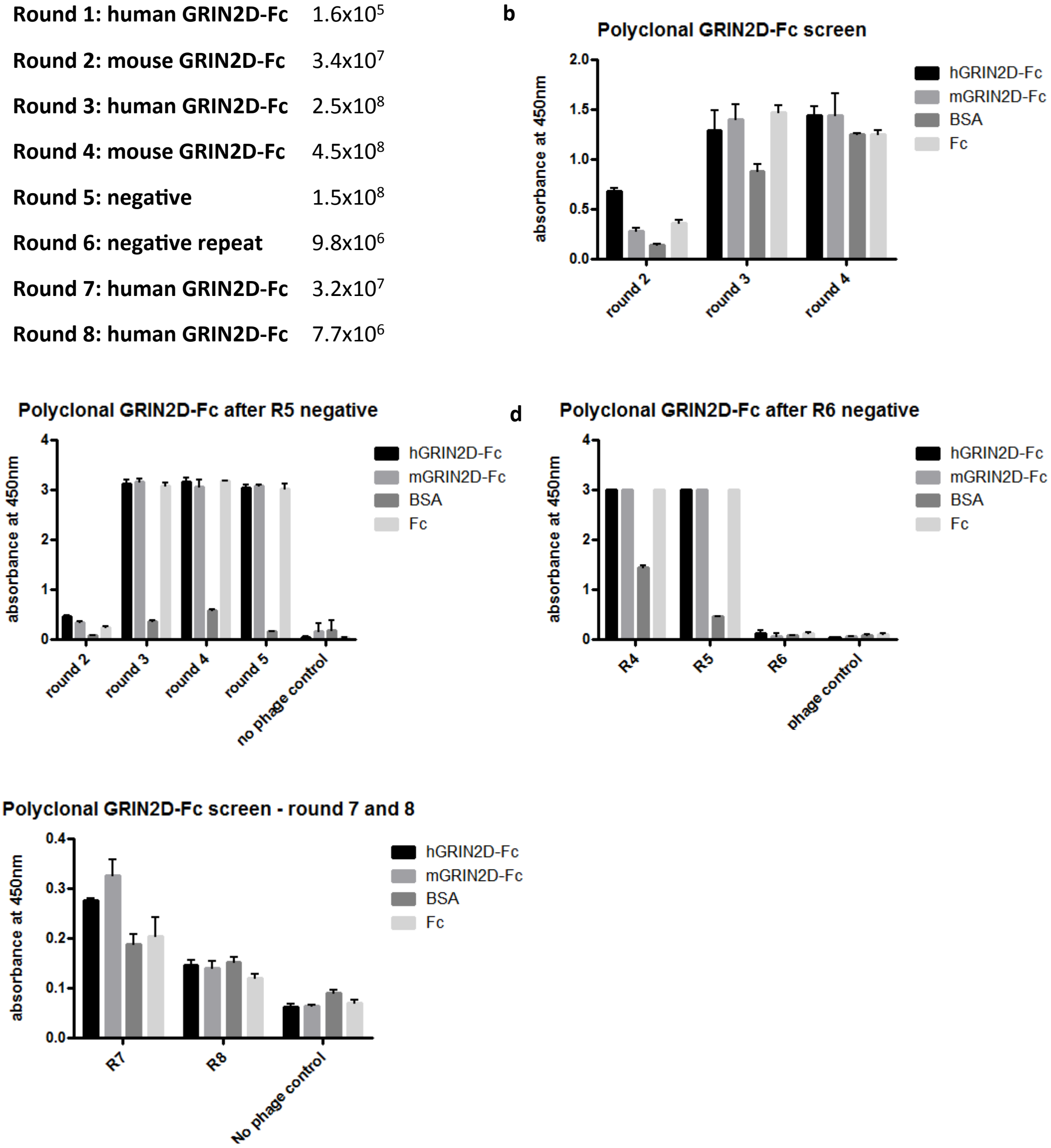

Figure 0.11: phage selection to biotinylated GRIN2D-Fc. (a) The phage rescue titre from each round of selection is summarised. (b-e) Polyclonal phage ELISAs using streptavidin coated 96 well plates were performed, screening phage (or no phage control where specified) for specificity to the biotinylated proteins: hGRIN2D-Fc, mGRIN2D-Fc, BSA and Fc.

5.5 An introduction to MCAM

Melanoma cell adhesion molecule (MCAM), also known as CD146, is a cell adhesion molecule and a member of the immunoglobulin superfamily. It was first identified as a marker in melanoma which correlated with poor prognosis, tumour progression and metastasis (Lehmann et al. 1989) (Sers et al. 1993). It is highly expressed during embryonic development in a range of tissues including the CNS, kidney and retina, however expression is limited in adult tissue (Ouhtit et al. 2009). As well as a developmental function it has been found in a variety of other roles. Found on rare groups of lymphocytes, it can help promote rolling on inflamed endothelium (Guezguez et al. 2007). It has been detected as a marker of mesochymal stem cells (MSCs) where an increased MCAM expression correlates with increased differentiation potential (Baksh et al. 2007). Of most interest is its role in angiogenesis, especially tumour angiogenesis.

It was soon recognised that MCAM was also expressed within the endothelium and smooth muscle associated with melanoma (Sers et al. 1993; Sers et al. 1994). Several studies have identified a pro-angiogenic role for MCAM. The use of an MCAM blocking antibody or siRNA to MCAM has resulted in inhibition of endothelial cell proliferation, migration and tubule formation in vitro (Kang et al. 2006; Jiang et al. 2012; Zheng et al. 2009) (Yan et al. 2003),(Bu et al. 2006) (Tu et al. 2015). Similarly, the same strategies have inhibited tumour growth and angiogenesis in xenograft human tumour mouse models. The use of an MCAM blocking antibody in combination with the anti-VEGF (bevacizumab) has resulted in a further increased anti-tumour effect (Jiang et al. 2012). In fact, endothelial MCAM was shown to directly interact with VEGFR2 to promote angiogenesis. MCAM mediated-angiogenesis has also been found to require MCAM homodimerization as well as an interaction with netrin-1(Zheng et al. 2009) (Tu et al. 2015). MCAM has now been identified as a potential TEM in renal cell carcinoma (RCC) and colorectal cancer (Wragg et al. 2016). Freshly isolated endothelium from tumours and matched control tissues from the same patients found MCAM to be highly overexpressed within tumour endothelium. qPCR found MCAM's relative expression in the tumour endothelium compared with normal endothelium to be greater than 5-fold. Interestingly, a higher MCAM expression within the endothelium of RCC tumours correlated with decreased survival.

5.5.1 Selection of antibodies to MCAM

The extracellular domain of human MCAM fused to Fc protein and the extracellular domain of murine MCAM fused to a His tag were purchased and used to screen the phage library using the biotinylated protein approach described above. After successful human MCAM biotinylation (figure 5.12a), 1nM of protein was added to a 5ml phage mixture for round 1 of selection. After 1 hour of orbital rotation, streptavidin-coated dynabeads were added and phage amplification and purification were performed as before. Round 2 was repeated as above using biotinylated mouse MCAM-His with a 5ml reaction mixture and an hour of rotation. Rounds 3 and 4 were performed with human and mouse MCAM respectively, this time with a 1.5ml reaction mixture and a 30 minute rotation. Amplification and purification were performed as normal for each round. A polyclonal StreptaWell ELISA was performed for all 4 rounds and the round titres were noted (figure 5.12b-c). Round 1 showed a clear enrichment for human MCAM specific phage with no background to BSA or Fc proteins. However, by round 2, specificity to human MCAM has been lost. On top of this, no murine MCAM specificity was observed at any round. This was despite high phage rescue titres at the end of each round.

To try and recover MCAM specific phage from round 1 of selection that could recognise both human and mouse forms of the protein, round 2 of selection was repeated to mouse MCAM, with 1nM of protein in a 5ml reaction mixture. Again, despite a high titre of phage rescue, there was no specificity to mouse MCAM (figure 5.12d-e). Human MCAM specificity was still present this time. An alternative strategy is to start round 1 of selection to murine MCAM followed by human MCAM in round 2. Both rounds used 1nM of biotinylated protein and a 5ml reaction mixture, with an hour of orbital rotation. Amplification and purification were performed as usual. The StreptaWell polyclonal ELISA showed no enrichment of phage to either murine or human MCAM, or the control proteins (figure 5.12f). High phage rescue titres were also noted for each round here (figure 5.12g).

a b

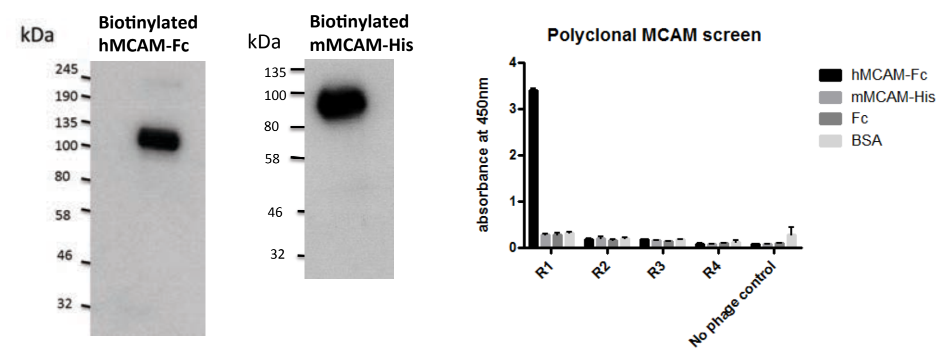

c

	Titre
Round 1	2.4x10^{6}
Round 2	5.3x10^{7}
Round 3	2.6x10^{5}
Round 4	1.7x10^{8}

d

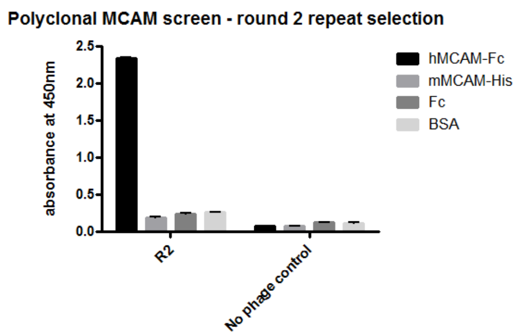

e

	Titre
Round 2	4.6x10^{7}

f

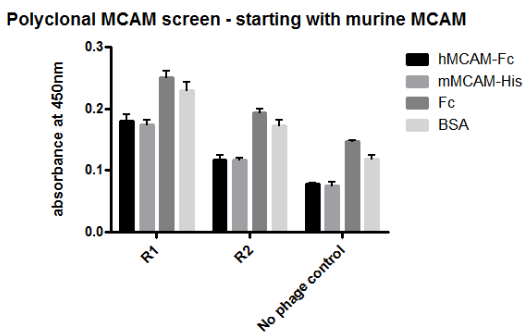

g

	Titre
Round 1	1.3x10^{8}
Round 2	8.7x10^{6}

Figure 0.12: phage selection to biotinylated MCAM. (a) Human MCAM-Fc (hMCAM) and mouse MCAM-His (mMCAM) were biotinylated at a ratio of 50:1 biotin to protein. Samples were tested in a western blot for biotinylation using streptavidin-HRP. Both bands where at the expected kDa of 125kDa for hMCAM and 95kDa for mMCAM. (b) Phage selection was performed using biotinylated hMCAM in rounds (R) 1 and 3 and biotinylated mMCAM in rounds 2 and 4. A polyclonal ELISA using a streptavidin coated 96 well plates was performed, screening phage for specificity to the biotinylated proteins: hMCAM-Fc, mMCAM-His, BSA and Fc. (c) The phage rescue titres from the corresponding rounds in (b) are summarised. (d) Phage selection from (b) was repeated at round 2 by selection with hMCAM-Fc. The polyclonal ELISA was then repeated as before. (e) The phage rescue titre from the corresponding round in (d) is summarised. (f) Phage selection was started again from the beginning firstly using mMCAM (round 1; R1) and then hMCAM (round 2; R2). The polyclonal ELISA was repeated as before. The phage rescue titre from the corresponding rounds in (f) are summarised. All data shown in histograms represent mean of triplicate wells with error bars shown the SD)

5.6 End of chapter discussion

Antibody phage display was used in an attempt to generate CARs to the recently identified TEMs ELTD1 (Masiero et al. 2013), GRIN2D (Ferguson et al. 2016) and

MCAM (Wragg et al. 2016). Significant problems were encountered in each of these selections. The choice of phage display library and the problems encountered are discussed below.

5.9.1 Antibody phage selection libraries

George P Smith first demonstrated the concept of phage display when peptides were linked to the PIII coat protein of filamentous phage (Smith 1985). Antibody phage display and subsequent selection were later demonstrated through the display of scFv molecules on filamentous phage (McCafferty et al. 1990). Antibody phage display libraries come in different forms: the immune library and the single pot library. The immune library is composed of antibody DNA derived from the B cells of immunised hosts, either animal or human. All variability from this library is derived from the host and the host's immune system. Common applications for the immune library include recovering antibodies that can neutralise viruses or antibodies specific to cancer antigens (Ponsel et al. 2011). High affinity antibodies may be recovered from such libraries due to the effects of the affinity maturation under the immune system. Furthermore, following immunisation a higher proportion of recovered antibodies are likely to be antigen specific. The relative clonal size of the library can be less critical in this respect. The major drawback to the immune library is the potential difficulty in recovering antibodies to self-antigens, due to immune tolerance. This will make it very difficult to recover antibodies to TEMs, since most are overexpressed self-antigens. Considerable effort is also required, as each desired antibody specificity first requires immunisation and library generation. For these reasons, an immune library would be a poor choice to recover a cross-reactive antibody to a conserved TEM.

The single pot library is designed so that it can be used to recover antibodies of any specificity. Rather than requiring immunisation before library generation, single pot libraries are pre-made and can be frozen into library phage aliquots. Any protein antigen may be used to recover specific antibodies. A crucial feature of a single pot library is the size of the repertoire of antibody phage clones. The number of clones in the library correlate with the chances of recovering high affinity antibodies (Griffiths et al. 1994). Single pot libraries may be derived from antibody DNA from the B cells of naïve hosts or non-immunised humans (Hoogenboom et al. 1991). Again such a library will struggle to generate antibodies to self-antigen and any recovered clones may be of low affinity. The content of the library is also relatively unknown and uncontrolled, due to the lack of immunisation and the host-to-host variability in B cell rearrangements. Although larger libraries have identified high affinity clones (Ponsel et al. 2011), the naïve library would also be a poor choice for isolating an antibody specific for a TEM.

Alternatively, a single pot library may be synthetic. Here, antibody diversity is generated in vitro. All antibodies have been randomly generated in the absence of immune selection/tolerance. Critically, the synthetic library is therefore ideal for recovering antibodies to self-proteins, such as TEMs. Furthermore, one can choose a framework antibody with desirable properties such as stability and select CDR regions for a controlled random variability. The ETH2 GOLD library is a synthetic scFv based library. The chosen human framework genes, variable heavy chain gene DP47 with the light chain genes DPK22 and DPL16 are the most commonly found genes in the human antibody repertoire (Kirkham et al. 1992). Furthermore, DP47 is known to be thermodynamically stable and may be purified/detected using protein A (Ewert et al. 2003). The high number of clones ($3x10^9$) and the synthetic nature of this library made it ideal to search for antibodies specific to human and mouse-conserved regions within TEMs.

Several studies have successfully used the ETH2 GOLD phage display library to isolate high affinity scFv to cancer related targets using both the immunotube and the biotinylated antigen methods (Silacci et al. 2005; Brack et al. 2006; Lovato et al. 2007; Romani et al. 2009; Ronca et al. 2010; Sgier et al. 2010). Most of these studies haven't directly selected for antibodies that cross-react with human and mouse forms of the target antigen. However one study ended up generating an anti-fibroblast growth factor receptor 1 scFv that was cross-reactive to human and mouse homologs after two rounds of selection only to the human protein, although the murine homolog is 98% identical (Ronca et al. 2010).

Despite a nigh number of different potential clones, it is believed that the ETH2 GOLD library suffers from a selection bias (Villa et al. 2011). Variability has only been introduced to the CDR3 regions. Although in vitro affinity maturation of CDR1 and CDR2 may improve affinity after selection, it is believed that the germline CDR2 loops bias initial epitope recognition. The Philo1 and Philo2 phage display libraries are derived from the ETH2 GOLD library, but with the substitution from Serine into a charged/hydrophilic amino acid at position 52 in CDR2. Such a substitution is believed to assist in potential epitope hydrogen bond interactions, thus reducing epitope recognition bias.

A further improvement is the PHILODiamond phage display library which contains over 4.1×10^{10} individual clones(Weber et al. 2014). This library incorporates more diversity in the CDR3 region as well as an Asparagine at position 52 of CDR2. PHILODiamond outperformed ETH2 GOLD by recovering a greater number of specific clones to most antigens tested. Future phage display experiments may wish to this library and make use of the larger repertoire of clones. The theoretical size of the library and the potential sectional bias may not have been the issue in this project. Several other factors can affect the outcome of phage selection, from the method of selection to the purity and condition of the protein.

5.9.2 Selection problems in this project

The extracellular domain of human and mouse ELTD1 share 63% sequence identity. Using the immunotube method of selection with alternate rounds to human and mouse ELTD1, multiple cross-reactive phage clones were identified. Yet after cloning a reactive scFv into a second generation CAR molecule, transduced T cells failed to react to ELTD1 protein (figure 5.7). T cells were also tested against an ELTD1 overexpression cell line, but again no response was seen (data not shown). Furthermore, although phage clones recognised recombinant protein, they failed to recognise ELTD1 on the HEK293 overexpression cell lines in the form of a whole-cell ELISA and in flow cytometry (data not shown). It is unknown why the scFv in the form of a CAR failed to recognise recombinant ELTD1 protein. CAR sequencing confirmed the scFv was correctly inserted. It is possible that once the scFv is fused to a CAR molecule, it can no longer recognise its epitope, due to some form of hindrance. A spacer domain may be required in the CAR to provide the scFv better epitope access. Another possibility is that, despite clear CD34 expression, the actual CAR protein may not be expressed on the cell surface. The issue of protein adsorption during selection was also a concern and an updated method was investigated.

Due to the possibility of selection of scFv specific to epitopes only available on protein that has been adsorbed onto plastic and thus not in a natural confirmation, an updated selection method was attempted. The biotinylation of protein antigen followed by phage selection while in solution has previously been used to isolate specific scFv (Brack et al. 2006). Since very little ELTD1 protein was available, this method was initially used in selection of GRIN2D. Selection against human GRIN2D-gst protein successfully generated specific monoclonal phage (figure 5.8). However, once it was discovered that a large portion of this protein was cleaved during production in the bacterial host (Henry Ferguson, personal communication), analysis and selection was continued with human and mouse GRIN2D-Fc produced in HEK293 cells. Unfortunately, the human specific clones originally enriched to GRIN2D-gst were not cross-reactive to mGRIN2D-Fc and were no longer considered. Selection was restarted using alternate selection to human and mouse GRIN2D-Fc protein. Significant problems were encountered due to an apparent selection to the Fc protein rather than GRIN2D despite attempts of negative Fc selection. An alternative strategy would be to include an excess of soluble, non-biotinylated Fc protein in the phage reaction mix. This way, any Fc reactive phage should bind to the soluble Fc rather than the Fc tag of the biotinylated GRIN2D protein. This method has been successfully used in another study (Ronca et al. 2010). Another potential issue with the GRIN2D protein is the fact that the Fc tag is by far the larger protein (26kDa) compared to the GRIN2D segment (7-8kDa). This may be the reason why phage were enriched to Fc rather than GRIN2D.

The biotinylated method of selection was also used in an attempt to isolate scFv to MCAM. For this, human MCAM-Fc and murine MCAM-His were used in alternate rounds of selection. This way, any phage specific to the tag rather than the protein should be lost in the next round of selection when the alternate protein is used. However, despite a clear selection to human MCAM, selection did not occur using murine MCAM. Since phage could be enriched to human MCAM but couldn't be enriched at all to murine MCAM, it is likely that the issue is with the murine protein rather than the selection method. Surprisingly, the phage rescue titre did not drop upon selection with murine MCAM despite the clear loss of human MCAM specificity. It was also surprising that even if selection began with murine MCAM, there was no enrichment to this protein despite the high phage rescue titres (figure 5.12). If protein was not biotinylated, or if protein was simply not recognisable by any phage, then no phage would be rescued after selection. One possibility is that after initial phage selection in solution, non-specific phage may bind to the dynabeads. Dynabead-specific phage could potentially be rescued and this may be seen in the selection titre, but won't be seen in a phage ELISA. A longer blocking incubation for the dynabeads or a more concentrated tween 20 in the wash may help prevent this. However, it is unknown why murine MCAM protein failed to induce phage selection.

Clearly, the selection method and choice of protein (and tag) can significantly affect the outcome of phage selection. Future experiments using phage display require a good quality protein with a small tag. Negative selection methods should also be incorporated against the tag. Alternative selection methods could also be explored. One recent method incubated biotinylated antigen into 8 wells of a StreptaWell plate (Weber et al. 2014). Phage selection is then performed against the immobilised antigen by adding phage library to the wells, following the same concept as immunotubes, except protein is not adsorbed and should remain in its native conformation. In this protocol dynabeads are not used, eliminating the risk of selection for dynabead specific phage.

Despite the issues with each selection attempt, phage clones specific to human protein only were recovered. These clones could still potentially be used to generate human specific CAR T cells. However, these CARs would not be able to be tested for safety and efficacy in mouse models, since the targeted TEM in mice, even with a human derived tumour, would still be a mouse protein on the endothelium. One way around this issue would be to use CRISPR technology to knock-in the human version of the TEM gene (Singh et al. 2015). Assuming the knock-in TEM model has a similar expression profile to that seen in humans, the model could be used to test the safety and efficacy of human TEM specific CAR T cells. The major drawback to this method is the cost and timescale to develop such a model, making it well outwith the scope of this PhD project. If a clone that was only specific to the mouse protein was recovered, this could be used to generate mouse specific CAR T cells. These cells could be tested for safety and efficacy in mouse models. However, the clinical translation of this into humans will be difficult as the mouse specific CAR will likely recognise a different epitope to any human-specific CAR.

6. General Discussion

Having explored the use of CARs targeting ROBO4 and demonstrated evidence of toxicity in healthy mice, given more time the next stage of the project would be to clarify the nature of this toxicity and investigating whether ROBO4 can be safely targeted with CARs. As discussed in chapter 4, ROBO4 knockout mice could help determine whether toxicity is due to ROBO4 or a crossreactive antigen. Given that both R1 and R2 CARs resulted in toxicity, both recognise separate epitopes and previous studies have identified ROBO4 in the lung and liver, it is likely that the toxicity is a result of ROBO4 expression in normal tissues. Various approaches to further control the specificity of CAR T-cells in vivo were discussed in chapter 4. This project could therefore also explore these in the context of ROBO4-specific CARs.

One major drawback to targeting the tumour vasculature is the potential for a viable rim of tumour cells within the perimeter of tumours. This viable rim has been demonstrated in models using vascular disrupting agents (VDAs). Despite a collapse in the tumours vasculature network, viable cells in the perimeter appear more resistant and are a source for tumour regrowth (figure 5.13). These cells appear less sensitive to the hypoxia induced by vascular disruption and may obtain suitable nutrients and oxygen from surrounding vasculature in normal tissues (Siemann et al. 2004). The combination of VDA's with traditional therapies have shown improved anti-tumour efficacy in several models. This may be due to a double-barrelled approach, where VDAs can target the internal tumour cells and traditional cytotoxic reagents or irradiation can target rapidly grown tumour cells (such as those in the perimeter)(Siemann et al. 2004).

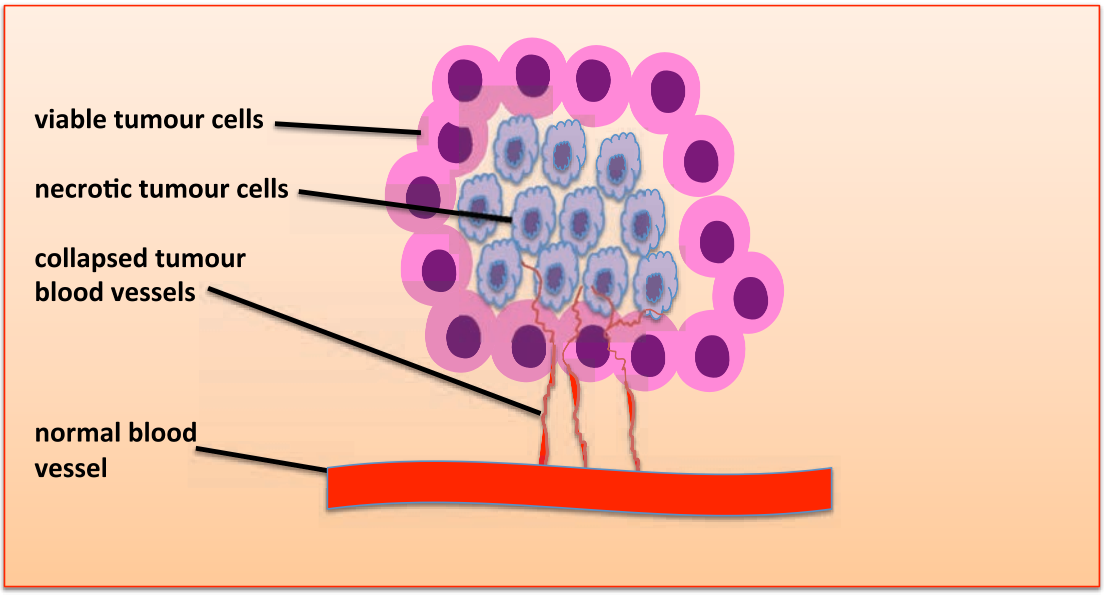

Figure **5.13:** The effect of vascular disrupting agents on tumours. Vascular disrupting agents can cause a selective destruction of the tumour blood vessels, resulting in a collapse in the tumour vasculature network. This can induce tumour necrosis due to a lack of oxygen and nutrients, especially in the centre of the tumour. Animal models have identified a perimeter of viable tumour cells that are less sensitive to the effects of vascular disruption. These viable cells can continue to regrow and reform the tumour.

Most CAR trials already implement pre-conditioning with irradiation and/or chemotherapy before T cell infusion. Viable rims of tumour cells may therefore be avoided in the context of CAR therapy. CAR T cells to TEMs may also be combined with CAR T cells to tumour antigens. The combination of VEGFR2 CARs and CARs to the tumour antigens gp100 or TRP-1 resulted in a synergistic improvement in anti-tumour efficacy as well as improved T cell infiltration of tumours (Chinnasamy et al. 2013). This effect may depend greatly on antigen choice and tumour model since there could be hindrance caused by vasculature disruption preventing sufficient infiltration of tumour specific CAR T cells.

Many more general roadblocks for the future of CAR T cell therapy exist. CAR therapy has only ever been used to treat a matter of hundreds of patients within specialised centres. There is considerable cost involved in patient transport, blood collection, generation of CAR T cells (under good manufacturing practice), implementing chemotherapy, patient management and surveillance while in intensive care and continued assessment. The cost of CAR treatment will likely be a major obstacle to overcome. Currently, CAR T cell therapy is an individualised treatment, using patient derived autologous T cells. This adds to the cost and scope of CAR therapy. Furthermore, sufficient numbers of autologous T cells may not be recovered from patients, such as in infants, to undergo CAR therapy treatment. The use of allogeneic donor derived T cells would allow a large-scale CAR T cell manufacture, cutting out individual blood collection and CAR T cell generation. Essential, CAR therapy could be an off-the-shelf treatment. This would make CAR therapy significantly cheaper and more practical.

Several studies have investigated the use of allogeneic donor CD19 CAR T cells in patients following allogeneic HSCTs to treat B cell malignancies (Kochenderfer et al. 2013; Brudno et al. 2016; Cruz et al. 2013). The development of GVHD, due to histocompatibility differences, is a potential side effect of allogeneic CAR T cells. However, no cases of acute GVHD have been reported so far using allogeneic CAR T cells. Overall, however, anti-tumour effects have been poor compared to autologous CD19 CAR T cells. This may be due to the lack of pre-conditioning therapy before CAR T cell infusion in these studies and the low dose of CAR T cells administered.

The use of lentiviral CAR vectors in combination with transcription activator-like effector nucleases (TALENs) to disrupt TCR expression is being pioneered by Cellectis to create universal allogeneic CAR T cells (UCARTs). Disruption of the TCR gene in the UCARs eliminates the risk of GVHD. Further disruption of CD52 makes UCARTs immune to anti-CD52 chemotherapy. Allogeneic UCARTs to CD19 (UCART19) have already resulted in complete remission in two infants with relapsed refractory ALL in a proof of principle study(Qasim et al. 2017). A phase 1 clinical trial for UCART19 is now recruiting ALL patients (http://clinicaltrials.gov NCT02746952). Further trials are investigating CD123 specific UCARTs in AML and blastic plasmacytoid dendritic cell neoplasm (http://clinicaltrials.gov NCT03190278 and NCT03203369 respectively). If results are as good as those seen with the initial UCART19 study, the approach to CAR T cell therapy could completely shift to allogeneic donors.

CAR T cell therapy would also require approval from the relevant government authorities before it becomes a widely available therapy. Three CD19 CAR products (CTL019 from Novartis; JCAR015 from Juno; KTE-C19 from Kite) have been designated FDA Breakthrough Therapy which means they are essentially fast tracked for potential approval, although JCAR015 has since been discontinued after trial termination due to five fatal neurological incidents (http://clinicaltrials.gov NCT02535364) (5). In August 2017, CTL019 from Novartis was FDA approved to treat paediatric and young adult relapsed/refractory B cell ALL.

Even with approval, CTL019 will likely require continued trials to confirm efficacy as part of post-marking surveillance and will remain in specialised treatment centres (Locke & Davila 2017). Meanwhile, CAR therapy to solid tumours has so far been less successful. Similar to the toxicity issues described in this project, finding a suitable antigen that is not expressed in normal tissue at levels resulting in on-target off-tumour toxicity has proved challenging.

An scFv phage display library was used to recover scFv and generate CARs to three alternative TEMs: ELTD1, GRIN2D and MCAM. However, all of these TEMs are also found in the endothelium of normal tissue. ELTD1 has also been found in non-endothelial cells of the heart and lungs (Nechiporuk et al. 2001). GRIND2 is expressed in the adult brain albeit at low levels. The blood brain barrier (BBB) should effectively inhibit CAR T cells from crossing into the brain and causing off-target toxicity. However, a recent report has shown CD19 CAR T cells to cross the BBB and cause cerebral CRS (Hu et al. 2016). Toxicity from GRIN2D CAR T cells that cross the BBB could be catastrophic. In addition, CARs to MCAM may cause the destruction of MSCs (Baksh et al. 2007). It is possible that CAR T cells to any of these markers may cause off-tumour toxicity. Unfortunately, there are no TEMs 100% specific to tumour tissue. Despite this, the TEM CLEC14A has been safely targeted with CAR T cells in mice in the Lee lab (unpublished data). Until a TEM with 100% tumour specificity can be found, current novel TEMs must be investigated to uncover any possible antibodies/CARs that can safely and effectively target the TEMs.

7. References

Agrawal, A. et al., 2008. An autosomal linkage scan for cannabis use disorders in the nicotine addiction genetics project. *Archives of general psychiatry*, 65(6), pp.713–21.

Ahmadzadeh, M. et al., 2009. Tumor antigen-specific CD8 T cells infiltrating the tumor express high levels of PD-1 and are functionally impaired. *Blood*, 114(8), pp.1537–1544.

Ahmed, N. et al., 2015. Human Epidermal Growth Factor Receptor 2 (HER2) - Specific Chimeric Antigen Receptor-Modified T Cells for the Immunotherapy of HER2-Positive Sarcoma. *Journal of clinical oncology : official journal of the American Society of Clinical Oncology*, 33(15), pp.1688–96.

Aird, W.C., 2009. Molecular heterogeneity of tumor endothelium. *Cell and tissue research*, 335(1), pp.271–81.

Akbarian, S. et al., 1996. Selective alterations in gene expression for NMDA receptor subunits in prefrontal cortex of schizophrenics. *The Journal of neuroscience : the official journal of the Society for Neuroscience*, 16(1), pp.19–30.

Akino, T. et al., 2009. Cytogenetic abnormalities of tumor-associated endothelial cells in human malignant tumors. *The American journal of pathology*, 175(6), pp.2657–67.

Aleksic, M. et al., 2012. Different affinity windows for virus and cancer-specific T-cell receptors: implications for therapeutic strategies. *European journal of immunology*, 42(12), pp.3174–9.

Allen, E. et al., 2017. Combined antiangiogenic and anti–PD-L1 therapy stimulates tumor immunity through HEV formation. *Science Translational Medicine*, 9(385).

Allie, N. et al., 2013. Prominent role for T cell-derived Tumour Necrosis Factor for sustained control of Mycobacterium tuberculosis infection. *Scientific Reports*, 3.

Alvarez-Vallina, L. & Hawkins, R.E., 1996. Antigen-specific targeting of CD28-mediated T cell co-stimulation using chimeric single-chain antibody variable fragment-CD28 receptors. *European journal of immunology*, 26(10), pp.2304–2309.

Antony, P.A. et al., 2005. CD8+ T cell immunity against a tumor/self-antigen is augmented by CD4+ T helper cells and hindered by naturally occurring T regulatory cells. *Journal of immunology (Baltimore, Md. : 1950)*, 174(5), pp.2591–2601.

Asahara, T. et al., 1999. Bone marrow origin of endothelial progenitor cells responsible for postnatal vasculogenesis in physiological and pathological neovascularization. *Circulation research*, 85(3), pp.221–8.

Asahara, T. et al., 1997. Isolation of putative progenitor endothelial cells for angiogenesis. *Science (New York, N.Y.)*, 275(5302), pp.964–967.

Bachmann, M.F. et al., 2007. Differential role of IL-2R signaling for CD8+ T cell responses in acute and chronic viral infections. *European Journal of Immunology*, 37(6), pp.1502–1512.

Badovinac, V.P., Tvinnereim, A.R. & Harty, J.T., 2000. Regulation of Antigen-

Specific CD8+ T Cell Homeostasis by Perforin and Interferon-γ. *Science*, 290(5495).
Baksh, D., Yao, R. & Tuan, R.S., 2007. Comparison of Proliferative and Multilineage Differentiation Potential of Human Mesenchymal Stem Cells Derived from Umbilical Cord and Bone Marrow. *Stem Cells*, 25(6), pp.1384–1392.
Ballesteros-Tato, A. et al., 2012. Interleukin-2 inhibits germinal center formation by limiting T follicular helper cell differentiation. *Immunity*, 36(5), pp.847–56.
Barber, A., Rynda, A. & Sentman, C.L., 2009. Chimeric NKG2D expressing T cells eliminate immunosuppression and activate immunity within the ovarian tumor microenvironment. *Journal of immunology (Baltimore, Md. : 1950)*, 183(11), pp.6939–47.
Barber, D.L. et al., 2006. Restoring function in exhausted CD8 T cells during chronic viral infection. *Nature*, 439(7077), pp.682–687.
Barrett, D.M. et al., 2016. Interleukin 6 Is Not Made By Chimeric Antigen Receptor T Cells and Does Not Impact Their Function. *Blood*, 128(22).
Barrett, D.M. et al., 2013. Regimen-specific effects of RNA-modified chimeric antigen receptor T cells in mice with advanced leukemia. *Human gene therapy*, 24(8), pp.717–27.
Barron, L. et al., 2010. Cutting Edge: Mechanisms of IL-2-Dependent Maintenance of Functional Regulatory T Cells. *The Journal of Immunology*, 185(11), pp.6426–6430.
Bedell, V.M. et al., 2005. roundabout4 is essential for angiogenesis in vivo. , 1.
Berger, C. et al., 2008. Adoptive transfer of effector CD8+ T cells derived from central memory cells establishes persistent T cell memory in primates. *The Journal of clinical investigation*, 118(1), pp.294–305.
Berger, C. et al., 2006. Analysis of transgene-specific immune responses that limit the in vivo persistence of adoptively transferred HSV-TK-modified donor T cells after allogeneic hematopoietic cell transplantation. *Blood*, 107(6), pp.2294–302.
Bergers, G. & Hanahan, D., 2008. Modes of resistance to anti-angiogenic therapy. *Nature reviews. Cancer*, 8(8), pp.592–603.
Bernhard, H. et al., 2008. Adoptive transfer of autologous, HER2-specific, cytotoxic T lymphocytes for the treatment of HER2-overexpressing breast cancer. *Cancer immunology, immunotherapy : CII*, 57(2), pp.271–80.
Besser, M.J. et al., 2009. Minimally cultured or selected autologous tumor-infiltrating lymphocytes after a lympho-depleting chemotherapy regimen in metastatic melanoma patients. *Journal of immunotherapy (Hagerstown, Md. : 1997)*, 32(4), pp.415–423.
Betts, M.R. et al., 2006. HIV nonprogressors preferentially maintain highly functional HIV-specific CD8+ T cells. *Blood*, 107(12), pp.4781–9.
Boissonnas, A. et al., 2007. In vivo imaging of cytotoxic T cell infiltration and elimination of a solid tumor. *The Journal of Experimental Medicine*, 204(2), pp.345–356.
Bonini, C., 1997. HSV-TK Gene Transfer into Donor Lymphocytes for Control of Allogeneic Graft-Versus-Leukemia. *Science*, 276(5319), pp.1719–1724.
Boon, T. et al., 2006. Human T cell responses against melanoma. *Annual review of immunology*, 24, pp.175–208.

Boyman, O. & Sprent, J., 2012. The role of interleukin-2 during homeostasis and activation of the immune system. *Nature Reviews Immunology*, 12(3), p.180.

Brack, S.S. et al., 2006. Tumor-Targeting Properties of Novel Antibodies Specific to the Large Isoform of Tenascin-C. *Clinical Cancer Research*, 12(10).

Brahmer, J.R. et al., 2012. Safety and Activity of Anti–PD-L1 Antibody in Patients with Advanced Cancer. *New England Journal of Medicine*, 366(26), pp.2455–2465.

Brentjens, R. et al., 2010. Treatment of Chronic Lymphocytic Leukemia With Genetically Targeted Autologous T Cells: Case Report of an Unforeseen Adverse Event in a Phase I Clinical Trial. *Molecular Therapy*, 18(4), pp.666–668.

Brentjens, R.J. et al., 2013. CD19-Targeted T Cells Rapidly Induce Molecular Remissions in Adults with Chemotherapy-Refractory Acute Lymphoblastic Leukemia. *Science Translational Medicine*, 5(177), p.177ra38-177ra38.

Brentjens, R.J. et al., 2003. Eradication of systemic B-cell tumors by genetically targeted human T lymphocytes co-stimulated by CD80 and interleukin-15. *Nature medicine*, 9(3), pp.279–86.

Brentjens, R.J. et al., 2007. Genetically targeted T cells eradicate systemic acute lymphoblastic leukemia xenografts. *Clinical cancer research : an official journal of the American Association for Cancer Research*, 13(18 Pt 1), pp.5426–35.

Brentjens, R.J. et al., 2011. Safety and persistence of adoptively transferred autologous CD19-targeted T cells in patients with relapsed or chemotherapy refractory B-cell leukemias. *Blood*, 118(18), pp.4817–28.

Bretscher, P. & Cohn, M., 1970. A Theory of Self-Nonself Discrimination: Paralysis and induction involve the recognition of one and two determinants on an antigen, respectively. *Science*, 169(3950), pp.1042–1049.

Brocker, T., 2000. Chimeric Fv-zeta or Fv-epsilon receptors are not sufficient to induce activation or cytokine production in peripheral T cells. *Blood*, 96(5), pp.1999–2001.

Brocker, T., 1995. Signals through T cell receptor-zeta chain alone are insufficient to prime resting T lymphocytes. *Journal of Experimental Medicine*, 181(5), pp.1653–1659.

Brose, K. et al., 1999. Slit Proteins Bind Robo Receptors and Have an Evolutionarily Conserved Role in Repulsive Axon Guidance. *Cell*, 96(6), pp.795–806.

Brown, C.E. et al., 2015. Bioactivity and Safety of IL13R 2-Redirected Chimeric Antigen Receptor CD8+ T Cells in Patients with Recurrent Glioblastoma. *Clinical Cancer Research*, 21(18), pp.4062–4072.

Brudno, J.N. et al., 2016. Allogeneic T Cells That Express an Anti-CD19 Chimeric Antigen Receptor Induce Remissions of B-Cell Malignancies That Progress After Allogeneic Hematopoietic Stem-Cell Transplantation Without Causing Graft-Versus-Host Disease. *Journal of Clinical Oncology*, 34(10), pp.1112–1121.

Bu, P. et al., 2006. Anti-CD146 monoclonal antibody AA98 inhibits angiogenesis via suppression of nuclear factor-κB activation. *Molecular Cancer Therapeutics*, 5(11).

Buckanovich, R.J. et al., 2007. Tumor vascular proteins as biomarkers in ovarian cancer. *Journal of clinical oncology : official journal of the American Society of*

Clinical Oncology, 25(7), pp.852–61.
Budde, L.E. et al., 2013. Combining a CD20 chimeric antigen receptor and an inducible caspase 9 suicide switch to improve the efficacy and safety of T cell adoptive immunotherapy for lymphoma. *PloS one*, 8(12), p.e82742.
Burri, P.H., Hlushchuk, R. & Djonov, V., 2004. Intussusceptive angiogenesis: its emergence, its characteristics, and its significance. *Developmental dynamics : an official publication of the American Association of Anatomists*, 231(3), pp.474–488.
Burrows, F.J. & Thorpe, P.E., 1993. Eradication of large solid tumors in mice with an immunotoxin directed against tumor vasculature. *Proceedings of the National Academy of Sciences*, 90(19), pp.8996–9000.
Caccamo, N. et al., 2010. Multifunctional CD4(+) T cells correlate with active Mycobacterium tuberculosis infection. *European journal of immunology*, 40(8), pp.2211–20.
Cai, H., Xue, Y., Liu, W., et al., 2015. Overexpression of Roundabout4 predicts poor prognosis of primary glioma patients via correlating with microvessel density. *Journal of neuro-oncology*, 123(1), pp.161–9.
Cai, H., Xue, Y., Li, Z., et al., 2015. Roundabout4 Suppresses Glioma-Induced Endothelial Cell Proliferation, Migration and Tube Formation ***in Vitro*** by Inhibiting VEGR2-Mediated PI3K/AKT and FAK Signaling Pathways. *Cellular Physiology and Biochemistry*, 35(5), pp.1689–1705.
Calzascia, T. et al., 2007. TNF-alpha is critical for antitumor but not antiviral T cell immunity in mice. *The Journal of clinical investigation*, 117(12), pp.3833–45.
Cameron, B.J. et al., 2013. Identification of a Titin-derived HLA-A1-presented peptide as a cross-reactive target for engineered MAGE A3-directed T cells. *Science translational medicine*, 5(197), p.197ra103.
Cao, Y. et al., 2016. Design of Switchable Chimeric Antigen Receptor T Cells Targeting Breast Cancer. *Angewandte Chemie International Edition*, 55(26), pp.7520–7524.
Carmeliet, P. et al., 1996. Abnormal blood vessel development and lethality in embryos lacking a single VEGF allele. *Nature*, 380(6573), pp.435–439.
Carmeliet, P., 2003. Blood vessels and nerves: common signals, pathways and diseases. *Nature reviews. Genetics*, 4(9), pp.710–720.
Carpenito, C. et al., 2009. Control of large, established tumor xenografts with genetically retargeted human T cells containing CD28 and CD137 domains. *Proceedings of the National Academy of Sciences of the United States of America*, 106(9), pp.3360–5.
Cartellieri, M. et al., 2010. Chimeric antigen receptor-engineered T cells for immunotherapy of cancer. *Journal of biomedicine & biotechnology*, 2010, p.956304.
Chatzidakis, I. et al., 2007. An essential role for TNF in modulating thresholds for survival, activation, and tolerance of CD8+ T cells. *Journal of immunology (Baltimore, Md. : 1950)*, 178(11), pp.6735–45.
Chaudhary, A. et al., 2012. TEM8/ANTXR1 blockade inhibits pathological angiogenesis and potentiates tumoricidal responses against multiple cancer types. *Cancer cell*, 21(2), pp.212–26.
Chen, X. & Oppenheim, J.J., 2011. Contrasting effects of TNF and anti-TNF on the activation of effector T cells and regulatory T cells in autoimmunity. *FEBS*

Letters, 585(23), pp.3611–3618.
Chen, Y.-K. et al., 2015. Clinical and prognostic implications of Roundabout 4 (robo4) in adult patients with acute myeloid leukemia. *PloS one*, 10(3), p.e0119831.
Cheng, J.C.-H. et al., 2013. Early detection of Lewis lung carcinoma tumor control by irradiation using diffusion-weighted and dynamic contrast-enhanced MRI. *PloS one*, 8(5), p.e62762.
Cherkassky, L. et al., 2016. Human CAR T cells with cell-intrinsic PD-1 checkpoint blockade resist tumor-mediated inhibition. *Journal of Clinical Investigation*, 126(8), pp.3130–3144.
Chinnasamy, D. et al., 2010. Gene therapy using genetically modified lymphocytes targeting VEGFR-2 inhibits the growth of vascularized syngenic tumors in mice. *The Journal of clinical investigation*, 120(11), pp.3953–68.
Chinnasamy, D. et al., 2012. Local delivery of interleukin-12 using T cells targeting VEGF receptor-2 eradicates multiple vascularized tumors in mice. *Clinical cancer research : an official journal of the American Association for Cancer Research*, 18(6), pp.1672–83.
Chinnasamy, D. et al., 2013. Simultaneous targeting of tumor antigens and the tumor vasculature using T lymphocyte transfer synergize to induce regression of established tumors in mice. *Cancer research*, 73(11), pp.3371–80.
Chinnasamy, N. et al., 2011. A TCR targeting the HLA-A*0201-restricted epitope of MAGE-A3 recognizes multiple epitopes of the MAGE-A antigen superfamily in several types of cancer. *Journal of immunology (Baltimore, Md. : 1950)*, 186(2), pp.685–96.
Chmielewski, M. et al., 2011. IL-12 release by engineered T cells expressing chimeric antigen receptors can effectively Muster an antigen-independent macrophage response on tumor cells that have shut down tumor antigen expression. *Cancer research*, 71(17), pp.5697–706.
Choi, K. et al., 1998. A common precursor for hematopoietic and endothelial cells. *Development (Cambridge, England)*, 125(4), pp.725–732.
Chu, T.J. & Peters, D.G., 2008. Serial analysis of the vascular endothelial transcriptome under static and shear stress conditions. *Physiological Genomics*, 34(2), pp.185–192.
Chun, T.-H. et al., 2004. MT1-MMP-dependent neovessel formation within the confines of the three-dimensional extracellular matrix. *The Journal of cell biology*, 167(4), pp.757–767.
Cieri, N. et al., 2013. IL-7 and IL-15 instruct the generation of human memory stem T cells from naive precursors. *Blood*, 121(4), pp.573–84.
Clay, T.M. et al., 1999. Efficient transfer of a tumor antigen-reactive TCR to human peripheral blood lymphocytes confers anti-tumor reactivity. *Journal of immunology (Baltimore, Md. : 1950)*, 163(1), pp.507–13.
Cohen, C.J. et al., 2006. Enhanced antitumor activity of murine-human hybrid T-cell receptor (TCR) in human lymphocytes is associated with improved pairing and TCR/CD3 stability. *Cancer research*, 66(17), pp.8878–8886.
Cohen, C.J. et al., 2007. Enhanced antitumor activity of T cells engineered to express T-cell receptors with a second disulfide bond. *Cancer research*, 67(8), pp.3898–3903.

Cohen, C.J. et al., 2015. Isolation of neoantigen-specific T cells from tumor and peripheral lymphocytes. *The Journal of clinical investigation*, 125(10), pp.3981–91.
Cohen, C.J. et al., 2005. Recognition of fresh human tumor by human peripheral blood lymphocytes transduced with a bicistronic retroviral vector encoding a murine anti-p53 TCR. *Journal of immunology (Baltimore, Md. : 1950)*, 175(9), pp.5799–5808.
Conway, E.M., Collen, D. & Carmeliet, P., 2001. Molecular mechanisms of blood vessel growth. *Cardiovascular research*, 49(3), pp.507–521.
Craddock, J.A. et al., 2010. Enhanced tumor trafficking of GD2 chimeric antigen receptor T cells by expression of the chemokine receptor CCR2b. *Journal of immunotherapy (Hagerstown, Md. : 1997)*, 33(8), pp.780–8.
Croft, M., 2003. Costimulation of T cells by OX40, 4-1BB, and CD27. *Cytokine & Growth Factor Reviews*, 14(3–4), pp.265–273.
Cruz, C.R.Y. et al., 2013. Infusion of donor-derived CD19-redirected virus-specific T cells for B-cell malignancies relapsed after allogeneic stem cell transplant: a phase 1 study. *Blood*, 122(17).
Curiel, T.J. et al., 2003. Blockade of B7-H1 improves myeloid dendritic cell–mediated antitumor immunity. *Nature Medicine*, 9(5), pp.562–567.
Curran, M.A. et al., 2010. PD-1 and CTLA-4 combination blockade expands infiltrating T cells and reduces regulatory T and myeloid cells within B16 melanoma tumors. *Proceedings of the National Academy of Sciences*, 107(9), pp.4275–4280.
Dalton, D.K. et al., 2000. Interferon gamma eliminates responding CD4 T cells during mycobacterial infection by inducing apoptosis of activated CD4 T cells. *The Journal of experimental medicine*, 192(1), pp.117–22.
Darcy, P.K. et al., 2000. Redirected perforin-dependent lysis of colon carcinoma by ex vivo genetically engineered CTL. *Journal of immunology (Baltimore, Md. : 1950)*, 164(7), pp.3705–12.
Darrah, P.A. et al., 2007. Multifunctional TH1 cells define a correlate of vaccine-mediated protection against Leishmania major. *Nature medicine*, 13(7), pp.843–50.
Davila, M.L. et al., 2014. Efficacy and toxicity management of 19-28z CAR T cell therapy in B cell acute lymphoblastic leukemia. *Science translational medicine*, 6(224), p.224ra25.
Davila, M.L. et al., 2012. How do CARs work?: Early insights from recent clinical studies targeting CD19. *Oncoimmunology*, 1(9), pp.1577–1583.
Deol, A. & Lum, L.G., 2010. Role of donor lymphocyte infusions in relapsed hematological malignancies after stem cell transplantation revisited. *Cancer treatment reviews*, 36(7), pp.528–538.
Dieterich, L.C. et al., 2012. Transcriptional profiling of human glioblastoma vessels indicates a key role of VEGF-A and TGFβ2 in vascular abnormalization. *The Journal of pathology*, 228(3), pp.378–90.
Dudley, A.C., 2012. Tumor endothelial cells. *Cold Spring Harbor perspectives in medicine*, 2(3), p.a006536.
Dudley, M.E. et al., 2001. Adoptive transfer of cloned melanoma-reactive T lymphocytes for the treatment of patients with metastatic melanoma. *Journal of immunotherapy (Hagerstown, Md. : 1997)*, 24(4), pp.363–73.
Dudley, M.E. et al., 2002. Cancer regression and autoimmunity in patients after

clonal repopulation with antitumor lymphocytes. *Science (New York, N.Y.)*, 298(5594), pp.850–854.
Dudley, M.E. & Rosenberg, S.A., 2003. Adoptive-cell-transfer therapy for the treatment of patients with cancer. *Nature reviews. Cancer*, 3(9), pp.666–75.
Duvall, M.G. et al., 2008. Polyfunctional T cell responses are a hallmark of HIV-2 infection. *European journal of immunology*, 38(2), pp.350–63.
Egen, J.G. & Allison, J.P., 2002. Cytotoxic T lymphocyte antigen-4 accumulation in the immunological synapse is regulated by TCR signal strength. *Immunity*, 16(1), pp.23–35.
Einsele, H. et al., 2002. Infusion of cytomegalovirus (CMV)-specific T cells for the treatment of CMV infection not responding to antiviral chemotherapy. *Blood*, 99(11), pp.3916–3922.
Engels, B. et al., 2005. Redirecting human T lymphocytes toward renal cell carcinoma specificity by retroviral transfer of T cell receptor genes. *Human gene therapy*, 16(7), pp.799–810.
Engels, B. et al., 2003. Retroviral Vectors for High-Level Transgene Expression in T Lymphocytes. *Human Gene Therapy*, 14(12), pp.1155–1168.
Enomoto, S. et al., 2016. *Suppression of Slit2/Robo1 mediated HUVEC migration by Robo4*,
Eshhar, Z. et al., 1993. Specific activation and targeting of cytotoxic lymphocytes through chimeric single chains consisting of antibody-binding domains and the gamma or zeta subunits of the immunoglobulin and T-cell receptors. *Proceedings of the National Academy of Sciences of the United States of America*, 90(2), pp.720–4.
Ewert, S. et al., 2003. Biophysical properties of human antibody variable domains. *Journal of molecular biology*, 325(3), pp.531–53.
Fallarino, F. et al., 2003. Modulation of tryptophan catabolism by regulatory T cells. *Nature Immunology*, 4(12), pp.1206–1212.
Farolfi, A. et al., 2012. Ipilimumab in advanced melanoma. *Melanoma Research*, 22(3), pp.263–270.
Favara, D.M., Banham, A.H. & Harris, A.L., 2014. A review of ELTD1, a pro-angiogenic adhesion GPCR. *Biochemical Society transactions*, 42(6), pp.1658–64.
Feau, S. et al., 2011. Autocrine IL-2 is required for secondary population expansion of CD8(+) memory T cells. *Nature immunology*, 12(9), pp.908–13.
Fedorov, V.D., Themeli, M. & Sadelain, M., 2013. PD-1- and CTLA-4-based inhibitory chimeric antigen receptors (iCARs) divert off-target immunotherapy responses. *Science translational medicine*, 5(215), p.215ra172.
Fehse, B. et al., 2000. CD34 Splice Variant: An Attractive Marker for Selection of Gene-Modified Cells. *Molecular Therapy*, 1(5), pp.448–456.
Ferguson, H.J.M. et al., 2016. Glutamate dependent NMDA receptor 2D is a novel angiogenic tumour endothelial marker in colorectal cancer. *Oncotarget*, 7(15), pp.20440–54.
Ferrara, N. et al., 1996. Heterozygous embryonic lethality induced by targeted inactivation of the VEGF gene. *Nature*, 380(6573), pp.439–442.
Ferrara, N., Gerber, H.-P. & LeCouter, J., 2003. The biology of VEGF and its receptors. *Nature medicine*, 9(6), pp.669–676.
Finney, H.M. et al., 1998. Chimeric receptors providing both primary and

costimulatory signaling in T cells from a single gene product. *Journal of immunology (Baltimore, Md. : 1950)*, 161(6), pp.2791–7.
Finney, H.M., Akbar, A.N. & Lawson, A.D.G., 2003. Activation of Resting Human Primary T Cells with Chimeric Receptors: Costimulation from CD28, Inducible Costimulator, CD134, and CD137 in Series with Signals from the TCR Chain. *The Journal of Immunology*, 172(1), pp.104–113.
Fisher, D.T. et al., 2011. IL-6 trans-signaling licenses mouse and human tumor microvascular gateways for trafficking of cytotoxic T cells. *Journal of Clinical Investigation*, 121(10), pp.3846–3859.
Folkman, J., 1971. Tumor angiogenesis: therapeutic implications. *The New England journal of medicine*, 285(21), pp.1182–6.
Fong, G.H. et al., 1999. Increased hemangioblast commitment, not vascular disorganization, is the primary defect in flt-1 knock-out mice. *Development (Cambridge, England)*, 126(13), pp.3015–3025.
Fontenot, J.D. et al., 2005. A function for interleukin 2 in Foxp3-expressing regulatory T cells. *Nature Immunology*, 6(11), pp.1142–1151.
Forsberg, E.C. et al., 2005. Differential expression of novel potential regulators in hematopoietic stem cells. *PLoS genetics*, 1(3), p.e28.
Foster, A.E. et al., 2008. Antitumor activity of EBV-specific T lymphocytes transduced with a dominant negative TGF-beta receptor. *Journal of immunotherapy (Hagerstown, Md. : 1997)*, 31(5), pp.500–5.
Francisco, L.M. et al., 2009. PD-L1 regulates the development, maintenance, and function of induced regulatory T cells. *The Journal of Experimental Medicine*, 206(13), pp.3015–3029.
Fratta, E. et al., 2011. The biology of cancer testis antigens: putative function, regulation and therapeutic potential. *Molecular oncology*, 5(2), pp.164–82.
Friedmann-Morvinski, D. et al., 2005. Redirected primary T cells harboring a chimeric receptor require costimulation for their antigen-specific activation. *Blood*, 105(8), pp.3087–3093.
Frumento, G. et al., 2013. Cord blood T cells retain early differentiation phenotype suitable for immunotherapy after TCR gene transfer to confer EBV specificity. *American journal of transplantation : official journal of the American Society of Transplantation and the American Society of Transplant Surgeons*, 13(1), pp.45–55.
Fukuhara, N. et al., 2008. Structural and functional analysis of slit and heparin binding to immunoglobulin-like domains 1 and 2 of Drosophila Robo. *The Journal of biological chemistry*, 283(23), pp.16226–34.
Furuya, M., Yonemitsu, Y. & Aoki, I., 2009. III. Angiogenesis: complexity of tumor vasculature and microenvironment. *Current pharmaceutical design*, 15(16), pp.1854–1867.
Gale, N.W. et al., 2004. Haploinsufficiency of delta-like 4 ligand results in embryonic lethality due to major defects in arterial and vascular development. *Proceedings of the National Academy of Sciences of the United States of America*, 101(45), pp.15949–15954.
Galon, J. et al., 2006. Type, density, and location of immune cells within human colorectal tumors predict clinical outcome. *Science (New York, N.Y.)*, 313(5795), pp.1960–1964.
Garon, E.B. et al., 2015. Pembrolizumab for the Treatment of Non–Small-Cell Lung Cancer. *New England Journal of Medicine*, 372(21), pp.2018–2028.

Gattinoni, L. et al., 2011. A human memory T cell subset with stem cell–like properties. *Nature Medicine*, 17(10), pp.1290–1297.
Gattinoni, L., Klebanoff, C.A., et al., 2005. Acquisition of full effector function in vitro paradoxically impairs the in vivo antitumor efficacy of adoptively transferred CD8+ T cells. *The Journal of clinical investigation*, 115(6), pp.1616–26.
Gattinoni, L., Finkelstein, S.E., et al., 2005. Removal of homeostatic cytokine sinks by lymphodepletion enhances the efficacy of adoptively transferred tumor-specific CD8+ T cells. *The Journal of experimental medicine*, 202(7), pp.907–912.
Geiger, T.L. et al., 2001. Integrated src kinase and costimulatory activity enhances signal transduction through single-chain chimeric receptors in T lymphocytes. *Blood*, 98(8), pp.2364–71.
Gerhardt, H. et al., 2003. VEGF guides angiogenic sprouting utilizing endothelial tip cell filopodia. *The Journal of cell biology*, 161(6), pp.1163–1177.
Germain, R.N., 2002. T-cell development and the CD4–CD8 lineage decision. *Nature Reviews Immunology*, 2(5), pp.309–322.
Ghajar, C.M. et al., 2013. The perivascular niche regulates breast tumour dormancy. *Nature cell biology*, 15(7), pp.807–17.
Ghassemi, S. et al., 2016. Shortened T cell culture with IL-7 and IL-15 provides the most potent chimeric antigen receptor (CAR)-modified T cells for adoptive immunotherapy. *The Journal of Immunology*, 196(1 Supplement), p.214.23-214.23.
Gimmi, C.D. et al., 1993. Human T-cell clonal anergy is induced by antigen presentation in the absence of B7 costimulation. *Proceedings of the National Academy of Sciences*, 90(14), pp.6586–6590.
Gong, M.C. et al., 1999. Cancer patient T cells genetically targeted to prostate-specific membrane antigen specifically lyse prostate cancer cells and release cytokines in response to prostate-specific membrane antigen. *Neoplasia (New York, N.Y.)*, 1(2), pp.123–7.
Green, A.M., Difazio, R. & Flynn, J.L., 2013. IFN-γ from CD4 T cells is essential for host survival and enhances CD8 T cell function during Mycobacterium tuberculosis infection. *Journal of immunology (Baltimore, Md. : 1950)*, 190(1), pp.270–7.
Griffiths, A.D. et al., 1994. Isolation of high affinity human antibodies directly from large synthetic repertoires. *The EMBO journal*, 13(14), pp.3245–60.
Grinberg-Bleyer, Y. et al., 2010. Pathogenic T cells have a paradoxical protective effect in murine autoimmune diabetes by boosting Tregs. *The Journal of clinical investigation*, 120(12), pp.4558–68.
Gröne, J. et al., 2006. Robo1/Robo4: differential expression of angiogenic markers in colorectal cancer. *Oncology reports*, 15(6), pp.1437–43.
Gross, G., Waks, T. & Eshhar, Z., 1989. Expression of immunoglobulin-T-cell receptor chimeric molecules as functional receptors with antibody-type specificity. *Proceedings of the National Academy of Sciences*, 86(24), pp.10024–10028.
Grupp, S.A. et al., 2013. Chimeric antigen receptor-modified T cells for acute lymphoid leukemia. *The New England journal of medicine*, 368(16), pp.1509–18.
Guezguez, B. et al., 2007. Dual Role of Melanoma Cell Adhesion Molecule

(MCAM)/CD146 in Lymphocyte Endothelium Interaction: MCAM/CD146 Promotes Rolling via Microvilli Induction in Lymphocyte and Is an Endothelial Adhesion Receptor. *The Journal of Immunology*, 179(10).
Hall, A., 2012. Rho family GTPases. *Biochemical Society transactions*, 40(6), pp.1378–82.
Hall, M. et al., 2016. Expansion of tumor-infiltrating lymphocytes (TIL) from human pancreatic tumors. *Journal for ImmunoTherapy of Cancer*, 4(1), p.61.
Han, Q. et al., 2012. Polyfunctional responses by human T cells result from sequential release of cytokines. *Proceedings of the National Academy of Sciences*, 109(5), pp.1607–1612.
Harding, F.A. et al., 1992. CD28-mediated signalling co-stimulates murine T cells and prevents induction of anergy in T-cell clones. *Nature*, 356(6370), pp.607–609.
Haring, J.S., Badovinac, V.P. & Harty, J.T., 2006. Inflaming the CD8+ T cell response. *Immunity*, 25(1), pp.19–29.
Harkensee, C. et al., 2013. Microsatellite scanning of the immunogenome associates MAPK14 and ELTD1 with graft-versus-host disease in hematopoietic stem cell transplantation. *Immunogenetics*, 65(6), pp.417–27.
Hayashi, N. et al., 2002. Antigen challenge leads to in vivo activation and elimination of highly polarized TH1 memory T cells. *Proceedings of the National Academy of Sciences of the United States of America*, 99(9), pp.6187–91.
Haynes, N.M. et al., 2001. Redirecting Mouse CTL Against Colon Carcinoma: Superior Signaling Efficacy of Single-Chain Variable Domain Chimeras Containing TCR- vs Fc RI- . *The Journal of Immunology*, 166(1), pp.182–187.
Haynes, N.M. et al., 2002. Rejection of Syngeneic Colon Carcinoma by CTLs Expressing Single-Chain Antibody Receptors Codelivering CD28 Costimulation. *The Journal of Immunology*, 169(10), pp.5780–5786.
Haynes, N.M. et al., 2002. Single-chain antigen recognition receptors that costimulate potent rejection of established experimental tumors. *Blood*, 100(9), pp.3155–3163.
Hellström, M. et al., 2007. Dll4 signalling through Notch1 regulates formation of tip cells during angiogenesis. *Nature*, 445(7129), pp.776–780.
Herbert, J.M.J. et al., 2008. A novel method of differential gene expression analysis using multiple cDNA libraries applied to the identification of tumour endothelial genes. *BMC genomics*, 9, p.153.
Heslop, H.E., 2009. How I treat EBV lymphoproliferation. *Blood*, 114(19), pp.4002–4008.
Hida, K., Hida, Y. & Shindoh, M., 2008. Understanding tumor endothelial cell abnormalities to develop ideal anti-angiogenic therapies. *Cancer science*, 99(3), pp.459–66.
Hinrichs, C.S. et al., 2009. Adoptively transferred effector cells derived from naive rather than central memory CD8+ T cells mediate superior antitumor immunity. *Proceedings of the National Academy of Sciences of the United States of America*, 106(41), pp.17469–74.
Hinrichs, C.S. et al., 2011. Human effector CD8+ T cells derived from naive rather than memory subsets possess superior traits for adoptive immunotherapy. *Blood*, 117(3), pp.808–14.
van Hinsbergh, V.W.M. & Koolwijk, P., 2008. Endothelial sprouting and

angiogenesis: matrix metalloproteinases in the lead. *Cardiovascular Research*, 78(2), pp.203–212.
Hock, H. et al., 1993. Mechanisms of rejection induced by tumor cell-targeted gene transfer of interleukin 2, interleukin 4, interleukin 7, tumor necrosis factor, or interferon gamma. *Proceedings of the National Academy of Sciences of the United States of America*, 90(7), pp.2774–8.
Hodi, F.S. et al., 2010. Improved Survival with Ipilimumab in Patients with Metastatic Melanoma. *New England Journal of Medicine*, 363(8), pp.711–723.
Hohenester, E. et al., 2006. Interaction of the guidance molecule Slit with cellular receptors. *Biochemical Society transactions*, 34(Pt 3), pp.418–21.
Hombach, A. et al., 2001. Tumor-Specific T Cell Activation by Recombinant Immunoreceptors: CD3 Signaling and CD28 Costimulation Are Simultaneously Required for Efficient IL-2 Secretion and Can Be Integrated Into One Combined CD28/CD3 Signaling Receptor Molecule. *The Journal of Immunology*, 167(11), pp.6123–6131.
Hombach, A. & Abken, H., 2007. Costimulation tunes tumor-specific activation of redirected T cells in adoptive immunotherapy. *Cancer immunology, immunotherapy : CII*, 56(5), pp.731–7.
Hoogenboom, H.R. et al., 1991. Multi-subunit proteins on the surface of filamentous phage: methodologies for displaying antibody (Fab) heavy and light chains. *Nucleic acids research*, 19(15), pp.4133–7.
Houck, K.A. et al., 1992. Dual regulation of vascular endothelial growth factor bioavailability by genetic and proteolytic mechanisms. *The Journal of biological chemistry*, 267(36), pp.26031–26037.
Hu, Y. et al., 2016. Predominant cerebral cytokine release syndrome in CD19-directed chimeric antigen receptor-modified T cell therapy. *Journal of Hematology & Oncology*, 9(1), p.70.
Huang, X. et al., 2008. Sleeping Beauty transposon-mediated engineering of human primary T cells for therapy of CD19+ lymphoid malignancies. *Molecular therapy : the journal of the American Society of Gene Therapy*, 16(3), pp.580–9.
Hughes, M.S. et al., 2005. Transfer of a TCR gene derived from a patient with a marked antitumor response conveys highly active T-cell effector functions. *Human gene therapy*, 16(4), pp.457–472.
Huminiecki, L. et al., 2002. Magic roundabout is a new member of the roundabout receptor family that is endothelial specific and expressed at sites of active angiogenesis. *Genomics*, 79(4), pp.547–52.
Huminiecki, L. & Bicknell, R., 2000. In silico cloning of novel endothelial-specific genes. *Genome research*, 10(11), pp.1796–806.
Hurwitz, H. et al., 2004. Bevacizumab plus irinotecan, fluorouracil, and leucovorin for metastatic colorectal cancer. *The New England journal of medicine*, 350(23), pp.2335–42.
Ikeda, H., Old, L.J. & Schreiber, R.D., 2002. The roles of IFNγ in protection against tumor development and cancer immunoediting. *Cytokine & Growth Factor Reviews*, 13(2), pp.95–109.
Imai, C. et al., 2004. Chimeric receptors with 4-1BB signaling capacity provoke potent cytotoxicity against acute lymphoblastic leukemia. *Leukemia*, 18(4), pp.676–84.
Intlekofer, A.M. & Thompson, C.B., 2013. At the bench: preclinical rationale for

CTLA-4 and PD-1 blockade as cancer immunotherapy. *Journal of leukocyte biology*, 94(1), pp.25–39.
Ishii, T. et al., 1993. Molecular characterization of the family of the N-methyl-D-aspartate receptor subunits. *Journal of Biological Chemistry*, 268(4), pp.2836–2843.
Jäger, E. et al., 1998. Simultaneous humoral and cellular immune response against cancer-testis antigen NY-ESO-1: definition of human histocompatibility leukocyte antigen (HLA)-A2-binding peptide epitopes. *The Journal of experimental medicine*, 187(2), pp.265–70.
Jain, R.K., 1988. Determinants of tumor blood flow: a review. *Cancer research*, 48(10), pp.2641–58.
Jensen, M.C. et al., 2010. Antitransgene rejection responses contribute to attenuated persistence of adoptively transferred CD20/CD19-specific chimeric antigen receptor redirected T cells in humans. *Biology of blood and marrow transplantation : journal of the American Society for Blood and Marrow Transplantation*, 16(9), pp.1245–56.
Jiang, T. et al., 2012. CD146 is a coreceptor for VEGFR-2 in tumor angiogenesis. *Blood*, 120(11).
John, L.B. et al., 2013. Anti-PD-1 Antibody Therapy Potently Enhances the Eradication of Established Tumors By Gene-Modified T Cells. *Clinical Cancer Research*, 19(20).
John, L.B., Kershaw, M.H. & Darcy, P.K., 2013. Blockade of PD-1 immunosuppression boosts CAR T-cell therapy. *Oncoimmunology*, 2(October), p.e26286.
Johnson, J.W. & Ascher, P., 1987. Glycine potentiates the NMDA response in cultured mouse brain neurons. *Nature*, 325(6104), pp.529–531.
Johnson, L.A. et al., 2009. Gene therapy with human and mouse T-cell receptors mediates cancer regression and targets normal tissues expressing cognate antigen. *Blood*, 114(3), pp.535–46.
Johnson, L.A. et al., 2006. Gene Transfer of Tumor-Reactive TCR Confers Both High Avidity and Tumor Reactivity to Nonreactive Peripheral Blood Mononuclear Cells and Tumor-Infiltrating Lymphocytes. *The Journal of Immunology*, 177(9), pp.6548–6559.
Johnston, R.J. et al., 2012. STAT5 is a potent negative regulator of TFH cell differentiation. *The Journal of experimental medicine*, 209(2), pp.243–50.
Jones, C.A. et al., 2008. Robo4 stabilizes the vascular network by inhibiting pathologic angiogenesis and endothelial hyperpermeability. *Nature medicine*, 14(4), pp.448–53.
Jones, C.A. et al., 2009. Slit2–Robo4 signalling promotes vascular stability by blocking Arf6 activity. *Nature Cell Biology*, 11(11), pp.1325–1331.
Jungbluth, A.A. et al., 2001. Monophasic and biphasic synovial sarcomas abundantly express cancer/testis antigen NY-ESO-1 but not MAGE-A1 or CT7. *International journal of cancer. Journal international du cancer*, 94(2), pp.252–6.
Kalos, M. et al., 2011. T cells with chimeric antigen receptors have potent antitumor effects and can establish memory in patients with advanced leukemia. *Science translational medicine*, 3(95), p.95ra73.
Kang, Y. et al., 2006. Knockdown of CD146 reduces the migration and proliferation of human endothelial cells. *Cell Research*, 16(3), pp.313–318.

Kannanganat, S. et al., 2007. Multiple-Cytokine-Producing Antiviral CD4 T Cells Are Functionally Superior to Single-Cytokine-Producing Cells. *Journal of Virology*, 81(16), pp.8468–8476.
Karagiannis, E.D. & Popel, A.S., 2006. Distinct modes of collagen type I proteolysis by matrix metalloproteinase (MMP) 2 and membrane type I MMP during the migration of a tip endothelial cell: insights from a computational model. *Journal of theoretical biology*, 238(1), pp.124–45.
Katz, S.C. et al., 2015. Phase I Hepatic Immunotherapy for Metastases Study of Intra-Arterial Chimeric Antigen Receptor–Modified T-cell Therapy for CEA+ Liver Metastases. *Clinical Cancer Research*, 21(14).
Kaur, S. et al., 2006. Robo4 signaling in endothelial cells implies attraction guidance mechanisms. *The Journal of biological chemistry*, 281(16), pp.11347–56.
Kaur, S. et al., 2008. Silencing of directional migration in roundabout4 knockdown endothelial cells. *BMC Cell Biology*, 9(1), p.61.
Kawalekar, O.U. et al., 2016. Distinct Signaling of Coreceptors Regulates Specific Metabolism Pathways and Impacts Memory Development in CAR T Cells. *Immunity*, 44(2), pp.380–390.
Keefe, D. et al., 2005. Perforin triggers a plasma membrane-repair response that facilitates CTL induction of apoptosis. *Immunity*, 23(3), pp.249–62.
Kerkar, S.P. et al., 2010. Tumor-specific CD8+ T cells expressing interleukin-12 eradicate established cancers in lymphodepleted hosts. *Cancer research*, 70(17), pp.6725–34.
Kershaw, M.H. et al., 2006. A phase I study on adoptive immunotherapy using gene-modified T cells for ovarian cancer. *Clinical cancer research : an official journal of the American Association for Cancer Research*, 12(20 Pt 1), pp.6106–15.
Kershaw, M.H. et al., 2002. Redirecting migration of T cells to chemokine secreted from tumors by genetic modification with CXCR2. *Human gene therapy*, 13(16), pp.1971–80.
Kidd, T. et al., 1998. Roundabout Controls Axon Crossing of the CNS Midline and Defines a Novel Subfamily of Evolutionarily Conserved Guidance Receptors. *Cell*, 92(2), pp.205–215.
Kim, K.J. et al., 1993. Inhibition of vascular endothelial growth factor-induced angiogenesis suppresses tumour growth in vivo. *Nature*, 362(6423), pp.841–844.
Kirkham, P.M. et al., 1992. Immunoglobulin VH clan and family identity predicts variable domain structure and may influence antigen binding. *The EMBO journal*, 11(2), pp.603–9.
Klebanoff, C.A. et al., 2005. Central memory self/tumor-reactive CD8+ T cells confer superior antitumor immunity compared with effector memory T cells. *Proceedings of the National Academy of Sciences of the United States of America*, 102(27), pp.9571–6.
Kleijwegt, F.S. et al., 2010. Critical role for TNF in the induction of human antigen-specific regulatory T cells by tolerogenic dendritic cells. *Journal of immunology (Baltimore, Md. : 1950)*, 185(3), pp.1412–8.
Kloss, C.C. et al., 2013. Combinatorial antigen recognition with balanced signaling promotes selective tumor eradication by engineered T cells. *Nature biotechnology*, 31(1), pp.71–5.

Koch, A.W. et al., 2011. Robo4 maintains vessel integrity and inhibits angiogenesis by interacting with UNC5B. *Developmental cell*, 20(1), pp.33–46.
Kochenderfer, J.N. et al., 2010. Adoptive transfer of syngeneic T cells transduced with a chimeric antigen receptor that recognizes murine CD19 can eradicate lymphoma and normal B cells. *Blood*, 116(19), pp.3875–86.
Kochenderfer, J.N. et al., 2012. B-cell depletion and remissions of malignancy along with cytokine-associated toxicity in a clinical trial of anti-CD19 chimeric-antigen-receptor-transduced T cells. *Blood*, 119(12), pp.2709–20.
Kochenderfer, J.N. et al., 2015. Chemotherapy-Refractory Diffuse Large B-Cell Lymphoma and Indolent B-Cell Malignancies Can Be Effectively Treated With Autologous T Cells Expressing an Anti-CD19 Chimeric Antigen Receptor. *Journal of Clinical Oncology*, 33(6), pp.540–549.
Kochenderfer, J.N. et al., 2013. Donor-derived CD19-targeted T cells cause regression of malignancy persisting after allogeneic hematopoietic stem cell transplantation. *Blood*, 122(25), pp.4129–4139.
Koehler, H. et al., 2007. CD28 costimulation overcomes transforming growth factor-beta-mediated repression of proliferation of redirected human CD4+ and CD8+ T cells in an antitumor cell attack. *Cancer research*, 67(5), pp.2265–73.
Kofler, D.M. et al., 2011. CD28 costimulation Impairs the efficacy of a redirected t-cell antitumor attack in the presence of regulatory t cells which can be overcome by preventing Lck activation. *Molecular therapy : the journal of the American Society of Gene Therapy*, 19(4), pp.760–7.
Koike, T. et al., 2002. MT1-MMP, but not secreted MMPs, influences the migration of human microvascular endothelial cells in 3-dimensional collagen gels. *Journal of Cellular Biochemistry*, 86(4), pp.748–758.
Kolb, H.J. et al., 1990. Donor leukocyte transfusions for treatment of recurrent chronic myelogenous leukemia in marrow transplant patients. *Blood*, 76(12), pp.2462–2465.
Konerding, M.A. et al., 1999. Evidence for characteristic vascular patterns in solid tumours: quantitative studies using corrosion casts. *British journal of cancer*, 80(5–6), pp.724–732.
Kramer, S.G. et al., 2001. Switching repulsion to attraction: changing responses to slit during transition in mesoderm migration. *Science (New York, N.Y.)*, 292(5517), pp.737–40.
Krause, A. et al., 1998. Antigen-dependent CD28 Signaling Selectively Enhances Survival and Proliferation in Genetically Modified Activated Human Primary T Lymphocytes. *Journal of Experimental Medicine*, 188(4), pp.619–626.
Krueger, A., Ziętara, N. & Łyszkiewicz, M., 2017. T Cell Development by the Numbers. *Trends in Immunology*, 38(2), pp.128–139.
Kuang, D.-M. et al., 2009. Activated monocytes in peritumoral stroma of hepatocellular carcinoma foster immune privilege and disease progression through PD-L1. *The Journal of Experimental Medicine*, 206(6), pp.1327–1337.
Kuball, J. et al., 2005. Cooperation of human tumor-reactive CD4+ and CD8+ T cells after redirection of their specificity by a high-affinity p53A2.1-specific TCR. *Immunity*, 22(1), pp.117–129.
Kundig, T. et al., 1993. Immune responses in interleukin-2-deficient mice.

Science, 262(5136).
Labrecque, N. et al., 2001. How much TCR does a T cell need? *Immunity*, 15(1), pp.71–82.
Lamers, C.H. et al., 2013. Treatment of Metastatic Renal Cell Carcinoma With CAIX CAR-engineered T cells: Clinical Evaluation and Management of On-target Toxicity. *Molecular Therapy*, 21(4), pp.904–912.
Lamers, C.H.J. et al., 2011. Immune responses to transgene and retroviral vector in patients treated with ex vivo-engineered T cells. *Blood*, 117(1), pp.72–82.
Lamers, C.H.J. et al., 2006. Treatment of Metastatic Renal Cell Carcinoma With Autologous T-Lymphocytes Genetically Retargeted Against Carbonic Anhydrase IX: First Clinical Experience. *Journal of Clinical Oncology*, 24(13), pp.e20–e22.
Lawrence, M.S. et al., 2013. Mutational heterogeneity in cancer and the search for new cancer-associated genes. *Nature*, 499(7457), pp.214–8.
Lee, D.W. et al., 2015. T cells expressing CD19 chimeric antigen receptors for acute lymphoblastic leukaemia in children and young adults: a phase 1 dose-escalation trial. *The Lancet*, 385(9967), pp.517–528.
Lee, K.-T. et al., 2011. Neuronal genes for subcutaneous fat thickness in human and pig are identified by local genomic sequencing and combined SNP association study. *PloS one*, 6(2), p.e16356.
Legg, J. a et al., 2008. Slits and Roundabouts in cancer, tumour angiogenesis and endothelial cell migration. *Angiogenesis*, 11(1), pp.13–21.
Lehmann, J.M., Riethmüller, G. & Johnson, J.P., 1989. MUC18, a marker of tumor progression in human melanoma, shows sequence similarity to the neural cell adhesion molecules of the immunoglobulin superfamily. *Proceedings of the National Academy of Sciences of the United States of America*, 86(24), pp.9891–5.
Lenschow, D.J., Walunas, T.L. & Bluestone, J.A., 1996. CD28/B7 system of T cell costimulation. *Annual review of immunology*, 14, pp.233–58.
Liang, W.-C. et al., 2006. Cross-species Vascular Endothelial Growth Factor (VEGF)-blocking Antibodies Completely Inhibit the Growth of Human Tumor Xenografts and Measure the Contribution of Stromal VEGF. *Journal of Biological Chemistry*, 281(2), pp.951–961.
Liao, W. et al., 2011. Modulation of cytokine receptors by IL-2 broadly regulates differentiation into helper T cell lineages. *Nature Immunology*, 12(6), pp.551–559.
Lin, G., Finger, E. & Gutierrez-Ramos, J.C., 1995. Expression of CD34 in endothelial cells, hematopoietic progenitors and nervous cells in fetal and adult mouse tissues. *European Journal of Immunology*, 25(6), pp.1508–1516.
Lindenstrøm, T. et al., 2009. Tuberculosis subunit vaccination provides long-term protective immunity characterized by multifunctional CD4 memory T cells. *Journal of immunology (Baltimore, Md. : 1950)*, 182(12), pp.8047–55.
Linette, G.P. et al., 2013. Cardiovascular toxicity and titin cross-reactivity of affinity-enhanced T cells in myeloma and melanoma. *Blood*, 122(6), pp.863–71.
Liu, X. et al., 2016. A Chimeric Switch-Receptor Targeting PD1 Augments the Efficacy of Second-Generation CAR T Cells in Advanced Solid Tumors. *Cancer research*, 76(6), pp.1578–90.
Liu, X. et al., 2015. Affinity-Tuned ErbB2 or EGFR Chimeric Antigen Receptor T

Cells Exhibit an Increased Therapeutic Index against Tumors in Mice. *Cancer research*, 75(17), pp.3596–607.
Liu, Z.-J. et al., 2003. Regulation of Notch1 and Dll4 by Vascular Endothelial Growth Factor in Arterial Endothelial Cells: Implications for Modulating Arteriogenesis and Angiogenesis. *Molecular and Cellular Biology*, 23(1), pp.14–25.
Lobov, I.B. et al., 2007. Delta-like ligand 4 (Dll4) is induced by VEGF as a negative regulator of angiogenic sprouting. *Proceedings of the National Academy of Sciences of the United States of America*, 104(9), pp.3219–3224.
Locke, F.L. & Davila, M.L., 2017. Regulatory challenges and considerations for the clinical application of CAR-T cell anti-cancer therapy. *Expert Opinion on Biological Therapy*, 17(6), pp.659–661.
London, N.R. et al., 2010. Targeting Robo4-dependent Slit signaling to survive the cytokine storm in sepsis and influenza. *Science translational medicine*, 2(23), p.23ra19.
Long, A.H. et al., 2015. 4-1BB costimulation ameliorates T cell exhaustion induced by tonic signaling of chimeric antigen receptors. *Nature medicine*, 21(6), pp.581–90.
Louis, C.U. et al., 2011. Antitumor activity and long-term fate of chimeric antigen receptor-positive T cells in patients with neuroblastoma. *Blood*, 118(23), pp.6050–6056.
Lovato, V. et al., 2007. A monoclonal antibody prevents aggregation of the NBD1 domain of the cystic fibrosis transmembrane conductance regulator. *Protein engineering, design & selection : PEDS*, 20(12), pp.607–14.
Lu, C. et al., 2007. Gene alterations identified by expression profiling in tumor-associated endothelial cells from invasive ovarian carcinoma. *Cancer research*, 67(4), pp.1757–68.
Lu, X. et al., 2004. The netrin receptor UNC5B mediates guidance events controlling morphogenesis of the vascular system. *Nature*, 432(7014), pp.179–186.
Ma, J.S.Y. et al., 2016. Versatile strategy for controlling the specificity and activity of engineered T cells. *Proceedings of the National Academy of Sciences of the United States of America*, 113(4), pp.E450-8.
MacDermott, A.B. et al., 1986. NMDA-receptor activation increases cytoplasmic calcium concentration in cultured spinal cord neurones. *Nature*, 321(6069), pp.519–522.
MacPhee, P.J., Schmidt, E.E. & Groom, A.C., 1995. Intermittence of blood flow in liver sinusoids, studied by high-resolution in vivo microscopy. *The American journal of physiology*, 269(5 Pt 1), pp.G692-8.
Madden, S.L. et al., 2004. Vascular gene expression in nonneoplastic and malignant brain. *The American journal of pathology*, 165(2), pp.601–8.
Maher, J. et al., 2002. Human T-lymphocyte cytotoxicity and proliferation directed by a single chimeric TCRzeta /CD28 receptor. *Nature biotechnology*, 20(1), pp.70–5.
Maher, J., 2012. Immunotherapy of malignant disease using chimeric antigen receptor engrafted T cells. *ISRN oncology*, 2012, p.278093.
Mahnke, Y.D. et al., 2013. The who's who of T-cell differentiation: Human memory T-cell subsets. *European Journal of Immunology*, 43(11), pp.2797–2809.

Manuri, P.V.R. et al., 2010. piggyBac transposon/transposase system to generate CD19-specific T cells for the treatment of B-lineage malignancies. *Human gene therapy*, 21(4), pp.427–37.
Marlow, R. et al., 2010. Vascular Robo4 restricts proangiogenic VEGF signaling in breast. *Proceedings of the National Academy of Sciences of the United States of America*, 107(23), pp.10520–5.
Masiero, M. et al., 2013. A core human primary tumor angiogenesis signature identifies the endothelial orphan receptor ELTD1 as a key regulator of angiogenesis. *Cancer cell*, 24(2), pp.229–41.
Masuda, Y. et al., 2001. Vascular endothelial growth factor enhances glomerular capillary repair and accelerates resolution of experimentally induced glomerulonephritis. *The American journal of pathology*, 159(2), pp.599–608.
Maude, S.L. et al., 2015. CD19-targeted chimeric antigen receptor T-cell therapy for acute lymphoblastic leukemia. *Blood*, 125(26), pp.4017–23.
Maude, S.L. et al., 2014. Chimeric Antigen Receptor T Cells for Sustained Remissions in Leukemia. *New England Journal of Medicine*, 371(16), pp.1507–1517.
Maus, M. V et al., 2013. T cells expressing chimeric antigen receptors can cause anaphylaxis in humans. *Cancer immunology research*, 1, pp.26–31.
McCafferty, J. et al., 1990. Phage antibodies: filamentous phage displaying antibody variable domains. *Nature*, 348(6301), pp.552–554.
McDermott, D.F. et al., 2015. Survival, Durable Response, and Long-Term Safety in Patients With Previously Treated Advanced Renal Cell Carcinoma Receiving Nivolumab. *Journal of Clinical Oncology*, 33(18), pp.2013–2020.
McDonald, D.M. & Choyke, P.L., 2003. Imaging of angiogenesis: from microscope to clinic. *Nature medicine*, 9(6), pp.713–725.
McGray, A.J.R. et al., 2014. Immunotherapy-induced CD8+ T Cells Instigate Immune Suppression in the Tumor. *Molecular Therapy*, 22(1), pp.206–218.
Meador-Woodruff, J.H., Hogg, A.J. & Smith, R.E., 2001. Striatal ionotropic glutamate receptor expression in schizophrenia, bipolar disorder, and major depressive disorder. *Brain Research Bulletin*, 55(5), pp.631–640.
Miller, C.H.T., Maher, S.G. & Young, H.A., 2009. Clinical Use of Interferon-γ. *Annals of the New York Academy of Sciences*, 1182(1), pp.69–79.
Milone, M.C. et al., 2009. Chimeric receptors containing CD137 signal transduction domains mediate enhanced survival of T cells and increased antileukemic efficacy in vivo. *Molecular therapy : the journal of the American Society of Gene Therapy*, 17(8), pp.1453–64.
Mitsuyasu, R.T. et al., 2000. Prolonged survival and tissue trafficking following adoptive transfer of CD4zeta gene-modified autologous CD4(+) and CD8(+) T cells in human immunodeficiency virus-infected subjects. *Blood*, 96(3), pp.785–93.
Moeller, M. et al., 2005. Adoptive transfer of gene-engineered CD4+ helper T cells induces potent primary and secondary tumor rejection. *Blood*, 106(9), pp.2995–3003.
Moghaddam, B. & Javitt, D., 2012. From revolution to evolution: the glutamate hypothesis of schizophrenia and its implication for treatment. *Neuropsychopharmacology : official publication of the American College of Neuropsychopharmacology*, 37(1), pp.4–15.
Monyer, H. et al., 1994. Developmental and regional expression in the rat brain

and functional properties of four NMDA receptors. *Neuron*, 12(3), pp.529–540.
Monyer, H. et al., 1992. Heteromeric NMDA receptors: molecular and functional distinction of subtypes. *Science (New York, N.Y.)*, 256(5060), pp.1217–21.
Moon, E.K. et al., 2014. Multifactorial T-cell hypofunction that is reversible can limit the efficacy of chimeric antigen receptor-transduced human T cells in solid tumors. *Clinical cancer research : an official journal of the American Association for Cancer Research*, 20(16), pp.4262–73.
Morgan, D., Ruscetti, F. & Gallo, R., 1976. Selective in vitro growth of T lymphocytes from normal human bone marrows. *Science*, 193(4257).
Morgan, R.A. et al., 2013. Cancer regression and neurological toxicity following anti-MAGE-A3 TCR gene therapy. *Journal of immunotherapy (Hagerstown, Md. : 1997)*, 36(2), pp.133–51.
Morgan, R.A. et al., 2006. Cancer regression in patients after transfer of genetically engineered lymphocytes. *Science (New York, N.Y.)*, 314(5796), pp.126–9.
Morgan, R.A. et al., 2010. Case report of a serious adverse event following the administration of T cells transduced with a chimeric antigen receptor recognizing ERBB2. *Molecular therapy : the journal of the American Society of Gene Therapy*, 18(4), pp.843–51.
Morgan, R.A. et al., 2003. High efficiency TCR gene transfer into primary human lymphocytes affords avid recognition of melanoma tumor antigen glycoprotein 100 and does not alter the recognition of autologous melanoma antigens. *Journal of immunology (Baltimore, Md. : 1950)*, 171(6), pp.3287–3295.
Morgan, R.A. et al., 2012. Recognition of glioma stem cells by genetically modified T cells targeting EGFRvIII and development of adoptive cell therapy for glioma. *Human gene therapy*, 23(10), pp.1043–53.
Morse, M.A. et al., 2007. Long term disease-free survival and T cell and antibody responses in women with high-risk Her2+ breast cancer following vaccination against Her2. *Journal of translational medicine*, 5, p.42.
Motz, G.T. et al., 2014. Tumor endothelium FasL establishes a selective immune barrier promoting tolerance in tumors. *Nature medicine*, 20(6), pp.607–15.
Mura, M. et al., 2012. Identification and angiogenic role of the novel tumor endothelial marker CLEC14A. *Oncogene*, 31(3), pp.293–305.
Muthukkaruppan, V.R., Kubai, L. & Auerbach, R., 1982. Tumor-induced neovascularization in the mouse eye. *Journal of the National Cancer Institute*, 69(3), pp.699–708.
Muul, L.M. et al., 1987. Identification of specific cytolytic immune responses against autologous tumor in humans bearing malignant melanoma. *Journal of immunology (Baltimore, Md. : 1950)*, 138(3), pp.989–995.
Nechiporuk, T., Urness, L.D. & Keating, M.T., 2001. ETL, a novel seven-transmembrane receptor that is developmentally regulated in the heart. ETL is a member of the secretin family and belongs to the epidermal growth factor-seven-transmembrane subfamily. *The Journal of biological chemistry*, 276(6), pp.4150–7.
Newick, K. et al., 2016. Augmentation of CAR T-cell Trafficking and Antitumor Efficacy by Blocking Protein Kinase A Localization. *Cancer Immunology Research*, 4(6).

Newrzela, S. et al., 2011. Retroviral insertional mutagenesis can contribute to immortalization of mature T lymphocytes. *Molecular medicine (Cambridge, Mass.)*, 17(11–12), pp.1223–32.
Nicholaou, T. et al., 2006. Directions in the immune targeting of cancer: lessons learned from the cancer-testis Ag NY-ESO-1. *Immunology and cell biology*, 84(3), pp.303–17.
Oestreich, K.J., Mohn, S.E. & Weinmann, A.S., 2012. Molecular mechanisms that control the expression and activity of Bcl-6 in TH1 cells to regulate flexibility with a TFH-like gene profile. *Nature immunology*, 13(4), pp.405–11.
Ouhtit, A. et al., 2009. Towards understanding the mode of action of the multifaceted cell adhesion receptor CD146. *Biochimica et Biophysica Acta (BBA) - Reviews on Cancer*, 1795(2), pp.130–136.
Paoletti, P., Bellone, C. & Zhou, Q., 2013. NMDA receptor subunit diversity: impact on receptor properties, synaptic plasticity and disease. *Nature Reviews Neuroscience*, 14(6), pp.383–400.
Park, J.E. et al., 1994. Placenta growth factor. Potentiation of vascular endothelial growth factor bioactivity, in vitro and in vivo, and high affinity binding to Flt-1 but not to Flk-1/KDR. *The Journal of biological chemistry*, 269(41), pp.25646–25654.
Park, J.E., Keller, G.A. & Ferrara, N., 1993. The vascular endothelial growth factor (VEGF) isoforms: differential deposition into the subepithelial extracellular matrix and bioactivity of extracellular matrix-bound VEGF. *Molecular biology of the cell*, 4(12), pp.1317–1326.
Park, J.R. et al., 2007. Adoptive transfer of chimeric antigen receptor re-directed cytolytic T lymphocyte clones in patients with neuroblastoma. *Molecular therapy : the journal of the American Society of Gene Therapy*, 15(4), pp.825–33.
Park, J.S. et al., 2014. Synthetic control of mammalian-cell motility by engineering chemotaxis to an orthogonal bioinert chemical signal. *Proceedings of the National Academy of Sciences of the United States of America*, 111(16), pp.5896–901.
Park, K.W. et al., 2003. Robo4 is a vascular-specific receptor that inhibits endothelial migration. *Developmental Biology*, 261(1), pp.251–267.
Parker, B.S. et al., 2004. Alterations in vascular gene expression in invasive breast carcinoma. *Cancer research*, 64(21), pp.7857–66.
Parkhurst, M.R. et al., 2009. Characterization of genetically modified T-cell receptors that recognize the CEA:691-699 peptide in the context of HLA-A2.1 on human colorectal cancer cells. *Clinical cancer research : an official journal of the American Association for Cancer Research*, 15(1), pp.169–80.
Parkhurst, M.R. et al., 2011. T cells targeting carcinoembryonic antigen can mediate regression of metastatic colorectal cancer but induce severe transient colitis. *Molecular therapy : the journal of the American Society of Gene Therapy*, 19(3), pp.620–6.
Patel, S.D. et al., 1999. Impact of chimeric immune receptor extracellular protein domains on T cell function. *Gene therapy*, 6(3), pp.412–419.
Paul, J.D. et al., 2013. SLIT3-ROBO4 activation promotes vascular network formation in human engineered tissue and angiogenesis in vivo. *Journal of molecular and cellular cardiology*, 64, pp.124–31.

Pircher, A. et al., 2016. Biomarkers of evasive resistance predict disease progression in cancer patients treated with antiangiogenic therapies. *Oncotarget*, 7(15), pp.20109–20123.
Pircher, A. et al., 2013. Favorable prognosis of operable non-small cell lung cancer (NSCLC) patients harboring an increased expression of tumor endothelial markers (TEMs). *Lung Cancer*, 81(2), pp.252–258.
Ponsel, D. et al., 2011. High Affinity, Developability and Functional Size: The Holy Grail of Combinatorial Antibody Library Generation. *Molecules*, 16(12), pp.3675–3700.
Porter, D.L. et al., 2015. Chimeric antigen receptor T cells persist and induce sustained remissions in relapsed refractory chronic lymphocytic leukemia. *Science Translational Medicine*, 7(303), p.303ra139.
Porto Neto, L.R. et al., 2011. DNA variation in the gene ELTD1 is associated with tick burden in cattle. *Animal genetics*, 42(1), pp.50–5.
Precopio, M.L. et al., 2007. Immunization with vaccinia virus induces polyfunctional and phenotypically distinctive CD8(+) T cell responses. *The Journal of experimental medicine*, 204(6), pp.1405–16.
Presta, L.G. et al., 1997. Humanization of an anti-vascular endothelial growth factor monoclonal antibody for the therapy of solid tumors and other disorders. *Cancer research*, 57(20), pp.4593–4599.
Pule, M.A. et al., 2008. Virus-specific T cells engineered to coexpress tumor-specific receptors: persistence and antitumor activity in individuals with neuroblastoma. *Nature medicine*, 14(11), pp.1264–70.
Pulè, M. a et al., 2005. A chimeric T cell antigen receptor that augments cytokine release and supports clonal expansion of primary human T cells. *Molecular therapy : the journal of the American Society of Gene Therapy*, 12(5), pp.933–41.
Qasim, W. et al., 2017. Molecular remission of infant B-ALL after infusion of universal TALEN gene-edited CAR T cells. *Science Translational Medicine*, 9(374).
Qin, L. et al., 2017. Incorporation of a hinge domain improves the expansion of chimeric antigen receptor T cells. *Journal of Hematology & Oncology*, 10(1), p.68.
Qureshi, O.S. et al., 2011. Trans-Endocytosis of CD80 and CD86: A Molecular Basis for the Cell-Extrinsic Function of CTLA-4. *Science*, 332(6029), pp.600–603.
Rama, N. et al., 2015. Slit2 signaling through Robo1 and Robo2 is required for retinal neovascularization. *Nature Medicine*, 21(5), pp.483–491.
Rangarajan, S. & Mariuzza, R.A., 2014. T cell receptor bias for MHC: co-evolution or co-receptors? *Cellular and Molecular Life Sciences*, 71(16), pp.3059–3068.
Ravelli, A. et al., 2017. Tumor-infiltrating lymphocytes and breast cancer: Beyond the prognostic and predictive utility. *Tumor Biology*, 39(4), p.101042831769502.
Read, S. et al., 2006. Blockade of CTLA-4 on CD4+CD25+ regulatory T cells abrogates their function in vivo. *Journal of immunology (Baltimore, Md. : 1950)*, 177(7), pp.4376–83.
Reece, W.H.H. et al., 2004. A CD4+ T-cell immune response to a conserved epitope in the circumsporozoite protein correlates with protection from natural Plasmodium falciparum infection and disease. *Nature Medicine*,

10(4), pp.406–410.
Ritter, L.M., Unis, A.S. & Meador-Woodruff, J.H., 2001. Ontogeny of ionotropic glutamate receptor expression in human fetal brain. *Developmental Brain Research*, 127(2), pp.123–133.
Robbins, P.F. et al., 2013. Mining exomic sequencing data to identify mutated antigens recognized by adoptively transferred tumor-reactive T cells. *Nature medicine*, 19(6), pp.747–52.
Robbins, P.F. et al., 2008. Single and dual amino acid substitutions in TCR CDRs can enhance antigen-specific T cell functions. *Journal of immunology (Baltimore, Md. : 1950)*, 180(9), pp.6116–31.
Robbins, P.F. et al., 2011. Tumor regression in patients with metastatic synovial cell sarcoma and melanoma using genetically engineered lymphocytes reactive with NY-ESO-1. *Journal of clinical oncology : official journal of the American Society of Clinical Oncology*, 29(7), pp.917–24.
Rodgers, D.T. et al., 2016. Switch-mediated activation and retargeting of CAR-T cells for B-cell malignancies. *Proceedings of the National Academy of Sciences of the United States of America*, 113(4), pp.E459-68.
Rodig, N. et al., 2003. Endothelial expression of PD-L1 and PD-L2 down-regulates CD8+ T cell activation and cytolysis. *European Journal of Immunology*, 33(11), pp.3117–3126.
Romani, C. et al., 2009. Development and characterization of a human single-chain antibody fragment against claudin-3: a novel therapeutic target in ovarian and uterine carcinomas. *American Journal of Obstetrics and Gynecology*, 201(1), p.70.e1-70.e9.
Ronca, R. et al., 2010. Antiangiogenic Activity of a Neutralizing Human Single-Chain Antibody Fragment against Fibroblast Growth Factor Receptor 1. *Molecular Cancer Therapeutics*, 9(12).
van Rooij, N. et al., 2013. Tumor exome analysis reveals neoantigen-specific T-cell reactivity in an ipilimumab-responsive melanoma. *Journal of clinical oncology : official journal of the American Society of Clinical Oncology*, 31(32), pp.e439-42.
Rooney, C.M. et al., 1998. Infusion of cytotoxic T cells for the prevention and treatment of Epstein-Barr virus-induced lymphoma in allogeneic transplant recipients. *Blood*, 92(5), pp.1549–1555.
Rooney, C.M. et al., 1995. Use of gene-modified virus-specific T lymphocytes to control Epstein-Barr-virus-related lymphoproliferation. *Lancet*, 345(8941), pp.9–13.
Rosenberg, S.A. et al., 2008. Adoptive cell transfer: a clinical path to effective cancer immunotherapy. *Nature reviews. Cancer*, 8(4), pp.299–308.
Rosenberg, S.A. et al., 2011. Durable complete responses in heavily pretreated patients with metastatic melanoma using T-cell transfer immunotherapy. *Clinical cancer research : an official journal of the American Association for Cancer Research*, 17(13), pp.4550–7.
Rosenberg, S.A. et al., 1988. Use of tumor-infiltrating lymphocytes and interleukin-2 in the immunotherapy of patients with metastatic melanoma. A preliminary report. *The New England journal of medicine*, 319(25), pp.1676–1680.
Rosenberg, S., Spiess, P. & Lafreniere, R., 1986. A new approach to the adoptive immunotherapy of cancer with tumor-infiltrating lymphocytes. *Science*,

233(4770), pp.1318–1321.
Rossy, J. et al., 2012. The integration of signaling and the spatial organization of the T cell synapse. *Frontiers in immunology*, 3, p.352.
Roszkowski, J.J. et al., 2005. Simultaneous generation of CD8+ and CD4+ melanoma-reactive T cells by retroviral-mediated transfer of a single T-cell receptor. *Cancer research*, 65(4), pp.1570–6.
Roy, D. et al., 2009. 3D Cryo-Imaging: A Very High-Resolution View of the Whole Mouse. *The Anatomical Record: Advances in Integrative Anatomy and Evolutionary Biology*, 292(3), pp.342–351.
Roybal, K.T. et al., 2016. Precision Tumor Recognition by T Cells With Combinatorial Antigen-Sensing Circuits. *Cell*, 164(4), pp.770–779.
Ruhrberg, C. et al., 2002. Spatially restricted patterning cues provided by heparin-binding VEGF-A control blood vessel branching morphogenesis. *Genes & development*, 16(20), pp.2684–98.
Sakaguchi, S. et al., 2008. Regulatory T Cells and Immune Tolerance. *Cell*, 133(5), pp.775–787.
Sampson, J.H. et al., 2014. EGFRvIII mCAR-modified T-cell therapy cures mice with established intracerebral glioma and generates host immunity against tumor-antigen loss. *Clinical cancer research : an official journal of the American Association for Cancer Research*, 20(4), pp.972–84.
Saunders, B.M., Briscoe, H. & Britton, W.J., 2004. T cell-derived tumour necrosis factor is essential, but not sufficient, for protection against Mycobacterium tuberculosis infection. *Clinical and experimental immunology*, 137(2), pp.279–87.
Savoldo, B. et al., 2011. CD28 costimulation improves expansion and persistence of chimeric antigen receptor-modified T cells in lymphoma patients. *The Journal of clinical investigation*, 121(5), pp.1822–6.
Scherzer, C.R. et al., 1998. Expression of N-methyl-D-aspartate receptor subunit mRNAs in the human brain: hippocampus and cortex. *The Journal of comparative neurology*, 390(1), pp.75–90.
Schlaepfer, D.D. et al., 2000. FAK integrates growth-factor and integrin signals to promote cell migration. *Nature Cell Biology*, 2(5), pp.249–256.
Seder, R.A., Darrah, P.A. & Roederer, M., 2008. T-cell quality in memory and protection: implications for vaccine design. *Nature Reviews Immunology*, 8(4), pp.247–258.
Seeger, M. et al., 1993. Mutations affecting growth cone guidance in drosophila: Genes necessary for guidance toward or away from the midline. *Neuron*, 10(3), pp.409–426.
Sers, C. et al., 1993. Genomic organization of the melanoma-associated glycoprotein MUC18: implications for the evolution of the immunoglobulin domains. *Proceedings of the National Academy of Sciences of the United States of America*, 90(18), pp.8514–8.
Sers, C., Riethmüller, G. & Johnson, J.P., 1994. MUC18, a melanoma-progression associated molecule, and its potential role in tumor vascularization and hematogenous spread. *Cancer research*, 54(21), pp.5689–94.
Seth, P. et al., 2005. Magic roundabout, a tumor endothelial marker: expression and signaling. *Biochemical and biophysical research communications*, 332(2), pp.533–41.
Sfanos, K.S. et al., 2009. Human prostate-infiltrating CD8+ T lymphocytes are

oligoclonal and PD-1+. *The Prostate*, 69(15), pp.1694–703.
Sgier, D. et al., 2010. Isolation and characterization of an inhibitory human monoclonal antibody specific to the urokinase-type plasminogen activator, uPA. *Protein Engineering Design and Selection*, 23(4), pp.261–269.
Shalaby, F. et al., 1995. Failure of blood-island formation and vasculogenesis in Flk-1-deficient mice. *Nature*, 376(6535), pp.62–66.
Sheldon, H. et al., 2008. Active involvement of Robo1 and Robo4 in filopodia formation and endothelial cell motility mediated via WASP and other actin nucleation-promoting factors. *The FASEB Journal*, 23(2), pp.513–522.
Shrimali, R.K. et al., 2010. Antiangiogenic Agents Can Increase Lymphocyte Infiltration into Tumor and Enhance the Effectiveness of Adoptive Immunotherapy of Cancer. *Cancer Research*, 70(15), pp.6171–6180.
Shutter, J.R. et al., 2000. Dll4, a novel Notch ligand expressed in arterial endothelium. *Genes & development*, 14(11), pp.1313–1318.
Siemann, D.W. et al., 2004. Efficacy of combined antiangiogenic and vascular disrupting agents in treatment of solid tumors. *International journal of radiation oncology, biology, physics*, 60(4), pp.1233–40.
Silacci, M. et al., 2005. Design, construction, and characterization of a large synthetic human antibody phage display library. *Proteomics*, 5(9), pp.2340–50.
Simpson, A.J.G. et al., 2005. Cancer/testis antigens, gametogenesis and cancer. *Nature reviews. Cancer*, 5(8), pp.615–25.
Simpson, T.R. et al., 2013. Fc-dependent depletion of tumor-infiltrating regulatory T cells co-defines the efficacy of anti–CTLA-4 therapy against melanoma. *Journal of Experimental Medicine*, 210(9).
Singh, P., Schimenti, J.C. & Bolcun-Filas, E., 2015. A mouse geneticist's practical guide to CRISPR applications. *Genetics*, 199(1), pp.1–15.
Smith-Berdan, S. et al., 2012. Dynamic expression of the Robo ligand Slit2 in bone marrow cell populations. *Cell Cycle*, 11(4), pp.675–682.
Smith-Berdan, S. et al., 2011. Robo4 Cooperates with Cxcr4 to Specify Hematopoietic Stem Cell Localization to Bone Marrow Niches. *Cell Stem Cell*, 8(1), pp.72–83.
Smith, G.P., 1985. Filamentous fusion phage: novel expression vectors that display cloned antigens on the virion surface. *Science (New York, N.Y.)*, 228(4705), pp.1315–7.
St Croix, B. et al., 2000. Genes expressed in human tumor endothelium. *Science (New York, N.Y.)*, 289(5482), pp.1197–202.
Stanislawski, T. et al., 2001. Circumventing tolerance to a human MDM2-derived tumor antigen by TCR gene transfer. *Nature immunology*, 2(10), pp.962–70.
Di Stasi, A. et al., 2011. Inducible apoptosis as a safety switch for adoptive cell therapy. *The New England journal of medicine*, 365(18), pp.1673–83.
van der Stegen, S.J.C. et al., 2013. Preclinical In Vivo Modeling of Cytokine Release Syndrome Induced by ErbB-Retargeted Human T Cells: Identifying a Window of Therapeutic Opportunity? *The Journal of Immunology*, 191(9), pp.4589–4598.
Steyer, G.J. et al., 2009. Cryo-Imaging of Fluorescently-Labeled Single Cells in a Mouse. *Proceedings of SPIE--the International Society for Optical Engineering*, 7262, p.72620W–72620W8.
Stoler, D.L. et al., 1999. The onset and extent of genomic instability in sporadic

colorectal tumor progression. *Proceedings of the National Academy of Sciences*, 96(26), pp.15121–15126.
Su, S. et al., 2016. CRISPR-Cas9 mediated efficient PD-1 disruption on human primary T cells from cancer patients. *Scientific Reports*, 6, p.20070.
Suchting, S. et al., 2004. Soluble Robo4 receptor inhibits in vivo angiogenesis and endothelial cell migration. , 17(3), pp.1–17.
Szymczak, A.L. et al., 2004. Correction of multi-gene deficiency in vivo using a single “self-cleaving” 2A peptide–based retroviral vector. *Nature Biotechnology*, 22(5), pp.589–594.
Takahashi, Y. et al., 1997. Vessel counts and expression of vascular endothelial growth factor as prognostic factors in node-negative colon cancer. *Archives of surgery (Chicago, Ill. : 1960)*, 132(5), pp.541–546.
Tamada, K. et al., 2012. Redirecting Gene-Modified T Cells toward Various Cancer Types Using Tagged Antibodies. *Clinical Cancer Research*, 18(23).
Tassev, D. V, Cheng, M. & Cheung, N.-K. V, 2012. Retargeting NK92 cells using an HLA-A2-restricted, EBNA3C-specific chimeric antigen receptor. *Cancer gene therapy*, 19(2), pp.84–100.
Textor, A. et al., 2014. Efficacy of CAR T-cell Therapy in Large Tumors Relies upon Stromal Targeting by IFNγ. *Cancer Research*, 74(23).
Thiery, J. et al., 2011. Perforin pores in the endosomal membrane trigger the release of endocytosed granzyme B into the cytosol of target cells. *Nature immunology*, 12(8), pp.770–7.
Till, B.G. et al., 2008. Adoptive immunotherapy for indolent non-Hodgkin lymphoma and mantle cell lymphoma using genetically modified autologous CD20-specific T cells. *Blood*, 112(6), pp.2261–71.
Topalian, S.L. et al., 2012. Safety, Activity, and Immune Correlates of Anti–PD-1 Antibody in Cancer. *New England Journal of Medicine*, 366(26), pp.2443–2454.
Towner, R.A. et al., 2013. ELTD1, a potential new biomarker for gliomas. *Neurosurgery*, 72(1), p.77–90; discussion 91.
Tu, T. et al., 2015. CD146 acts as a novel receptor for netrin-1 in promoting angiogenesis and vascular development. *Cell Research*, 25(3), pp.275–287.
Turtle, C.J. et al., 2015. Anti-CD19 Chimeric Antigen Receptor-Modified T Cell Therapy for B Cell Non-Hodgkin Lymphoma and Chronic Lymphocytic Leukemia: Fludarabine and Cyclophosphamide Lymphodepletion Improves In Vivo Expansion and Persistence of CAR-T Cells and Clinical Outcomes. *Blood*, 126(23).
Turtle, C.J. et al., 2016. CD19 CAR-T cells of defined CD4+:CD8+ composition in adult B cell ALL patients. *Journal of Clinical Investigation*, 126(6), pp.2123–2138.
Uckun, F.M. et al., 1988. Detailed studies on expression and function of CD19 surface determinant by using B43 monoclonal antibody and the clinical potential of anti-CD19 immunotoxins. *Blood*, 71(1), pp.13–29.
Ueda, J. et al., 2014. The hypoxia-inducible epigenetic regulators Jmjd1a and G9a provide a mechanistic link between angiogenesis and tumor growth. *Molecular and cellular biology*, 34(19), pp.3702–20.
Urbanska, K. et al., 2012. A Universal Strategy for Adoptive Immunotherapy of Cancer through Use of a Novel T-cell Antigen Receptor. *Cancer Research*, 72(7).

Urbich, C. & Dimmeler, S., 2004. Endothelial progenitor cells: characterization and role in vascular biology. *Circulation research*, 95(4), pp.343–353.
Del Valle-Pinero, A.Y. et al., 2007. Expression of the N-methyl-D-aspartate receptor NR1 splice variants and NR2 subunit subtypes in the rat colon. *Neuroscience*, 147(1), pp.164–73.
Villa, A. et al., 2011. A novel synthetic naïve human antibody library allows the isolation of antibodies against a new epitope of oncofetal fibronectin. *mAbs*, 3(3), pp.264–272.
Walker, L.S.K. & Sansom, D.M., 2015. Confusing signals: recent progress in CTLA-4 biology. *Trends in immunology*, 36(2), pp.63–70.
Wallgard, E. et al., 2008. Identification of a core set of 58 gene transcripts with broad and specific expression in the microvasculature. *Arteriosclerosis, thrombosis, and vascular biology*, 28(8), pp.1469–76.
Walter, E.A. et al., 1995. Reconstitution of cellular immunity against cytomegalovirus in recipients of allogeneic bone marrow by transfer of T-cell clones from the donor. *The New England journal of medicine*, 333(16), pp.1038–1044.
Wang, B. et al., 2003. Induction of tumor angiogenesis by Slit-Robo signaling and inhibition of cancer growth by blocking Robo activity. *Cancer cell*, 4(1), pp.19–29.
Wang, W. et al., 2013. Specificity redirection by CAR with human VEGFR-1 affinity endows T lymphocytes with tumor-killing ability and anti-angiogenic potency. *Gene Therapy*, 20(10), pp.970–978.
Warren, B.A. et al., 1978. The microcirculation in two transplantable melanomas of the hamster. I. In vivo observations in transparent chambers. *Cancer letters*, 4(2), pp.109–116.
Waterhouse, P. et al., 1995. Lymphoproliferative disorders with early lethality in mice deficient in Ctla-4. *Science (New York, N.Y.)*, 270(5238), pp.985–8.
Weber, J.S. et al., 2015. Nivolumab versus chemotherapy in patients with advanced melanoma who progressed after anti-CTLA-4 treatment (CheckMate 037): a randomised, controlled, open-label, phase 3 trial. *The Lancet Oncology*, 16(4), pp.375–384.
Weber, M. et al., 2014. A Highly Functional Synthetic Phage Display Library Containing over 40 Billion Human Antibody Clones M. Isalan, ed. *PLoS ONE*, 9(6), p.e100000.
Whitmire, J.K., Tan, J.T. & Whitton, J.L., 2005. Interferon-gamma acts directly on CD8+ T cells to increase their abundance during virus infection. *The Journal of experimental medicine*, 201(7), pp.1053–9.
Williams, M.A., Tyznik, A.J. & Bevan, M.J., 2006. Interleukin-2 signals during priming are required for secondary expansion of CD8+ memory T cells. *Nature*, 441(7095), pp.890–893.
Wilson, D. et al., 2008. Whole Mouse Cryo-Imaging. *Proceedings of SPIE--the International Society for Optical Engineering*, 6916, p.69161I–69161I9.
Wing, K. et al., 2008. CTLA-4 Control over Foxp3+ Regulatory T Cell Function. *Science*, 322(5899), pp.271–275.
Wragg, J. et al., 2016. MCAM and LAMA4 are highly enriched in tumor blood vessels of renal cell carcinoma and predict patient outcome. *Cancer Research*, 76(8), pp.2314–2326.
Wu, C.-Y. et al., 2015. Remote control of therapeutic T cells through a small

molecule-gated chimeric receptor. *Science*, 350(6258).
Wu, J.Y. et al., 2001. The neuronal repellent Slit inhibits leukocyte chemotaxis induced by chemotactic factors. *Nature*, 410(6831), pp.948–952.
Xiao, J. et al., 2012. Augmented cardiac hypertrophy in response to pressure overload in mice lacking ELTD1. *PloS one*, 7(5), p.e35779.
Yadav, S.S. & Narayan, G., 2014. Role of ROBO4 signalling in developmental and pathological angiogenesis. *BioMed research international*, 2014, p.683025.
Yan, X. et al., 2003. A novel anti-CD146 monoclonal antibody, AA98, inhibits angiogenesis and tumor growth. *Blood*, 102(1).
Yana, I. et al., 2007. Crosstalk between neovessels and mural cells directs the site-specific expression of MT1-MMP to endothelial tip cells. *Journal of cell science*, 120(Pt 9), pp.1607–14.
Yee, C. et al., 2002. Adoptive T cell therapy using antigen-specific CD8+ T cell clones for the treatment of patients with metastatic melanoma: in vivo persistence, migration, and antitumor effect of transferred T cells. *Proceedings of the National Academy of Sciences of the United States of America*, 99(25), pp.16168–73.
Yoshikawa, M. et al., 2013. Robo4 is an effective tumor endothelial marker for antibody-drug conjugates based on the rapid isolation of the anti-Robo4 cell-internalizing antibody. *Blood*, 121(14), pp.2804–2813.
Younes, S.-A. et al., 2003. HIV-1 Viremia Prevents the Establishment of Interleukin 2–producing HIV-specific Memory CD4 $^{+}$ T Cells Endowed with Proliferative Capacity. *The Journal of Experimental Medicine*, 198(12), pp.1909–1922.
Yu, J. et al., 2014. Slit2N and Robo4 regulate lymphangiogenesis through the VEGF-C/VEGFR-3 pathway. *Cell Communication and Signaling*, 12(1), p.25.
Zhang, B. et al., 2009. Repulsive axon guidance molecule Slit3 is a novel angiogenic factor. *Blood*, 114(19), pp.4300–9.
Zhang, L. et al., 2003. Intratumoral T cells, recurrence, and survival in epithelial ovarian cancer. *The New England journal of medicine*, 348(3), pp.203–213.
Zhao, H. et al., 2016. Endothelial Robo4 suppresses breast cancer growth and metastasis through regulation of tumor angiogenesis. *Molecular Oncology*, 10(2), pp.272–281.
Zhao, H., Anand, A.R. & Ganju, R.K., 2014. Slit2-Robo4 pathway modulates lipopolysaccharide-induced endothelial inflammation and its expression is dysregulated during endotoxemia. *Journal of immunology (Baltimore, Md. : 1950)*, 192(1), pp.385–93.
Zhao, Y. et al., 2009. A herceptin-based chimeric antigen receptor with modified signaling domains leads to enhanced survival of transduced T lymphocytes and antitumor activity. *Journal of immunology (Baltimore, Md. : 1950)*, 183(9), pp.5563–74.
Zhao, Y. et al., 2005. Primary human lymphocytes transduced with NY-ESO-1 antigen-specific TCR genes recognize and kill diverse human tumor cell lines. *Journal of immunology (Baltimore, Md. : 1950)*, 174(7), pp.4415–4423.
Zhao, Z. et al., 2015. Structural Design of Engineered Costimulation Determines Tumor Rejection Kinetics and Persistence of CAR T Cells. *Cancer Cell*, 28(4), pp.415–428.
Zheng, C. et al., 2009. Endothelial CD146 is required for in vitro tumor-induced angiogenesis: The role of a disulfide bond in signaling and dimerization.

International Journal of Biochemistry and Cell Biology, 41(11), pp.2163–2172.
Zhong, X.S. et al., 2010. Chimeric antigen receptors combining 4-1BB and CD28 signaling domains augment PI3kinase/AKT/Bcl-XL activation and CD8+ T cell-mediated tumor eradication. *Mol Ther*, 18(2), pp.413–420.
Zhou, Q. & Nicholas Verne, G., 2008. NMDA Receptors and Colitis: Basic Science and Clinical Implications. *Reviews in analgesia*, 10(1), pp.33–43.
Zhou, Z. et al., 2000. Impaired endochondral ossification and angiogenesis in mice deficient in membrane-type matrix metalloproteinase I. *Proceedings of the National Academy of Sciences of the United States of America*, 97(8), pp.4052–4057.
Zhu, J. & Paul, W.E., 2008. CD4 T cells: fates, functions, and faults. *Blood*, 112(5), pp.1557–69.
Zhuang, X. et al., 2015. Robo4 vaccines induce antibodies that retard tumor growth. *Angiogenesis*, 18(1), pp.83–95.
Zhuang, X. et al., 2011. Shear stress, tip cells and regulators of endothelial migration. *Biochemical Society transactions*, 39(6), pp.1571–5.
Zou, W. & Chen, L., 2008. Inhibitory B7-family molecules in the tumour microenvironment. *Nature Reviews Immunology*, 8(6), pp.467–477.

Appendix

In vitro experimental repeats and control data

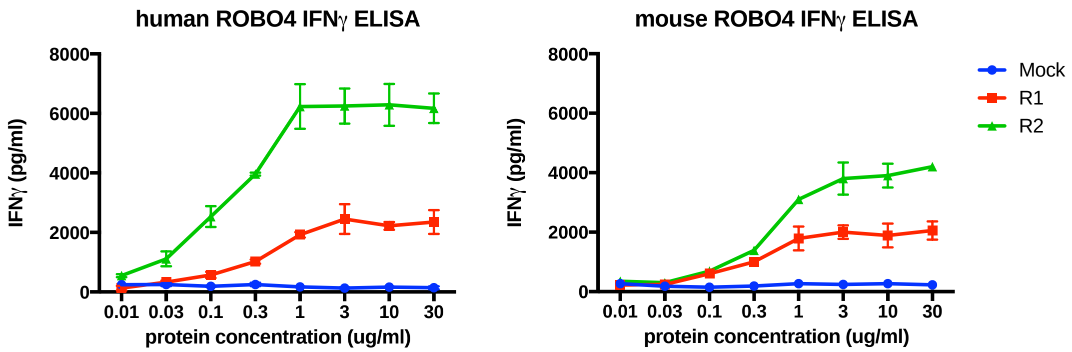

Figure 13: IFNγ response to recombinant human and mouse ROBO4 protein. R1 and R2 CAR Transduced R1 and R2 T cells were matched for transduction percentage by dilution with mock-transduced T cells. R1, R2 and mock-transduced T cells were incubated with an increasing concentration of recombinant human or mouse extracellular ROBO4 protein. After an overnight incubation the supernatant was analysed for IFNγ production. Graphs show the comparison of mock, R1 and R2 transduced T cells to either human or mouse ROBO4 protein.

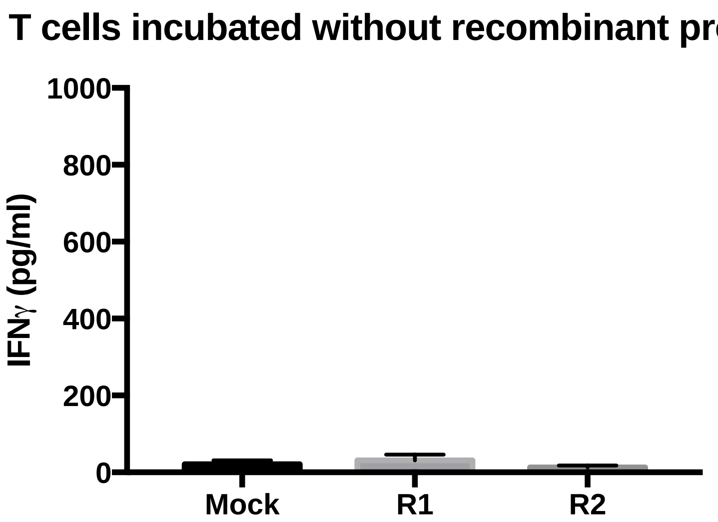

Figure 14: IFNγ ELISA to T cells incubated alone, without recombinant protein. R1 and R2 CAR Transduced T cells were matched for transduction percentage by dilution with mock-transduced T cells. R1, R2 and mock-transduced T cells were resuspended in ELISA medium and added to empty wells at a concentration of $2x10^5$ cells/well. The supernatant was then analysed for the presence of IFNγ. Data is the mean of triplicate wells with error bars shown the (SD).

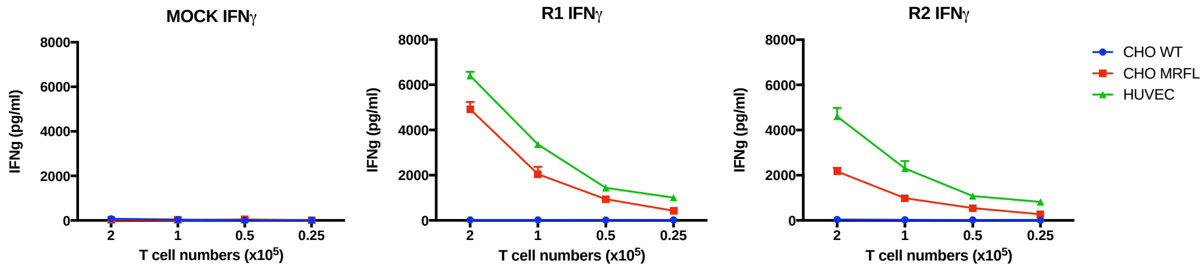

Figure 15 IFNγ ELISA to T cells incubated with target cells. R1 and R2 CAR Transduced T cells were matched for transduction percentage by dilution with mock-transduced T cells. R1, R2 and mock-transduced T cells were incubated at decreasing concentrations with the cell lines CHO WT, CHO MRFL or HUVECs overnight. The supernatant was then analysed for the presence of IFNγ. Data is the mean of triplicate wells with error bars shown the (SD).

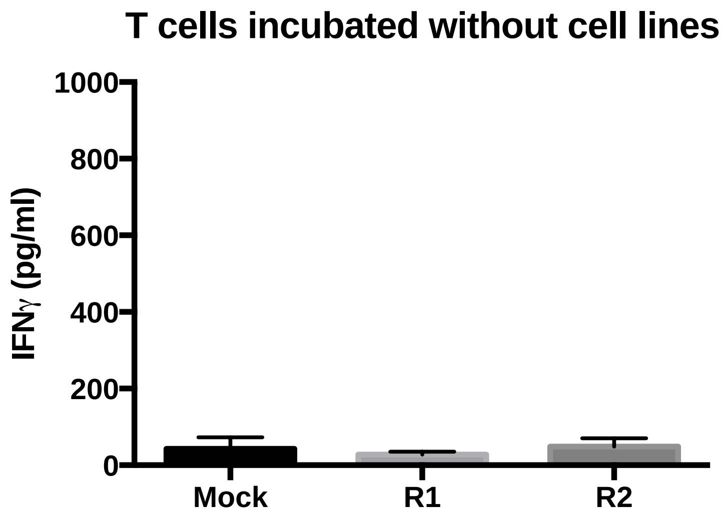

Figure 16: IFNγ ELISA to T cells incubated alone, without target cells. R1 and R2 CAR Transduced T cells were matched for transduction percentage by dilution with mock-transduced T cells. R1, R2 and mock-transduced T cells were resuspended in ELISA medium and added to empty wells at a concentration of $2x10^5$ cells/well. The supernatant was then analysed for the presence of IFNγ. Data is the mean of triplicate wells with error bars shown the (SD).

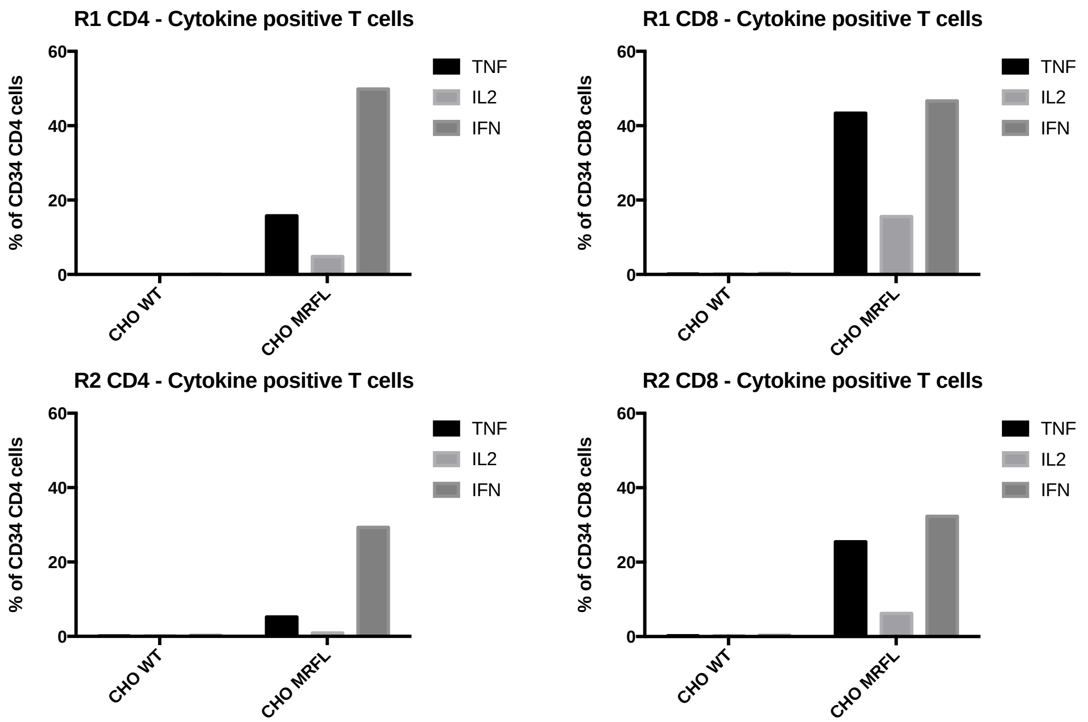

Figure 17: production of single cytokines by CD4 and CD8 CAR T cells. R1 and R2 CAR transduced T cells were matched for transduction percentage by dilution with mock-transduced T cells. Mock, R1 or R2 transduced T cells were incubated with the cell lines CHO WT or CHO MRFL overnight. T cells were stained for surface markers then permeabilised before intracellular cytokine staining was performed for IFNγ, TNFα and IL2. Data shows the percentage of CD34 (transduced) CD4 or CD8 T cells that are expressing only a single cytokine in response to CHO WT or CHO MRFL. Data is from a single well from a single assay.

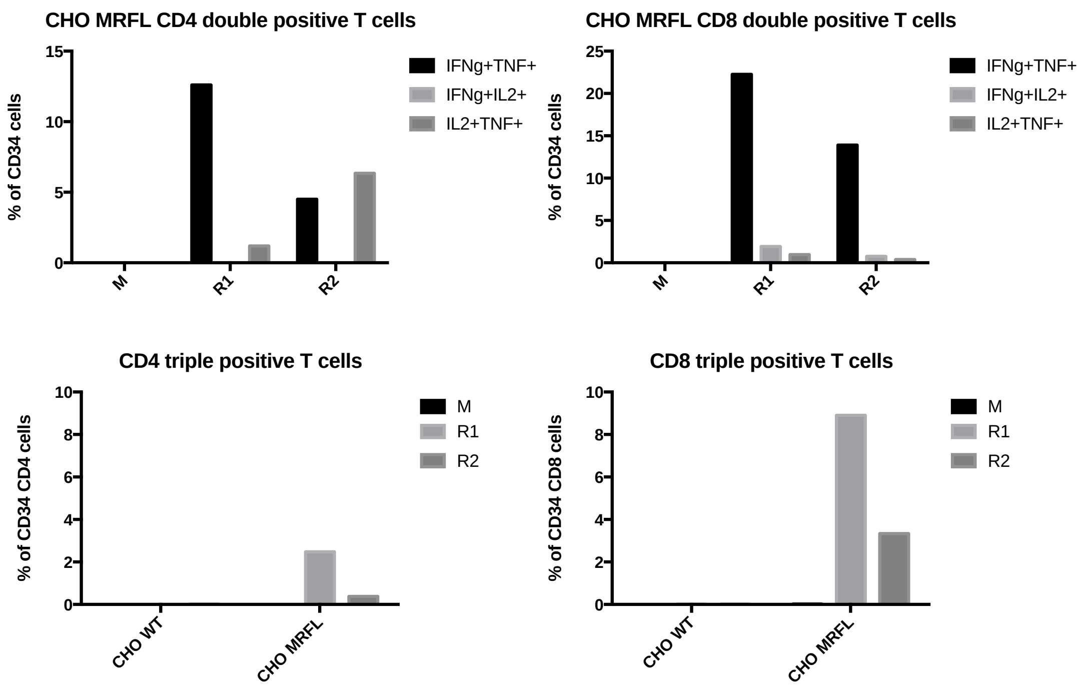

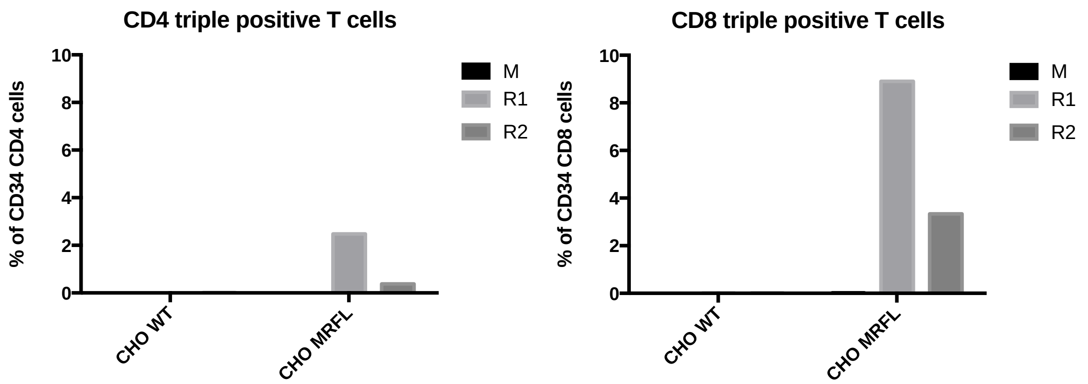

Figure 18: multicytokine production by CAR T cells. R1 and R2 CAR Transduced T cells were matched for transduction percentage by dilution with mock-transduced T cells. Mock (m), R1 or R2 transduced T cells were incubated with the cell lines CHO WT or CHO MRFL overnight. T cells were stained for surface markers then permeabilised before intracellular cytokine staining was performed for IFNγ, TNFα and IL2. Data shows the percentage of CD34 (transduced) CD4 or CD8 T cells that are expressing only two cytokines or produced all three cytokines (triple positive) in response to CHO WT or CHO MRFL. Data is from a single well from a single assay. Results are representative of three individual experiments

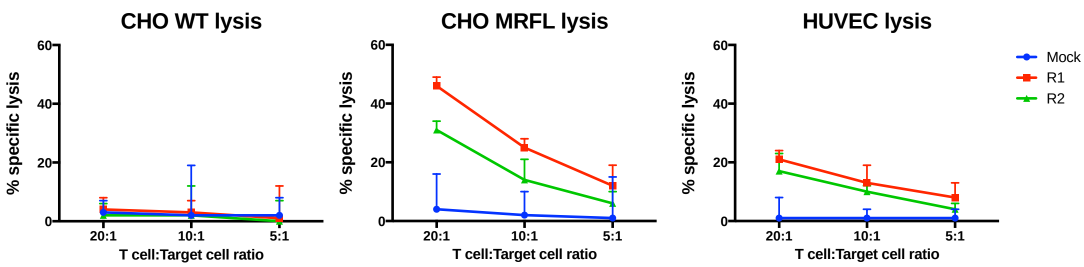

Figure 19 Chromium release assay. The target cells CHO WT, CHO MRFL or HUVEC were pre-labelled with ^{51}Cr. Labelled Target cells were then incubated with either Mock, R1 or R2 transduced T cells at different ratios for 8 hours. The % specific lysis was measured for all T cells and the target cells. Data shows the mean value from triplicate wells with the SD

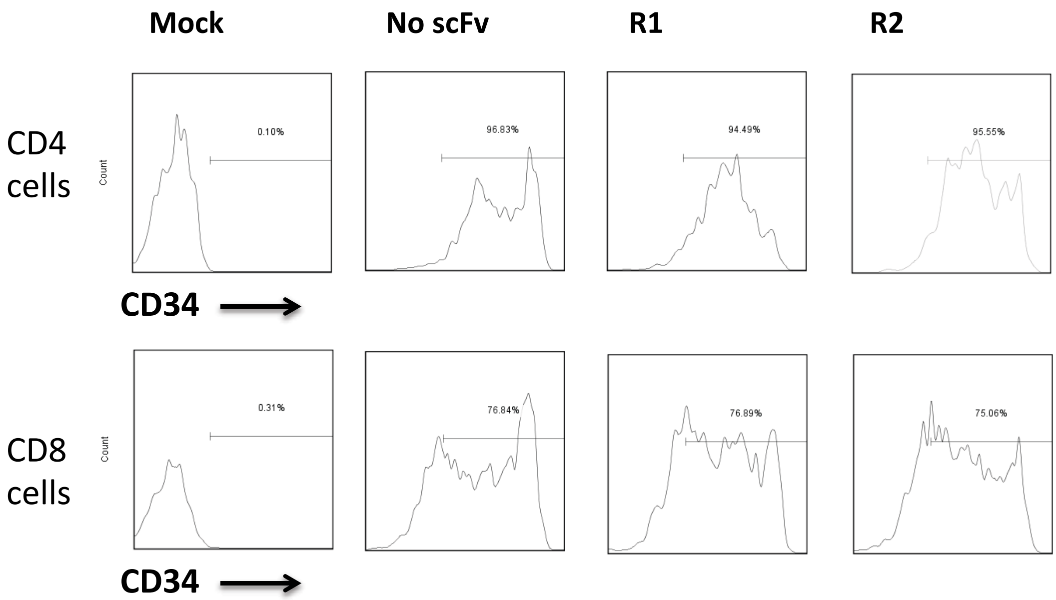

Figure 20 Mouse T cell transduction. Mouse T cells were transduced with R1, R2 or No scFv CAR DNA or mock transduced with no DNA. The following day, cells were stained for live cells then CD4 and CD8 T cells. Cells were stained for CD34 to analyse CAR transduction.